For Reference

NOT TO BE TAKEN FROM THIS ROOM

Ex libris
Universitatis
Albertaensis

QUAECUMQUE VERA

THE UNIVERSITY OF ALBERTA

MASS SPECTROMETRIC INVESTIGATION OF THE ION-MOLECULE REACTIONS AND EQUILIBRIA OF

(a) METHANE CONTAINING TRACES OF ETHANE

(b) THE SOLVATION OF Cl^- BY VARIOUS SOLVENT MOLECULES

BY

© MARGARET ANN FRENCH

A THESIS

SUBMITTED TO THE FACULTY OF GRADUATE STUDIES AND RESEARCH

IN PARTIAL FULFILMENT OF THE REQUIREMENTS FOR THE DEGREE

OF

DOCTOR OF PHILOSOPHY

DEPARTMENT OF CHEMISTRY

EDMONTON, ALBERTA

SPRING, 1977

Digitized by the Internet Archive
in 2023 with funding from
University of Alberta Library

https://archive.org/details/French1977

ABSTRACT

A commercial mass spectrometer was modified in order to observe the temporal behaviour of ions in a high pressure ion source. An ion source was constructed so that pressures up to 5 torr could be flowed through it. Electrical circuits were added which pulsed the electron beam. High speed amplifiers were installed so that the ion intensities could be stored in a multichannel scaler. The instrument could be used to measure rate constants and equilibria of ion-molecule reactions at thermal energies.

The first part of the thesis is concerned with the sequence of ion-molecule reactions occurring in methane containing traces of ethane. Studies of the reaction $CH_5^+ + C_2H_6 = CH_4 + C_2H_7^+$ showed that proton transfer occurred from left to right and equilibrium was not established even at the lowest ethane pressures used, 10^{-5} torr. This enabled a lower limit of 10^6 to be placed on the equilibrium constant for the proton transfer reaction and a proton affinity difference between methane and ethane of >8.7 kcal/mol.

$C_2H_7^+$ was found to decompose thermally to $C_2H_5^+$ by the reaction

$$C_2H_7^+ \longrightarrow C_2H_5^+ + H_2$$

The rate constant for the decomposition of $C_2H_7^+$ was

ABSTRACT

A conventional mass spectrometer was modified in order to measure the temporal behaviour of ions in a high pressure ion source. An ion source was constructed so that pressures up to 5 torr could be placed therein. Electrical circuitry was added which pulsed the electron beam. High speed amplifiers were installed so that the ion intensities could be followed in a multichannel scaler. The instrument could be used to measure rate constants and equilibria of ion-molecule reactions at thermal energies.

The first part of the thesis is concerned with the sequence of ion-molecule reactions occurring in methane containing traces of ethane. Studies of the reaction $CH_5^+ + C_2H_6 = CH_4 + C_2H_7^+$ showed that proton transfer occurred from left to right and equilibrium was not established even at the lowest ethane pressures used, 10^{-6} torr. This enabled a lower limit of 10^4 to be placed on the equilibrium constant for the proton transfer reaction and a proton affinity difference between methane and ethane of ≥ 5.5 kcal/mol.

$C_2H_7^+$ was found to decompose thermally to $C_2H_5^+$ by the reaction

$$C_2H_7^+ \longrightarrow C_2H_5^+ + H_2$$

The rate constant for the decomposition of $C_2H_7^+$ was measured at several temperatures which led to an activation energy of 10.5 kcal/mol. This enabled a value for $\Delta H_f(C_2H_7^+)$ to be calculated which led to an estimation of the proton affinity difference between methane and ethane of 10.3 kcal/mol. This value agreed with that obtained from the direct proton transfer measurement.

The $C_2H_5^+$ ion was observed to react with methane as well as ethane in the reactions

$$\begin{aligned} C_2H_5^+ + C_2H_6 &\longrightarrow C_4H_9^+ + H_2 \\ &\longrightarrow C_3H_7^+ + CH_4 \\ C_2H_5^+ + CH_4 &\longrightarrow C_3H_7^+ + H_2 \end{aligned}$$

The rate constant for the reaction of $C_2H_5^+$ with ethane was 5.3×10^{-11} cm^3 molecule^{-1} s^{-1} at 304°K and the rate constant for the reaction with methane was 1×10^{-14} cm^3 molecule^{-1} s^{-1} at 304°K. The reaction scheme was tested by fitting the results using an analog computer program. The rate constants agreed within 20%.

The second part of the thesis describes the investigation of a proposed correlation between the gas phase acidity of a compound RH and the chloride affinity of RH described by the enthalpy of the reaction

$$Cl^- + RH \rightleftharpoons RHCl^-$$

The chloride affinities were measured for RH = oxygen acids, ketones, carbon acids and substituted benzenes. The correlation was found to hold for the oxygen acids measured at several temperatures which led to an activation energy of 19.5 kcal/mol. This enabled a value for $\Delta H_f^\circ(C_2H_5)^+$ to be calculated which led to an estimation of the proton affinity difference between methane and ethane of 10.7 kcal/mol. This value agreed well with that obtained from the direct proton transfer measurements.

The $C_2H_5^+$ ion was observed to react with methane as well as ethane in the reactions:

$$C_2H_5^+ + C_2H_6 \longrightarrow C_4H_9^+ + H_2$$

$$\longrightarrow C_3H_7^+ + CH_4$$

$$C_2H_5^+ + CH_4 \longrightarrow C_3H_7^+ + H_2$$

The rate constant for the reaction of $C_2H_5^+$ with ethane was 5.0×10^{-11} cm^3 molecule^{-1} s^{-1} at 415°K and the rate constant for the reaction with methane was 1×10^{-12} cm^3 molecule^{-1} s^{-1} at 415°K. The reaction scheme was tested by fitting the results using an analog computer program. The rate constants agreed within 10%.

The second part of this thesis describes the investigation of a proposed correlation between the gas phase acidity of a compound AH and the chloride affinity of AH determined by the enthalpy of the reaction

$$Cl^- + AH \rightleftharpoons AHCl^-$$

The chloride affinities were measured for RH = oxygen acids: alcohols, carbon acids and substituted phenols. The correlation was found to hold for the oxygen acids

and ketones but when all of the compounds were considered the overall correlation was not good. In the case of the oxygen acids the chloride ion was found to attach *via* a hydrogen bond. The interaction with Cl^- varied from 13.7 kcal/mol for acetone to 33.7 kcal/mol for p-cyanophenol. The chloride affinities for the carbon acids and substituted benzenes were much weaker. The possible modes of the attachment of Cl^- are discussed for each type of compound.

ACKNOWLEDGEMENTS

I wish to express my sincere appreciation to Dr. Paul Kebarle for his advice and encouragement throughout the course of this work.

Some of the work described in Chapter 5 was done in collaboration with Dr. J. B. Cumming, who collected the data for the phenols.

The author would like to thank the members of the mass spectrometry group for their assistance and valuable discussions during the course of this study, particularly Dr. R. Yamdagni, Dr. K. Hiraoka and Dr. J. D. Payzant. Permission by Dr. O. P. Strausz for the use of the Atlas CH4 is acknowledged and also the assistance of Dr. E. Hardwidge.

The author wishes to thank Mrs. Mary Waters for her care and patience in typing the manuscript.

I would like to thank the members of the Chemistry Department Machine Shop and Electronics Shops. Special thanks are due to Mr. Hubert Hoffman for his care and skill in constructing the ion source and Mr. Terry Nord for his assistance in maintenance of the apparatus.

The financial assistance provided by the University of Alberta and the National Research Council of Canada is gratefully acknowledged.

TABLE OF CONTENTS

Page

1. INTRODUCTION 1

1.1 The Present Study........................ 1

1.2 The Development of Ion-Molecule Reaction Investigations.......................... 1

A. Studies at Low Pressures............ 1

B. Limitations of Low Pressure Studies. 7

C. Studies at High Pressures........... 10

1.3 Types of Ion-Molecule Reactions......... 16

a) Charge Transfer...................... 16

b) Abstraction or Transfer of Atoms or Atomic Ions........................ 17

i) Proton Transfer.................. 18

ii) Hydrogen Abstraction............ 19

iii) Hydride Ion Abstraction....... 19

iv) Atom-Ion Interchange 19

c) Condensation Reactions.............. 20

d) Exchange Reactions.................. 21

1.4 Recent Theories of Ion-Molecule Collisions................................ 22

1.5 Mechanisms of the Formation of Negative Ions...................................... 26

1.6 The Present Investigation............... 27

2. EXPERIMENTAL.............................. 29

2.1 Introduction............................ 29

2.2 Description of the Apparatus........... 30

2.3 The Ion Source.......................... 33

Page

2.4 Temperature Control and Measurement... 38

2.5 The Gas Handling Plant................ 39

2.6 Electron Gun Assembly................ 43

2.7 Pulsing Circuitry.................... 45

2.8 The Ion Detection System............. 48

2.9 Description of the Second Mass Spectometer............................. 52

2.10 Time of Flight...................... 57

2.11 Physical Conditions in the Ion Source. 59

A. Number of Collisions in the Ion Source............................ 59

B. Ion Sampling...................... 61

C. Charged Particle Recombination..... 69

D. Diffusion of Ions.................. 72

2.12 Normalization of the Data............ 75

3. ASSESSMENT OF SYSTEM OPERATION............ 78

3.1 Auxiliary Filament Test.............. 78

3.2 Electron Gun Test.................... 80

3.3 Testing of the Pulsing Circuits....... 83

4. ION-MOLECULE REACTIONS IN METHANE CONTAINING TRACES OF ETHANE........................... 89

4.1 Introduction.......................... 89

4.2 Experimental.......................... 95

4.3 Results and Discussion: Major Reactions in the Methane/Ethane System.......... 96

Page

4.4 Kinetics of the Reaction $CH_5^+ + C_2H_6 \longrightarrow C_2H_7^+ + CH_4$ 130

4.5 The Equilibrium $CH_5^+ + C_2H_6 \rightleftarrows C_2H_7^+ + CH_4$ 143

4.6 The Kinetics of the Reaction of $C_2H_5^+$ ... 149

4.7 Pyrolysis of $C_2H_7^+$ 159

4.8 Thermochemical Calculations........ 176

4.9 Analog Computer Analysis of Results...... 180

4.10 Recent Results........ 187

4.11 Other Reactions Observed........ 198

4.12 Conclusion........ 199

5. SOLVATION OF Cl^- BY VARIOUS SOLVENT MOLECULES. 201

5.1 Introduction........ 201

5.2 Previous Work on Gas Phase Acidities..... 204

5.3 Previous Work on Chloride Affinities and Other Related Complexes........ 210

5.4 Experimental........ 216

5.5 Measurement of Ionic Equilibria........ 221

5.6 Results........ 224

5.7 Discussion........ 259

(a) General Inspection of Data Obtained.. 259

(b) Chloride Affinities of Oxygen Acids: Substituted Phenols and Others....... 260

(c) Chloride Affinities of Ketones....... 265

(d) Chloride Affinities of Carbon Acids.. 270

Page

(e) Chloride Affinities of the Substituted Benzenes................ 277

(f) Correlation of Chloride Affinities with Dipole Moment................ 280

(g) Comparison with Recent Studies of $RHCl^-$ Complexes in Solution....... 281

5.8 Conclusions........................... 284

6. REMEASUREMENT OF THE RELATIVE GAS PHASE ACIDITIES OF ACETONE AND ACETONITRILE....... 287

6.1 Introduction........................... 287

6.2 Experimental........................... 288

6.3 Results and Discussion................. 289

7. SUGGESTIONS FOR FURTHER WORK................ 295

REFERENCES................................... 299

LIST OF TABLES

Table		Page
I	Typical Operating Voltages	46
II	Ions Observed when Methane is Bombarded by 70 eV Electrons	79
III	Thermodynamic Parameters Obtained for the Reaction $NH_4^+(NH_3)_{n-1} + NH_3 = NH_4^+(NH_3)_n$	88
IV	Summary of Reactions in Mixtures of Methane and Ethane	131
V	Summary of Rate Constants Obtained for the Reaction $CH_5^+ + C_2H_6 = C_2H_7^+ + CH_4$	142
VI	Calculated Equilibrium Constants at 30°C	145
VII	Relative Intensities of $C_3H_7^+$ and $C_4H_9^+$ at 86°C	151
VIII	Summary of Rate Constants k_{2s}, for the Decay of $C_2H_7^+$	174
IX	Average Rate Constants	184
X	Theoretical Calculations by J. A. Pople (147) of the Relative Energies of $C_2H_5^+$ Isomers Using Different Basis Sets	196
XI	The Effect of the Relative Intensity of Ions if 10% Collisional Dissociation Occurs	222
XII	Thermodynamic Data Obtained for the Reaction $Cl^- + RH = RHCl^-$	241
XIII	The Thermochemical Data Obtained for the Reaction $Cl^- + RH = RHCl^-$	247
XIV	Chloride Affinities, ΔG^o_T with Respect to 1,4 Pentadiene	257
XV	ΔG^o values for the Equilibrium $CH_3COCH_3 + CH_2CN^- \rightleftharpoons CH_3CN + CH_3COCH_2^-$ at 257°C	293

LIST OF FIGURES

Figure		Page
2.1	Schematic Diagram of Apparatus	32
2.2	Pulsed Electron Beam High Pressure Ion Source	35
2.3	Gas Handling System	40
2.4	Circuit Diagram for Electron Gun and Ion Source	44
2.5	Schematic Diagram of Experimental Apparatus	47
2.6	Signal Observed as a Function of Discriminator Gate Level	50
2.7	Schematic Diagram of Second Apparatus Used	54
2.8	Pressure Drop in the Ion Source	63
2.9	Schematic Diagram of Gas Flow Through the Ion Source	65
2.10	Measured Equilibrium Constant for the Reaction $Cl^- + (CH_3)_3COH \rightleftharpoons (CH_3)_3COH.Cl^-$ at 215°C with Flow Capillary Closed	67
2.11	Time Dependence of Total Positive Ion Signal	71
3.1	Normalized Intensity as a Function of Pressure of Methane	82
3.2	Measured Equilibrium Constants $K_{n-1,n}$ for the system $NH_4^+(NH_3)_{n-1} + NH_3 = NH_4^+(NH_3)_n$	86
4.1	Time Dependence of Normalized Intensities with No Ethane Added	97
4.2	Normalized Intensities of Major Ions at Short Reaction Times	99
4.3 to 4.31	Time Dependence of Normalized Ion Intensities	100-128

Figure		Page
4.32 to 4.37	Logarithmic Plots of the Decay of CH_5^+	134-139
4.38	Plot of ν_1 as a Function of Ethane Concentration	140
4.39	Logarithmic Plots of the Decay of CH_5^+ at 30°C	149
4.40	Logarithmic Plots of the Decay of $C_2H_5^+$ at 86°C	154
4.41	Plot of $\nu_{ov}/[C_2H_6]$ *versus* $[CH_4]/[C_2H_6]$ at 86°C	156
4.42	Logarithmic Plots of the Decay of $C_2H_5^+$ at $[CH_4]:[C_2H_6] = 50:1$	158
4.43	Perspective Plot of the Intensity of $C_2H_7^+$ as a Function of Temperature and Reaction Time	160
4.44 to 4.53	Logarithmic Plots of the Decay of $C_2H_7^+$	162-171
4.54	Plot of $\nu_2/[CH_4]$ *versus* Ethane Pressure at 86°C	173
4.55	Arrhenius Plot for the Rate Constant k_2 at Various Temperatures	175
4.56	Schematic Potential Energy Diagram for the Reaction $C_2H_7^+ \longrightarrow C_2H_5^+ + H_2$	179
4.57	Analog Computer Program to Produce Best Fit for the Normalized Intensity Curves	182
4.58	Plot of $\nu_{ov}/[C_2H_6]$ *versus* $[CH_4]/[C_2H_6]$ at 30°C Using Values of ν_{ov} Calculated from the Best Computer Fits	185
4.59	Plot of $\nu_{ov}/[C_2H_6]$ *versus* $[CH_4]/[C_2H_6]$ at 86°C Using Values Calculated from the Best Computer Fit	186

Figure Page

4.60 van't Hoff Plot for the Equilibrium $C_2H_5^+ + H_2 = C_2H_7^+$ Studied at Two Different Temperature Ranges 191

4.61 Schematic Potential Energy Diagram for the Reaction of Protonated Ethane 193

5.1 Plot of Equilibrium Constant $K_{0,1}$ for the Reaction $Cl^- + (CH_3)_3COH = (CH_3)_3COH.Cl^-$ versus the Time After the Reactants Were Mixed in the Bulb 218

5.2 Time Dependence of Cl^- and $CH_3COCH_3.Cl^-$ Ions in 2.75 torr CH_4 Containing 0.15 torr Acetone at 114°C 220

5.3 Measured Equilibrium Constants for the Reaction $Cl^- + (CH_3)_3COH = (CH_3)_3COH.Cl^-$ at Various Temperatures 226

5.4 Measured Equilibrium Constants for the Reaction $Cl^- + HCOOH = HCOOH.Cl^-$ at Various Temperatures 227

5.5 Measured Equilibrium Constants for the Reaction $Cl^- + CH_3COCH_3 = CH_3COCH_3.Cl^-$ at Various Temperatures 228

5.6 Measured Equilibrium Constants for the Reaction $Cl^- + C_6H_5OH = C_6H_5OH.Cl^-$ at Various Temperatures 229

5.7 Measured Equilibrium Constants for the Reaction $Cl^- + p\text{-}CH_3.C_6H_4OH = p\text{-}CH_3.C_6H_4OH.Cl^-$ at Various Temperatures 230

5.8 Measured Equilibrium Constants for the Reaction $Cl^- + p\text{-}Cl.C_6H_4OH = p\text{-}Cl.C_6H_4OH.Cl^-$ at Various Temperatures 231

Figure | Page

5.9 Measured Equilibrium Constants for the Reaction $Cl^- + p\text{-}F.C_6H_4OH = p\text{-}F.C_6H_4OH.Cl^-$ as a Function of Total Ion Source Pressure 232

5.10 Measured Equilibrium Constants for the Reaction $Cl^- + p\text{-}F.C_6H_4OH = p\text{-}F.C_6H_4OH.Cl^-$ as a Function of Total Ion Source Pressure After Changing the Ion Source Slits 233

5.11 Measured Equilibrium Constants for the Reaction $Cl^- + p\text{-}CN.C_6H_4OH = p\text{-}CN.C_6H_4OH.Cl^-$ at Various Temperatures 234

5.12 van't Hoff Plots for the Reaction $Cl^- + RH = RHCl^-$ where RH = Acetone, Formic Acid, t-Butanol and Phenol 235

5.13 van't Hoff Plots for Phenol and Substituted Phenols for the Reaction $Cl^- + RH = RHCl^-$ 236

5.14 Measured Equilibrium Constants for the Reaction $Cl^- + t\text{-}BuOH = t\text{-}BuOH.Cl^-$ at 231°C for a Mixture of t-BuOH in CH_4 and pure t-BuOH 238

5.15 van't Hoff Plot for the Reaction $Y\text{-}C_6H_4\text{-}OH.Cl^- + X\text{-}C_6H_4OH = X\text{-}C_6H_4OH\text{-}Cl^- + Y\text{-}C_6H_4OH$ for Various X and Y 244

5.16 Relative Hydrogen Bond Strengths to Cl^- for Various Phenols 246

5.17 Possible Deviations from the True van't Hoff Plot 250

5.18 Measured Equilibrium Constants for the Reaction $Cl^- + RH + RHCl^-$ at 26°C 253

Figure | Page

5.19 Measured Equilibrium Constants for the Reaction $Cl^- + RH = RHCl^-$ at 148°C 254

5.20 Correlation of Gas Phase Acidities *versus* Chloride Affinities for Various Oxygen Acids and Pyrrole 261

5.21 Correlation of Gas Phase Acidities *versus* Chloride Affinities for a series of Ketones and Acetonitrile 267

5.22 Correlation of Gas Phase Acidities *versus* Chloride Affinities for Various Carbon Acids 271

5.23 Plot of ΔG^o_T for the Substituted Benzenes versus the σ^o Values of Taft 278

5.24 Plot of $-\Delta G^o_T$ for all the Compounds Studied *versus* Their Dipole Moment 283

6.1 Observed Ion Signal in 2.8 torr CH_4 Containing a 1:1 Ratio of Acetone to Acetonitrile at 257°C 290

6.2 Observed Ion Signal in 3.2 torr CH_4 Containing a 10:1 Ratio of Acetone to Acetonitrile at 257°C 291

CHAPTER I

INTRODUCTION

1.1 The Present Study

This thesis describes an investigation of the kinetics and thermodynamics of selected ion-molecule reactions at pressures of about 1 to 5 torr. The ion-molecule reactions were followed in a pulsed electron beam, high pressure ion source mass spectrometer and multichannel scaler. This method enabled the reactions mechanisms to be analyzed and the rate or equilibrium constants to be measured.

1.2 The Development of Ion-Molecule Reaction Investigations.

A. Studies at Low Pressures

The conventional analytical mass spectrometer operates with the ion source, and particularly the mass analysis region of the instrument at as low a pressure as possible. The low pressure reduces the probability of an ion striking a neutral gas molecule. Raising the pressure in the ion source results in collisions between ions and neutral molecules which may lead to ion-molecule reactions. This results in the appearance of new ions and the disappearance of the primary ions,which is generally undesirable in qualitative and quantitative analytical mass spectrometry.

The first observation of an ion-molecule reaction was reported by J. J. Thomson as early as 1912 (1). Thomson observed, with his first mass spectrograph, an ion with m/e = 3 as a product from an electrical discharge in hydrogen. Dempster (2) substantiated Thomson's observation and showed that the ion was due to H_3^+. The origin of this ion was later explained (3,4) as arising from the reaction

$$H_2^+ + H_2 \longrightarrow H_3^+ + H \qquad (1.1)$$

The presence of H_3^+ was undesirable in isotopic experiments when the abundance of HD^+ needed to be measured.

Until the 1950's most mass spectrometric measurements were involved with isotopic abundance experiments and quantitative determinations of hydrocarbon mixtures. It was not until this time that it was recognized that ion-molecule reactions may play a major role in radiation chemistry. The pioneers in this field were Tal'rose and Lyubimova (5), Stevenson and Schissler (6,7) and Gutbier (8). These workers raised the pressure in the ion source of a mass spectrometer to 10^{-3} to 10^{-4} torr. Under these conditions a small fraction of the primary ions undergo collisions with neutral gas molecules to produce secondary ions. By measuring the intensity of secondary ions as a function of ion source pressure, cross-sections for ion-

molecule reactions could be calculated (9).

Earlier workers in the investigation of ion-molecule reactions used a conventional ion source which employs a small constant electric field that repels the ions out of the ion source into the mass analysis region of the mass spectrometer.

When the pressure in the ion source is sufficiently high that collisions occur, (about 10^{-4} torr) the primary ion, P^+, undergoes an ion-molecule reaction which gives rise to a secondary ion, S^+.

$$P^+ + M \longrightarrow S^+ + N \tag{1.2}$$

The attenuation of P^+ is given by

$$\frac{I_s}{I_p} = Qnl \tag{1.3}$$

where I_p and I_s are the intensities of the primary and secondary ion respectively, Q is the reaction cross-section, n is the number density of the gas and l is the total path length of the ion. Equation (1.3) is valid only at low pressures where much less than one collision occurs during a distance l. This technique was employed by such workers as Stevenson (6,7,10), Hamill (11) and Field and Franklin (12-14). They found that the experimental cross-sections for bimolecular ion-molecule reactions were very large and of the order of 100 $\mathring{A}^2$. This

may be compared to the fastest neutral-neutral reactions which are free radical recombination reactions. These processes have cross-sections of less than 10 $\mathring{A}^2$.

The first detailed quantitative explanation of the large cross-sections obtained for ion-molecule reactions was attempted by Langevin (15) in 1905, who was interested in the mobility of ions through gases. Langevin's treatment was applied to ion-molecule reactions by Gioumousis and Stevenson (16) under conditions where both ion and molecule moved with thermal (Maxwell) velocities and also under conditions where the ion was accelerated by the repeller field. Their theory visualizes the attractive forces between the colliding ion and molecule as being electrostatic in nature. As the colliding particles approach each other, the ion induces a dipole moment in the neutral, (neglecting any permanent dipole moment) and the particles are drawn together. This attractive force becomes significant (i.e. ~kT) at intermolecular separations of the order of several Angstroms. van der Waal's forces due to the interaction of the electron clouds of the particles are negligible at these distances. Various trajectories of the approaching ion are possible. When the distance of closest approach is quite large, the ion is deviated only slightly from its original path and a "distant" collision occurs. As the distance of closest

approach decreases the ion deviates from its original path to a greater extent until the ion spirals or orbits around the molecule. The period of interaction between the two particles is therefore greatly increased and Langevin assumed that an orbiting collision leads to a reaction while a distant collision does not. Gioumousis and Stevenson (16) showed that the orbiting or capture rate coefficient, k_c for a reaction, where the reactants have thermal velocities, could be expressed by

$$k_c = 2\pi e\left(\frac{\alpha}{\mu}\right)^{\frac{1}{2}} \qquad (1.4)$$

where e is the electronic charge, α is the polarizability of the neutral and μ is the reduced mass of the colliding pair. Since the cross-section, Q is given by

$$Q = \frac{k_c}{v} \qquad (1.5)$$

where v is the velocity of the approach of the particles, therefore

$$Q = \frac{2\pi e}{v}\left(\frac{\alpha}{\mu}\right)^{\frac{1}{2}} \qquad (1.6)$$

This expression predicts the observed large cross-section. The theory also predicts that Q will not depend on temperature. Therefore ion-molecule reactions of the type (1.2) usually proceed without any activation energy. Experimental observations have largely confirmed this prediction (17). Stevenson's treatment gives the orbiting

rate constant, and many reactions are experimentally observed to proceed with this rate constant. The orbiting rate constant is therefore equal to the reaction rate constant.

Gioumousis and Stevenson extended equation (1.6) to the situation where the rate constant was determined in the presence of a repeller field. Equation (1.7) describes a simple theoretical calculation of the thermal rate constant under conditions where the ion possesses excess energy.

$$k_c = Q\sqrt{\frac{eE_r l}{2m_p}} \qquad (1.7)$$

where E_r is the repeller field and m_p is the mass of the primary ion. However, several examples have been found of systems where k_c was not proportional to $E_r^{\frac{1}{2}}$ (9).

Reactions of the type (1.2) occur in a large number of chemical systems, such as radiation chemistry, the ionosphere, flames and electrical discharges. It would therefore be desirable to determine the rate constant of such systems where ions and molecules are in thermal equilibrium. The pulse technique was developed so that ions could react under field free conditions and the measured rate constant would be the thermal rate constant.

The pulsing technique was developed by Tal'rose

(18,19). The method consisted of allowing the electron beam to enter the ion source for a brief period, t_e ($\sim 10^{-7}$ sec) during which ions were formed. The ion source was then maintained under equipotential conditions for a certain time, t_d, during which the ions could react in a thermal environment. A brief pulse, t_r, was then applied to the repeller electrode so that ions were expelled from the ion source. Tal'rose showed that

$$\frac{I_s}{I_p} = knt_d + f(t_e,t_r) \tag{1.8}$$

where I_s/I_p is the ratio of secondary to primary ion, k is the rate constant, n is the number density of the gas, $f(t_e,t_r)$ is a function of the pulse widths. Equation (1.8) expresses the normal kinetic formulation where the degree of conversion from primary to secondary ions is determined as a function of elapsed time. This method of pulsing has since been used by Harrison _et al_ (20) and Ryan and Futrell (21,22).

B. _Limitations of Low Pressure Studies_

The study of ion-molecule reactions by the continuous repulsion and later the pulsing method had certain limitations. The low pressure in the ion source ($\sim 10^{-4}$ torr) combined with the short reaction times ($\sim 10^{-6}$ sec) are such that only bimolecular reactions with large rate con-

stants may be studied i.e. reactions which occur with orbiting rate constants. The concentration of secondary ions was usually more than a hundred times smaller than that of the primary ions and therefore further reactions of the secondary ions could not be observed.

The difficulties due to short reaction times were overcome mainly by the application of various trapping techniques (23-26). Harrison _et al_ (24-26) have developed a technique in which the positive ions are trapped in the ion source by the space charge of an electron beam. The ions are trapped by passing a continuous low energy electron beam (~5 eV) through the ion source. After a given reaction time the ions are expelled from the ion source by applying a pulse to the repeller electrode. Ions have been retained in the ion source for several milliseconds, using this method.

A recent approach to ion trapping has been the use of ion cyclotron resonance spectroscopy. This technique involves capturing ions in crossed electric and magnetic fields and ions have been trapped up to 100 milliseconds. This method was pioneered by Baldeschwieler _et al_ (27) and the field has expanded rapidly in the last ten years due to the work of Beauchamp _et al_ (28,29), Brauman _et al_ (30-32) and others (33,34).

Low pressure techniques where the ions are produced by electron impact have some restrictions. The main dis-

advantage is that the ions produced by the method may be internally or translationally excited. The energy state of the reactant is unknown and the measured rate constant is not the thermal rate constant. Reactions which require third body stabilization cannot normally be studied at pressures below 10^{-3} torr because the lifetime of the excited complex is shorter than the time between collisions.

By operating with the pressure in the ion source in the torr range many of the limitations mentioned previously are eliminated and a wider range of reactions may be studied. The ions need not be retained in the ion source by specific trapping techniques since the movement of the ions is slowed down by the increased pressure. The ions must diffuse to the walls, undergoing collisions which were absent in the low pressure case. The long residence time of the ions in the ion source allows the investigation of complex reaction sequences of the type

$$A^+ \longrightarrow B^+ \longrightarrow C^+ \longrightarrow D^+ \longrightarrow \ldots \qquad (1.9)$$

The ions are involved in many thousands of collisions while they remain in the ion source. Such a number of collisions is sufficient to quench most excited species to the ground state and the reactions studied will be those of thermal species.

Although the pressure in the ion source may be in the torr range, once the ions have left the ion source any

Further collisions on their flight to mass analysis are undersirable since this may alter the reaction products. The pressure outside the ion source must therebore be maintained at about 10^{-4} torr to eliminate any collisions. The external low pressure can be achieved by high capacity pumping systems and by making the exit from the ion source into a small orifice. The ions escape through the orifice to the external chamber by a combination of mass flow and diffusion. Under field-free conditions, the translational energies of the ions reflect the temperature of the gas in which they are carried. High pressures in the ion source enable multiple collisions of individual ions to occur and termolecular reactions of the type

$$X^{+} + Y + M \rightleftharpoons X^{+}.Y + M \qquad (1.10)$$

which require third body stabilization, may be investigated.

C. Studies at High Pressures

Field and coworkers repeated their earlier low pressure investigations of hydrocarbons (12-14) with a modified instrument capable of using pressures up to 0.3 torr. They were able to observe high order reactions in methane (35) and ethylene (36). Further improvements to

their apparatus permitted pressures up to 2 torr to be used (37). Field found that in pure methane, CH_5^+ and $C_2H_5^+$ were essentially unreactive. Once the reactions of methane were well established, Field and coworkers investigated the effect of small amounts (~1%) of additives on the reactions of the ions observed in pure methane (38,39). Field et al found that small concentrations of additives changed the distribution of ions in methane drastically. This line of research eventually led Field et al to the development of the Chemical Ionization Method (40-44). This technique involves the electron bombardment of a carrier gas, normally methane, containing small amounts of substrate. The primary ions formed are rapidly converted to the CH_5^+ and $C_2H_5^+$ which may then undergo proton transfer to the substrate or hydride ion abstraction. The ionization of the substrate is therefore effected by ionic reaction rather than electron impact.

Electron impact spectra normally involve the use of 70 eV electrons and considerable fragmentation occurs. For large molecules the parent ion is rarely observed because the excess energy gained from electron bombardment results in fragmentation. The energy involved in proton transfer or hydride abstraction is normally of the order of 1 to 2 eV which may be removed by collisions with the neutral molecules of the carrier gas. Fragmentation therefore occurs to a lesser extent in the chemical ion-

ization spectrum and identification of unknown compounds is made simpler. For example, hydride abstraction is prevalent in the paraffin hydrocarbons (41),

$$n\text{-}C_{18}H_{38} + CH_5^+ \longrightarrow s\text{-}C_{18}H_{37}^+ + CH_4 + H_2 \quad (1.11)$$

and the $(M-1)^+$ ion is observed, where M is the molecular weight of the compound. In the chemical ionization spectrum the $C_{18}H_{37}^+$ ion represents almost 40% of the total ionization whereas the parent ion, $C_{18}H_{38}^+$ contributes only 0.5% to the total ionization in the electron impact spectrum.

Chemical ionization spectra are usually much simpler than electron impact spectra and this allows faster interpretation of the spectra. Chemical ionization is widely used as an analytical technique and such instruments are now sold commercially. The only difference to that of Field's instrument is the presence of a repeller electrode in the ion source. Field and coworkers have also extensively investigated equilibria and kinetics of ion-molecule clustering reactions (45-49).

One of the most useful modern techniques available for studying ion-molecule reactions is the flowing afterglow technique. This method was developed by Ferguson, Fehsenfeld and Schmeltekopf (50) mainly for the purpose of studying ionospheric reactions. A carrier gas, which is usually helium, is weakly ionized by electron impact or a microwave discharge. The gas is flowed down a tube

at a pressure of about 0.5 torr. Downstream from the ionization region, reactant gases are injected and these molecules are ionized by the helium ions and excited helium atoms. Further downstream a second reactant gas is added whose reactions with the primary ions are to be studied. The ions are sampled mass spectrometrically at the end of the tube. From knowledge of the fluid dynamics of the flowing plasma the reaction time and hence the rate constant may be deduced. Ferguson and coworkers have investigated many clustering reactions of ionospheric interest (9,51) and have also used this method to measure electron affinities (52).

Bohme and Schiff (53,54) have used the flowing afterglow technique to measure rate constants of reactions selected to test current reaction rate theories and have found this method to be equally useful in determining thermodynamic data for ion-molecule reactions such as heats of formation of ions, proton affinities, electron affinities and bond dissociation energies of molecules.

The stationary afterglow technique involves the production of a plasma in a cell using microwave discharge or photon absorption. The ionic species present can be detected mass spectrometrically as a function of time of the decaying plasma. Fite *et al* (55) and Sayers and Smith (56) first applied the technique to reactions of ionospheric interest and Lineberger and Puckett (57) have studied

hydration of negative ions, also aeronomically important.

Ion drift tubes can be used as mass spectrometers in the torr range. A short burst of ions is created at one end of the drift tube. The ions drift along the tube under the influence of a uniform axial electric field and can be detected mass spectrometrically at the far end of the tube. When low field gradients are applied, thermal conditions are approached. Drift tubes are mainly used to measure ion mobilities and ion diffusion coefficients. McDaniel et al have performed such experiments (58) as well as ion-molecule association reactions (59) for example

$$O^- + 2O_2 \longrightarrow O_3^- + O_2 \qquad (1.12)$$

Kebarle et al applied the pulsing technique to the investigation of ion-molecule reactions at high pressures (60). The pulsing method used was similar to that developed by Tal'rose (18,19) and others (20-22) but by using high pressures they eliminated the necessity of a repeller field to eject the ions from the ion source. The electron beam was pulsed by applying a voltage to an electrode in the electron gun assembly such that the beam was deflected away from the entrance of the ion source except for a short time Δt_e (~10 μsec) when the electron beam passed into the ion source. The ion signal emerging from the ion source passed through a cone and an assembly of focussing and accelerating electrodes before being mass analysed.

The ion signal was gated by applying suitable voltages to the cone. The ion gate was closed for a time t' after the beginning of the electron pulse and then opened for a short time, Δt_i (~10 μsec). The ions collected during Δt_i had a reaction time of t'. The electron beam was pulsed at such a rate that all ions had completely decayed before the next pulse occurred. The reaction time t' was varied manually and experiments therefore took a considerable time. The pulsing method was later improved (65) by collecting the data in a multichannel scaler where all the signal was utilized, instead of only a small fraction and where the ion gating was achieved automatically by the scaler.

Kebarle and coworkers studied the solvation of both positive and negative ions (61-69). For example, the investigation of the attachment of water molecules to ions such as H^+ (61,62), O_2^+ (63) and NO^+ (67) is of ionospheric interest whereas the study of the solvation of Cl^- and O_2^- by water, methanol and the aprotic solvent acetonitrile (66,68) yields information on the behaviour of these ions in solution. Kebarle _et al_ have also obtained an absolute gas phase acidity and basicity scale (70-73) for simple organic compounds. Studying ion-molecule reactions in simple hydrocarbons has led to information on the energetics and stabilities of many carbocations (74,75).

1.3 Types of Ion-Molecule Reactions

(a) Charge Transfer

The simplest type of an ion-molecule reaction is charge transfer. During a collision between an ion and molecule, the ion abstracts an electron from the molecule for example

$$N_2^+ + O_2 \longrightarrow O_2^+ + N_2 \qquad (1.13)$$

The exothermicity of the reaction is the difference between the ionization potentials of nitrogen and oxygen.

$$-\Delta H = IP(N_2) - IP(O_2) \qquad (1.14)$$

Generally, if a bimolecular ion-molecule reaction is exothermic, the reaction proceeds at the collision frequency (9). The rate constants for charge transfer reactions are normally of the order of 10^{-9} to 10^{-10} cm^3 $molecule^{-1}$ sec^{-1}.

The corresponding charge transfer reaction for a negative ion is

$$X^- + Y \longrightarrow Y^- + X \qquad (1.15)$$

In this case the direction of the reaction is determined by the relative electron affinities of X and Y.

Resonant charge transfer occurs when the exothermicity is approximately zero. ΔH is zero when the ion

and molecule are the same species

$$N_2^+ + N_2 \longrightarrow N_2 + N_2^+ \qquad (1.16)$$

but resonant charge transfer has been observed between ions of different species, for example (76),

$$Xe^+ + C_2H_2 \longrightarrow Xe + C_2H_2^+ \quad , \Delta H = 0.04 \text{ eV} \qquad (1.17)$$

If ΔH is large because of a large difference in ionization potentials, the ion produced possesses a large amount of excess energy and may dissociate (77) as in reaction (1.18). The process is known as charge transfer induced dissociation.

$$Kr^+(^2P_{\frac{1}{2}}) + CH_4 \longrightarrow CH_3^+ + H + Kr \qquad (1.18)$$

The recombination energy of Kr^+ is 1.55 eV greater than the ionization potential of methane. The excitation energy is sufficient to break a C-H bond.

(b) Abstraction or Transfer of Atoms or Atomic Ions

A large majority of ion-molecule reactions involve the abstraction by the ion of an ionic or neutral fragment from the molecule, or the transfer by the ion of such a fragment to the molecule. Reactions in which the fragment is large are termed condensation reactions. When the fragment is hydrogen several types of reactions are possible.

(i) Proton Transfer Reactions

Proton transfer reactions have been studied extensively in recent years because of the interest in gas phase acidity and basicity. The gas phase basicity of a substance can be measured by observing the reaction

$$M + H^+ \longrightarrow MH^+ \quad , \quad \Delta H = -PA(M) \qquad (1.19)$$

The proton affinity of M is defined as the exothermicity of reaction (1.19), where M may be a negative ion or a neutral molecule. Proton affinities of simple organic compounds are normally of the order of 100 to 200 kcal/mol (54,78). In instruments of the type that are designed to measure thermal reactions, such magnitudes of ΔH are impossible to measure directly. Therefore reactions where proton transfer occurs from one base to another are used to measure proton affinities for bases M_1 and M_2

$$M_1H^+ + M_2 \rightleftarrows M_2H^+ + M_1 \qquad (1.20)$$

If the reaction proceeds in the direction written then the reaction is exothermic. The proton affinity of M_2 is therefore greater than that of M_1 and the measured ΔH is given by

$$\Delta H = PA(M_2) - PA(M_1) \qquad (1.21)$$

Thus if one proton affinity is known the other can be calculated by this method. Proton transfer occurs when there

are no electron vacancies in the valence shell of the ion (79).

(ii) Hydrogen Abstraction

If the ion has one electron vacancy in its valence shell, it is known as a radical ion. An example of a hydrogen abstraction reaction is (80)

$$CD_4^+ + NH_3 = CD_4H^+ + NH_2 \qquad (1.22)$$

(iii) Hydride Ion Abstraction

An ion in which there are two electron vacancies in the valence orbital tends to abstract a hydride ion from saturated molecules (79). For example, equation (1.23) shows $C_3H_5^+$ abstracting a hydride ion from

$$C_3H_5^+ + \text{neo-}C_5H_{12} = C_5H_{11}^+ + C_3H_6 \qquad (1.23)$$

neo-C_5H_{12}, this type of reaction is also observed with CH_3^+ (81).

(iv) Atom-Ion Interchange

Reactions where elements larger than hydrogen are transferred are called atom-ion interchange. For example (82)

$$O^+ + N_2 = NO^+ + N \qquad (1.24)$$

(c) Condensation Reactions

When units larger than atoms or atomic ions are transferred, the reaction is termed a condensation or attachment reaction. An example of this type of reaction is the clustering of water around NH_4^+ to form $NH_4^+.H_2O$ (83).

$$NH_4^+ + H_2O = NH_4^+.H_2O \tag{1.25}$$

The general equation for this type of reaction is

$$A^+(S)_{n-1} + S + M \rightleftharpoons A^+(S)_n + M \tag{1.26}$$

where M is the third body, which is required to remove excess energy due to the exothermicity of the reaction.

Attachment reactions are very informative because the equilibria may be measured for each successive addition of a solvent molecule around an ion. Thermodynamic data obtained in this way may then be compared to the behaviour in solution and the intrinsic effect of the ion-solvent interactions can be ascertained.

Equation 1.26 can be broken down into various steps. When an ion and neutral solvent molecule react, an excited intermediate is formed (84)

$$A^+ + S \xrightarrow{k_c} [A^+S]^* \tag{1.27}$$

The lifetime of the excited intermediate may vary from a single rotation period (~10^{-13} sec) to the time required

for collisional stabilization. If the lifetime is short and no stabilizing collisions have occurred, the complex dissociates to the reactants.

$$[A^+S]^* \xrightarrow{k_d} A^+ + S \quad \text{decomposition} \qquad (1.28)$$

If the lifetime of the complex is considerably longer and collision occurs with a third body, a stable cluster is formed.

$$[A^+S]^* + M \xrightarrow{k_s} [A^+S] + M \quad \text{stabilization} \qquad (1.29)$$

The overall reaction is therefore

$$A^+ + S \underset{k_d}{\overset{k_c}{\rightleftarrows}} [A^+S]^* \xrightarrow[M]{k_s} A^+_{\cdot}S \qquad (1.30)$$

Applying steady state conditions, the expression for the experimental rate constant, k_f is given by (84).

$$k_f = \frac{k_c k_s}{k_d + k_s[M]} \qquad (1.31)$$

Under conditions of low pressure, $k_d >> k_s[M]$ and equation (1.31) becomes

$$k_f = \frac{k_c k_s}{k_d} \qquad (1.32)$$

The magnitude of the rate constants, k_f, for clustering reactions are normally 10^{-28} to 10^{-31} cm^6 $molecules^2$ sec^{-1} (69).

(d) Exchange Reactions

Reactions of this type involve the exchange of a

molecule attached to an ion for another neutral molecule. These reactions are also known as "switching reactions".

$$(CH_3OH)_2H^+ + CH_3OCH_3 \rightleftharpoons (CH_3OH)(CH_3OCH_3)H^+ + CH_3OH \tag{1.33}$$

The measurement of equilibria such as (1.33) and higher cluster exchange reactions can lead to information about preferential solvation in solution (85).

1.4 Recent Theories of Ion-Molecule Collisions

Gioumousis and Stevenson (16) first derived the theoretical expression for the capture rate constant for a point charge colliding with a point polarizable molecule.

$$k_c = 2\pi e\left(\frac{\alpha}{\mu}\right)^{\frac{1}{2}} \tag{1.34}$$

where e is the electronic charge, α is the polarizability of the neutral and μ is the reduced mass of the colliding ion-neutral pair. Gioumousis and Stevenson did not take into account any permanent dipole moment that the neutral molecule may possess. Moran and Hamill (86) determined that contributions of the ion-dipole interaction must be included in the calculations for target molecules with significant dipole moments. They suggested the Locked Dipole Approximation. If no alignment of the dipole with the approaching positive charge occurs, then the ion-

dipole interactions should average zero, and only the ion-induced dipole interaction will be important. The expression then reduces to the Gioumousis-Stevenson equation (1.34). However if the dipole of the rotating molecule "locks in" as the ion approaches, the ion-dipole interaction should be added to the ion-induced dipole interaction. Harrison et al (87) extended the calculations to thermal ion distributions

$$k_{LD} = \frac{2\pi e}{\mu^{\frac{1}{2}}}\left[\alpha^{\frac{1}{2}} + \mu_D\left(\frac{2}{\pi kT}\right)^{\frac{1}{2}}\right] \qquad (1.35)$$

where μ_D is the permanent dipole of the molecule, k is Boltzmann's constant and T is the absolute temperature.

Equation (1.35) was found to be useful for estimating the upper limit of rate constants but usually their magnitude was overestimated.

Bowers and Laudenslager (88) suggested that the ion field was not sufficient to lock the dipole of the molecule and only partial locking occurred. They assumed that the rate constant could be represented by the semi-empirical form

$$k_{PLD} = \frac{2\pi e}{\mu^{\frac{1}{2}}}\left[\alpha^{\frac{1}{2}} + C\mu_D\left(\frac{2}{\pi kT}\right)^{\frac{1}{2}}\right] \qquad (1.36)$$

where C is the locking dipole constant with values between 0 and 1. When C=0, no locking occurs and the equation reduces to k_c, equation (1.34). When C=1, complete locking

occurs and equation (1.35) is obtained. They tested equation (1.36) quantitatively by measuring the rate constant for the charge transfer from rare gas ions to a series of isomers with different dipole moments. They chose the trans, 1,1 and cis isomers of difluoroethylene and measured the incremental increase in the rate constant with increasing dipole moment of the molecule and assumed that this represented the degree of locking of the dipole. From equation (1.36)

$$C = \Delta k_{PLD}\left(\frac{kT\mu}{8\pi e^2 \mu_D^2}\right)^{\frac{1}{2}} \tag{1.37}$$

where Δk_{PLD} is the experimental increase in rate constant for the polar isomer, relative to the non-polar isomer. In this particular example, $C_{1,1} = 0.093$ and $C_{\underline{cis}} = 0.111$ which are close to the zero dipole limit. The cis isomer is oriented to a slightly greater extent than the 1,1 isomer.

The Average Dipole Orientation Theory was proposed by Su and Bowers in 1973 (89,91) and they visualized the effect of the approaching ion on the rotating molecule. As the ion approaches the molecule, the rotational motion of the dipole of the molecule is hindered by the field of the ion causing a net orientation of the dipole. Secondly they assumed that the net transfer of angular momentum between the rotor and the system is negligible.

Their third assumption was concerned with the rotational degrees of freedom of the rotor. They assumed that the rotor had two rotational degrees of freedom in the plane of collision and the third degree of freedom was aligned along the dipole and did not affect the angular momentum. This premise is valid for diatomic molecules but they estimated that errors introduced by using more complicated molecules would not change the final rate constant by more than 5%. The ADO theory, by considering the average orientation of the polar molecule is only valid for ion-molecule separations of 8 to 15 Å and therefore the rate of the reaction is independent of the size of the molecule for low ion energies.

Bohme has tested the ADO theory using proton transfer reactions (54). For example, the neutral molecule NH_3 was reacted with different proton donors and the rate constant for proton transfer for reaction (1.38) was measured where X = H_2, NH_2, CH_4, H_2O, CO, N_2, C_2H_4, C_2H_6, N_2O and C_4H_8. The experimental results gave good agreement with the predictions from the ADO theory.

$$XH^+ + NH_3 \longrightarrow NH_4^+ + X \qquad (1.38)$$

1.5 Mechanisms of the Formation of Negative Ions

Negative ions may be formed by several processes (92). Under the conditions used in most high pressure mass spectrometers the most important processes are electron capture, dissociative electron attachment and ion-pair production.

In an electron capture reaction, the electron encounters a neutral molecule which has a positive electron affinity. The resultant excited molecular ion is stabilized by collision with another molecule or autoionized.

$$\begin{aligned} e + O_2 &\rightleftharpoons [O_2^-]^* \\ [O_2^-]^* + M &\longrightarrow O_2^- + M^* \end{aligned} \qquad (1.39)$$

Dissociative electron attachment occurs when no stabilizing collision occurs within the lifetime of the excited molecular ion and the transient molecular ion dissociates into an ion and neutral fragments.

$$e + XY \longrightarrow X + Y^- \qquad (1.40)$$

Therefore the pressure of the gas, as well as the energy of the electron, is important in determining whether electron capture or dissociative attachment occurs. Both processes occur only over a narrow range of electron energy of about 2 - 5 eV (92).

When an electron and neutral molecule interact such that both a negative and positive ion are produced then the process is called ion-pair production.

$$e + XY \longrightarrow e + X^{+} + Y^{-} \qquad (1.41)$$

The electron acts as a source of energy and excites the molecule into an unstable state such that it dissociates into a positive and negative ion. There is a critical energy below which ion-pair production does not occur. Above the critical value, the probability of ion-pair production occurring depends on the energy of the electron.

1.6 The Present Investigation

The work described in the subsequent chapters was performed on two different mass spectrometers. The investigations described in Chapters 3 and 4 were performed on a mass spectrometer that was originally a commerical instrument but has been altered in several stages. Modifications were made to an Atlas CH4 mass spectrometer in order to observe ion-molecule reactions using pressures in the torr range. As mentioned in Section 1.2, three requirements are necessary to observe consecutive ion-molecule reactions at high pressures. First a high capacity pumping system is essential in the vacuum chamber outside the ion source to reduce the possibility of ions escaping

from the ion source and colliding with molecules on their path to mass analysis. This feature was already installed on the Atlas CH4 mass spectrometer. The second requirement is an ion source that can retain a pressure of several torr while the external pressure is kept at a minimum. This was achieved by making the orifices extremely small. A slit of approximate dimensions 1 x .01 mm was usually small enough to provide an adequate pressure difference between the ion source and the main vacuum chamber. Third, pulsing circuits are required to follow the temporal behaviour of the various reactant and product ions of a sequence of ion-molecule reactions. Suitable electronic equipment was added to this end.

The techniques used in the present experiments were developed by Durden (93) and the pulsing circuity, data collection and ion source design was improved by Payzant (94). These methods were incorporated into the design of the ion source used in the Atlas CH4 mass spectrometer.

The second mass spectrometer used was identical in principle to the Atlas CH4 but was constructed in our laboratory.

This thesis describes two major projects and an introduction to each is included in the relevant chapter.

CHAPTER 2

EXPERIMENTAL

2.1 Introduction

The investigations described in this thesis were conducted with two different mass spectrometers. The two instruments were very similar in their principles of operation. One machine will be described in detail and the other will be described briefly where it differs from the first.

There are several requirements which a high pressure ion source mass spectrometer must meet if the measurements are to be reliable and reproducible. First, the electrons used to ionize the gas must have sufficiently high energy to penetrate the gas sample, which is present at pressures of several torr. Therefore 1 to 2 KeV electron energies were used. Second, the incandescent filament which generates the electrons, must be sufficiently distant from the ion source that no temperature gradient across the ion source is caused by the heating effect of the filament. The lifetime of the filament is longer when operated at lower pressures. Third, it is important that the ion intensities detected are an accurate representation of the actual ion population in the ion source. Although the pressure in the ion source may be several torr, the mass spectrometer must be designed so that no collisions occur between ions and molecules as

they move from the ion exit slit to the mass analyzer. This criterion requires a high capacity pumping system in the chamber outside the ion source and an electrode geometry which allows free expansion of the gas escaping from the ion source. The vacuum outside the ion source should be such that the mean free path of an ion is much greater than the dimensions of the apparatus.

2.2 Description of the Apparatus

The mass spectrometer used for the project described in Chapter 4 was a commercial instrument, an Atlas CH4. A schematic diagram of the mass spectrometer is shown in Figure 2.1. The instrument was a conventional 60° sector magnetic deflection mass spectrometer which had previously been modified for high pressure work using flash photolysis (95) by adding a large stainless steel chamber which was mounted on the analyzer tube [3] of the mass spectrometer. The 10 in. diameter chamber was evacuated, *via* an 8 in. pumping lead [5], by a 6 in. NRC oil diffusion pump fitted with a 6 in. NRC water cooled baffle. Strausz *et al* (95) estimate the pumping speed at the ion source to be 500 l/sec. For the present work the ion acceleration system was also modified by mounting a series of acceleration and focussing slits and deflection plates on the analyzer tube. The voltages of these electrodes could be

FIGURE 2.1

Schematic Diagram of Apparatus

[1] Ion source

[2] Ion accelerating and focussing electrodes

[3] Atlas CH4 mass analyzer tube and magnet

[4] Electron multiplier followed by an amplifier and multi-channel scaler

[5] To a 6 in. vapor trap and diffusion pump

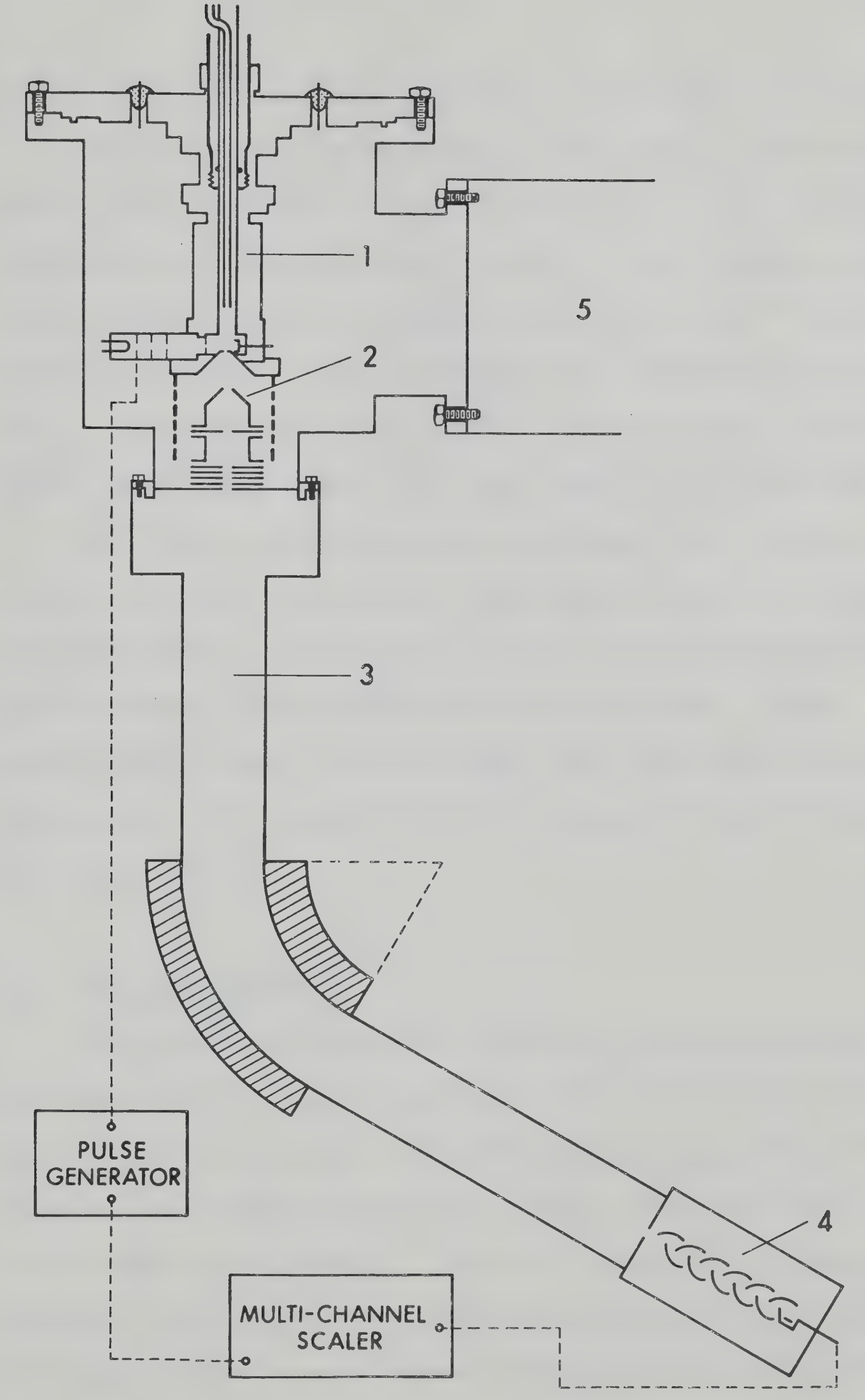
PULSE GENERATOR
MULTI-CHANNEL SCALER

selected to give optimum sensitivity and mass resolution.

An ion gauge was mounted on the side of the chamber which could be pumped to less than 1×10^{-7} torr overnight. During normal operation with 3 torr of gas passing through the ion source, the ion gauge registered 2×10^{-4} torr. A Penning gauge was also available for measuring the pressure in the analyzer tube itself. The pressure in this region was normally 5×10^{-5} torr during an experiment.

The mass spectrometer was equipped with heaters which could bake out most of the analyzer tube and electron multiplier. The magnet could be withdrawn and heaters placed around the narrowest part of the tube. These heaters were found to be necessary for the baking out of the system. The removal of last traces of water required particular effort.

2.3 The Ion Source

The design of the ion source was very similar to that used with other instruments in our laboratory (62). The ion source was made from non-magnetic stainless steel. The one difference to previous designs was the position of the electron filament. Since no separate flange was available for mounting the electron gun assembly it had to be mounted on a small tower attached to the side of the ion source as shown in Figure 2.2.

FIGURE 2.2

Pulsed Electron Beam High Pressure Ion Source

[1]	High pressure ion source
[2]	Slow gas flow inlet and outlet
[3]	Filament
[4]	Pulsed electron beam electrodes
[5]	Electron entrance slit
[6]	Ion exit slit
[7]	High transparency grid for electric field shielding
[8]	Heating mantle
[9]	Auxiliary electron filament

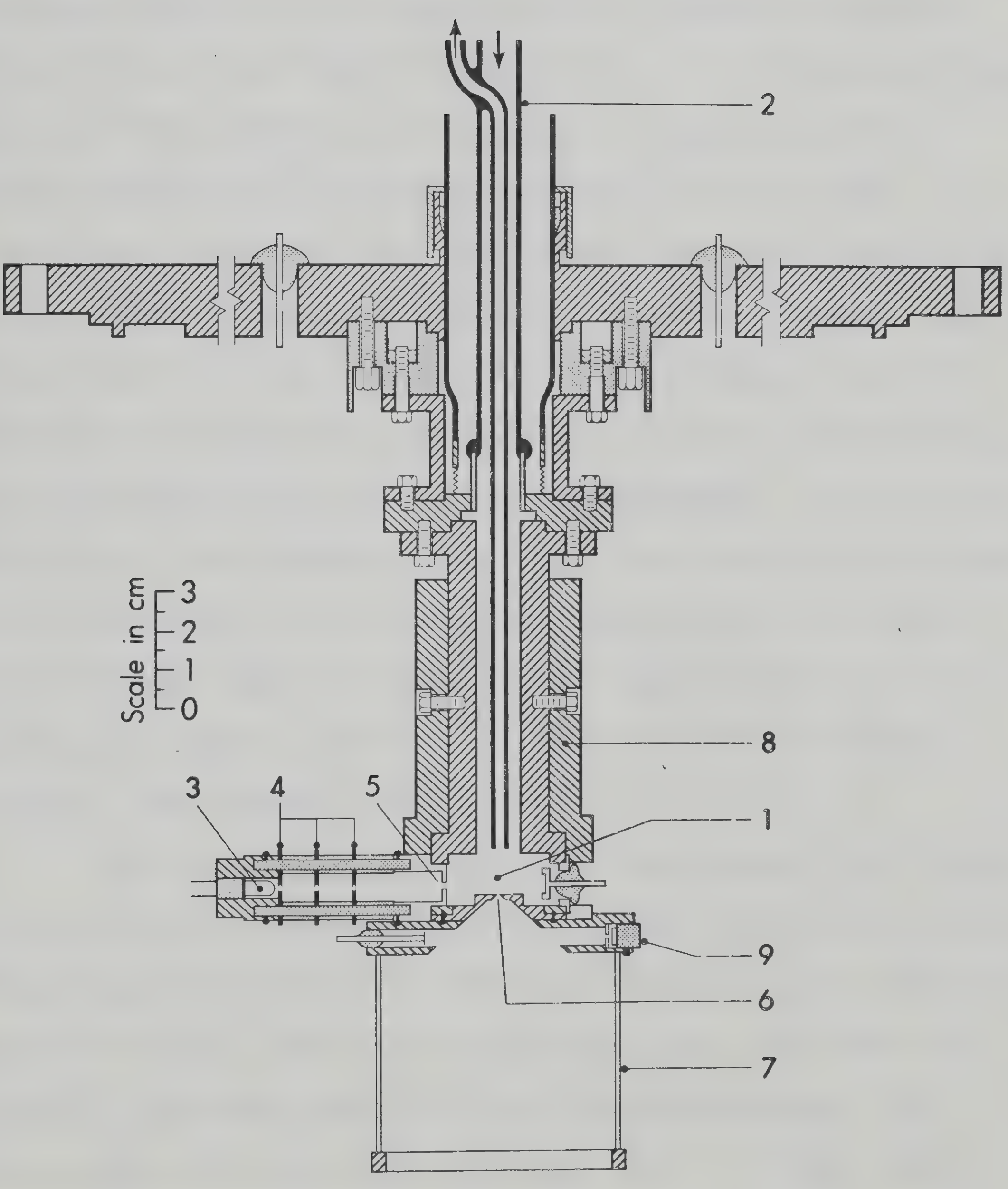
Scale in cm

The electron beam from the filament [3] passed through drawout, focus and deflection electrodes [4], then through a narrow slit mounted on the electron entrance cone [5] and into the ion source [1]. The narrow slit was made by spot welding two parallel pieces of stainless steel razor blades across a small hole in the cone. A stainless steel ring was spot welded over the top of the razor blades to ensure that their edges were even. The resultant slit was .008 x 2 mm. The filament was sufficiently distant from the ion source to be effectively at the same pressure as the vacuum chamber. The heating effect of the filament on the ion source was also minimal. The temperature rise in the ion source after turning on the filament was only about 1°C. Undeflected electrons were collected on the trap at the far side of the ion source. (See Figure 2.2).

The volume of the ion source was about 2 cm^3. The ions created in the ion source diffused through the field free region to the walls. Some of the ions reach the ion exit slit [9]. The slit was mounted on a cone and was made in the same manner as the electron entrance slit. The size of the ion exit slit was .017 x 1.6 mm. The plane of the electron beam was about 4 mm above the ion exit slit. Both entrance and exit cones were sealed to the ion source with gold 'O'-ring gaskets made from .015 in. gold wire.

Gas flowed into the ion source from a gas handling plant [2]. The gas from the gas handling plant entered the ion source in a slow flow and was pumped out of the ion source by a mechanical pump controlled by an intermediate capillary. The inlet/outlet tube was made of glass and was joined to the metal ion source by a silver-soldered kovar seal. Around the inlet/outlet tube was another glass tube which was mounted on bellows to allow flexibility. The outer glass tube was used to hold pencil heaters directly against the inlet/outlet tube. Five 90 watt Hotwatt heaters were used to ensure that no condensation occurred in the glass tubing and for bake-out purposes.

A stainless steel mantle [8] contained vertical grooves into which heaters could be installed. The heaters were held in place by two semicircular shields which were screwed to the mantle. The heaters consisted of 2½ in. cylindrical ceramic rods with 6 longitudinal holes, threaded with .010 in. molybdenum wire. A second set of heaters was mounted in the base of the ion source in order to make sure that there was no temperature gradient across the ion source.

An auxiliary filament [9] and trap were embedded in the base outside the ion source. This enabled conventional mass spectra to be measured in the low pressure region just outside the ion source in order to check the

the purity of reactant gases.

Below the base of the ion source an electrostatic shield [7] was mounted which provided a boundary for the electric field between the ion source and the ion acceleration tower. The cage consisted of eight longitudinal rods held rigid by the base at the top end and by a ring at the other. High transparency gauze was spot welded around the rods so that the high pumping speed was still maintained.

All electrical connections to the ion source assembly were made by electrical feed-throughs on the flange.

2.4 Temperature Control and Measurement

The temperature of the ion source was monitored in three places by iron-constantan thermocouples. The thermocouples were placed in the ion source, heating mantle and base of the ion source. The thermocouples have to be in intimate contact with the surface they are measuring and to ensure good contact, the middle of a screw was drilled out, the thermocouple inserted and the hole filled with silver solder. The screw was then screwed tightly into a tapped hole.

The temperature of the ion source was controlled by manual setting of the heater voltage. The heater voltage was supplied by an auto transformer (Variac) followed by an isolation transformer so that the heaters could float

at the same voltage as the ion source. It had been found (93) that allowing the ion source to reach a steady state gave a much more constant temperature than could be obtained by an automatic temperature controller.

The voltage of the thermocouples was read with a potentiometer. The reference thermocouple was immersed in an ice-water mixture.

Since the heaters and thermocouples all floated at high voltage, care was taken to insulate all heater and potentiometer controls.

2.5 The Gas Handling Plant

The gas inlet system provided with the Atlas CH4 mass spectrometer was an all-stainless steel system except for the valve seats which were made of Teflon. This was considered undesirable since Teflon can absorb substances and then gradually degas them over a long period of time. Also, the valves on the gas inlet system were the lever type which are either fully open or completely shut. Thus it was impossible to control the gas flow to the ion source from the gas inlet system. Because of these disadvantages a completely new gas handling plant was designed and built.

The gas handling system, shown in Figure 2.3, was made entirely of glass and stainless steel. The entire system was surrounded by a box made of 1 in. thick, hard

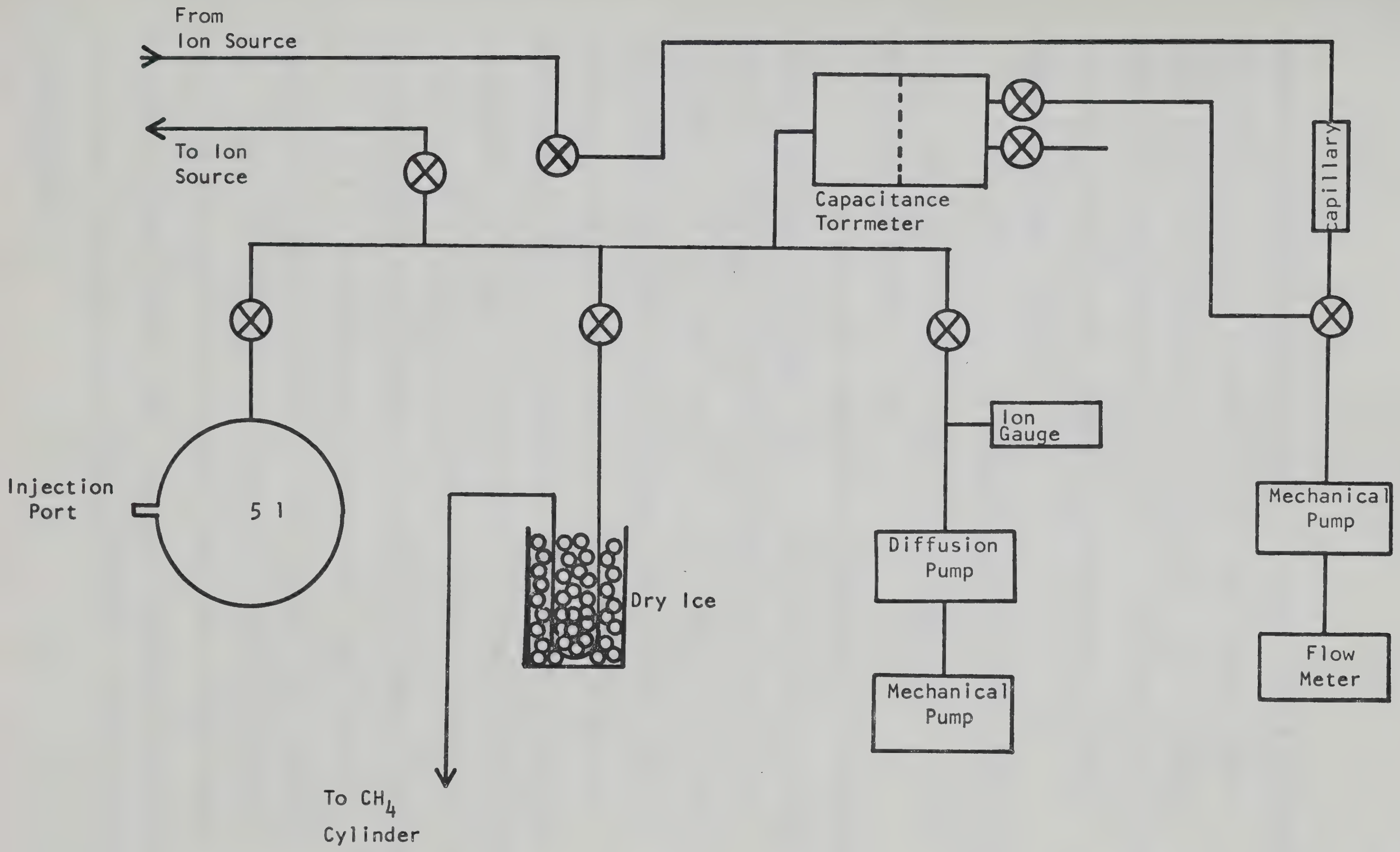
From
Ion Source
To Ion
Source
Capacitance
Torrmeter
capillary
Ion
Gauge
Injection
Port
5 l
Dry Ice
Diffusion
Pump
Mechanical
Pump
Mechanical
Pump
Flow
Meter
To CH_4
Cylinder

FIGURE 2.3 Gas Handling System

asbestos material, Marinite 36A. The box could be heated to 200°C to bake out impurities. The heaters were GE 1000 watt rod elements which were bent into suitable shapes and covered with a shield so that there was no possibility of initiating thermal decomposition if the heaters glowed red hot.

The valves were all metal Granville-Phillips ultra-high vacuum valves which used silver gaskets as a seal. The glass tubing was 14 mm.

The system was pumped by an Edwards oil diffusion pump and liquid nitrogen trap. The pressure in the manifold was measured by an Atlas-Bremen MCT capacitance manometer which could read pressures from 0.1 to 20 torr. The manometer head could be baked out at 350°C for degassing purposes. The reference side could either be evacuated or let up to atmospheric pressure so that one atmosphere of a gas could be admitted into the gas handling plant. The calibration of the capacitance manometer was checked periodically against a digital or mercury manometer.

A 5 litre bulb was used to make gas mixtures. The bulb has an injection port, access to which was obtained by a small sliding door on the front panel of the box. The injection port consisted of two rubber septa separated by a dead space. The septa were changed frequently to prevent leakage and disintegration due to the elevated temperature.

The most troublesome impurity for the experiments described in Chapter 4 was water. The entire mass spectrometer and gas handling system had to be completely free of any traces of water. To achieve this the mass spectrometer and gas handling system were repeatedly baked out. To prevent water from entering the system with the reactants the major gas, ultra high purity methane, was passed through a U-tube containing molecular sieve immersed in dry ice. Liquid nitrogen could not be used since the pressure of methane passed through the U-tube was 1 atmosphere and the vapor pressure of methane at -78°C is about 40 torr. Ethane was contained in a separate vacuum rack which was maintained at 1 atmosphere pressure and also passed over a molecular sieve. The ethane was Phillips Research Grade.

The glass tubes leading from the gas handling system to the ion sources were wrapped in heating tape for purposes of degassing and to prevent condensation. The tubing was 14 mm in diameter and was large enough that the pressure difference between the manifold of the gas handling system and the ion source was insignificant. Poiseville's Law (96) can be used to calculate the pressure gradient.

$$n_M = \frac{\pi a^4 (P_2^2 - P_1^2)}{16 \eta l RT} \qquad (2.1)$$

where n_M is the flow (moles/sec) through a tube of length l and radius a, R is the gas constant, T is the temperature and η the viscosity of the gas. P_2 and P_1 are the inlet and outlet pressures of the tubes to the ion source. To measure the flow a bubble flow meter was installed on the exhaust of the mechanical pump that controlled the flow through the ion source. When the pressure of methane was 3 torr the flow rate was about 20 cm^3 atm min^{-1}. The length of the tube from the manifold to the ion source was about 1 m, with a radius of 0.7 cm. The viscosity of methane is 1.09×10^{-4} poise (97). From equation (2.1) it may be calculated that the pressure difference between the manifold and the ion source is less than 0.5%. Therefore the pressure reading of the capacitance manometer is an accurate representation of the pressure in the ion source.

2.6 The Electron Gun Assembly

The electron gun assembly is shown in Figure 2.2. Since the filament was much closer to the electron entrance slit in the ion source than in previous designs (98), the arrangement of electrodes could be simplified.

The potential divider and wiring circuit for the various electrodes is shown in Figure 2.4. The voltage for the potential divider was supplied by a variable high voltage supply. The center of the filament was kept at

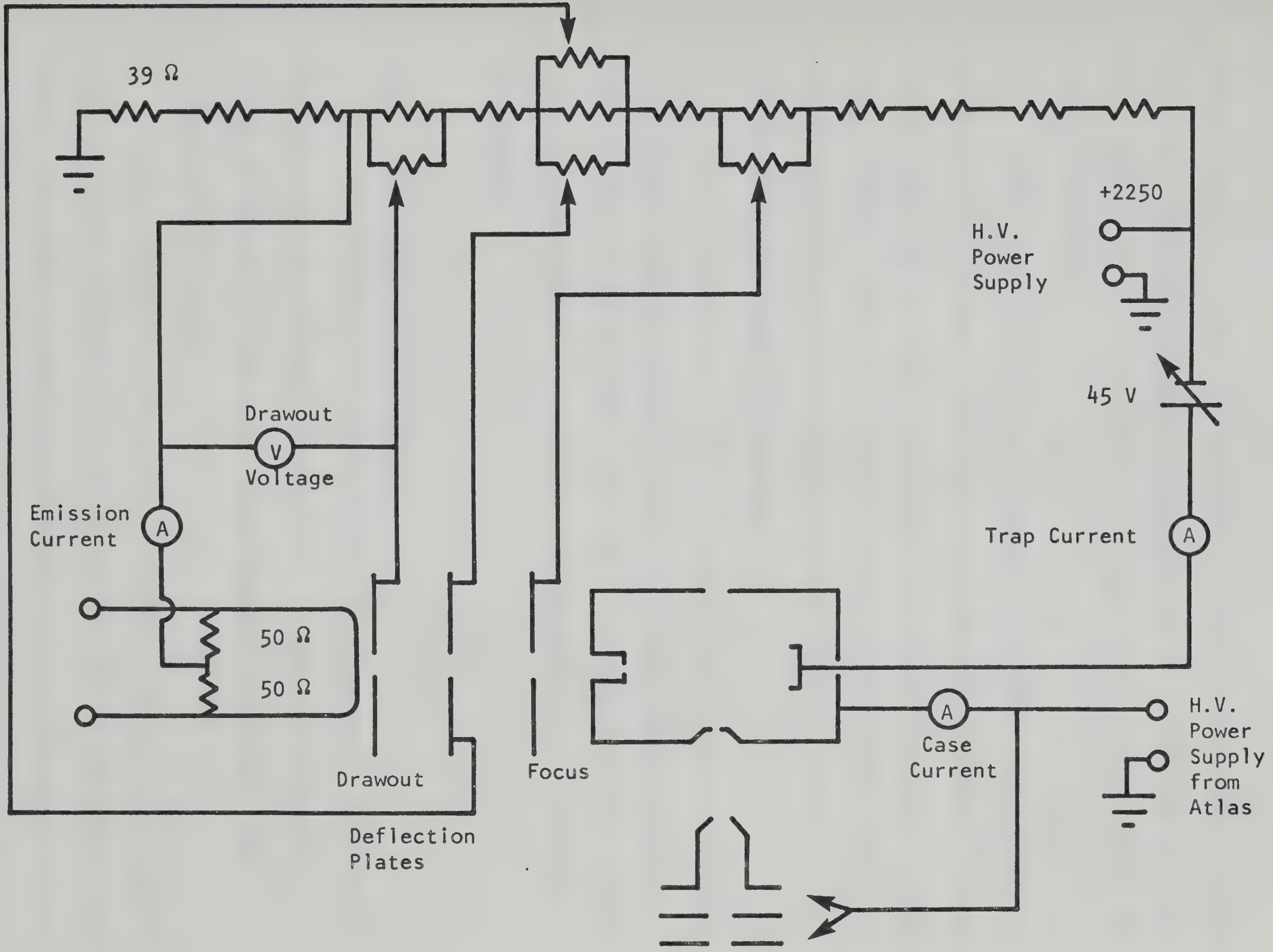
39 Ω
+2250
H.V.
Power
Supply
45 V
Drawout
V
Voltage
Emission
Current
A
Trap Current
A
50 Ω
50 Ω
Drawout
Focus
Deflection
Plates
A
Case
Current
H.V.
Power
Supply
from
Atlas

FIGURE 2.4 Circuit Diagram for Electron Gun and Ion Source

approximately -1200 V relative to the ion source. Various monitoring ammeters and voltmeters were installed and typical values of the electrode voltages and current flows are shown in Table I.

The filament of the electron gun was constructed of thoriated iridium. This material was used because it has been found to be very resistant to attack by gases, especially oxygen, which is a great advantage over the more commonly used tungsten filaments which are particularly vulnerable to attack by oxygen.

The voltages of the ion source and ion acceleration electrodes were supplied by the existing high voltage supply on the Atlas CH4. The ions leaving the ion source were accelerated to ground at the entrance to the mass analyzer.

2.7 The Pulsing Circuitry

The electron gun was pulsed by applying a suitable voltage to the drawout electrode. Figure 2.5 shows a block diagram of the mass spectrometer including the electronic circuits.

The electron gun pulse generator was battery powered and could be floated to the potential of the drawout plate which was kept at about 90 V negative with respect to the filament so that no electrons could pass into the ion source.

TABLE I

Typical Operating Voltages

Electrode	Voltage
Filament	860
Drawout	870
Deflection Plates	1150
Focus	1250
Ion Source	2240
Mass Analyzer Tube	0

Typical Meter Readings under Continuous Irradiation

Drawout Voltage	10V
Emission Current	1.2 ma
Case Current	13 μa
Trap Current	0.3 μa

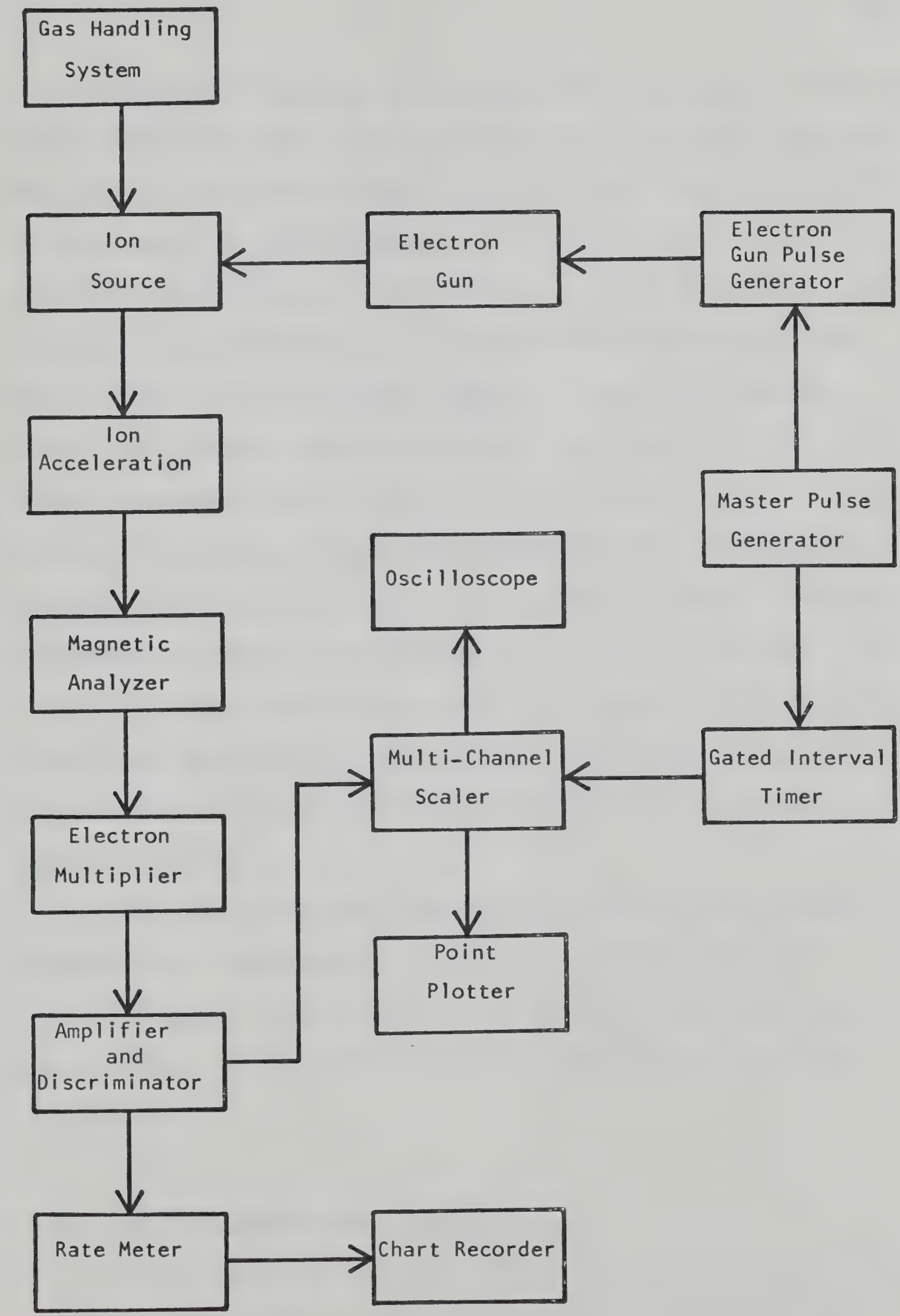
Gas Handling System
Ion Source
Electron Gun
Electron Gun Pulse Generator
Ion Acceleration
Master Pulse Generator
Oscilloscope
Magnetic Analyzer
Multi-Channel Scaler
Gated Interval Timer
Electron Multiplier
Point Plotter
Amplifier and Discriminator
Rate Meter
Chart Recorder

FIGURE 2.5 Schematic Diagram of Experimental Apparatus

When the floating pulse generator received a positive pulse from the master pulse generator, it raised the potential on the drawout plate until it was 10 volts positive with respect to the filament for a period which could be varied from 6-140 μs on the floating pulse generator. This allowed electrons to travel from the filament into the focussing and accelerating region of the electron gun. After the preset time had elapsed the floating pulse generator returned the potential of the drawout plate to its original voltage so that electrons could no longer pass through the drawout plate. This method allowed pulses of electrons of known duration to enter the ion source. The intensity and width of the pulse delivered to the drawout plate was governed by the floating pulse generator whereas the frequency of pulsing was determined by the master pulse generator.

When the electron beam was not pulsed the current measured at the electron trap in the ion source was 3×10^{-7} amps. From this it can be calculated that in a 10 μs pulse, approximately 2×10^{7} electrons enter the ion source.

2.8 The Ion Detection System

After mass analysis the ions were detected with an ion counting system. The input end of the system was a 16-stage copper-beryllium secondary electron multiplier.

The voltage across the multiplier could be varied from 1.6 to 2.5 KV. The pulses from the multiplier were fed into an SSR Instruments Limited amplifier-photon counter which also contained a discriminator. The level of the discriminator threshold could be varied so that low level noise could be rejected. The amplifier-discriminator was specially designed to eliminate the undesirable characteristics of photomultipliers. The amplifier-discriminator could resolve individual electron pulses separated by as little as 10 nanoseconds with sufficient sensitivity to detect individual secondary electron pulses equivalent to less than 10^6 electronic charges.

The condition of a secondary electron multiplier can be tested by measuring the signal intensity at various discriminator levels. Figure 2.6 shows the effect of the signal as a function of the gate level. When the gate level is low the signal is enormous and contains essentially all noise. As the gate level is increased a plateau is reached where only the signal is allowed through. At high gate levels the signal falls off entirely. It can be seen that as the voltage across the electron multiplier is increased the plateau becomes flatter. As the electron multiplier becomes older the plateau disappears even at the highest voltage across the dynodes, and the signal decreases almost linearly with increase in gate level. By operating well up on the plateau, fluctuations in secondary

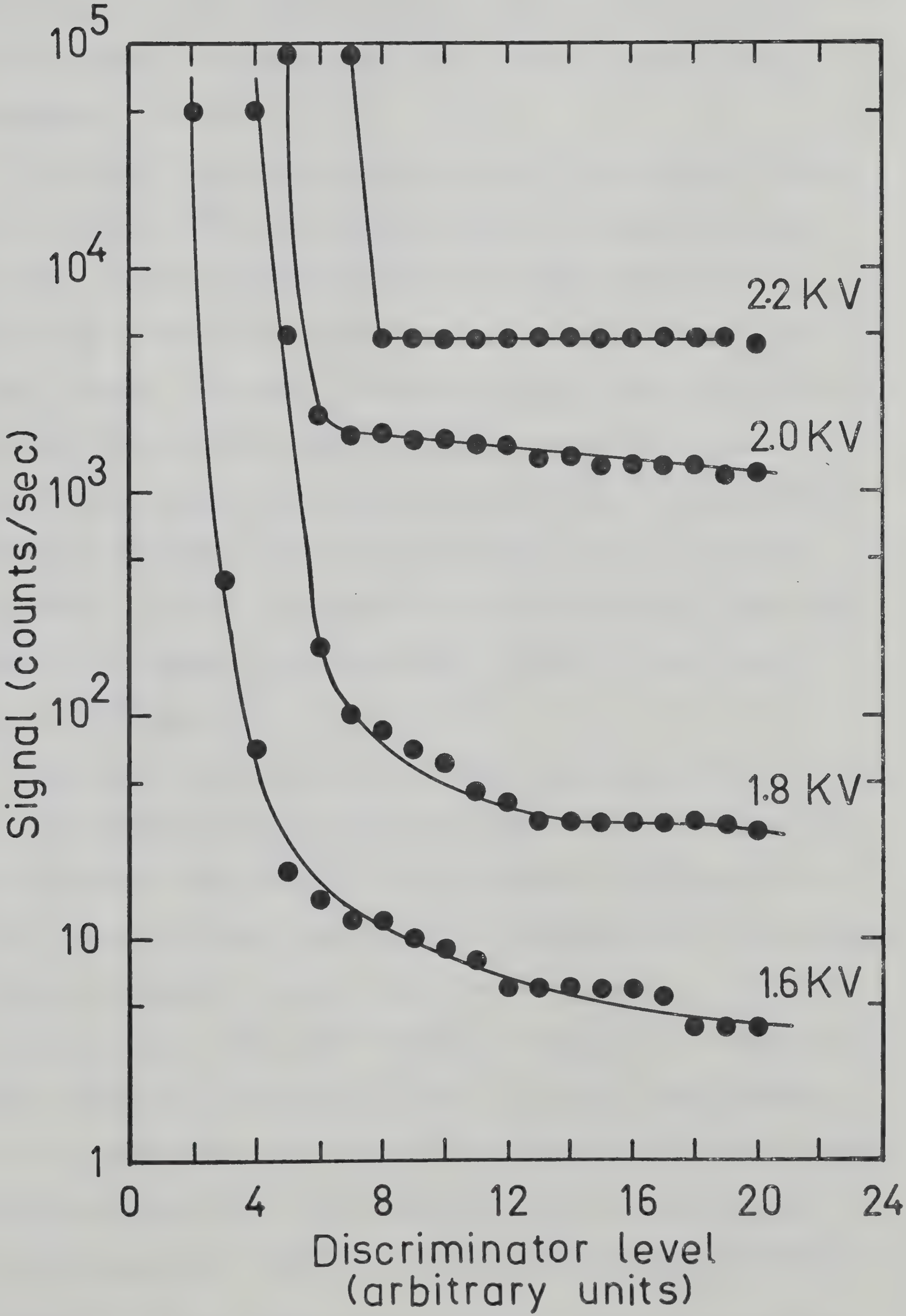

FIGURE 2.6. Signal Observed as a Function of Discriminator gate Level at Various Acceleration Voltages Across the Dynodes of the Electron Multiplier.

emission characteristics of the electron multiplier, fluctuations in the high voltage of detection threshold can be reduced to negligible levels and provide stable measurements.

The amplifier/discriminator could be used for counting rates up to 10^7 per second without corrections for dead time. This resolution was more than adequate for this system since the maximum count rate was never above 10^5 per second. The main disadvantage of the amplifier's wide bandwidth was its sensitivity to external noise. A low background count was only achieved when the amplifier was mounted directly next to the anode of the electron multiplier. In this position a background noise level of 10 counts per second was obtained. Signal rates were typically 10^4/second.

The amplified pulses were counted either with a rate meter and displayed on a chart recorder or a multichannel scaler (Nuclear Data 2200). The temporal fluctuation of an ion's intensity was observed by synchronizing the sweep of the multichannel scaler with the triggering pulse of the electron gun. The dwell time per channel in the multichannel scaler was selected to be 10 μs for 256 channels. Thus ions which were detected in the first 10 μs after the beginning of the pulse were stored in the first channel of the multichannel scaler. The ions which were detected

from 10 µs to 20 µs after the pulse were stored in the second channel and so on for 256 channels or 2560 µs. After 3 ms the signal had decayed by a factor of 10^4 and the electron gun could be pulsed again. The number of ions detected in each channel were added to the ones collected previously. Normally ion intensities were collected for a period of 30 to 60 seconds, selected by a gated interval timer.

2.9 Description of the Second Mass Spectrometer

The second machine could be used to study positive or negative ions and is shown in Figure 2.7. This mass spectrometer was not a commercial instrument and the major difference from the previously described Atlas CH4 was that the electron gun was mounted on a separate flange. The filament was about 25 cm from the electron entrance slit. For operation with negative ions, the ion source was maintained at -2KV and the filament at -4KV. This machine also used a 15 cm radius 60° magnet for mass analysis.

The electron beam was pulsed in a similar manner to that described in Section (2.6) by applying a gating pulse to the drawout electrode [2]. The potential divider supplying voltages to the electrodes in the electron gun included a switch to convert to monitoring positive ions.

FIGURE 2.7

Schematic Diagram of Second Apparatus Used

1.	Filament
2.	Draw out
3.	Extractor
4,5,6	Einzel lens
7,8	Deflection plates
9.	Shielding cylinders
10.	Heating Mantle
11.	Electrostatic shield
12.	Electron entrance slit
13.	Electron trap
14.	Ion exit slit cone
15.	Gas inlet
16.	Kovar seal flange
17.	Stainless steel support
18.	Ceramic spacer
19.	Cone
20.	Ion acceleration assembly support
21-26	Electrodes for focussing and ion beam into mass analyzer tube
27.	Mass analyzer tube

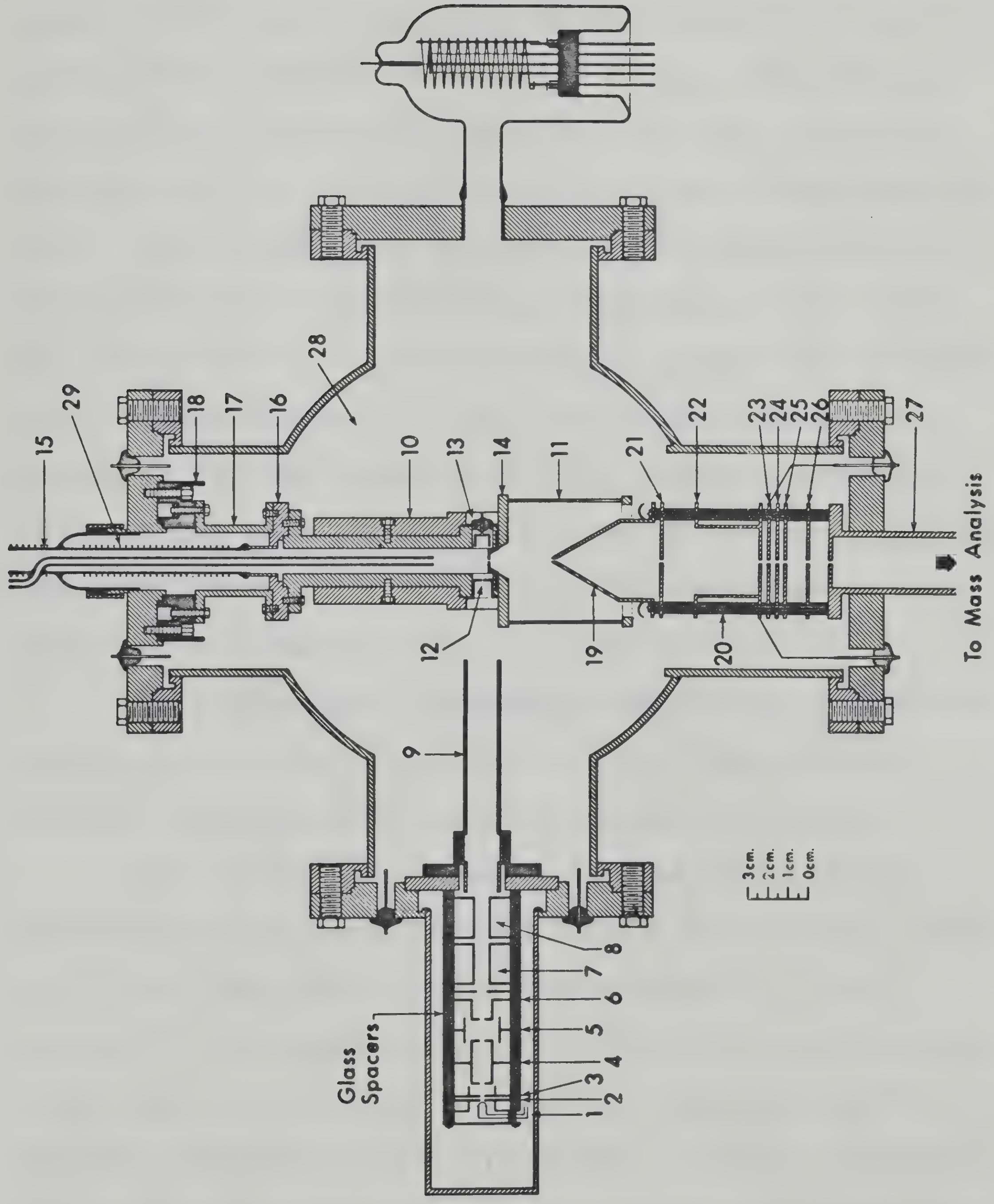
Glass Spacers
To Mass Analysis
3cm.
2cm.
1cm.
0cm.

The electron beam could be focussed and directed towards the electron entrance slit by means of a plexiglass window installed in a blank flange. The electron beam was made visible by mounting a shield in front of the electron entrance cone with a suitably sized hole to admit the electron beam and painting the outer surface of the shield with a phosphorescent substance. The shield was coated with a mixture of phosphor (type P-31 Sylvania) and sodium silicate solution. The shield extended the length of the ion source to prevent spurious ionization. The electron beam could be deflected on to the phosphored area, focussed to a spot and then directed through the hole into the electron entrance cone.

The electron gun and magnet were encased in magnetic shielding to minimize the deflection of the electron beam by the magnetic field of the analyzing magnet.

After mass analysis the ions were detected by a Spiraltron Electron Multiplier (Bendix Corporation). The spiraltron was operated such that a gain of 10^6 was achieved. For negative ions the voltage across the multiplier was varied between 3 to 4 kV. The output pulses from the multiplier were very narrow (~3 ns by manufacturer's specifications) and of very uniform size compared to the variable size of the output pulses from a conventional dynode structure. This uniformity has been attributed to space charge of the pulse of electrons as it moves through

the channels of the multiplier (99).

The efficiency of detection for the spiraltron is approximately unity for negative ions with more than 500 eV energy on impact (100) and about 90% for positive ions (101). The high efficiency for negative ions has been explained as due to the ease of removal of the loosely held electron of the negative ion compared to the more strongly bound electron of the positive ion (100).

The output pulses from the multiplier were then passed through a discriminator to eliminate low level noise. The discriminator curves were similar to those shown in Figure (2.6). The background count was much lower, about 3 counts/sec, than that observed with the dynode electron multiplier described earlier. The lower background count of the former is probably due to the more uniform output pulses of the spiraltron which gives rise to horizontal plateaus in the discriminator curves which are only observed at high acceleration energies with the dynode multiplier.

The pulse amplifier unit consisted of a preamplifier, amplifier and discriminator. The amplification unit delivered a 0.25 µs pulse for each input pulse. The response time of this amplifier was not as fast as the one previously used and it was found that at counting rates larger than 10^5 counts/second, the signal saturated the amplifier. This condition was easily detected as the ion

profile collected in the multichannel scaler would be flat-topped at the maximum of the curve. Normally the signal was adjusted such that the most intense ion count rate was no more than 5 x 10^4 counts/second.

The gas handling system was of the same design as that described in section (2.5) except for one extra feature. This instrument had been used for investigations of systems using condensible organic compounds. Therefore to protect the oil diffusion pump an extra valve was installed which led to a mechanical pump. Once the exeriment was finished the contents of the 5 litre bulb could be pumped from one atmosphere to about one torr with the roughing pump through a trap, then pumped with the oil diffusion pump. This arrangement kept the gas handling system clean and the oil in the diffusion pump needed to be changed less frequently.

2.10 Time of Flight

The time required for the ions to travel from the ion source to the detector is finite and should be calculated for each ion. The time of flight could be estimated by assuming that the gradient of the electric field from one electrode to another in the ion accelerating tower was uniform. The gradient was assumed to be the potential difference between the electrodes divided by the interelectrode distance. Using the geometry and

potential of the electrodes the time of flight may be calculated from the following expression.

$$x_{ij} = v_i t_{ij} + \frac{eE_{ij}t_{ij}^2}{2m} \qquad (2.2)$$

where x_{ij} is the spacing between the i^{th} and j^{th} electrode, v_i is the velocity of the particle at the i^{th} electrode, E_{ij} is the potential difference between electrodes i and j, m is the mass of the particle, e the electronic charge and t_{ij} the time of flight from electrode i to j. Since

$$v_i = v_{i-1} - \frac{eE_{ij}t_{ij}}{m} \qquad (2.3)$$

the quadratic equation (2.2) can be solved to give t_{ij}. The total time of flight, t_f, is therefore the sum of the individual t_{ij} for n electrodes.

$$t_f = \sum_{j=1}^{n} t_{ij}$$

For machines of this geometry in our laboratory it has been found that t_f is normally of the order of 5 to 10 µs (94). Since the time of flight is comparable in magnitude to the minimum time resolution of the multichannel scaler, the correction for t_f was not used in this investigation.

2.11 Physical Conditions in the Ion Source

A. Number of Collisions in the Ion Source

The conditions inside and the dimensions of the ion source must be chosen carefully to ensure that the signal received at the detector is an accurate representation of the ion population in the ion source. Simple kinetic theory can be applied to verify this assumption.

In studying ion-molecule reactions it is necessary to ensure that the ions have no excess energy when they emerge from the ion source. If no repeller voltage is applied then the source is field free but the ions may have obtained excess energy by chemical means. In reaction (2.6) an ion A collides with a neutral B and forms a cluster $[AB^+]^*$ with excess energy due to the

$$A^+ + B \underset{k_d}{\overset{k_c}{\rightleftharpoons}} [AB^+]^* \xrightarrow[M]{k_s} AB^+ \qquad (2.6)$$

bond formed. Depending on the lifetime of the excited species, it may decompose back to the original products before it collides with a third body, M, which removes the excess energy. In fact many collisions may be necessary for $[AB^+]^*$ to return to its ground state.

The number of collisions per molecule per second, Z, in a gas is given by

$$Z = \sqrt{2}N\bar{v}\pi\sigma^2 \qquad (2.7)$$

where N is the gas number density, σ is the diameter of the molecule (102, p.40) and $\bar{v}$ is the average velocity calculated from equation (2.8). $\pi\sigma^2$ is therefore the collision cross section.

$$\bar{v} = \left(\frac{8kT}{\pi m}\right)^{\frac{1}{2}} \tag{2.8}$$

For methane, σ is 4.1×10^{-8} cm. At a pressure of 1 torr of methane at 300°K a molecule will undergo 2300 collisions in a millisecond.

A charged particle will suffer more collisions since its collision cross section is larger than that of a neutral molecule. The collision cross section of an ion and a molecule is given by the Giomousis-Stevenson expression (16). Equation (1.6) predicts that collision cross sections for ions at room temperature are of the order of 100 Å^2. Using this value in equation (2.7) indicates that an ion will undergo about 10^5 collisions per millisecond at 1 torr pressure at 300°K. It may be assumed that after so many collisions the ion should be in the ground state. The half life for the disappearance of positive ions is about 300 μsec which represents the lifetime of an ion before it undergoes another reaction. During this time an ion will undergo about 3×10^4 collisions, therefore an ion undergoing a sequence of ion-molecule reactions will reach the ground state before it reacts further.

B. Ion Sampling

The size of the ion exit slit has an important effect upon the flow conditions. Previous experiments in this laboratory (103-105) have shown that the combination of high pressures (20 torr) and large orifices (0.1 mm) tends to make the flow through the orifice non-molecular. The consequence is that the ion population changes as it emerges from the ion source due to cooling effects and collisions in the expanding jet of gas. The cooling of the gas causes large clustered ions to grow in size while collision of the ions causes larger clusters to dissociate to smaller ones. It was found that molecular flow was most suitable to eradicate both of these problems (105).

Molecular flow occurs when the dimensions of the orifice are smaller than the average distance that a molecule travels between collisions, that is, the mean free path. The mean free path, λ is given by

$$\lambda = \frac{1}{\sqrt{2}\ N\pi\sigma^2} \qquad (2.9)$$

where N is the gas number density and σ is the diameter of the molecule (102, p.40). The mean free path of methane at 3 torr and 300°K is .014 mm. Therefore the flow through a 1.6 x .017 mm slit should be near molecular. Molecular flow through an orifice is proportional to $\sqrt{T/M}$ where T is the temperature and M is the molecular

weight of the compound. The flow to the ion source from the reservoir is viscous since the diameter of the tubing is large compared to the mean free path of the gas molecules. For viscous flow all of the components of the gas travel at the same velocity. However, the different components of the gas leave the ion source by molecular flow i.e. the lighter gases escape faster. Therefore the ion source will become enriched in the heavier components. To avoid this mass discrimination a flow system, described in section 2.5, is employed which continually refreshes the gas in the ion source and prevents any build-up of the heavier components. Normally the size of the capillary in the flow system is chosen so that the flow through the capillary is 3 to 4 times that leaking through the slits. This can be tested by monitoring the pressure drop with time when the gas handling system is filled with gas at 5 torr and opening the valve to the ion source. Figure 2.8 shows the relative rates of pressure decrease through the normal flow system and through the slits only. The relative rates of decrease with and without the capillary at 3 torr are 3:1 and this ratio is sufficiently large to assume that there is no accumulation of the heavier reactants in the ion source.

The flow behaviour can be analyzed by assuming steady state conditions in the ion source and that the

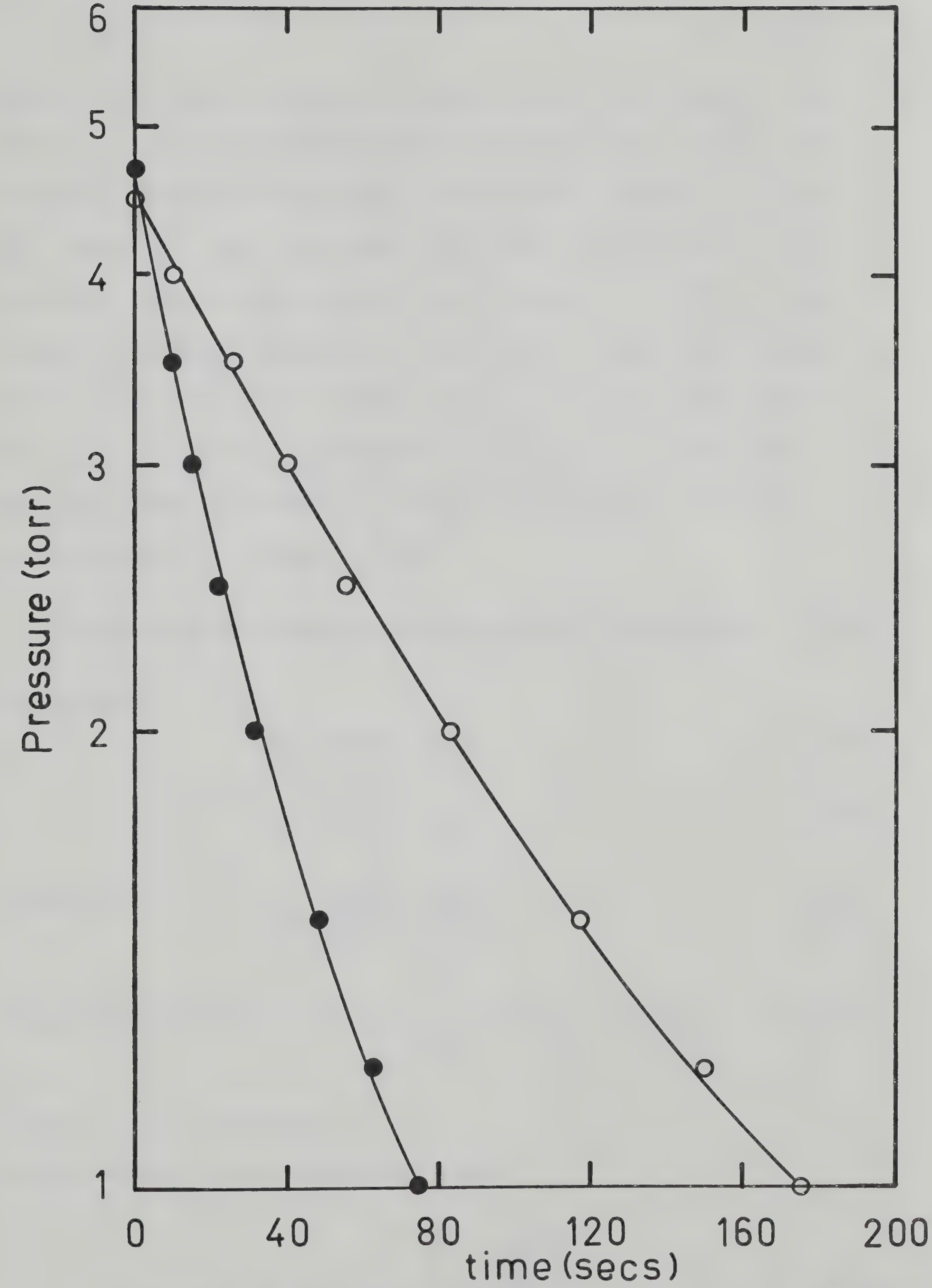

FIGURE 2.8. Pressure Drop in the Ion Source, ● with Capillary, ○ without Capillary.

only orifices are the inlet and outlet flow tubes and the exit slit as represented in Figure 2.9. If the gas mixture contains two gases of molecular weights M_1 and M_2, where $M_1 < M_2$, and the stationary concentrations in the ion source are a and b for components 1 and 2, the rate of flow of compound 1 into the ion source is equal to k_1 and that of compound 2 is k_2. The outflow rate by viscous flow of compound a is equal to ca and the outflow rate by molecular flow of compound a is d_1a and compound b is d_2b. Since

$$\text{Flow into ion source} = \text{Flow out of ion source} \tag{2.10}$$

Therefore

$$k_1 = a(c + d_1) \tag{2.11}$$

$$k_2 = b(c + d_2) \tag{2.12}$$

Therefore

$$\frac{a}{b} = \frac{k_1}{k_2}\frac{(c + d_2)}{(c + d_1)} \tag{2.13}$$

From Graham's Law: $d_1 = f.\dfrac{1}{\sqrt{M_1}}$ and $d_2 = f.\dfrac{1}{\sqrt{M_2}}$ (2.14)

where f is a constant.

Substituting into equation (2.13)

$$\frac{a}{b} = \frac{k_1}{k_2}\,\frac{\left(c + \dfrac{f}{\sqrt{M_2}}\right)}{\left(c + \dfrac{f}{\sqrt{M_1}}\right)} \tag{2.15}$$

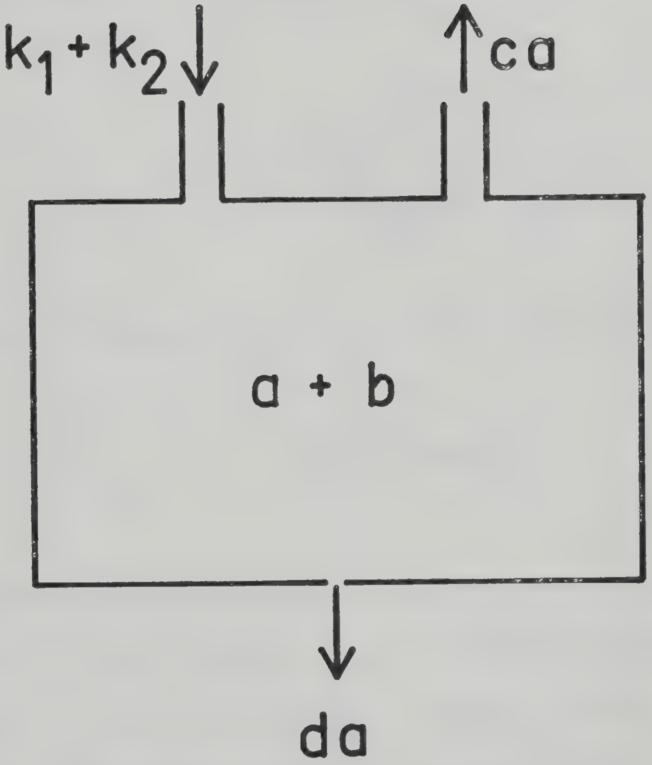

FIGURE 2.9. Schematic Diagram of Gas Flow through the Ion Source Showing Viscous Flow through Inlet and Outlet Tubes and Molecular Flow through a Narrow Slit.

If it is assumed that the viscous flow is x times larger than the molecular flow through the slit then

$$c = x \times \frac{f}{\sqrt{M_1}} \tag{2.16}$$

Substitution of equation (2.16) into equation (2.15) gives

$$\frac{a}{b} = \frac{k_1}{k_2}\left(\frac{\frac{x}{\sqrt{M_1}} + \frac{1}{\sqrt{M_2}}}{\frac{x}{\sqrt{M_1}} + \frac{1}{\sqrt{M_1}}}\right) \tag{2.17}$$

For a system where $M_1 = 16$, $M_2 = 64$ and $x = 3$

$$\frac{a}{b} = 0.88\,\frac{k_1}{k_2} \tag{2.18}$$

Therefore the ratio of gases in the bulb is different to that in the ion source. To test whether this could be detected a mixture of CH_4, t-BuOH and CCl_4 was flowed through the apparatus and the equilibrium constant, $K_{0,1}$ was measured for reaction (2.19).

$$Cl^- + (CH_3)_3COH \underset{}{\overset{K_{0,1}}{\rightleftharpoons}} (CH_3)_3COH.Cl^- \tag{2.19}$$

The capillary was then closed and the mixture was allowed to flow for 7 hours to see if there was any detectable difference in the equilibrium constant. The broken line in Figure 2.10 represents the average value of 9 experiments under normal flow conditions and the points show the

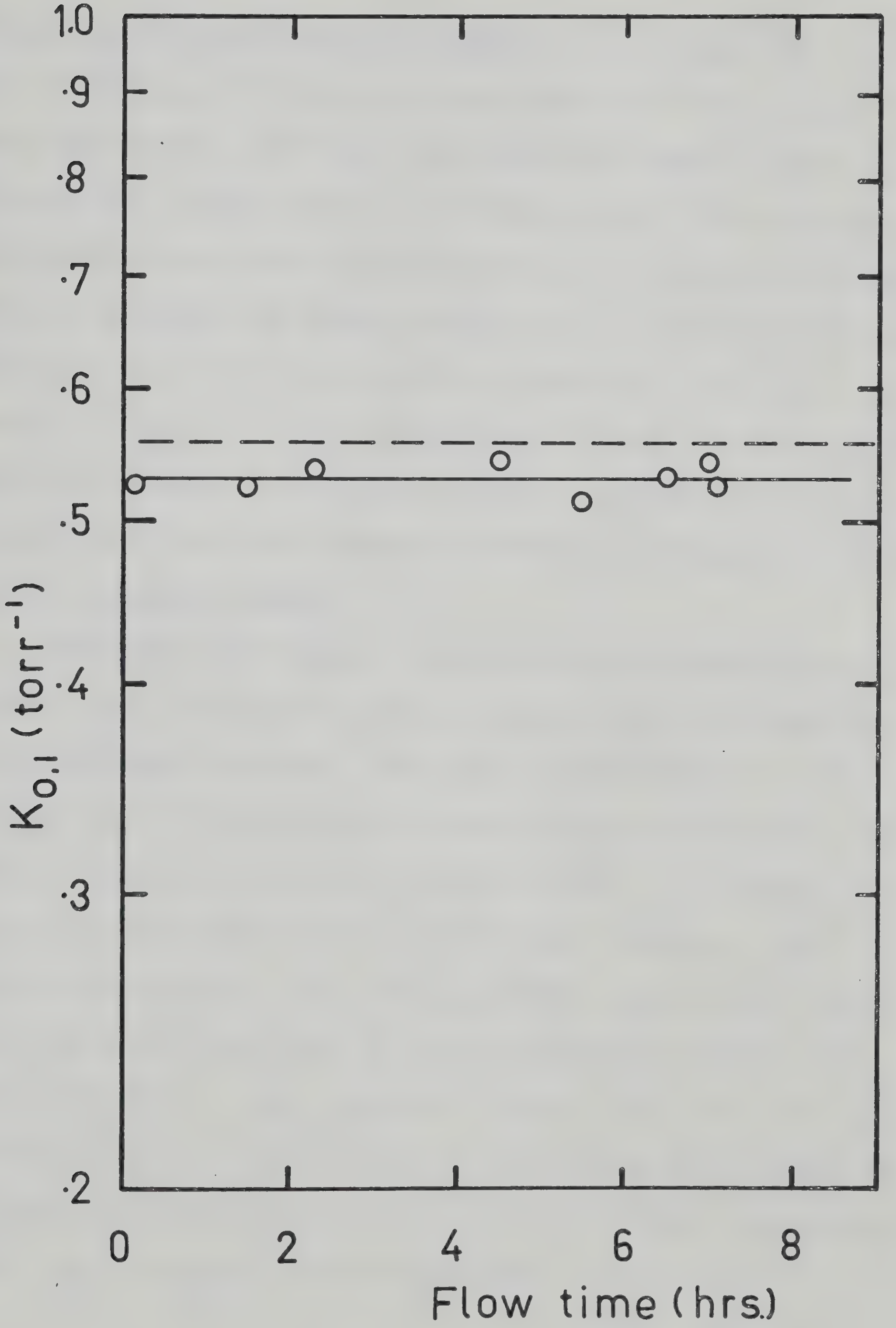

FIGURE 2.10. Measured Equilibrium Constant for the reaction $Cl^- + (CH_3)_3COH \rightleftharpoons (CH_3)_3COH.Cl^-$ at 215°C with Flow Capillary Closed. Broken Line is Average K with Normal Flow

measurements where the gas flowed only through the slits. The average equilibrium constant measured with normal flow was 0.557 $torr^{-1}$ and that measured under static conditions was 0.531 $torr^{-1}$, a difference of less than 5%. The equilibrium constant measured under static conditions did not undergo any steady change which would have occurred if there had been a gradual enrichment of t-butanol, the heavier compound. At a pressure of 3 torr the flow through the slits alone is 10 cc/min which is probably fast enough to flush out the ion source so that no enrichment of the heavier compound occurs.

The region of highest pressure outside the ion source is the space directly outside the ion exit slit due to escaping gases spraying into the vacuum chamber. The probability of a collision between anion and neutral molecule is therefore highest in this region. If methane is the major gas passing through the ion source at 300°K and the pressure in the vacuum chamber is 2×10^{-4} torr, then the mean free path of an ion is about 135 cm from equation (2.9). The distance from the ion exit slit to the detector is less than 1 m. Therefore under these conditions no collisions should occur while the ion travels from the ion source to the detector.

C. Charged Particle Recombination

The concentration of positive ions in the ion source may decrease by two pathways: diffusion to the walls and charged particle recombination. Charged particle recombination for positive ions is mainly due to ion-electron recombination. The half life for recombination is given by

$$\tau \approx (\alpha n_e)^{-1} \tag{2.20}$$

where α is the ion-electron recombination coefficient, n_e is the density of electrons. Values of α are quite well documented but n_e is more difficult to estimate.

The number of primary ions generated from one electron is given by

$$\frac{I_p}{I_e} = Qnl \tag{2.21}$$

Q is the ionization cross section and l is the electron path length. The distance from the electron entrance slit to the electron trap is about 1 cm. At a pressure of 3 torr at 300°K, $n = 1 \times 10^{17}$ molecules/cc. The ionization cross section CH_4 for 1400 eV electrons may be taken as 2.8×10^{-17} cm^2 (106). Therefore from equation (2.21) each electron in the primary beam generates about 3 ions, providing the electron energy remains constant. If it is assumed that

about 100 eV are lost per collision (107) the final electron energy will be 1100 eV where the ionization cross section is slightly larger. For each ion produced a secondary electron will also be created which will have an energy of about 70 eV. The secondary electrons will give rise to 2 more ions before they reach low energies (107). Therefore each primary electron which enters the ion source produces approximately 10 ions at a pressure of 3 torr. During a 10 μs electron pulse about 2×10^7 (section 2.7) electrons enter the ion source and give rise to 2×10^8 ions.

Although the total volume of the ion source is about 2 cc, the ions are only formed along the path of the primary electron beam. The electron entrance slit is 2 x .008 mm and the distance from the entrance slit to the trap is 1 cm but as the beam enters the source it will be spread by collisions. The volume in which the ions are generated can be estimated as $1 \times 0.2 \times 0.1$ cm^3 = 2×10^{-2} cm^3, which yields an initial density of about 10^{10} ions per cm^3. Since the volume in which ions are generated expands rapidly as secondary electrons are formed, this estimate of ion density is a maximum value. From equation (2.20) the half life for ion-electron recombination is 50 msec. The half life for the disappearance of the total positive ion signal shown in

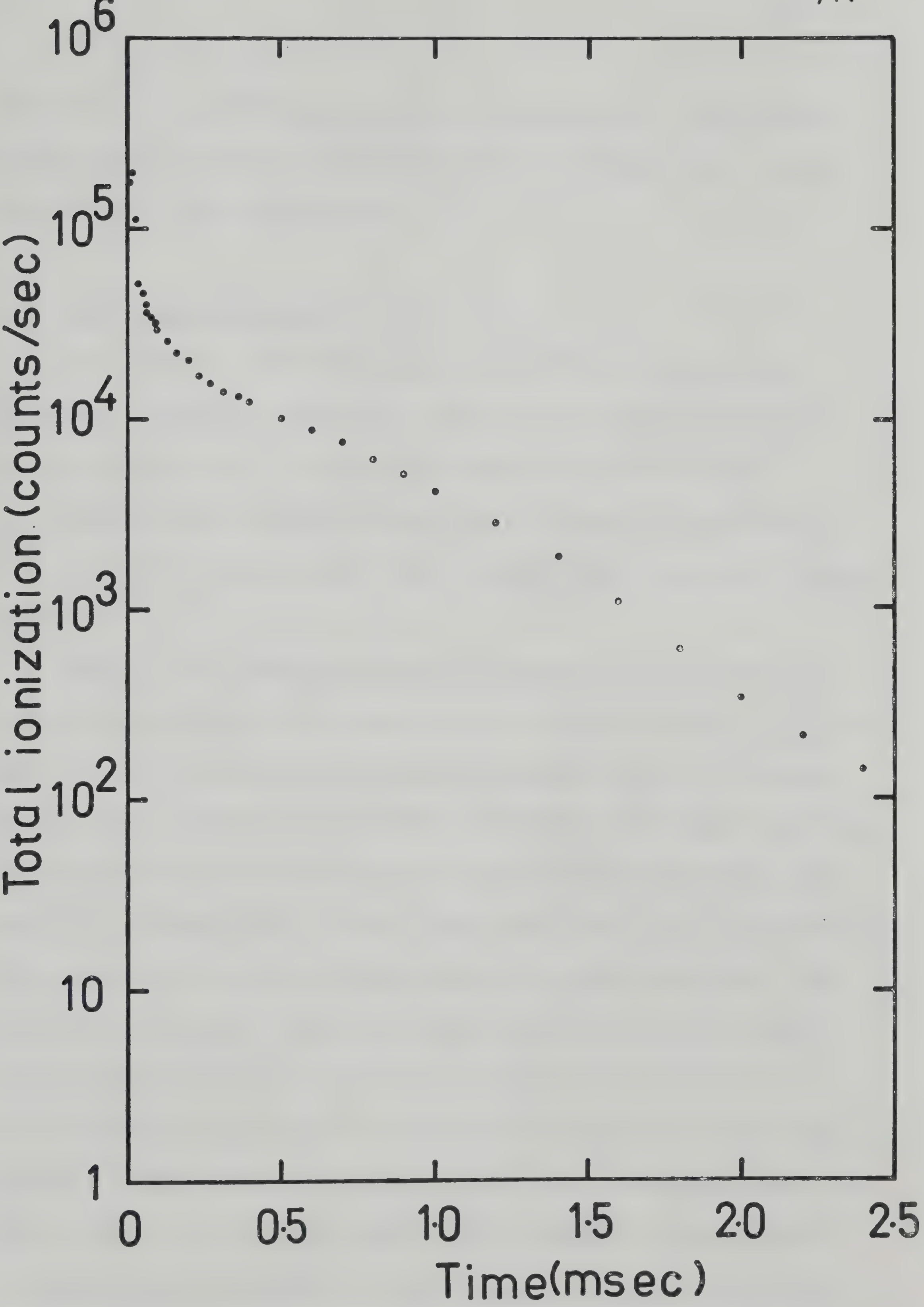

FIGURE 2.11. Time Dependence of Total Positive Ion Signal in 2.5 torr Methane and 0.5 mtorr Ethane at 104°C.

Figure 2.11 is about 0.1 msec. Therefore in the present experiments ion-electron recombination should not cause significant loss of signal.

D. Diffusion of Ions

The previous section discussed positive ion loss through recombination with an electron and was found to be unimportant. Above ion densities of $10^7/cm^3$ the interaction between charged particles during diffusion should be considered (102, p.512) due to space charge effects.

Figure 2.11 shows the total positive ion intensity with time for a mixture containing a ratio of $CH_4:C_2H_6$ of 5000:1. The pressure in the ion source was 2.5 torr at 104°C. The diagram shows that initially the total positive ion signal decays very rapidly and then at about 250 μsec there is a break after which the positive ions decay much more slowly. Previous experiments on other machines (94) have shown that if the instrument is then switched over to monitor negative ions, the negative ion signal is initially zero and then at the break in the curve of the positive ion signal, it rises rapidly to a maximum and then decays at the same rate as the positive ion signal. If substances are added to the flowing mixture that have a large capture cross section for thermal electrons then the break occurs earlier in the decay of the ions. Thus

when studying negative ions, compounds which are efficient electron capture agents are usually added to the gas flow to enhance the negative ion signal at short reaction times.

The transition point in the curve may be explained qualitatively in the following way. As the high energy electron beam traverses the ion source it initially creates mainly positive ions and the corresponding secondary electrons. These electrons cause further ionization until degraded to thermal energies by inelastic collisions. The electron capture cross section is very low for high energy electrons (102, p.382) and thus very few negative ions are formed initially.

Since the mobility of the electrons in the plasma is much larger than that of the ions (108) they start to move rapidly towards the walls of the ion source. However, the motion of the electrons is restrained by positive ions which are left behind and a space charge field is created. This field also has the effect of speeding up the positive ions and they diffuse at a faster rate than if the electrons were absent. Thus the positive ions and electrons diffuse at the same rate under the influence of their mutual electric fields. When charged particles diffuse through a gas at a rate controlled by the electrical forces between them, the diffusion is called ambipolar (109). Below ion densities of $10^7/cm^3$ the charged particles are far enough

away from each other that their mutual electrical forces are negligible compared to their thermal energies.

The ambipolar diffusion coefficient D_a is given by the relationship

$$D_a = \frac{D^+K^- + D^-K^+}{K^+ + K^-} \qquad (2.22)$$

where D^+ and D^- are the diffusion coefficients of the positive ions and electrons respectively, and K^+ and K^- are the mobilities of the respective species (102, p.513). Assuming that $K^- >> K^+$ and that $T^+ = T^- = T_{gas}$ it is found that

$$D_a \approx 2D^+ \qquad (2.23)$$

The slope of the two dashed lines in Figure 2.11 differ by a factor of two. The initial points on the curve are high because electrons are still entering the ion source.

The abundance of positive ions reaching the exit slit will be high during the period of positive ion-electron diffusion while that of the negative ions will be low, since they are trapped by the electric field. After a time a number of the positive ions and electrons will be discharged at the walls until the number density of the ions and electrons is insufficient to maintain the space charge field. The collapse of the field is shown by a break in the curve in Figure 2.11 where negative ions suddenly appear and decay at the same rate as the positive

ions. After the transition point therefore, the diffusion rate is probably determined by positive ion-negative ion ambipolar diffusion.

2.12 Normalization of the Data

Figure 2.11 shows that the total ion intensity changes with time. If rate constants were calculated using raw data, the values obtained would be inaccurate since ions are disappearing by diffusion to the walls as well as by reactions with other molecules. To eliminate the diffusion factor the ions are "normalized" by calculating the ion intensity at a time t as a fraction of the total ion intensity at that time. Therefore normalized ion intensities represent a system where the total number of ions remain constant.

For this method to yield meaningful results, the temporal profile of all observable ions must be measured. Also, the period between 2 successive electron pulses must be sufficiently long that the total ion intensity has decayed to a negligible amount so that any ions left from the previous pulse will not interfere. In Figure 2.11 the pulse of electrons entered the ion source every 3 ms and the total ion signal had decayed by a factor of almost 10^5, thus the number of ions left in the ion source at the start of the next electron pulse is minimal.

The normalization procedure assumes that all loss

mechanisms, other than ion-molecule reactions, affect all ions equally. Ion-electron recombination was shown to be a negligible loss mechanism in the previous section. Normalization assumes therefore that all ions diffuse to the slit at the same rate, i.e. their diffusion coefficients are the same. However, diffusion coefficients are inversely proportional to the square root of the reduced mass (102, p.435).

$$D \propto \left(\frac{1}{\mu}\right)^{\frac{1}{2}} \qquad (2.24)$$

where μ is the reduced mass of the colliding ion and molecule.

Consider two ions m_1 and m_2 of m/e 30 and 60 in methane. The reduced masses of the two ions colliding with a methane molecule are $\mu_1 = 10.4$ and $\mu_2 = 12.6$. Substituting into equation (2.24) gives the ratio of the diffusion coefficients of the two ions.

$$\frac{D_1}{D_2} = \left(\frac{\mu_2}{\mu_1}\right)^{\frac{1}{2}} \qquad (2.25)$$

Therefore $D_1/D_2 = 1.10$ and the diffusion coefficients differ by 10%. Since the mass range of ions detected in the kinetic study was of the same order as in the example given above, the diffusion coefficients of the various ions will not differ greatly. In most kinetic studies the rate of disappearance of an ion by reaction with a molecule is

much larger than by diffusion. Therefore it is expected that the normalization of the ions will not introduce serious error into the results of the experiment.

CHAPTER 3

ASSESSMENT OF SYSTEM OPERATION

3.1 Auxiliary Filament Test

Since the Atlas CH4 had been modified considerably and equipped with a new ion source the system was tested by studying reactions where the rate constants or equilibrium constants were well established.

After the high pressure ion source was installed, the low pressure auxiliary filament, placed just outside the ion source, was tested. At this time the original gas handling system and signal amplifier on the Atlas CH4 were still being used. Methane at pressure of the order of 10 mtorr were flowed through the ion source, the pressure was measured with a microcapacitance torrmeter in the flow system. Table II shows the ion distribution observed in 10 mtorr of methane using the 70 eV auxiliary filament, together with the accepted values. The auxiliary filament was not intended to be used as an accurate measure of electron impact spectra but rather as a check on the purity of the reactant gases. Therefore the agreement shown in Table II between the observed intensities and those in the literature is quite adequate for the intended purpose of the auxiliary filament.

TABLE II

Ions Observed When Methane Is Bombarded by 70 eV Electrons

m/e	Ion	Intensity as a % of largest peak This Work	ASTM[a]
12	C^+	0.2	1
13	CH^+	1.0	3
14	CH_2^+	5.0	7
15	CH_3^+	71.0	76
16	CH_4^+	100.0	100
17	CH_5^+	0.7	1

---

a. Reference 110.

3.2 Electron Gun Test

Before the pulsing circuits were installed only the intensities of ions under continuous irradiation could be observed. Probably the most documented system is that of ion-molecule reactions in methane. Successive workers have tended to work at increasingly higher ion source pressures as techniques have improved. This increase in ion source pressure results in the occurrence of more complex reactions.

The primary ions produced by electron impact in pure methane are shown in equation (3.1). The established ion-molecule reactions (5-7, 111-114) occurring after the

$$CH_4 + e \longrightarrow CH_4^+, CH_3^+, CH_2^+, CH^+, C^+, H_2^+, H^+ \quad (3.1)$$

formation of the primary ions are listed in equations (3.2 to 3.9).

$$CH_4^+ + CH_4 \longrightarrow CH_5^+ + CH_3 \quad (3.2)$$

$$CH_3^+ + CH_4 \longrightarrow C_2H_5^+ + H_2 \quad (3.3)$$

$$CH_2^+ + CH_4 \longrightarrow C_2H_4^+ + H_2 \quad (3.4)$$

$$CH_2^+ + CH_4 \longrightarrow C_2H_3^+ + H_2 + H \quad (3.5)$$

$$CH^+ + CH_4 \longrightarrow C_2H_2^+ + H_2 + H \quad (3.6)$$

$$CH_3^+ + 2CH_4 \longrightarrow C_2H_7^+ + CH_4 \quad (3.7)$$

$$CH_3^+ + 2CH_4 \longrightarrow C_3H_7^+ + 2H_2 \quad (3.8)$$

$$C_2H_3^+ + CH_4 \longrightarrow C_3H_5^+ + H_2 \quad (3.9)$$

Field (35,37) calculated the rate constants for the above reactions by studying the ion intensities as functions of pressure. To calculate the rate constants, the residence time of the ion in the ion source is required. However, the estimation of the residence times of the ions is quite complicated because reactant ions are not necessarily produced in the electron beam but can be formed in a diffuse region around it. Therefore the position of formation is not well-defined. Also, at high pressures the ion undergoes a large number of collisions before it passes out of the ion source and the position cannot easily be calculated. The drift velocities of the ion are not well known and their values change as the pressure is varied. The ion source residence time or reaction time changes as a consequence.

Figure 3.1 shows the ion intensities observed at different ion source pressures of methane. Field's results (35,37) are shown by the solid line and the present experimental results by the symbols. The data is rather scattered, but Field's original data, shown in reference (37), also shows considerable variance and the smooth lines are a result of a large number of experiments. The agreement between the low experimental relative intensities of CH_3^+ and CH_4^+ and Field's observations is good. The intensities of both CH_5^+ and $C_2H_5^+$ are generally lower than Field's results but this may be due to

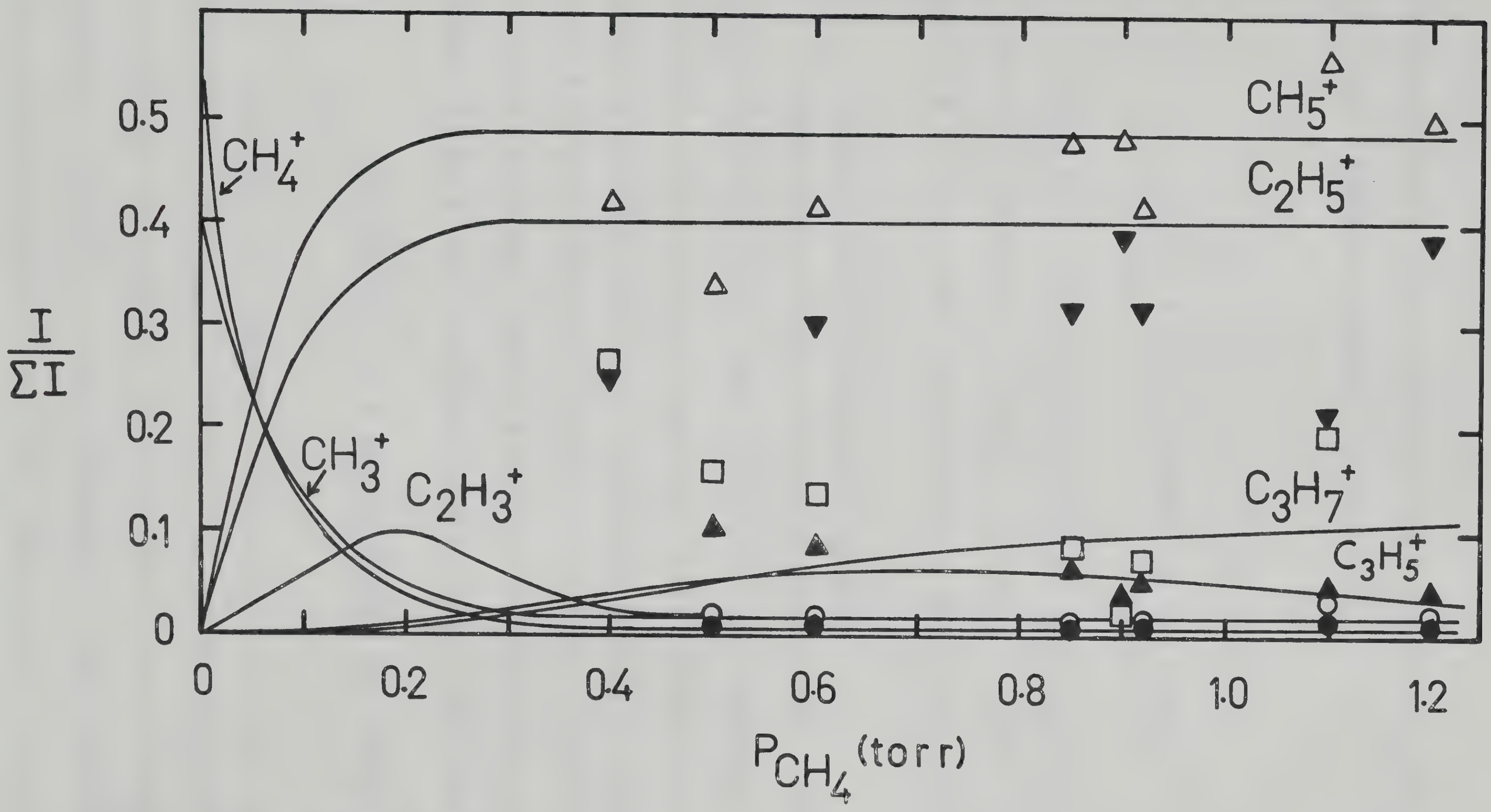

FIGURE 3.1. Normalized Intensity as a Function of Pressure of Methane. Solid lines indicate results obtained by Field (35,37). ○ CH_3^+, ● CH_4^+, △ CH_5^+, ▼ $C_2H_5^+$, □ $C_2H_3^+$, ▲ $C_3H_5^+$, ◆ $C_3H_7^+$.

the presence of water in the system because both CH_5^+ and $C_2H_5^+$ will proton transfer to water.

$$CH_5^+ + H_2O \longrightarrow H_3O^+ + CH_4 \qquad (3.10)$$

$$C_2H_5^+ + H_2O \longrightarrow H_3O^+ + C_2H_4 \qquad (3.11)$$

The observed relative intensities of CH_5^+ and $C_2H_5^+$ will therefore be smaller if water is present in the system. About 5% of the total ion intensity was due to H_3O^+.

3.3 Testing of the Pulsing Circuits

When the pulsing circuits and the fast response amplifier/discriminator were installed the temporal profile of the ion intensities could be collected and stored in the multichannel scalar. A reaction sequence was chosen which had been studied recently on another instrument in our laboratory and required only a simple flow system. The system studied was the solvation of NH_4^+ with ammonia.

$$NH_4^+(NH_3)_{n-1} + NH_3 \overset{K_{n-1,n}}{\rightleftarrows} NH_4^+(NH_3)_n \qquad (3.12)$$

Methane was flowed directly from the cylinder. The pressure was reduced to the torr range by a needle valve. The ammonia was treated similarly and the two gases were mixed by a capillary from the ammonia line projecting into the stream of methane. At low temperatures approximately

equal pressures of methane and ammonia were flowed through the ion source. At higher temperatures only ammonia was used.

Many ions were observed, most of them of the type $NH_4^+(NH_3)_n$ where n varied from 0 to 9 and also $NH_4^+(H_2O)_w$ where w varied from 1 to 5. Mixed clusters of the type $NH_4^+(NH_3)_n(H_2O)_w$ were also observed. The water impurity arose from the reactant gases and was also inherent in the system.

The equilibrium constant for the solvation reaction (3.13)

$$X^-.A_{n-1} + A \rightleftarrows X^-.A_n \tag{3.13}$$

can be denoted by $K_{n-1,n}$ for the addition of the n^{th} solvent molecule to the cluster. $K_{n-1,n}$ is given by

$$K_{n-1,n} = \frac{P_{X^-.A_n}}{P_{X^-.A_{n-1}}.P_A} \tag{3.14}$$

where P_A is the partial pressure of A. If it is assumed that the partial pressure of an ion is proportional to the observed ion intensity, then equation (3.14) can be rewritten

$$K_{n-1,n} = \frac{I_{X^-.A_n}}{I_{X^-.A_{n-1}}.P_A} \tag{3.15}$$

The free energy of reaction (n-1,n) is therefore given by

$$\Delta G^{\circ}_{n-1,n} = -RT \ln K_{n-1,n} \qquad (3.16)$$

where T is the absolute temperature and R is the gas constant. Since

$$\Delta G^{\circ}_{n-1,n} = \Delta H^{\circ}_{n-1,n} - T\Delta S^{\circ}_{n-1,n} \qquad (3.17)$$

equation (3.17) may be substituted into equation (3.16) to give

$$\ln K_{n-1,n} = -\frac{\Delta H^{\circ}_{n-1,n}}{RT} + \frac{\Delta S^{\circ}_{n-1,n}}{R} \qquad (3.18)$$

which is a form of the van't Hoff equation. Therefore measurement of $K_{n-1,n}$ at various temperatures enables a plot of $\ln K_{n-1,n}$ vs $\frac{1}{T}$ to be drawn. The slope is equal to $-\Delta H^{\circ}_{n-1,n}/R$ and the intercept is $\Delta S^{\circ}_{n-1,n}/R$. By selecting suitable pressures and temperatures, reactions with different values of n can be investigated.

The ammonia/water system has been studied by Kebarle et al (69,103). Figure 3.2 shows the van't Hoff plot for the measured equilibrium constants for reaction (3.12). The solid lines indicate the results of Kebarle et al (69) and the experimental points lie close to them. Most of the experimental points lie with ±20% of the line which is reasonable agreement between the same experiment performed on different instruments. The equilibrium for the reaction

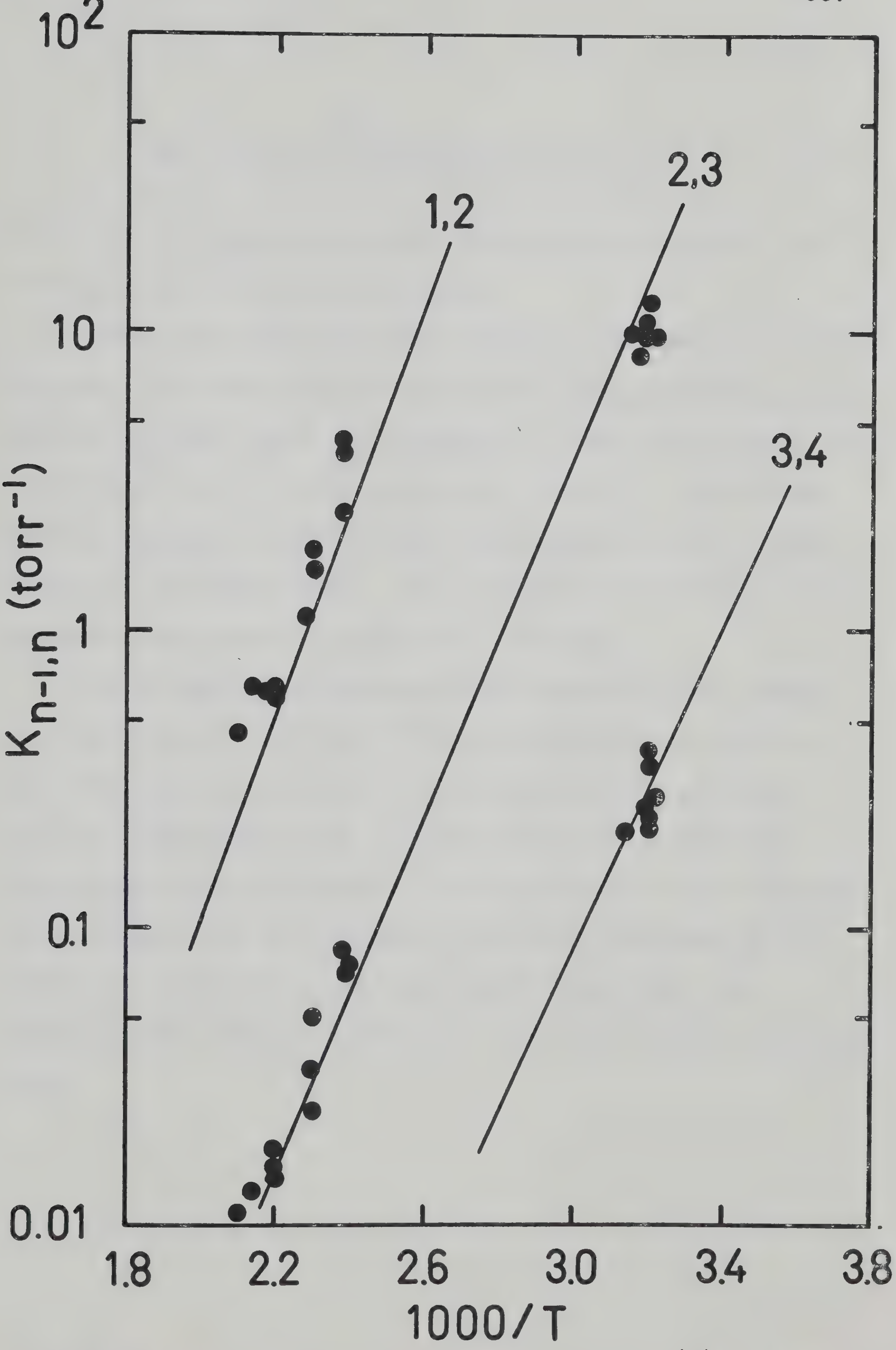

FIGURE 3.2. Measured equilibrium constants (●) $K_{n-1,n}$ for the system $NH_4^+(NH_3)_{n-1} + NH_3 = NH_4^+(NH_3)_n$. Lines show previous measurements.

$$NH_4^+(H_2O)_{w-1} + H_2O \rightleftharpoons NH_4^+(H_2O)_w \qquad (3.19)$$

could not be calculated since water was an impurity and its partial pressure was unknown.

Table III shows the thermodynamic parameters obtained for the (1,2) and (2,3) equilibrium. $\Delta H^o_{3,4}$ and $\Delta S^o_{3,4}$ were not calculated since the temperature range over which the (3,4) reaction was studied was very small. The thermodynamic quantities calculated agree satisfactorily with those of reference (69). The instrument therefore yields reproducible results within 20% precision.

The preceding experiments described in this chapter were performed using the existing gas handling system of the Atlas instrument. Before proceeding with any further experiments the all-glass/metal gas handling system described in section (2.5) was built and installed. This enabled the gas handling system to be baked up to 200°C to reduce the water and other impurities and eliminate the "memory" effect of the previous gas handling plant.

TABLE III

Thermodynamic Parameters Obtained for the Reaction

$$NH_4^+(NH_3)_{n-1} + NH_3 \rightleftarrows NH_4^+(NH_3)_n$$

Reaction (n-1,n)	$-\Delta H^o$(kcal/mol) This work	 a	 b	$-\Delta S^o$(e.u.) This work	 a	 b	$-\Delta G^o$(kcal/mol) This work	 a	 b
1,2	15.2 ± 1.5[c]	17.5	17	20.8 ± 3.3	23	26.8	9.0 ± 1.5	8.9	9.0
2,3	12.5 ± 0.2	13.8	16.5	22.1 ± 0.5	26	34	5.9 ± 0.2	6.1	6.4

---

a. Reference 69

b. Reference 103

c. Standard deviation from least squares analysis

CHAPTER 4

ION-MOLECULE REACTIONS IN METHANE CONTAINING TRACES OF ETHANE

4.1 Introduction

Interest in carbocations has been revived recently because of the possibility of observing them directly in highly acidic or "super acid" solvent systems (115). There are two distinct types of carbocations. The "classical" trivalent carbenium ion, such as CR_3^+, contains an sp^2 hybridized electron deficient central carbon atom, which is normally planar. The second type is the "nonclassical" penta or tetracoordinated carbonium ion, for example CR_5^+ and $C_2R_5^+$. The pentacoordinated species contains a five-coordinated carbon atom with eight valence electrons. The surrounding carbon atoms are bound to the central carbon by three single bonds and a two-electron, three-centre bond. For many years the transition state of S_E2 and S_N2 reactions has been represented by a pentacoordinated species which until recently had not been observed directly (115).

The structure of the tetracoordinated carbonium ion $C_2R_5^+$ can be respresented in two different ways as shown in (4.1).

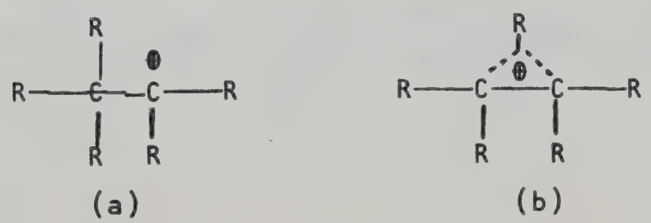

(4.1)

The existence of the nonclassical structure (b) has been controversial for the last two decades (116), but no direct experimental means were available to differentiate classical from nonclassical ions. The first direct observation of stable alkyl carbenium ions was reported in 1962 by Olah et al (115, p.16) when t-butyl fluoride was dissolved in excess antimony pentafluoride, which functioned as a Lewis acid as well as the solvent.

$$(CH_3)_3CF + (SbF_5)_2 \longrightarrow (CH_3)_3C^+Sb_2F_{11}^- \qquad (4.2)$$

The development of other superacids, such as magic acid, FSO_3H-SbF_5 and fluoroantimonic acid $HF-SbF_5$, has enabled many other carbenium ions to be observed using ^1H-NMR, ^{13}C-NMR, Infrared and Raman Spectra and ESCA.

The simplest pentacoordinated carbonium ion is the methonium ion, CH_5^+, which is well known in the gas phase from mass spectrometric studies. The reaction of methane in superacids and with strong electrophiles has been studied by Olah et al (117). Olah proposed that the interaction of the proton involves the main lobes of the covalent bonds, i.e. that the reaction proceeds by frontal attack (115).

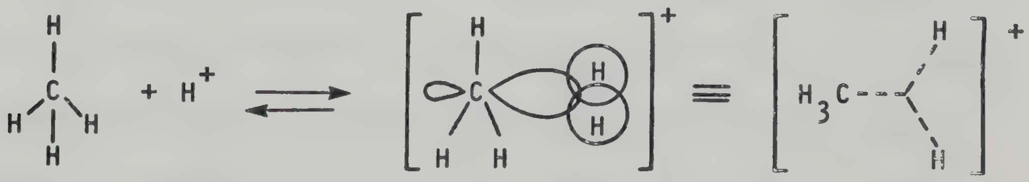

(4.3)

Electrophiles attack the points of highest electron density. Therefore Olah suggested that attack occurs on the covalent bonds and not on the back lobes.

Several possible structures exist for the methonium ion: D_{3h}, C_{4v}, C_s, symmetry. Olah and coworkers, on the basis of experiments on methane in superacids, suggested that C_s was the preferred form. Pople _et al_ (118,119) utilized _ab initio_ calculations and supported the C_s structure. Their calculations indicated that C_s is more stable than the C_{4v} structure by about 2 kcal/mol, and that the latter is 8 kcal/mol more stable than the D_{3h} structure. Other independent calculations also indicated that the C_s structure is the most stable (120,121). However, it should be noted that the theoretical calculations considered the isolated ion, whereas Olah's data would be influenced by solvation.

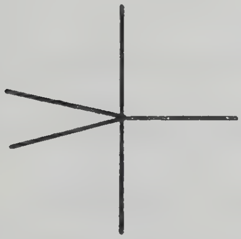

D_{3h}

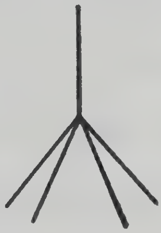

C_{4v}

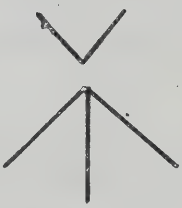

C_s .

The renewed interest in carbonium ions in superacids and the subsequent additional knowledge from theoretical calculations has led to further investigation of the behaviour of carbonium ions in the gas phase using mass spectrometry.

Two important properties that can be studied by means of ion-molecule reactions are ion-solvent interactions and the acidity or basicity of a substance. The former has been studied by Hiraoka and Kebarle (74) who investigated reaction (4.4)

$$CH_5^+(CH_4)_{n-1} + CH_4 \rightleftharpoons CH_5^+(CH_4)_n \qquad (4.4)$$

for n = 1-5. By studying the equilibrium reaction (4.4), the enthalpy changes $\Delta H^o_{n-1,n}$ can be determined and related to the structure of the cluster ions.

Although many investigations have been conducted on ion-molecule reactions in methane, ion-molecule reactions in ethane and the higher alkanes are not so well documented.

The basicity or proton affinity of a compound M, is the exothermicity of reaction (4.5).

$$M + H^+ \longrightarrow MH^+ \qquad (4.5)$$

The proton affinity of ethane was first measured by Munson, Franklin and Field (122). After exeriments with pure ethane they postulated that the protonated ethane ion $C_2H_7^+$ was formed from the excited parent ion by reaction (4.6). The

$$(C_2H_6^+)^* + C_2H_6 — C_2H_7^+ + C_2H_5 \qquad (4.6)$$

$\Delta H^o_f(C_2H_7^+)$ calculated from this mechanism was ≤ 229 kcal/mol, which gave a value for $PA(C_2H_6) > 120$ kcal/mol.

In 1965 Munson and Field (38) studied the ion-molecule reactions in a mixture of methane containing 1% ethane. They observed a simple proton transfer between methane and ethane by reaction (4.7). Since the reaction

$$CH_5^+ + C_2H_6 \longrightarrow C_2H_7^+ + CH_4 \qquad (4.7)$$

is observed it is exothermic and therefore the proton affinity of ethane is greater than the proton affinity of methane. From these experiments they estimated $PA(C_2H_6) > 120$ kcal/mol which agreed with their previous work (122).

Chong and Franklin (120) have also measured the proton affinity difference between methane and ethane by studying the equilibrium for the forward and reverse steps of reaction (4.7). They calculated ΔG^o to be -1.09 kcal/mol. Assuming that the entropy change was zero, they proposed that the proton affinity difference between ethane and methane is ~1 kcal/mol. When combined with $PA(C_2H_6) = 127$ kcal/mol, Franklin's result leads to $PA(C_2H_6) = 128$ kcal/mol.

In 1973 Bohme _et al_ (124) published results for the proton affinity of ethane which disagreed substantially with the previous measurements of Franklin (123). Bohme used the flowing afterglow technique (125) to determine the preferred direction of proton transfer reactions of the type

$$XH^{+} + Y \underset{k_r}{\overset{k_f}{\rightleftarrows}} YH^{+} + X \qquad (4.8)$$

by measuring the forward rate constant, k_f and the reverse rate constant, k_r. If reaction (4.8) occurs preferentially in the direction left to right then $k_f/k_r > 1$ and $PA(Y) > PA(X)$. By keeping X constant and using different compounds Y whose proton affinity is known, it becomes possible to bracket PA(X) within a narrow range of possible values. For example, Bohme studied reactions (4.9-4.11) and found that proton transfer occurs preferentially in the direction in which they are written.

$$N_2OH^{+} + C_2H_6 \rightleftarrows C_2H_7^{+} + N_2O \qquad (4.9)$$

$$COH^{+} + C_2H_6 \rightleftarrows C_2H_7^{+} + CO \qquad (4.10)$$

$$C_2H_7^{+} + C_2H_4 \rightleftarrows C_2H_5^{+} + C_2H_6 \qquad (4.11)$$

Therefore the proton affinity of C_2H_6 is greater than that of N_2O and CO but less than the proton affinity of C_2H_4. Since Bohme had previously established (126) that $PA(N_2O) =$ 134 kcal/mol and PA(CO) = 138 kcal/mol, the lower limit of $PA(C_2H_6)$ is 138 kcal/mol, almost 10 kcal/mol greater than Chong and Franklin's value (123). $C_2H_7^{+}$ was observed to transfer a proton to C_2H_4 preferentially, therefore, $PA(C_2H_6) < PA(C_2H_4)$. Bohme calculated $PA(C_2H_4) = 159$ kcal/mol from thermochemical data (127). Therefore the proton affinity of ethane can be narrowed down to the

proton affinity of ethane can be narrowed down to the range $138 < PA(C_2H_6) < 159$. A difference of 10 kcal/mol in the proton affinity measurement between Bohme's and Chong and Franklin's value implies that Franklin's equilibrium constant was in error by a factor of at least 10^6.

Bohme's range of values for $PA(C_2H_6)$ was substantiated by theoretical calculations by Lathan, Hehre and Pople (128), whose estimate of $PA(C_2H_6)$ was 140 kcal/mol.

In view of the vast disparity between Bohme's and Chong and Franklin's value of the proton affinity of ethane, an independent evaluation of the equilibrium reaction (4.7) was necessary in order to ascertain the proton affinity difference between ethane and methane. If the proton affinity difference between the two compounds is of the order of 10 kcal/mol, the measurement of the equilibrium constant for reaction (4.7) would be very difficult experimentally. The measurement would only be possible in methane containing traces of ethane. The investigation of ion-molecule reactions and their temperature dependences under such concentration conditions proved quite rewarding since the system proved to be a lot more complicated than was originally expected and several interesting processes were found which will be described separately in the following sections of this chapter.

4.2 Experimental

The apparatus used in the experiments shown in this

chapter is described in chapter 2. The methane used in this project was of Ultra High Purity grade. The quoted impurity concentration of ethane in the methane gas supply was 27 ppm or a ratio of $CH_4:C_2H_6 = 37,000:1$, thus amounts of ethane injected into the bulb to give higher ratios would be insignificant compared to the impurity already present. However, the methane gas was passed through a molecular sieve before entering the gas handling plant. In order to examine the effectiveness of the sieve in removing the ethane impurity, an experiment was conducted with pure methane after being passed through the molecular sieve. $C_2H_7^+$ could not be detected. The ion profiles are shown in Figure 4.1. $C_2H_7^+$ is absent and the disappearance of CH_5^+ is accompanied by an increase in H_3O^+ at the same rate due to a water impurity. Since no $C_2H_7^+$ was observed, the molecular sieve must remove residual ethane from the gas supply and the mixutres made with very small amounts of ethane will be accurate.

4.3 Results and Discussion : Major Reactions in the Methane/Ethane System

The measured ion intensities of 50 experiments were normalized. The ion source pressure was varied between 1 and 3.5 torr, but most experiments were conducted at about 2.5 torr. The ethane partial pressures in the ion source were varied from 0.07 to 5 mtorr. The temperature range was 30 to 210 ± 2°C.

Since the major component in all experiments was

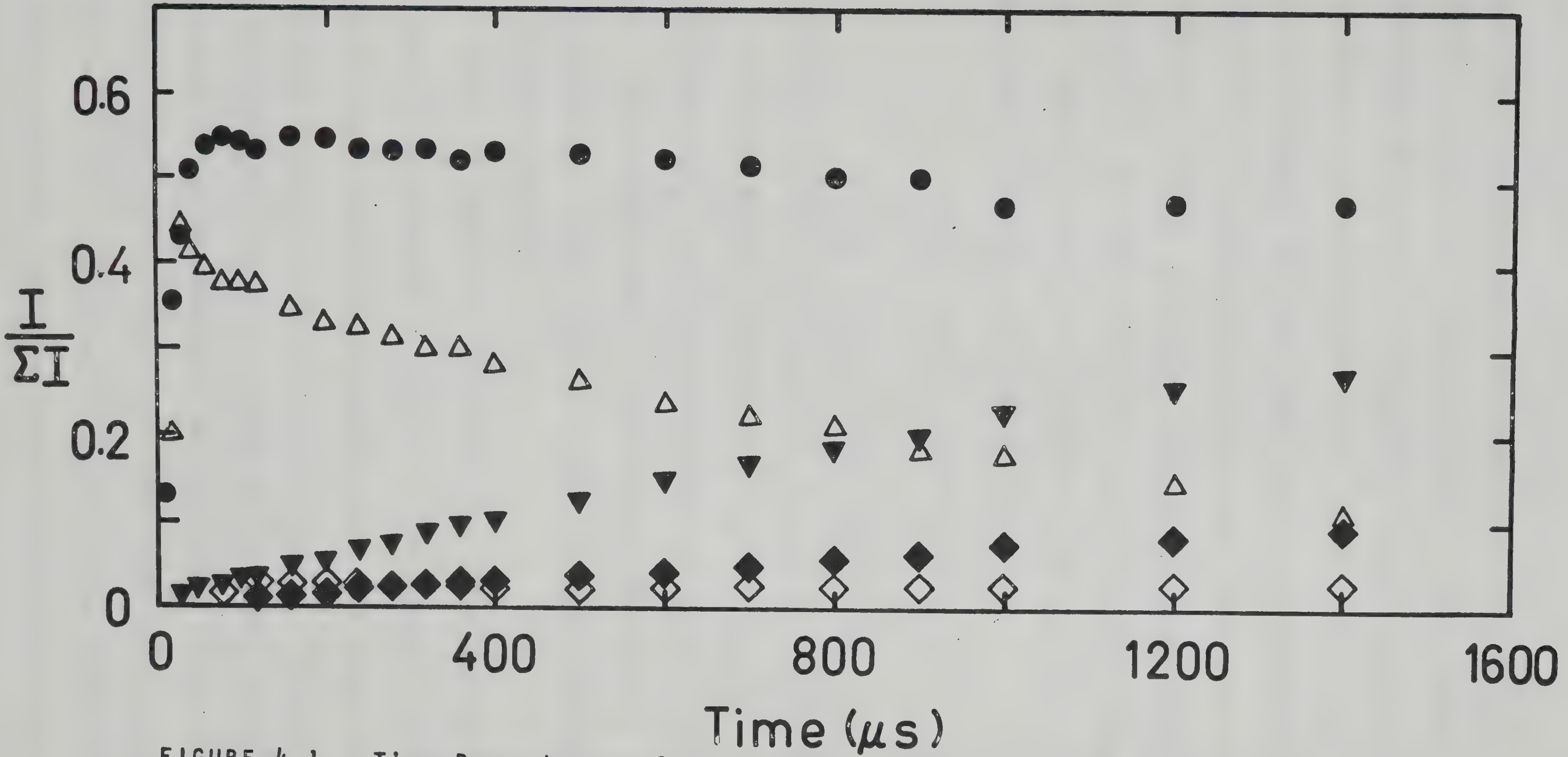

FIGURE 4.1 Time Dependence of Normalized Intensities P_{CH_4} = 2.5 torr. No C_2H_6 added, T = 110°C. ● CH_5^+, △ $C_2H_5^+$, ▼ $C_3H_7^+$, ◆ H_3O^+, ◇ $C_2H_4^+$.

methane, the primary ions produced by electron impact were almost exclusively due to methane. The primary ions observed were CH_3^+ and CH_4^+ which were present in the expected ratio of 5:4. In all experiments the first 10 μsec channel was not used in any calculations because the electron pulse was still on and ions were still being created. Figure 4.2 shows the observed concentration changes of the major ions at short reaction times at 30°C. CH_3^+ and CH_4^+ react very rapidly with methane in the well-known reactions (4.12) and (4.13).

$$CH_3^+ + CH_4 \longrightarrow C_2H_5^+ + H_2 \qquad (4.12)$$

$$CH_4^+ + CH_4 \longrightarrow CH_5^+ + CH_3 \qquad (4.13)$$

As CH_3^+ and CH_4^+ decrease in intensity with time, there is a simultaneous increase in CH_5^+ and $C_2H_5^+$ showing that CH_4^+ and CH_3^+ are the precursors of these ions. Under all conditions used in these experiments CH_3^+ and CH_4^+ disappeared within 40 μsec and will be omitted from subsequent diagrams.

The ion intensity profiles for 29 experiments are shown in Figures 4.3 to 4.31. The symbols indicate the normalized experimental points and the same symbols represent the same ion in each diagram. The solid lines are the best fits calculated by an analog computer. The analog computer analysis is described in section 4.9. The major products at long reaction times are represented by one curve. Figures 4.3 to 4.7 show experiments conducted at room temperature and illustrate the effect of

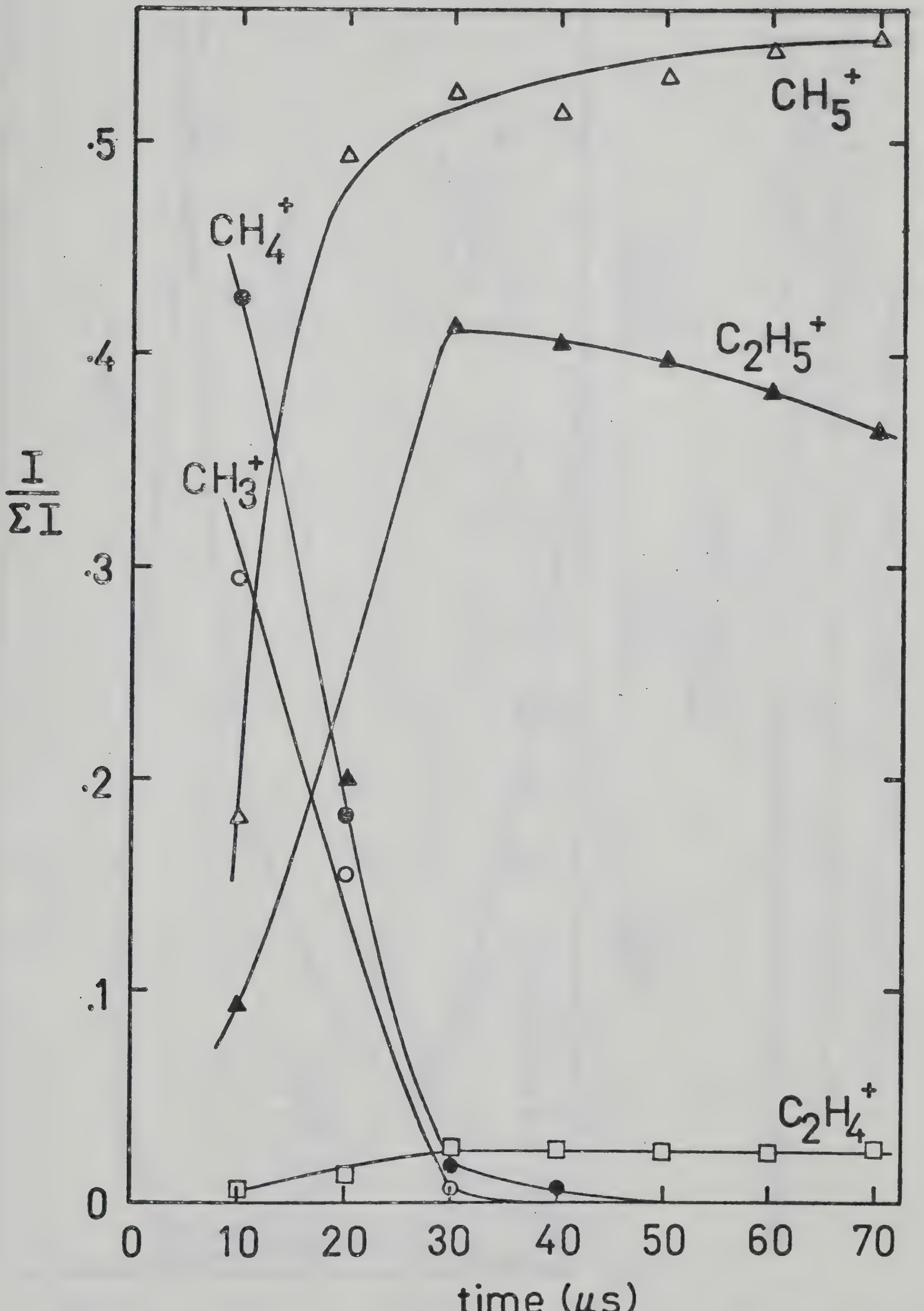

FIGURE 4.2 Normalized Intensities of Major Ions at Short Reaction Times. P_{CH_4} = 2.3 torr, $P_{C_2H_6}$ = 0.05 mtorr. T = 30°C.

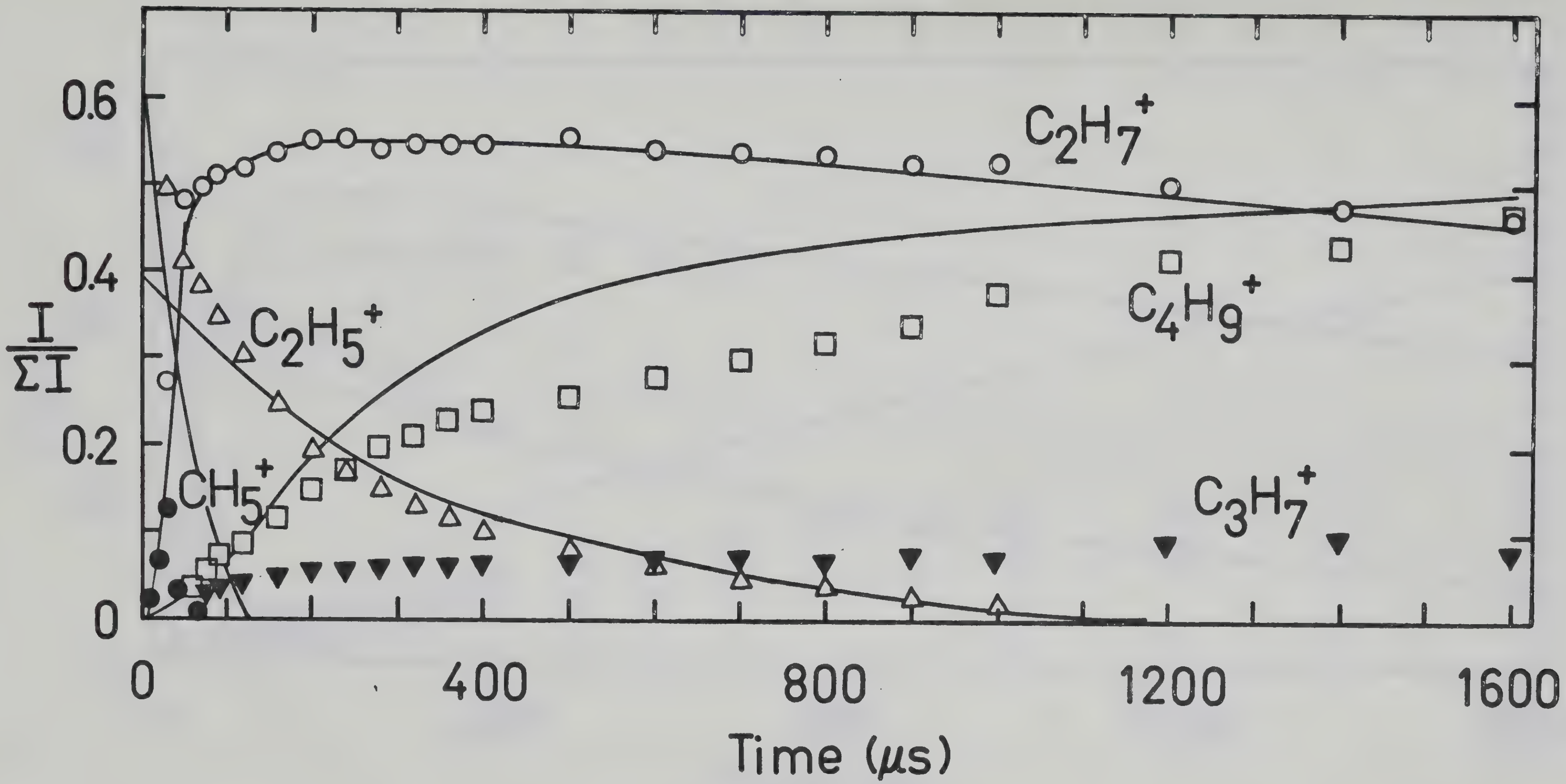

FIGURE 4.3 Time Dependence of Normalized Ion Intensities. P_{CH_4} = 2.3 torr CH_4, $P_{C_2H_6}$ = 4.6 mtorr. CH_4:C_2H_6 = 500:1 T = 32°C. ● CH_5^+, ○ $C_2H_7^+$, △ $C_2H_5^+$, ▼ $C_3H_7^+$, □ $C_4H_9^+$, ◇ $C_2H_4^+$, ▲ $C_4H_{10}^+$, ■ $C_4H_{11}^+$, ◆ H_3O^+. Symbols the same in all diagrams.

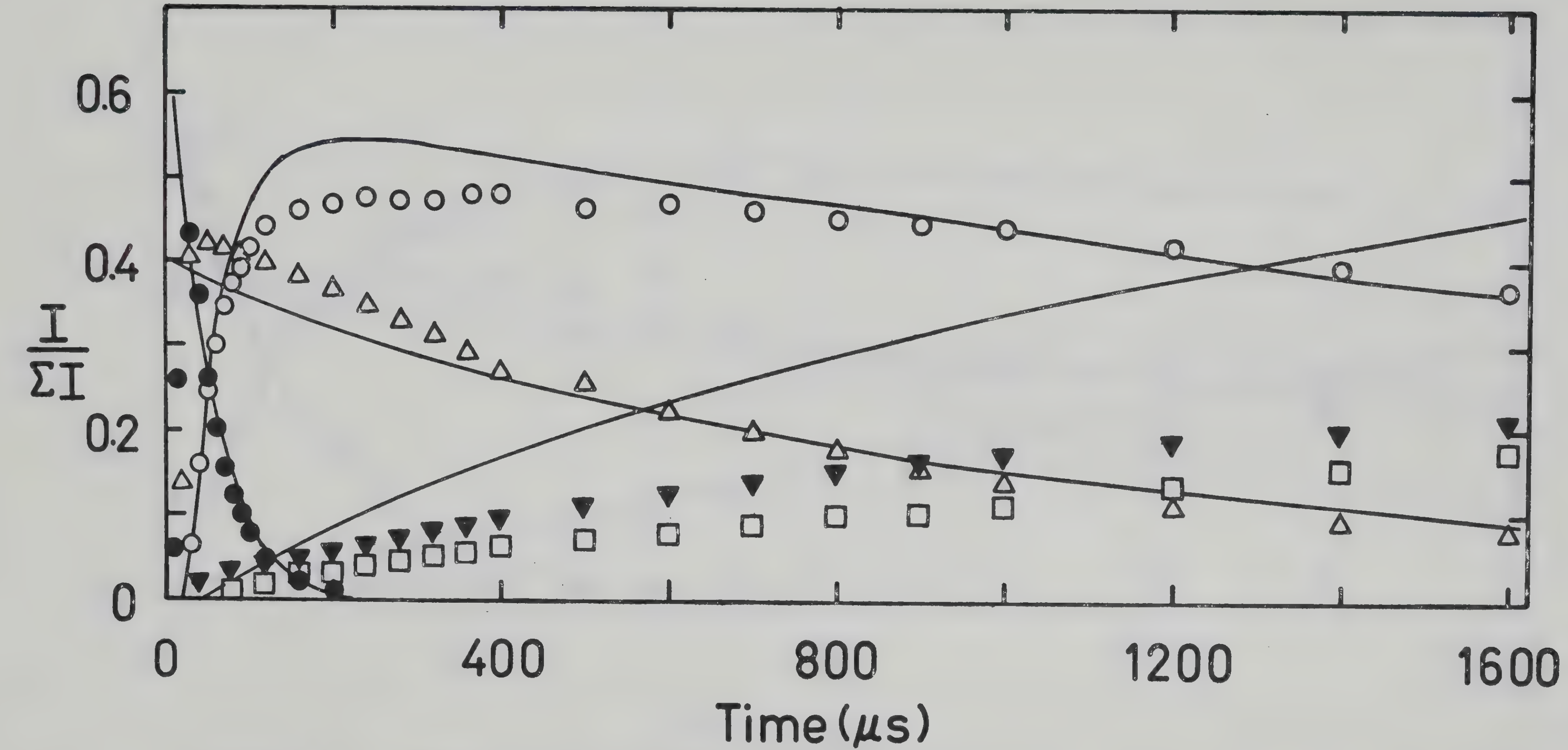

FIGURE 4.4. Time Dependence of Normalized Ion Intensities. P_{CH_4} = 2.4 torr CH_4, $P_{C_2H_6}$ = 0.48 mtorr. $CH_4:C_2H_6$ = 5000:1. T = 29°C. Symbols as in Figure 4.3. Solid lines are computer fitted.

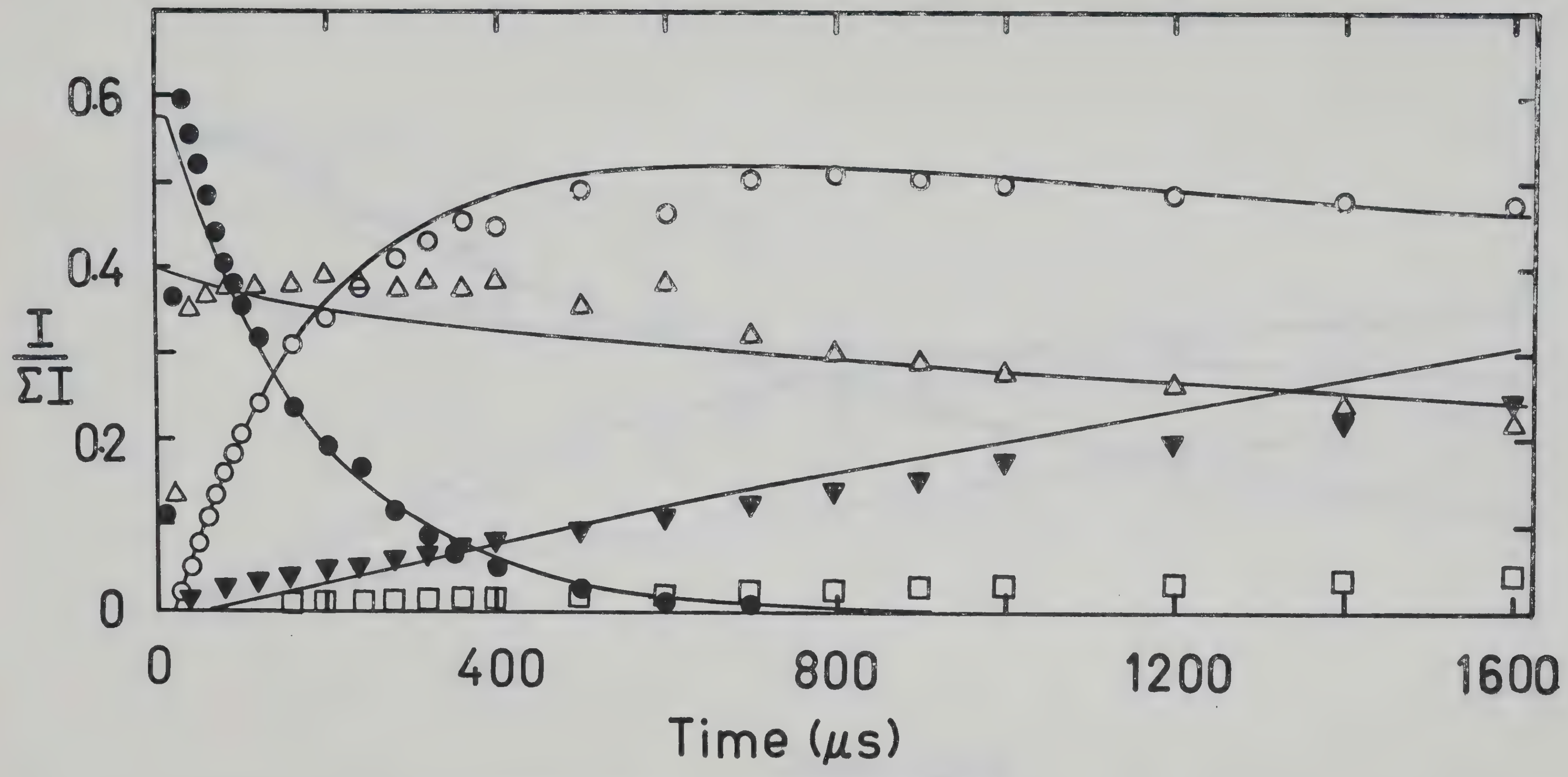

FIGURE 4.5. Time Dependence of Normalized Ion Intensities. P_{CH_4} = 2.3 torr, $P_{C_2H_6}$ = 0.12 mtorr. $CH_4:C_2H_6$ = 20,000:1. T = 29°C. Symbols as in Figure 4.3.

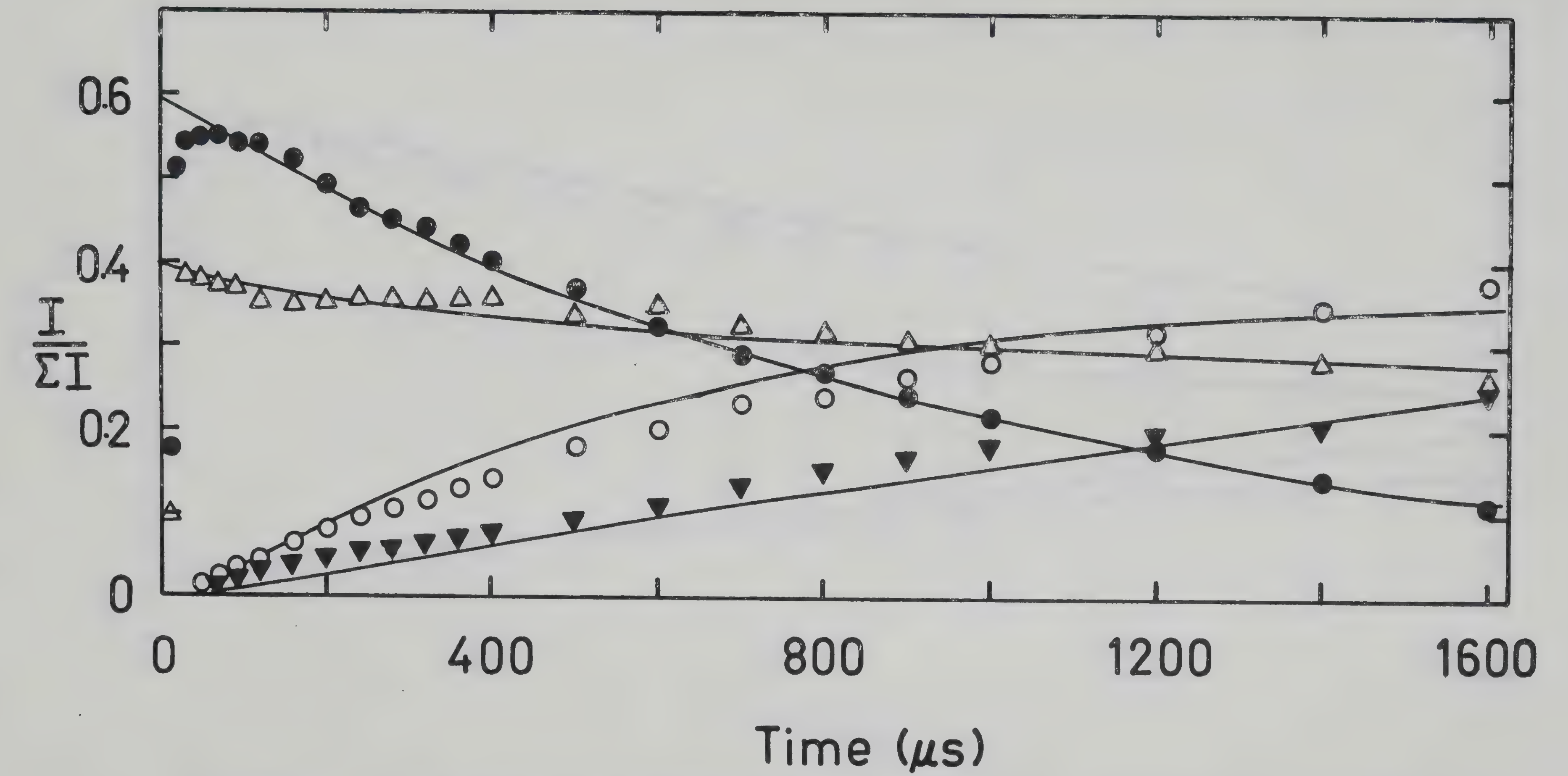

FIGURE 4.6. Time Dependence of Normalized Ion Intensities. P_{CH_4} = 2.3 torr, $P_{C_2H_6}$ = .012 mtorr. $CH_4:C_2H_6$ = 200,000:1. T = 30°C. Symbols as in Figure 4.3.

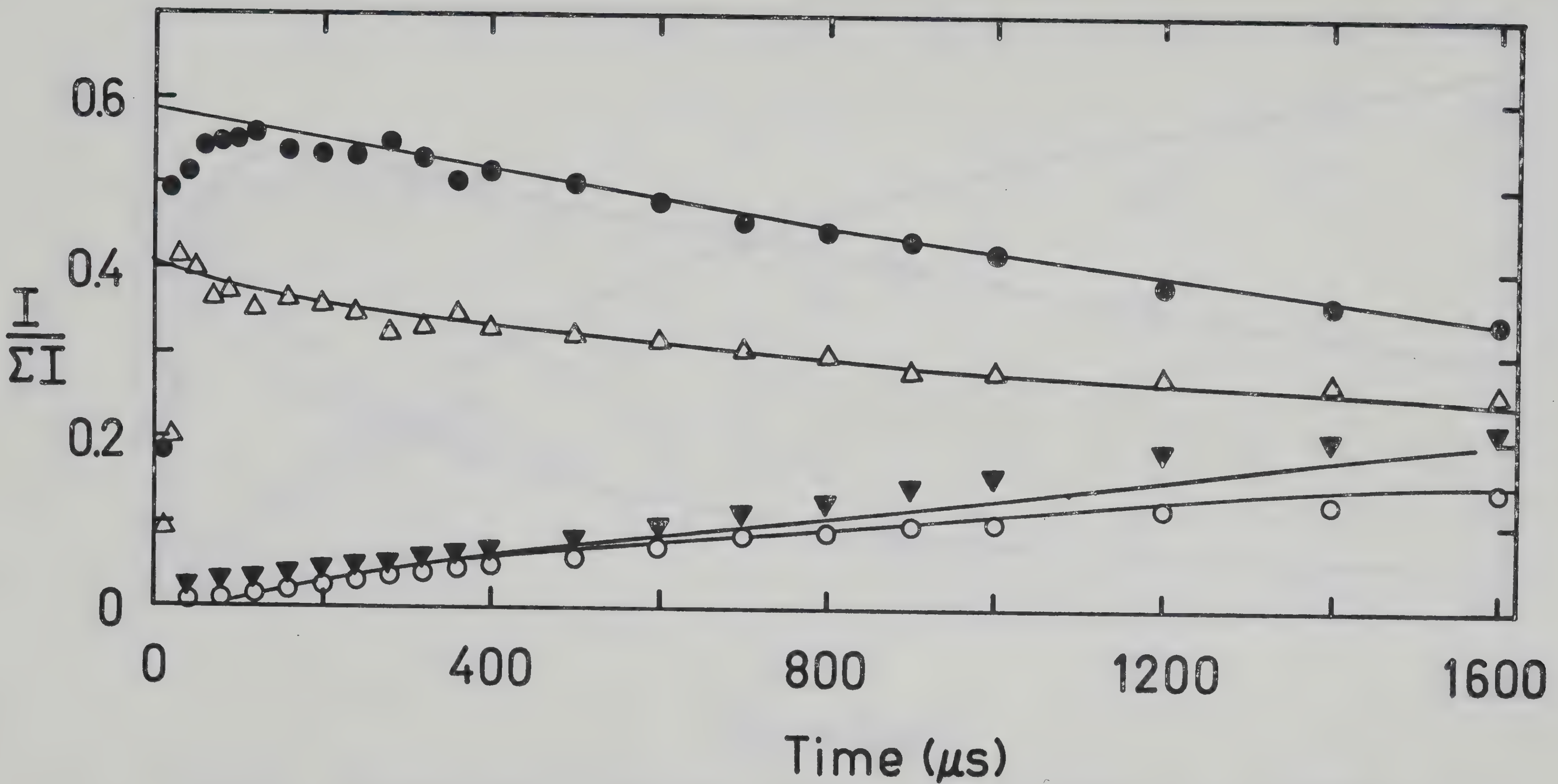

FIGURE 4.7. Time Dependence of Normalized Ion Intensities. P_{CH_4} = 2.3 torr, $P_{C_2H_6}$ = 0.046 mtorr. CH_4:C_2H_6 = 500,000:1. T = 29°C. Symbols as in Figure 4.3.

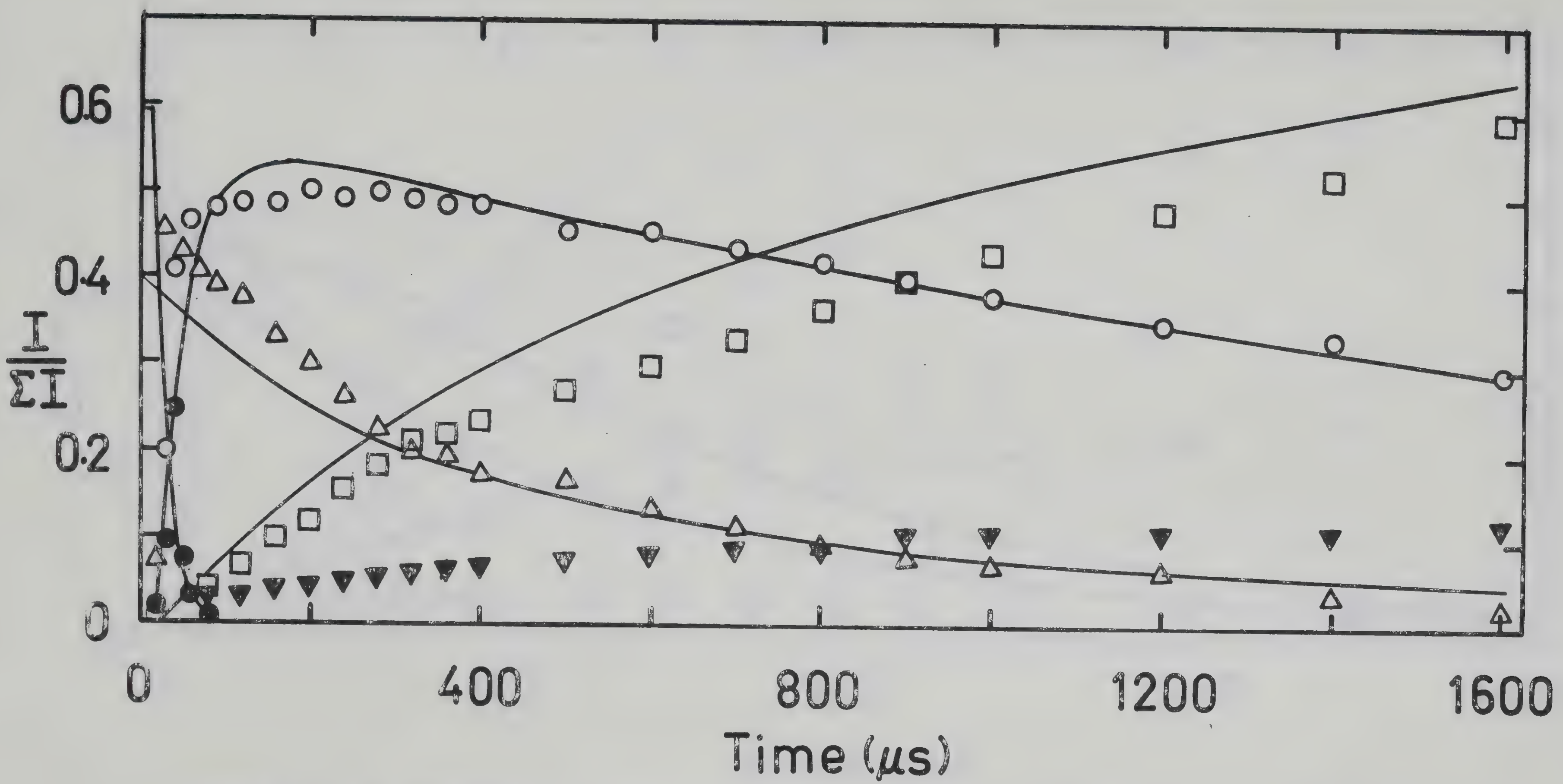

FIGURE 4.8. Time Dependence of Normalized Intensities. P_{CH_4} = 2.3 torr, $P_{C_2H_6}$ = 4.6 mtorr, $CH_4:C_2H_6$ = 500:1. T = 49°C. Symbols as in Figure 4.3.

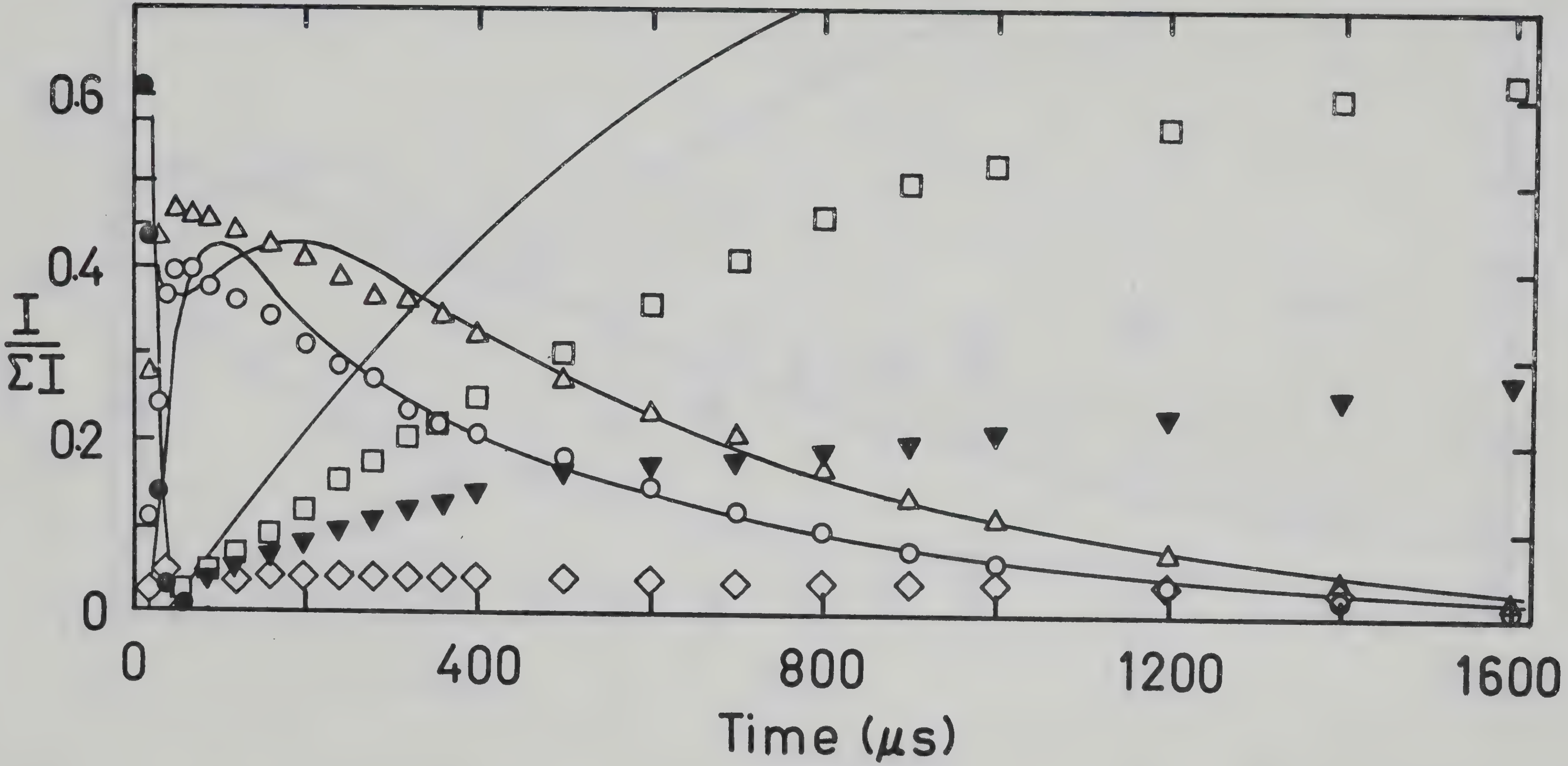

FIGURE 4.9. Time Dependence of Normalized Intensities. P_{CH_4} = 2.2 torr, $P_{C_2H_6}$ = 4.4 μ, $CH_4:C_2H_6$ = 500:1, T = 88°C. Symbols as in Figure 4.3.

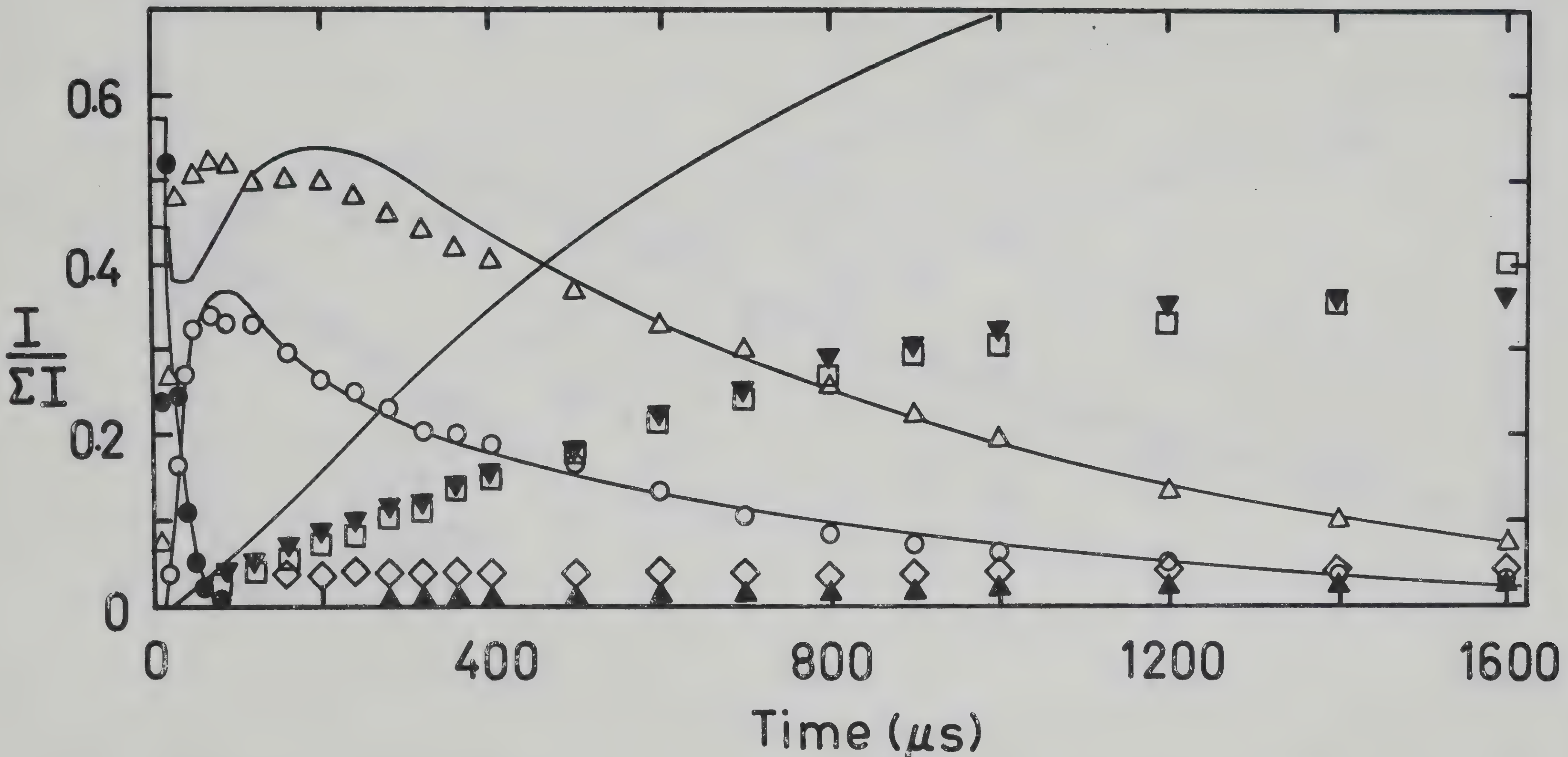

FIGURE 4.10. Time Dependence of Normalized Intensities. P_{CH_4} = 2.3 torr CH_4, $P_{C_2H_6}$ = 2.3 mtorr. CH_4:C_2H_6 = 1000:1. T = 85°C. Symbols as in Figure 4.3.

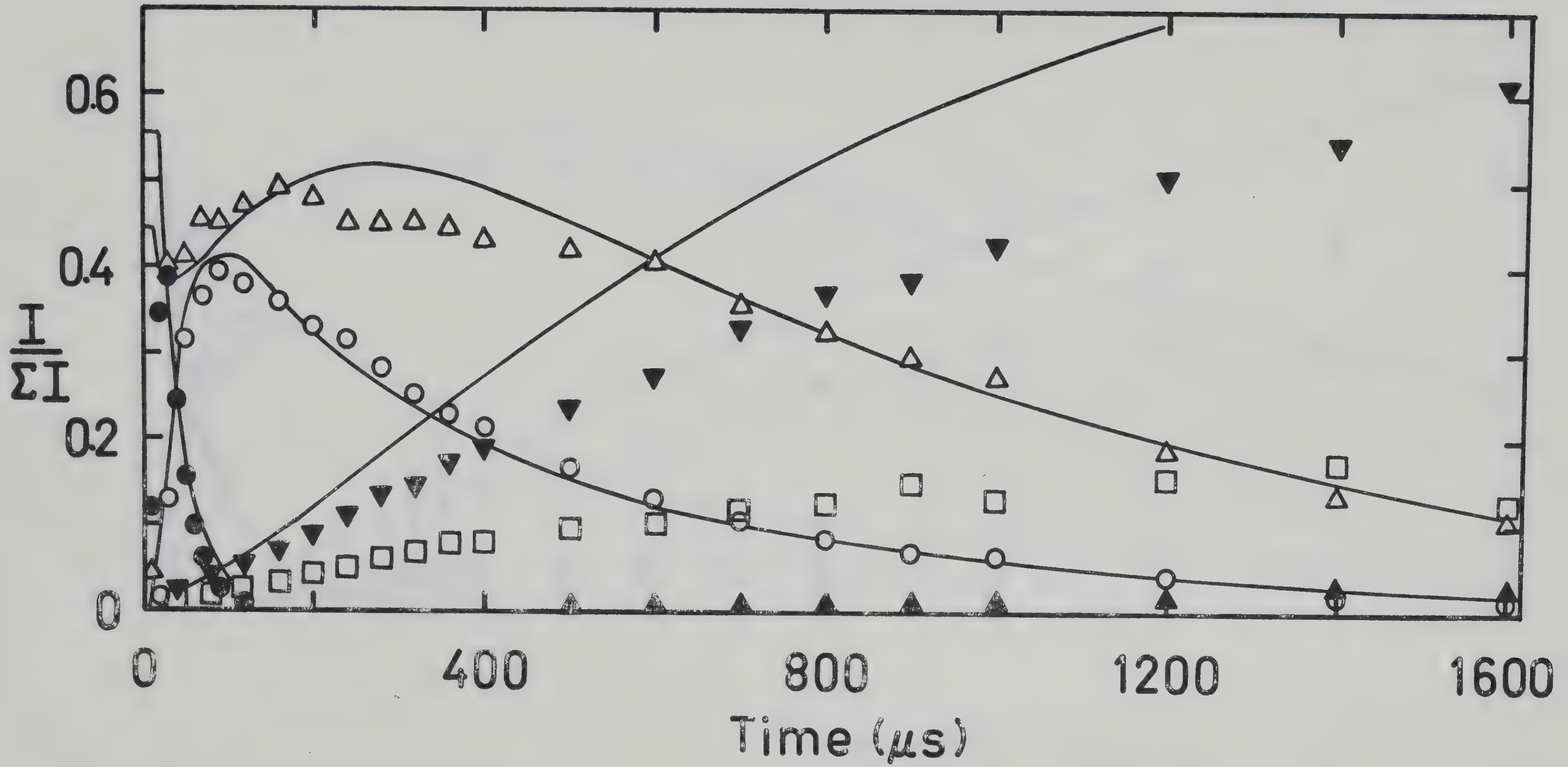

FIGURE 4.11. Time Dependence of Normalized Intensities. P_{CH_4} = 2.4 torr, $P_{C_2H_6}$ = 0.96 mtorr, $CH_4:C_2H_6$ = 2500:1. T = 84°C. Symbols as in Figure 4.3.

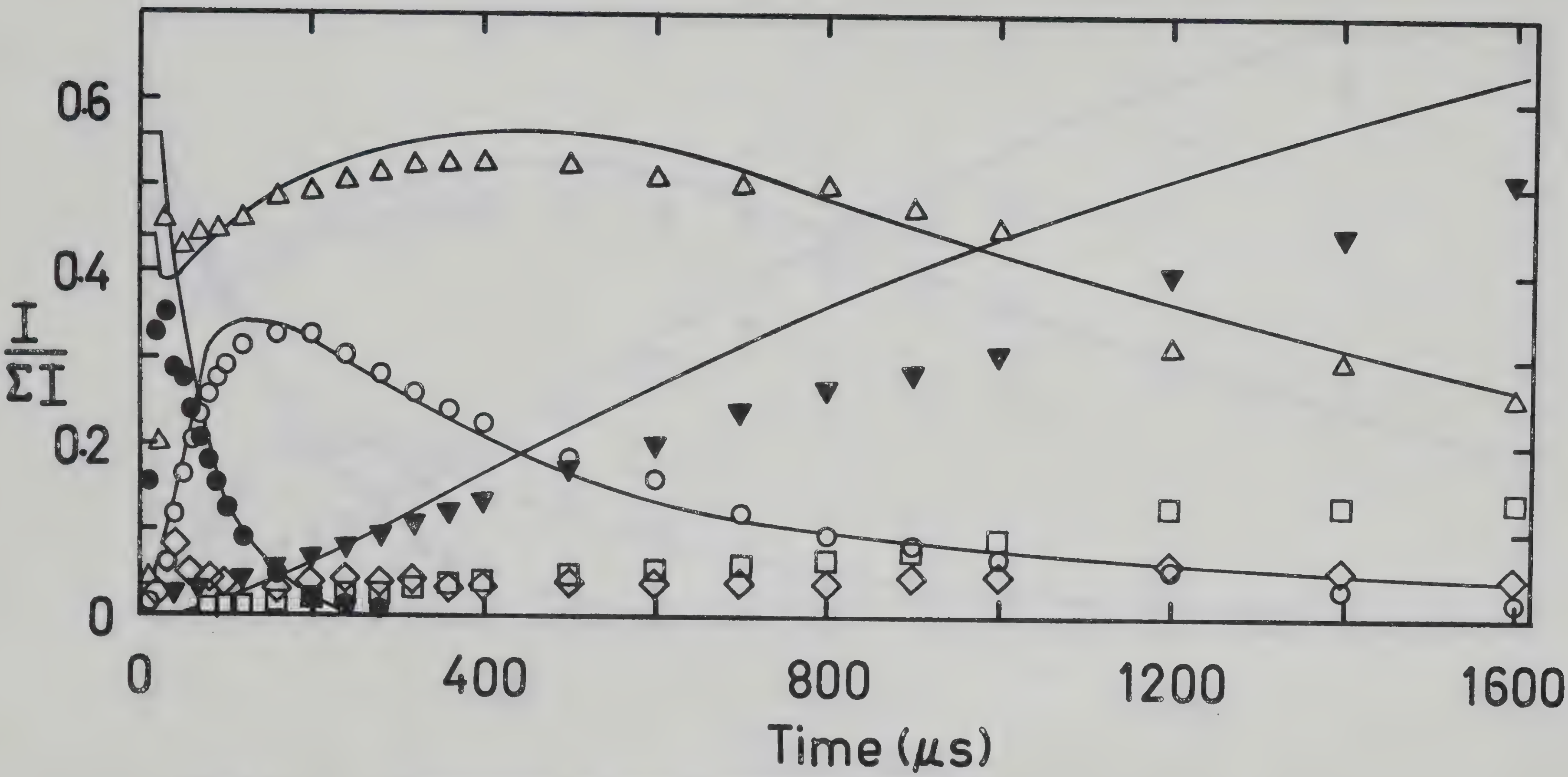

FIGURE 4.12. Time Dependence of Normalized Intensities. P_{CH_4} = 2.1 torr, $P_{C_2H_6}$ = 0.42 mtorr. CH_4:C_2H_6 = 5000:1. T = 84°C. Symbols as in Figure 4.3.

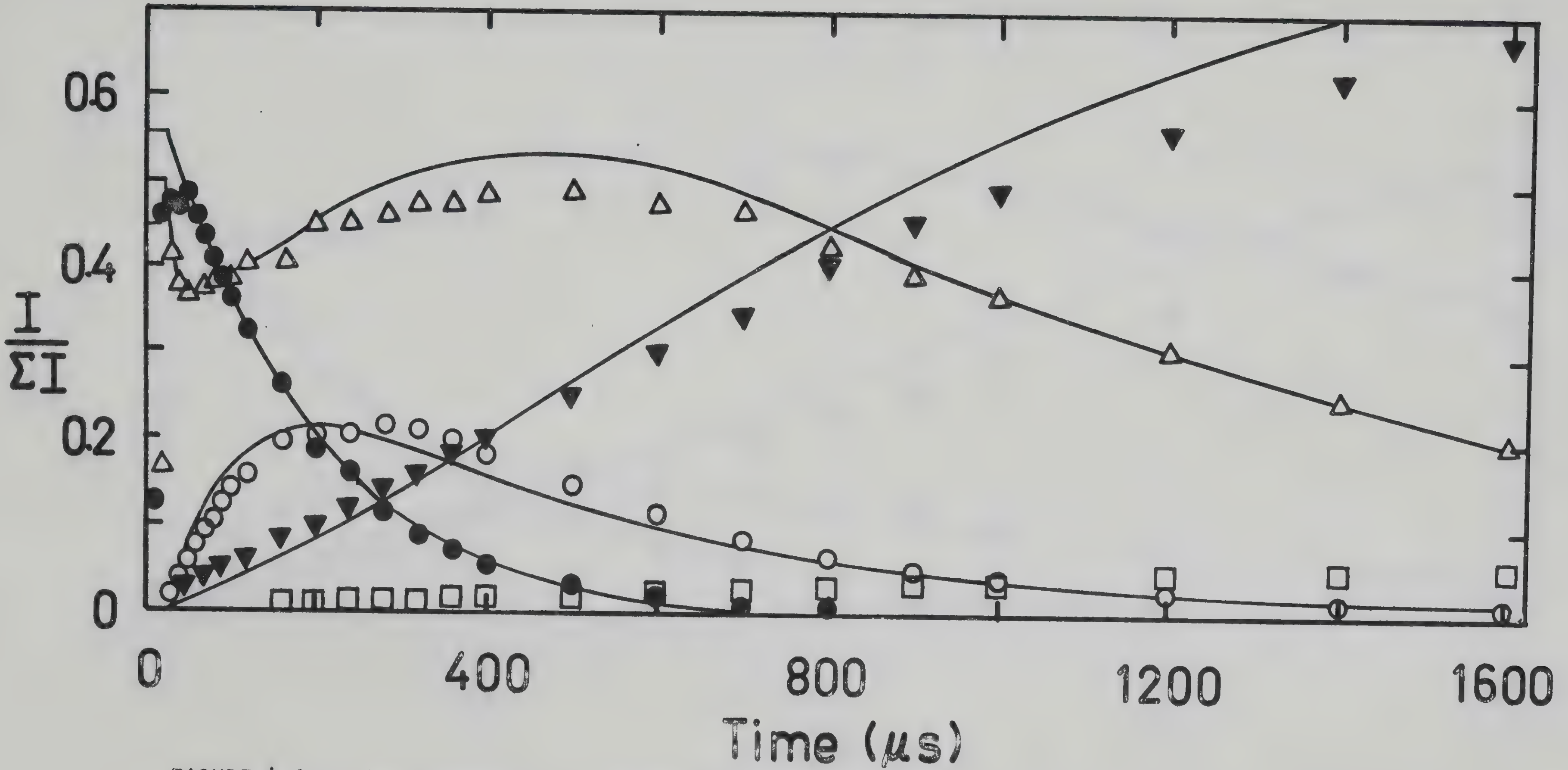

FIGURE 4.13. Time Dependence of Normalized Intensities. P_{CH_4} = 3.2 torr, $P_{C_2H_6}$ = 0.16 mtorr. $CH_4:C_2H_6$ = 20,000:1. T = 87°C. Symbols as in Figure 4.3.

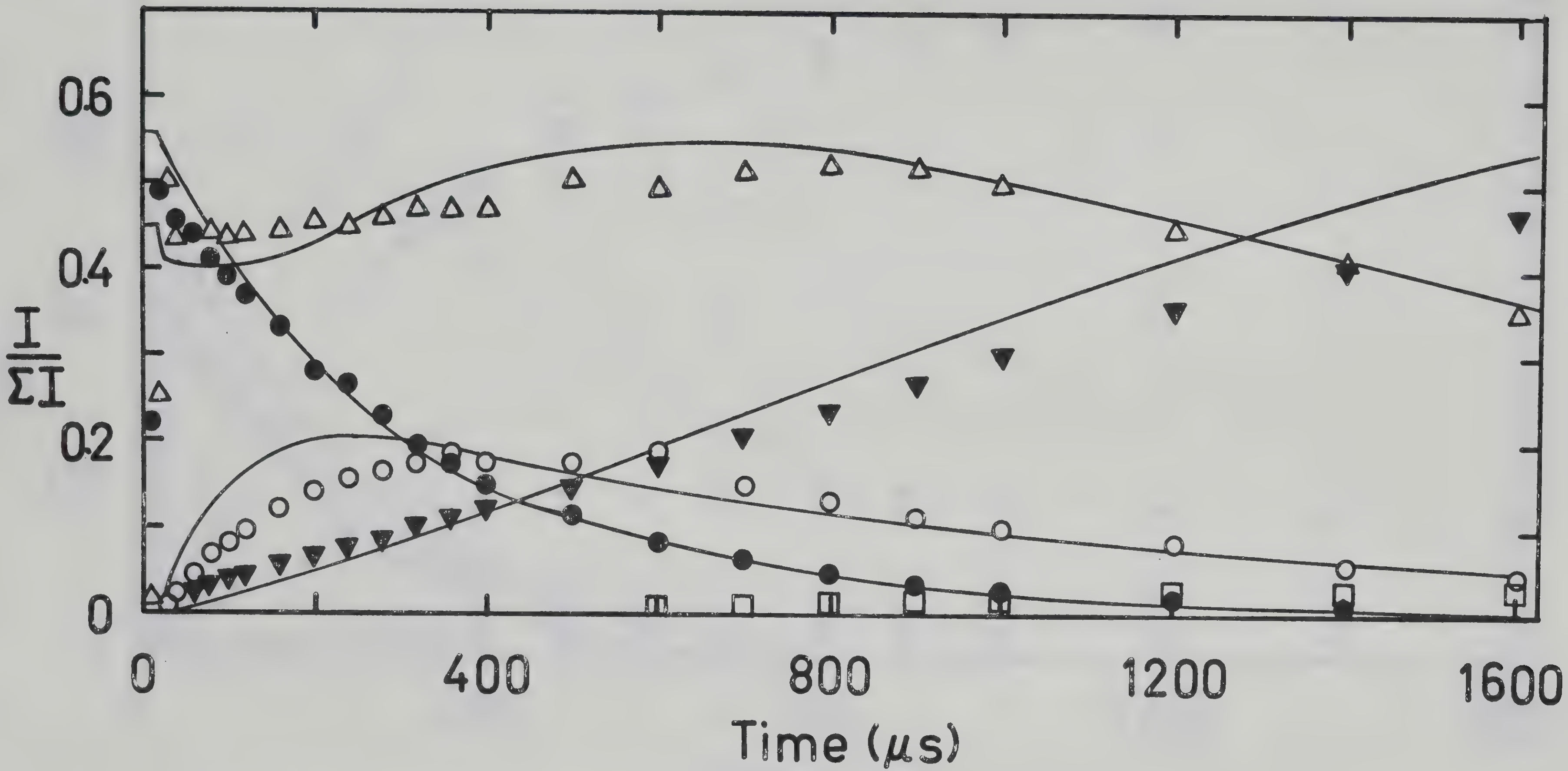

FIGURE 4.14. Time Dependence of Normalized Intensities. P_{CH_4} = 2.2 torr, $P_{C_2H_6}$ = .044 mtorr. $CH_4:C_2H_6$ = 50,000:1. T = 86°C. Symbols as in Figure 4.3.

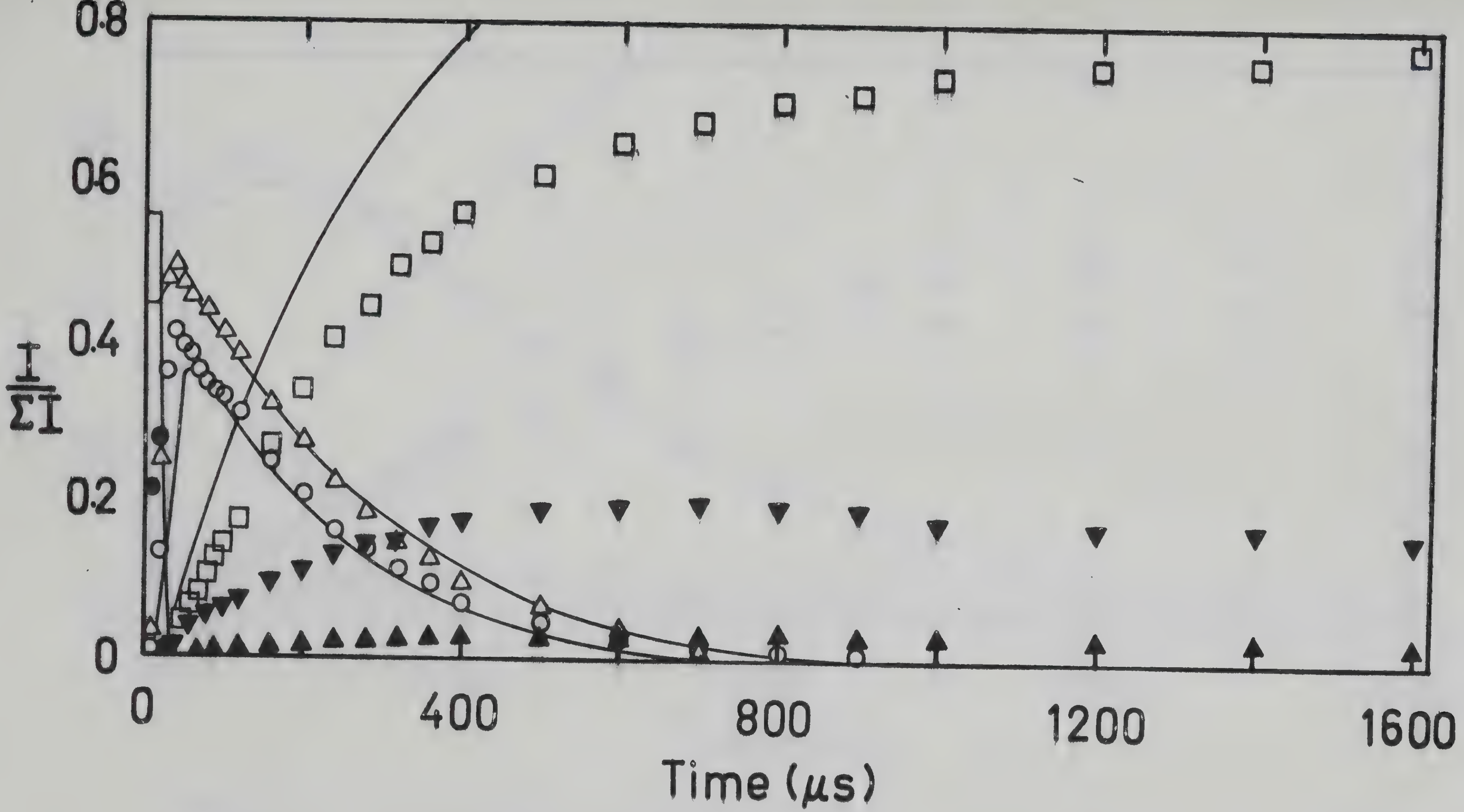

FIGURE 4.15. Time Dependence of Normalized Intensities. P_{CH_4} = 2.5 torr, $P_{C_2H_6}$ = 10 mtorr. $CH_4:C_2H_6$ = 250:1. T = 105°C. Symbols as in Figure 4.3.

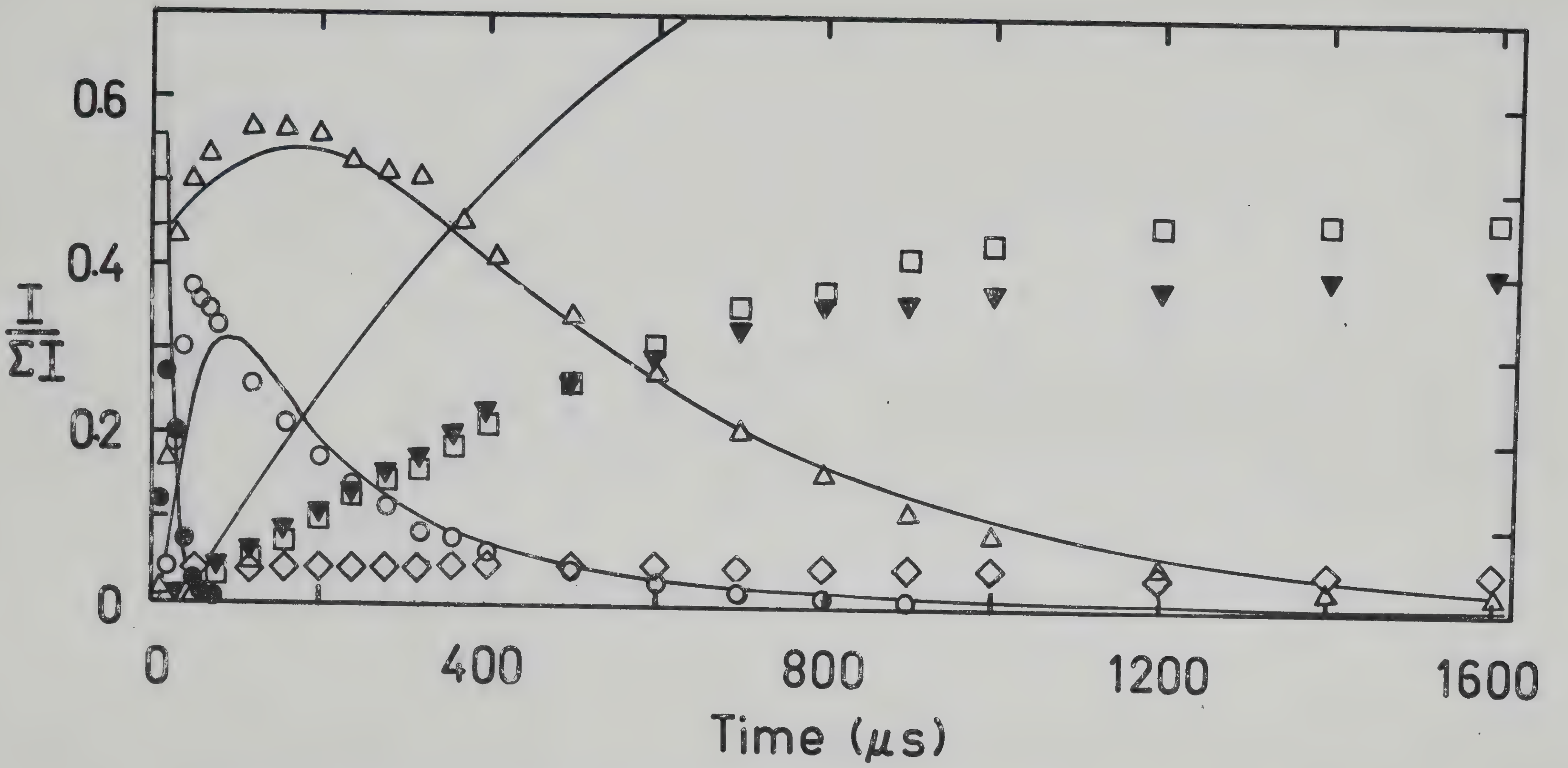

FIGURE 4.16. Time Dependence of Normalized Intensities. P_{CH_4} = 2.6 torr CH_4, $P_{C_2H_6}$ = 2.6 mtorr. CH_4:C_2H_6 = 1000:1. T = 105°C. Symbols as in Figure 4.3.

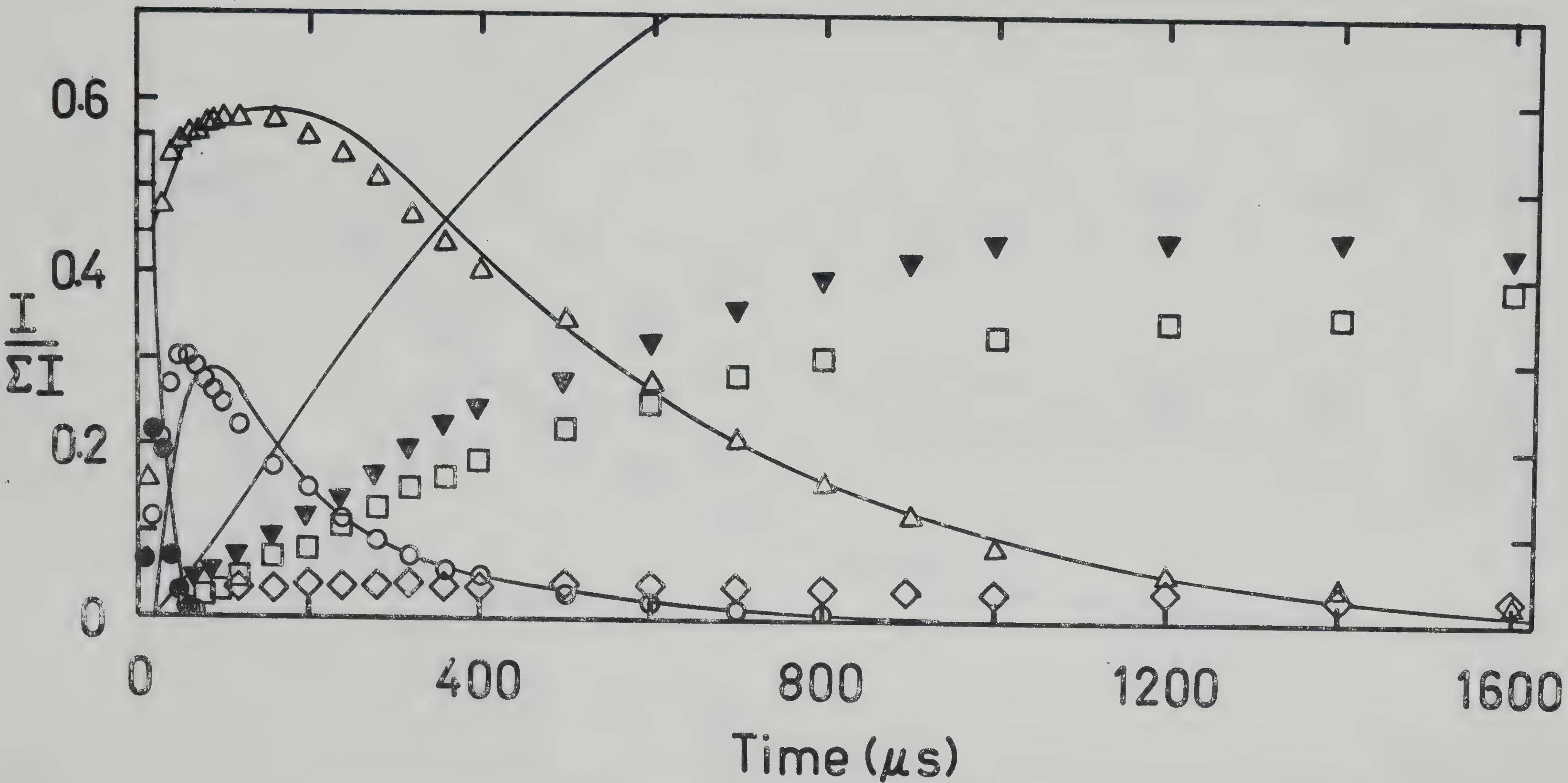

FIGURE 4.17. Time Dependence of Normalized Intensities. P_{CH_4} = 2.4 torr, $P_{C_2H_6}$ = 1.9 mtorr. $CH_4:C_2H_6$ = 1250:1. T = 106°C. Symbols as in Figure 4.3.

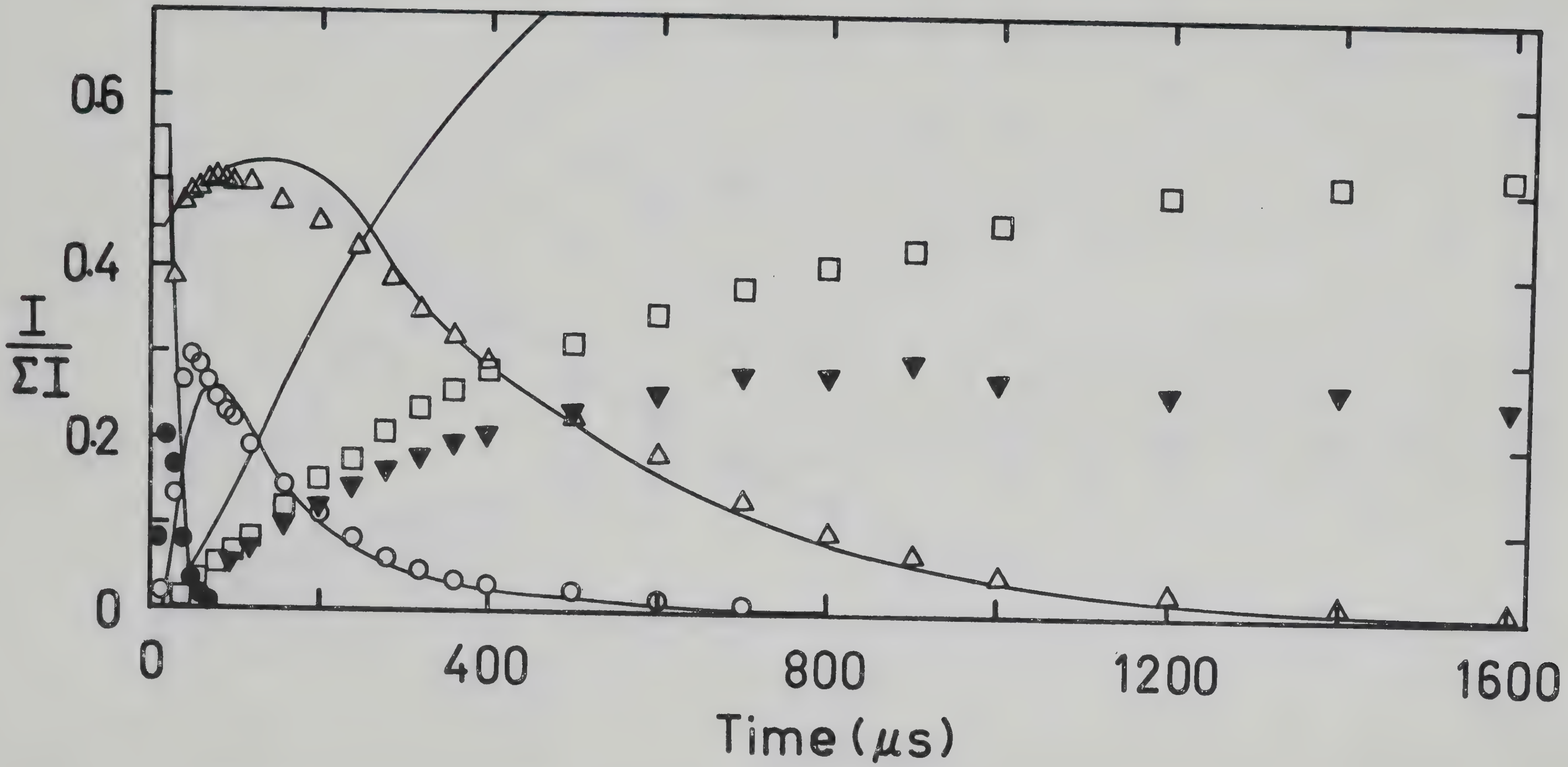

FIGURE 4.18. Time Dependence of Normalized Intensities. $P_{CH_4} = 2.5$ torr, $P_{C_2H_6} = 1.5$ mtorr. $CH_4:C_2H_6 = 1700:1$. T = 105°C. Symbols as in Figure 4.3.

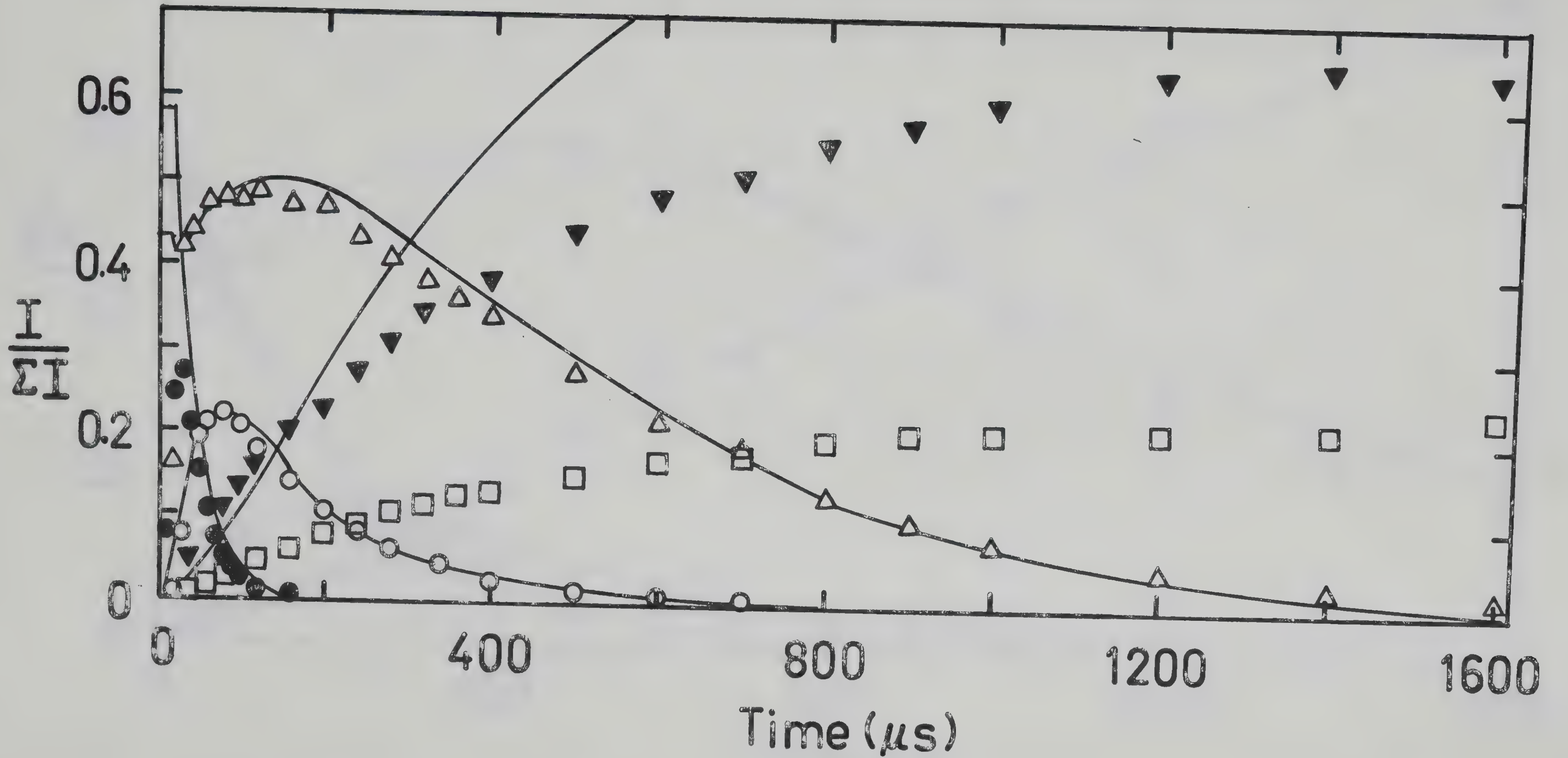

FIGURE 4.19. Time Dependence of Normalized Intensities. P_{CH_4} = 2.5 torr, $P_{C_2H_6}$ = 0.5 mtorr. CH_4:C_2H_6 = 5000:1. T = 104°C. Symbols as in Figure 4.3.

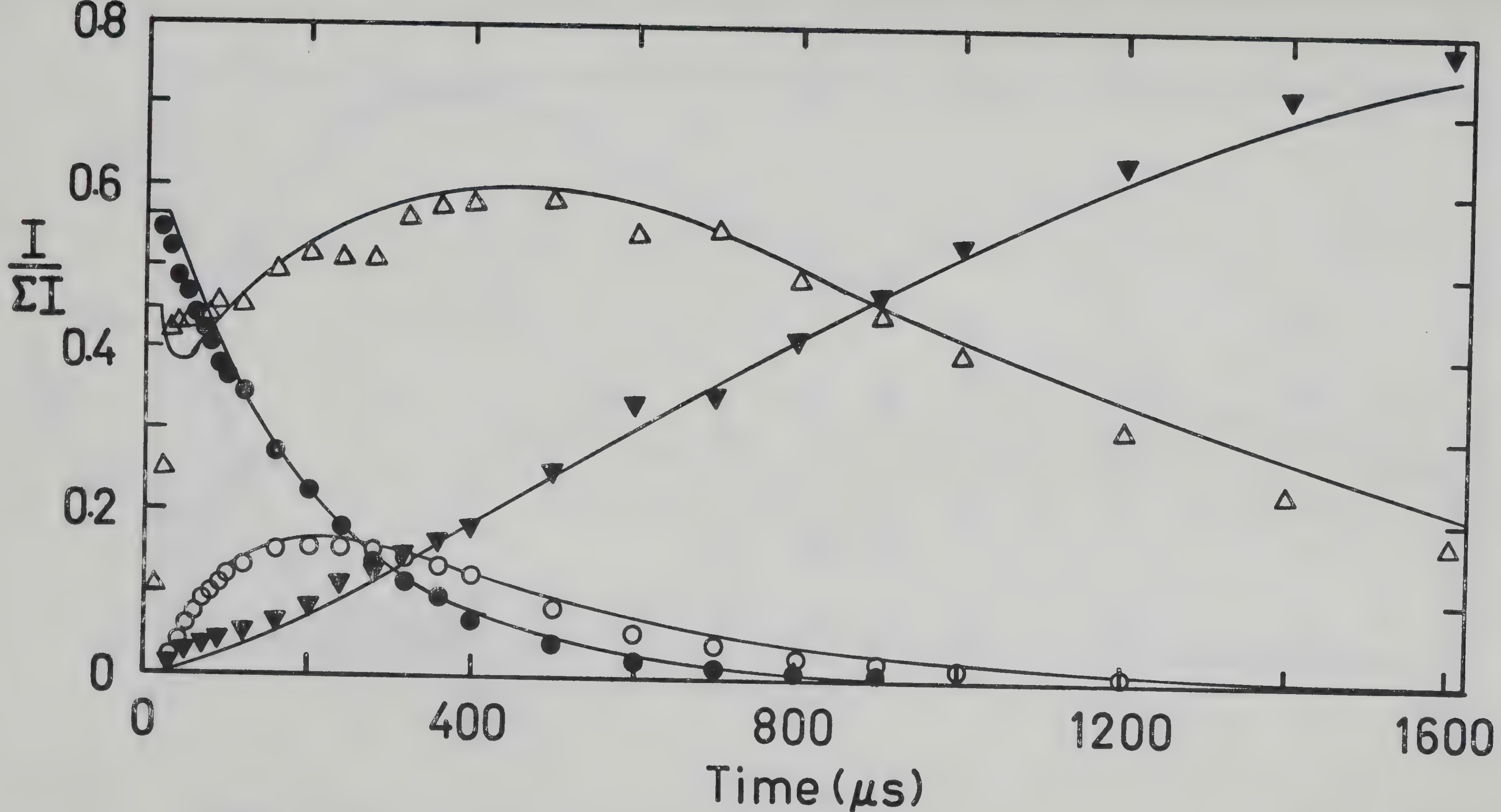

FIGURE 4.20. Time Dependence of Normalized Intensities. P_{CH_4} = 2.2 torr, $P_{C_2H_6}$ = 0.22 mtorr. $CH_4:C_2H_6$ = 10,000:1. T = 101°C. Symbols as in Figure 4.3.

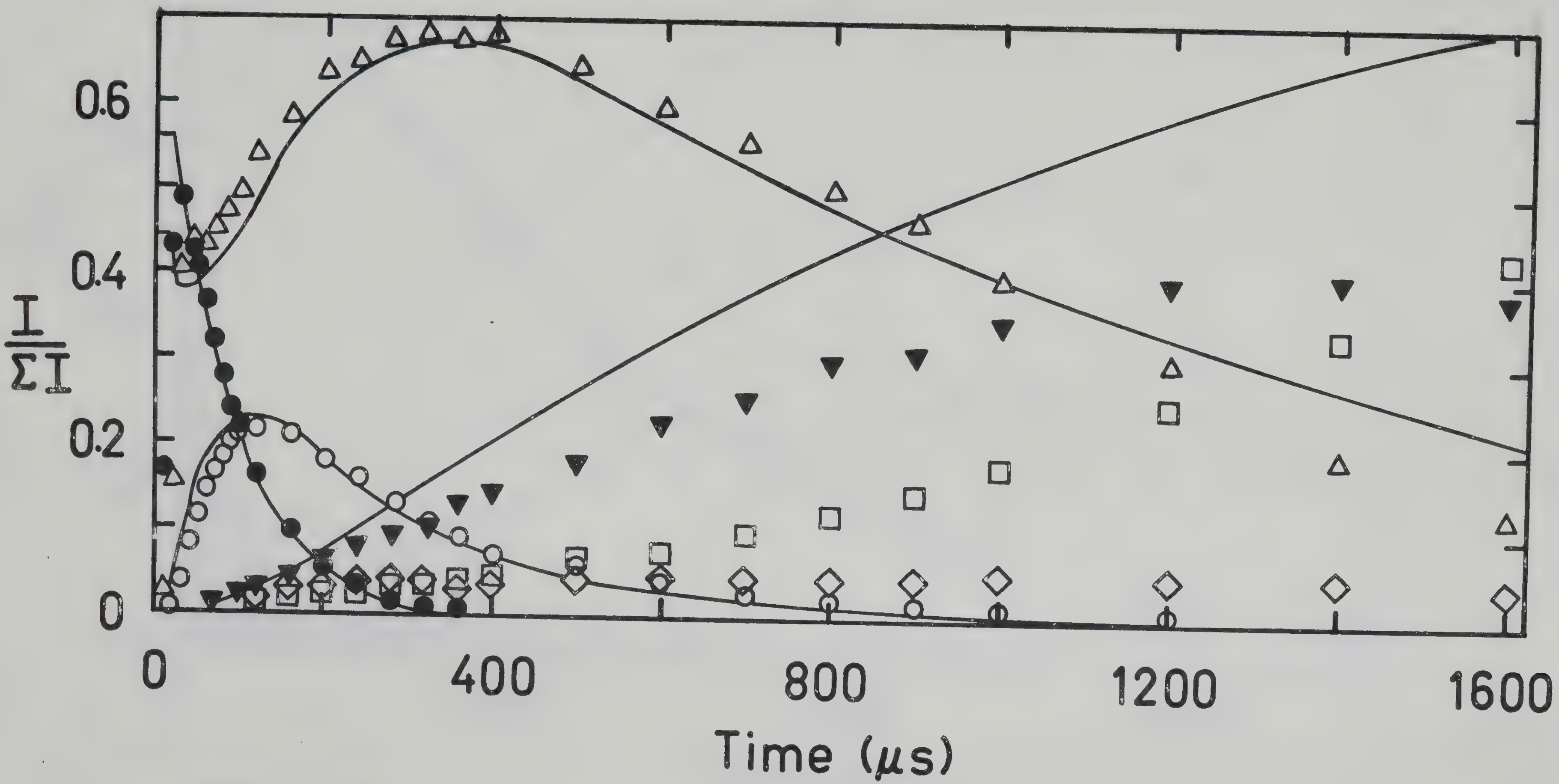

FIGURE 4.21. Time Dependence of Normalized Intensities. P_{CH_4} = 2.4 torr, $P_{C_2H_6}$ = 0.2 mtorr. $CH_4:C_2H_6$ = 12,000:1. T = 107°C. Symbols as in Figure 4.3.

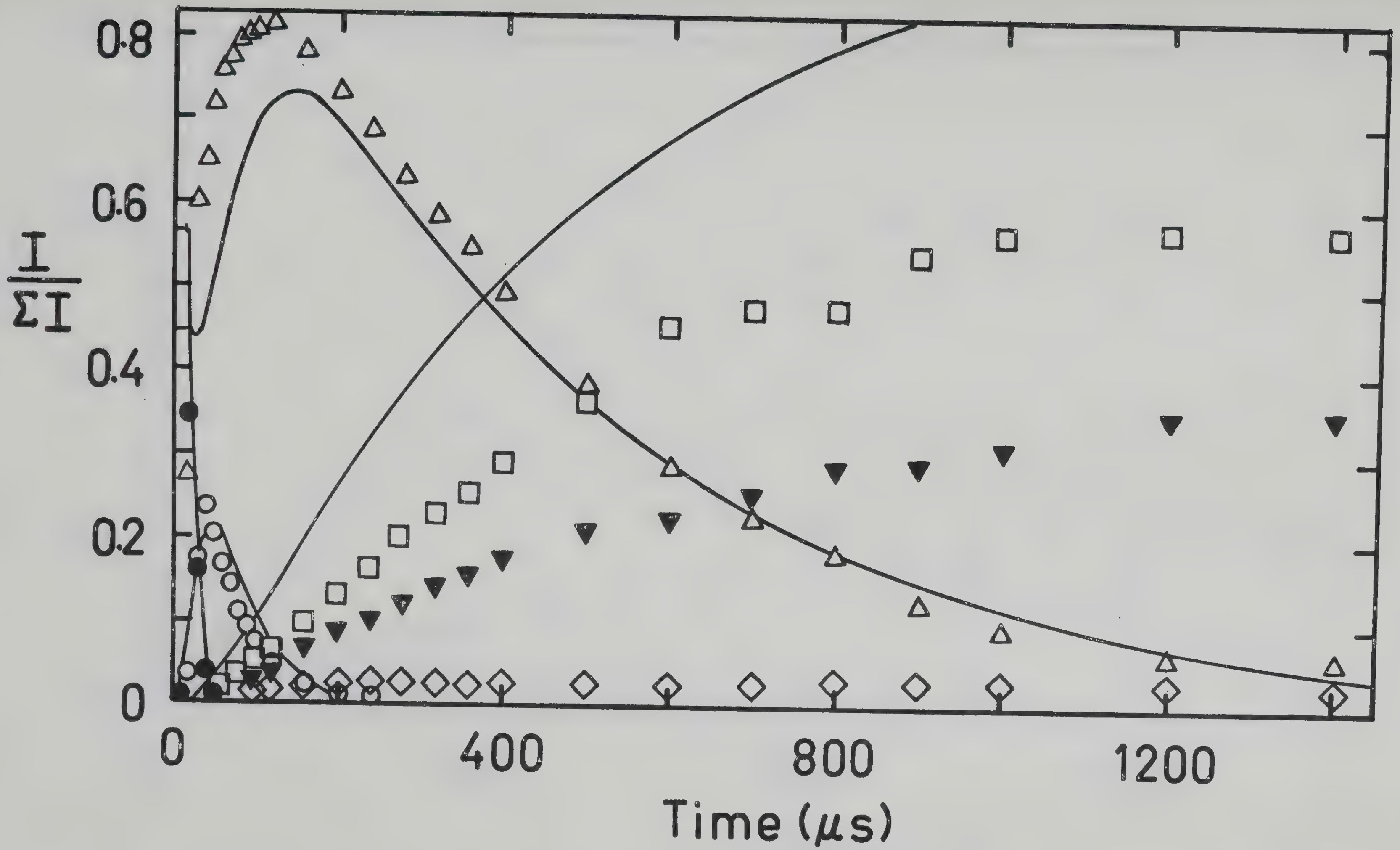

FIGURE 4.22. Time Dependence of Normalized Intensities. P_{CH_4} = 2.4 torr, $P_{C_2H_6}$ = 4.8 mtorr. $CH_4:C_2H_6$ = 500:1. T = 155°C. Symbols as in Figure 4.3.

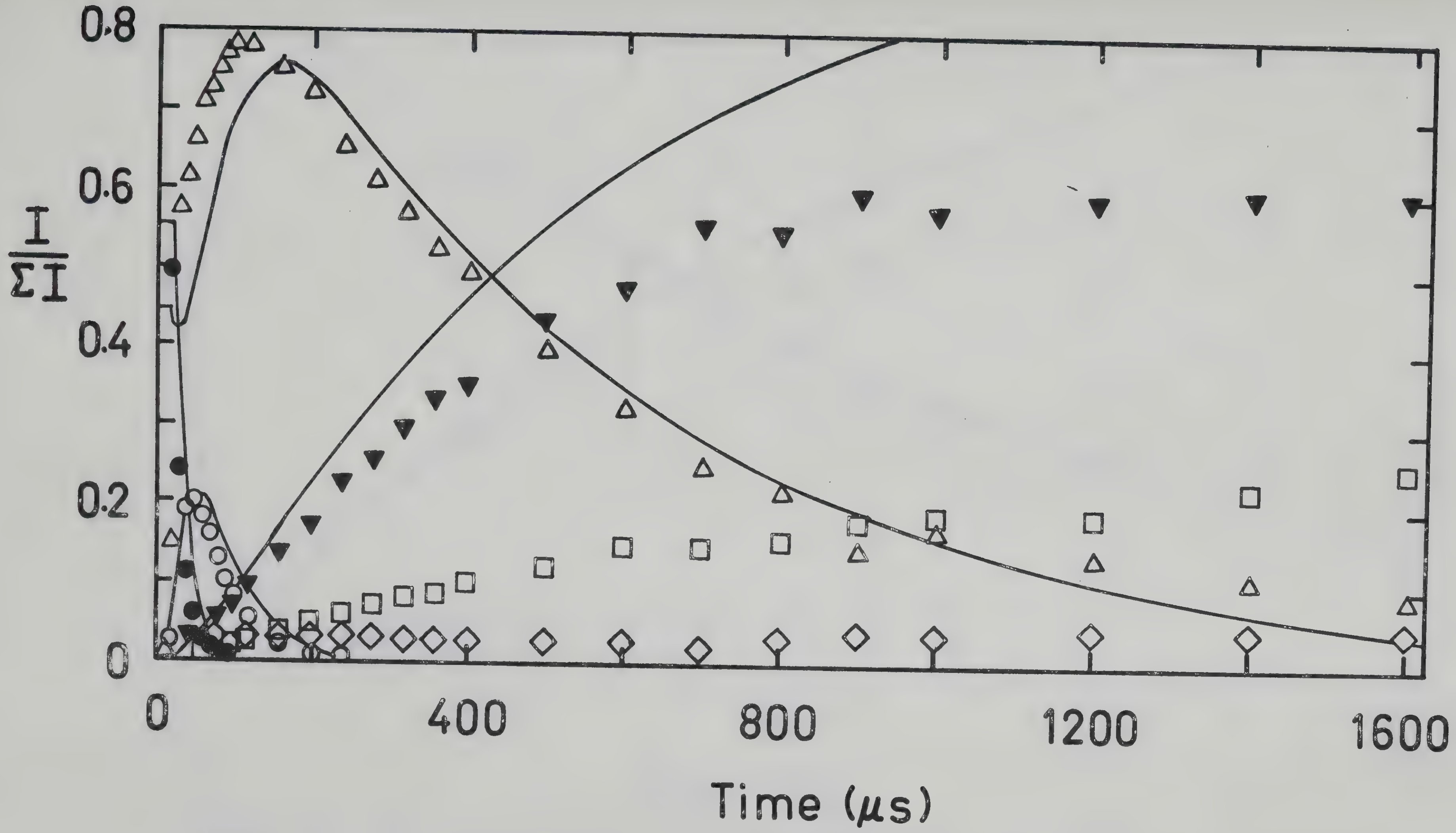

FIGURE 4.23. Time Dependence of Normalized Intensities. P_{CH_4} = 2.7 torr, $P_{C_2H_6}$ = 2.7 mtorr. $CH_4:C_2H_6$ = 1000:1. T = 157°C. Symbols as in Figure 4.3.

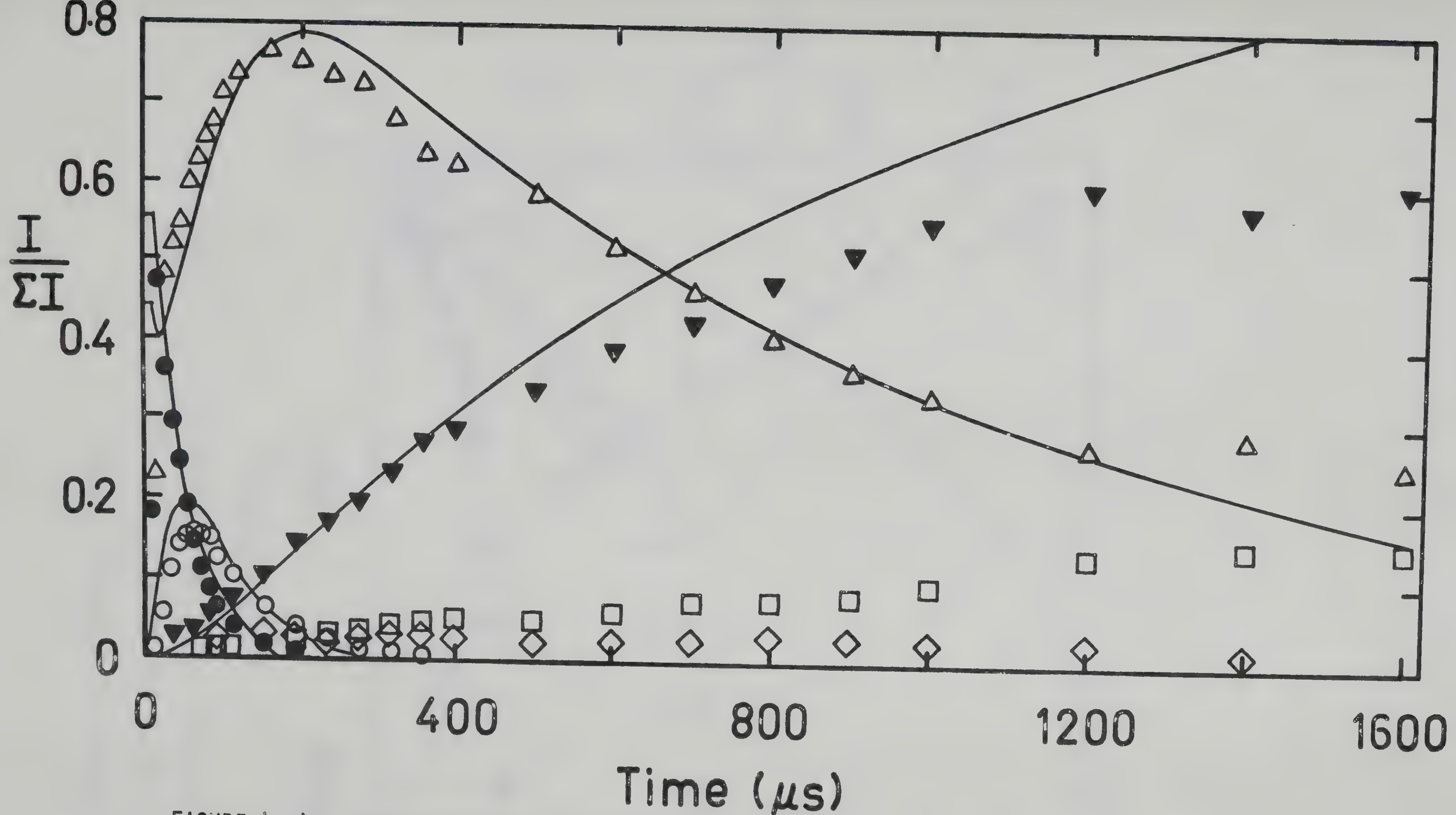

FIGURE 4.24. Time Dependence of Normalized Intensities. P_{CH_4} = 2.2 torr, $P_{C_2H_6}$ = 0.88 mtorr. CH_4:C_2H_6 = 2500:1. T = 157°C. Symbols as in Figure 4.3.

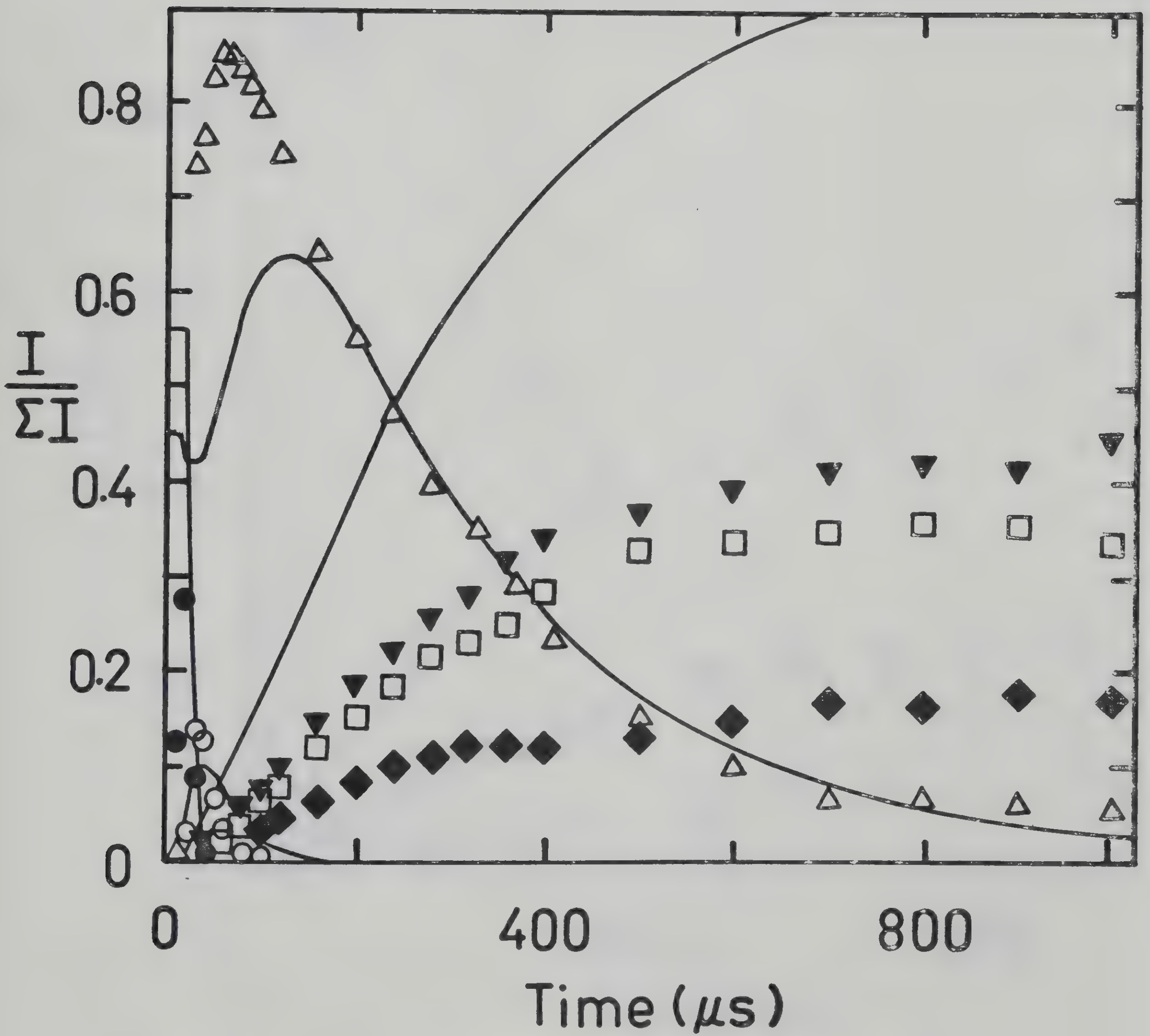

FIGURE 4.25. Time Dependence of Normalized Intensities.

P_{CH_4} = 2.5 torr, $P_{C_2H_6}$ = 10 mtorr. $CH_4:C_2H_6$ = 250:1. T = 209°C. Symbols as in Figure 4.3.

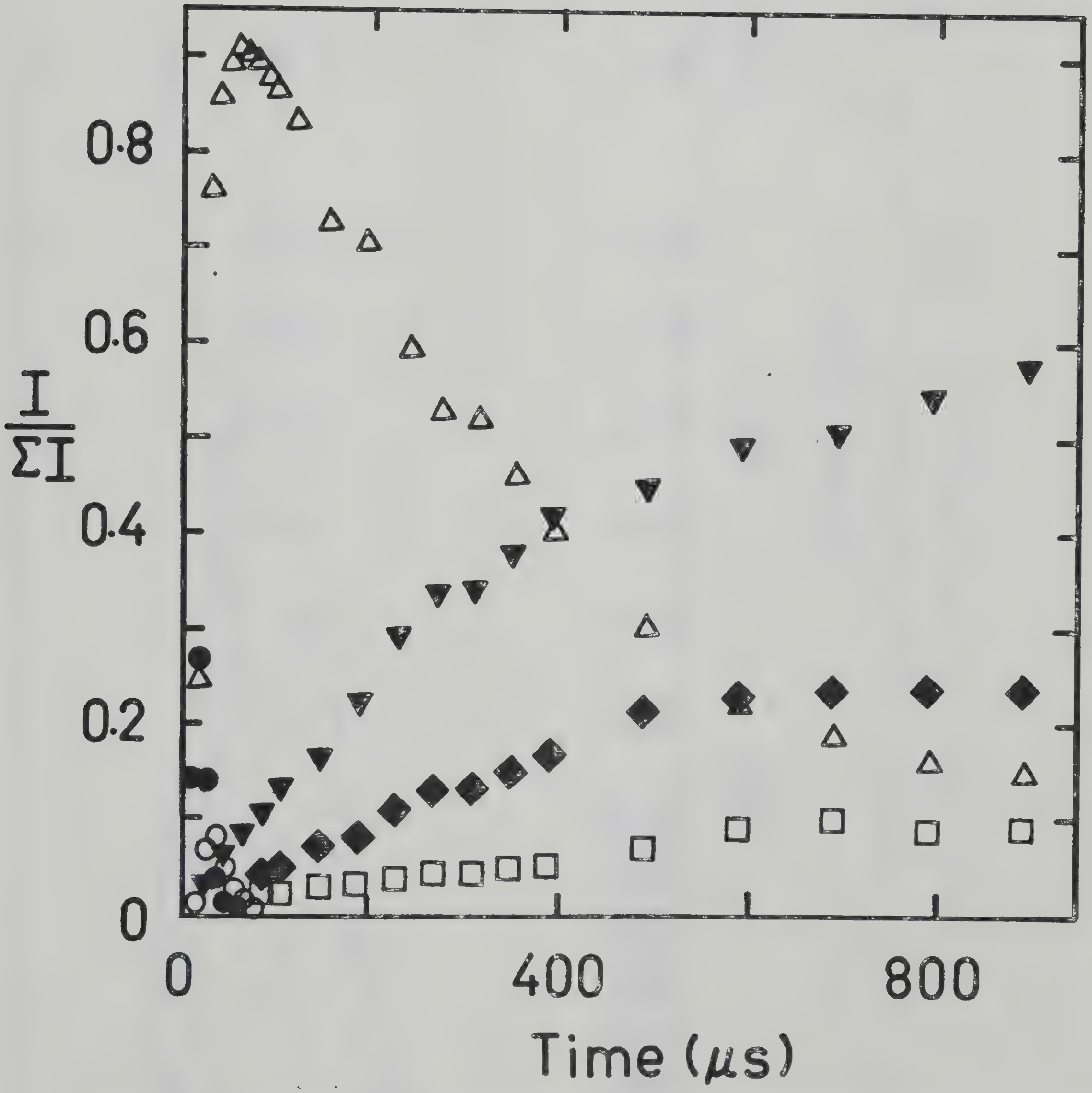

FIGURE 4.26. Time Dependence of Normalized Intensities.

P_{CH_4} = 2.7 torr, $P_{C_2H_6}$ = 5.4 mtorr. $CH_4:C_2H_6$ = 500:1. T = 210°C. Symbols as in Figure 4.3. CH_5^+ and $C_2H_7^+$ disappear too rapidly to be fitted.

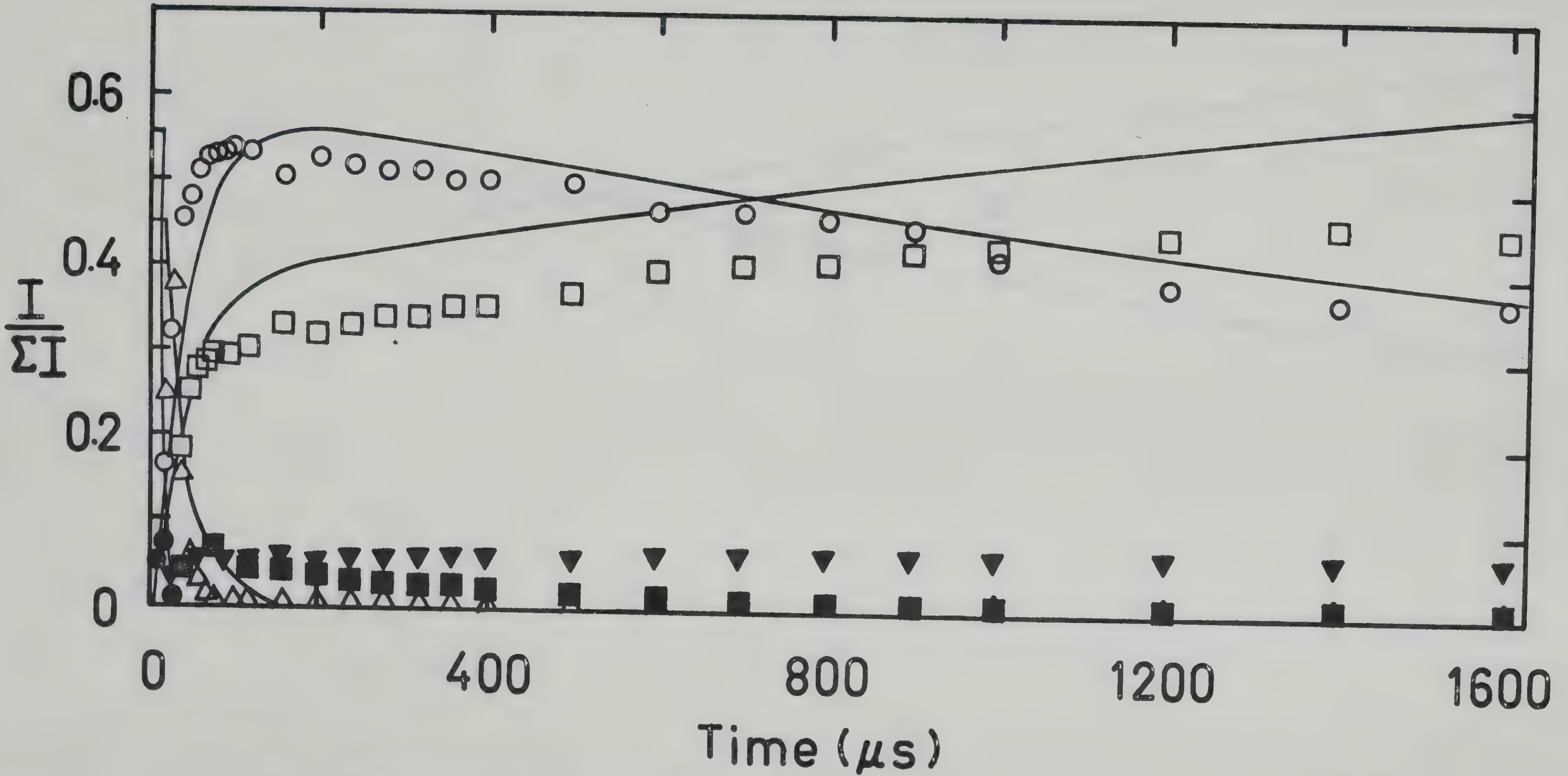

FIGURE 4.27. Time Dependence of Normalized Intensities. P_{CH_4} = 2.7 torr, $P_{C_2H_6}$ = 54 mtorr. $CH_4:C_2H_6$ = 50:1. T = 32°C. Symbols as in Figure 4.3.

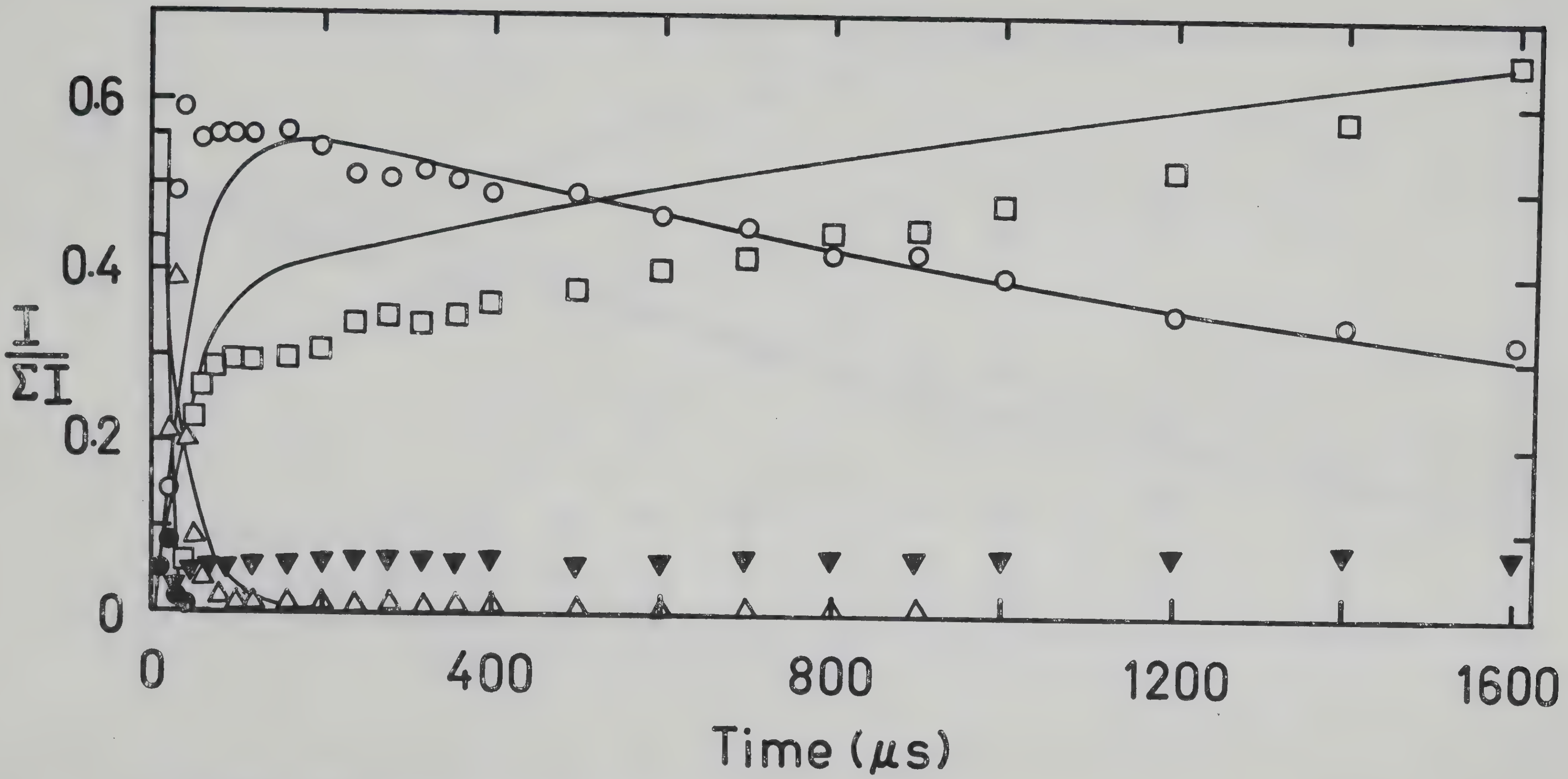

FIGURE 4.28. Time Dependence of Normalized Intensities. P_{CH_4} = 2.6 torr, $P_{C_2H_6}$ = 52 mtorr. $CH_4:C_2H_6$ = 50:1. T = 42°C. Symbols as in Figure 4.3.

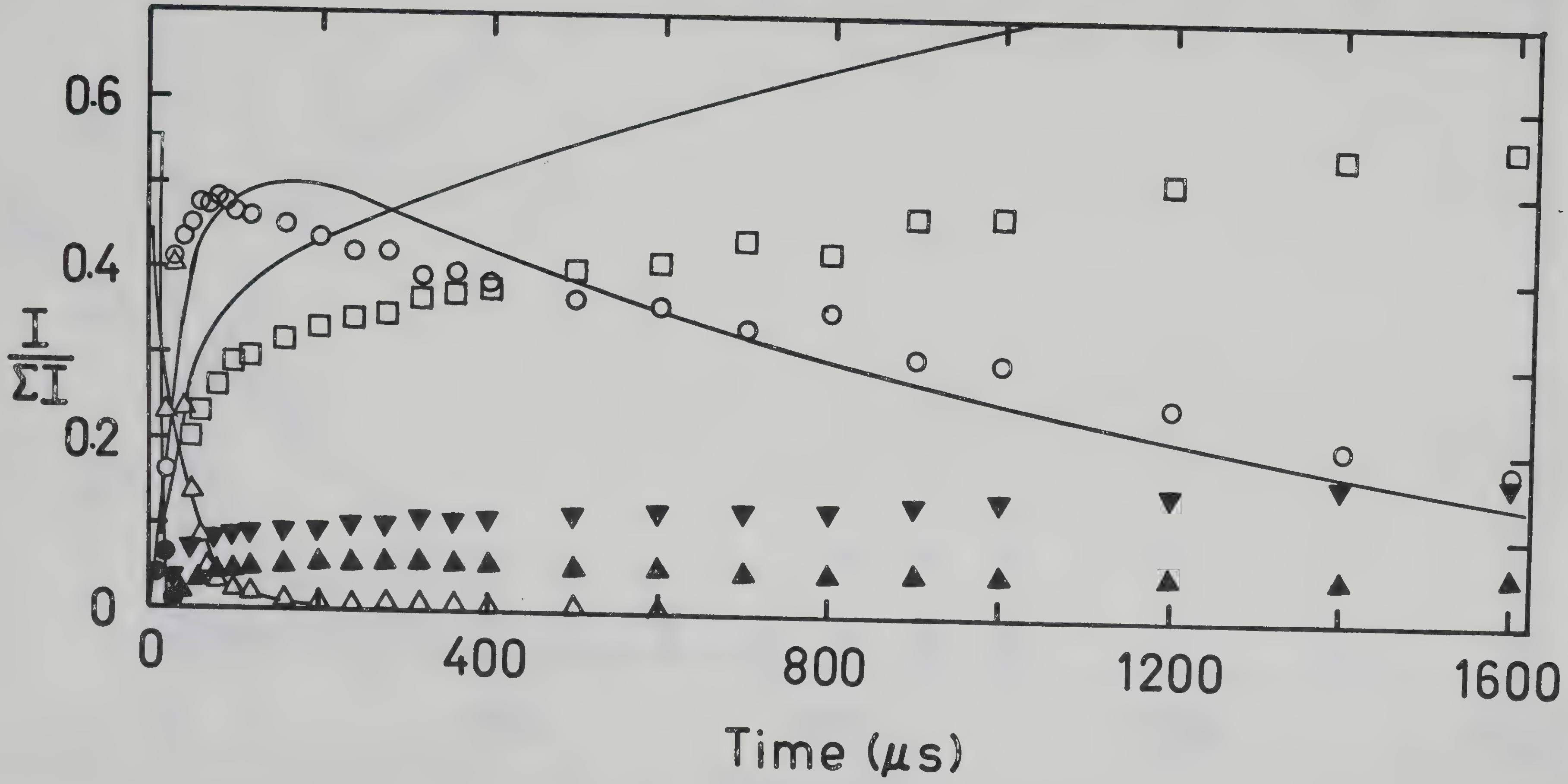

FIGURE 4.29. Time Dependence of Normalized Intensities. P_{CH_4} = 2.4 torr, $P_{C_2H_6}$ = 48 mtorr. CH_4:C_2H_6 = 50:1. T = 51°C. Symbols as in Figure 4.3.

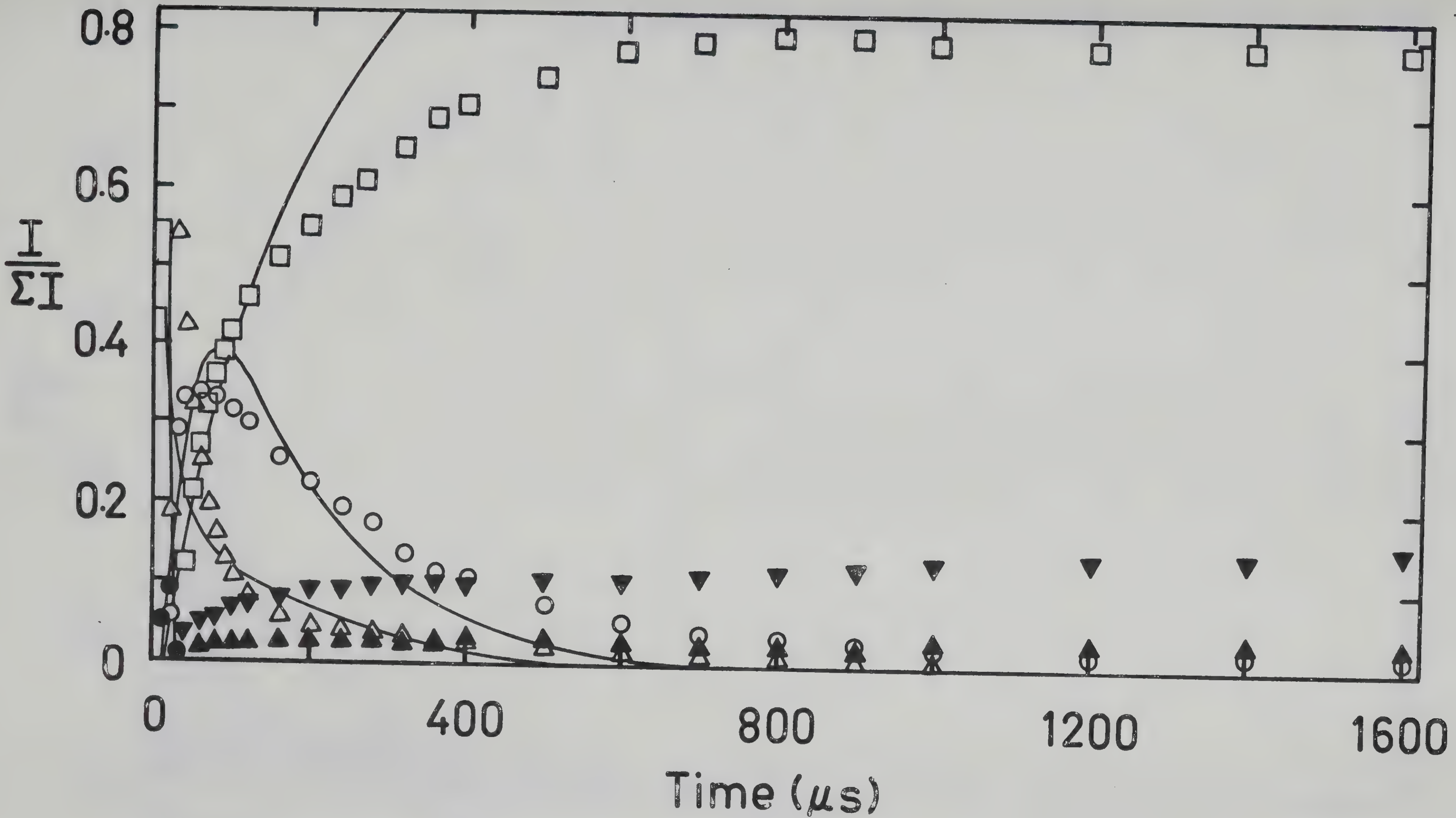

FIGURE 4.30. Time Dependence of Normalized Intensities. $P_{CH_4} = 2.6$ torr, $P_{C_2H_6} = 52$ mtorr. $CH_4:C_2H_6 = 50:1$. T = 97°C. Symbols as in Figure 4.3.

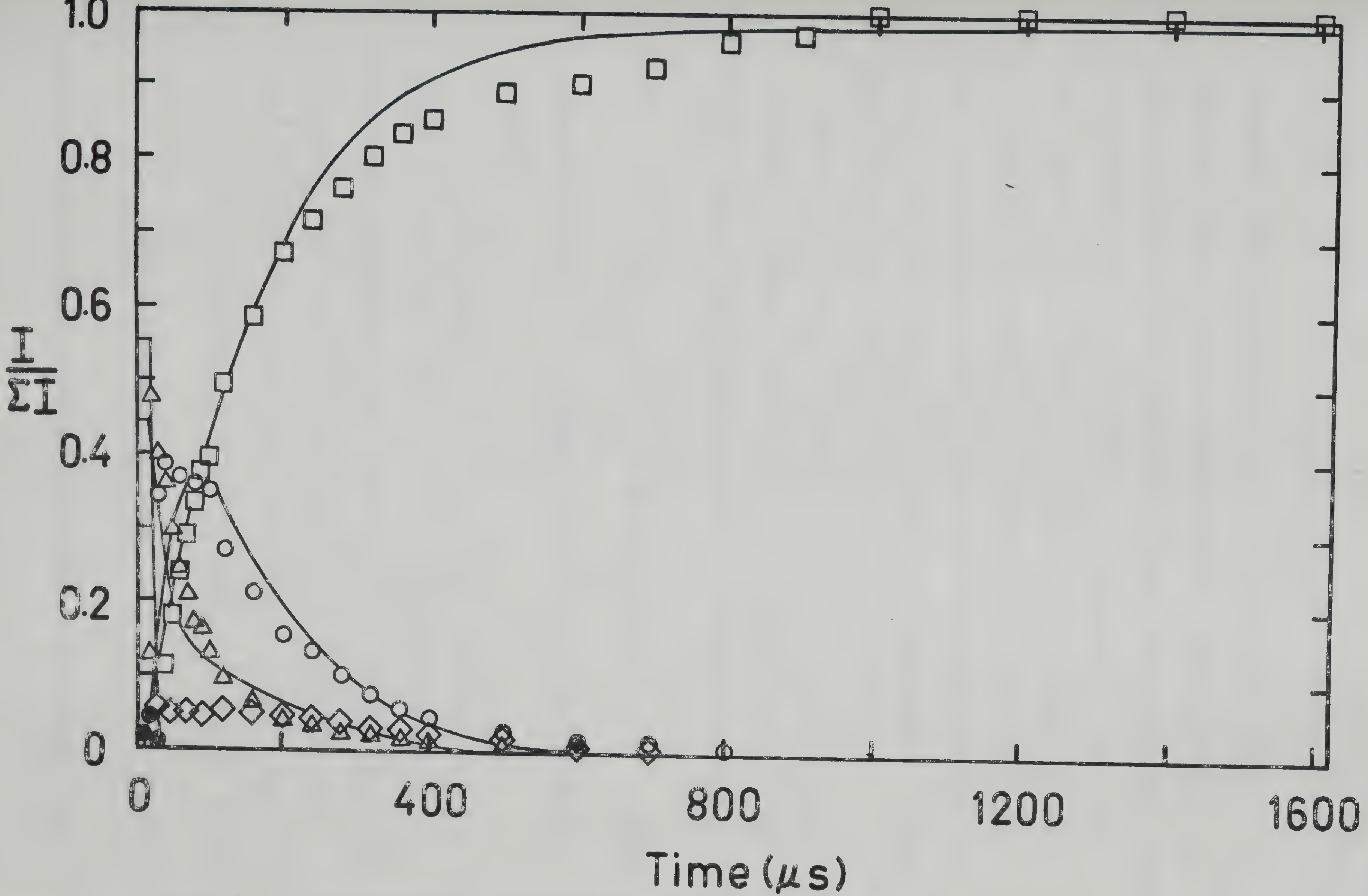

FIGURE 4.31. Time Dependence of Normalized Intensities. P_{CH_4} = 2.6 torr, $P_{C_2H_6}$ = 52 mtorr.

gradually decreasing the ethane concentration from a $CH_4:C_2H_6$ ratio of 500:1 to 500,000:1. Figure 4.9 to 4.14 were performed at 86°C and the ethane concentration is decreased from 500:1 to 50,000:1. Figures 4.15 to 4.21 show experiments at 110°C, Figures 4.22 to 4.24 at 156°C and Figures 4.25 and 4.26 at 210°C. A series of experiments were conducted at a constant high ethane concentration of 50:1 at gradually increasing temperatures. These experiments are shown in Figures 4.27 to 4.31.

The CH_5^+ produced by reaction (4.13) rapidly transfers a proton to ethane forming $C_2H_7^+$ by reaction (4.7). Figure 4.5 shows the intensity of CH_5^+ decreasing slowly

$$CH_5^+ + C_2H_6 \longrightarrow C_2H_7^+ + CH_4 \qquad (4.7)$$

accompanied by a simultaneous increase in the intensity of $C_2H_7^+$.

In the experiments at 30°C the $C_2H_7^+$ disappears very slowly (Figures 4.3 to 4.6) at all concentrations of ethane but disappears more rapidly as the temperature is increased. Figure 4.9 illustrates that the decay of $C_2H_7^+$ is followed closely by the decay of $C_2H_5^+$. $C_2H_7^+$ is therefore dissociating to give $C_2H_5^+$. Reaction (4.14)

$$C_2H_7^+ \longrightarrow C_2H_5^+ + H_2 \qquad (4.14)$$

has previously been reported in mixtures of methane and

ethane (38,123,129).

The $C_2H_5^+$ formed from reactions (4.12) and (4.14) reacts with ethane by reaction (4.15) but there are several

$$\begin{array}{lll} C_2H_5^+ + C_2H_6 \longrightarrow [C_4H_{11}^+]^* & \longrightarrow & C_4H_9^+ + H_2 \\ & \longrightarrow & C_3H_7^+ + CH_4 \\ & \xrightarrow{M} & C_4H_{11}^+ \end{array} \qquad (4.15)$$

products. The intermediate $[C_4H_{11}^+]^*$ ion may be stabilized by collision with a third body and was observed in these experiments as a minor product (for example see Figure 4.27), but only when the ethane concentration was high. At long reaction times the $C_4H_{11}^+$ intensity was usually about 2-3% of the total ionization. $C_4H_{11}^+$ has also been observed in pure ethane (130,131) and in mixtures of methane and ethane (131,132) . The formation of $C_4H_9^+$ and $C_3H_7^+$ will be discussed in detail later.

Other minor products observed were $C_2H_4^+$ and $C_4H_{10}^+$. At long reaction times $C_2H_4^+$ was normally less than 5% of the total ionization. $C_4H_{10}^+$ was only observed when the concentration of ethane was large.

Table IV includes the major reactions observed in the methane/ethane system.

4.4 Kinetics of the Reaction $CH_5^+ + C_2H_6 \longrightarrow C_2H_7^+ + CH_4$

The temporal profiles of the ion intensities shown

TABLE IV

Summary of Reactions in Mixtures of Ethane and Methane

	$CH_3^+ + CH_4 \longrightarrow C_2H_5^+ + H_2$	(4.12)
	$CH_4^+ + CH_4 \longrightarrow CH_5^+ + CH_3$	(4.13)
(1)	$CH_5^+ + C_2H_6 \longrightarrow C_2H_7$	(4.7)
(2)	$C_2H_7^+ \longrightarrow C_2H_5^+ + H_2$	(4.14)
(3)	$C_2H_5^+ + C_2H_6 \longrightarrow [C_4H_{11}^+]^* \longrightarrow C_4H_9^+ + H_2$ $\longrightarrow C_3H_7^+ + CH_4$ $\xrightarrow{M} C_4H_{11}^+$	(4.15)
(4)	$C_2H_5^+ + CH_4 \longrightarrow C_3H_7^+ + H_2$	(4.31)
(5)	$C_2H_4^+ + C_2H_6 \longrightarrow [C_4H_{10}^+]^* \longrightarrow C_3H_7^+ + CH_3$	(4.56)

in Figures 4.3 to 4.31 show that at high ethane concentration CH_5^+ disappears very rapidly accompanied by an increase in $C_2H_7^+$. As the ethane concentration is decreased the lifetime of CH_5^+ becomes longer. The forward rate constant, k_1 can be calculated for reaction (4.7)

$$CH_5^+ + C_2H_6 \xrightarrow{k_1} C_2H_7^+ + CH_4 \tag{4.7}$$

The forward rate constant for the general reaction

$$I^+ + A \xrightarrow{k_f} \text{products} \tag{4.16}$$

can be calculated from

$$\frac{d[I^+]}{dt} = -k_f[I^+][A] \tag{4.17}$$

where $[I^+]$ is the intensity of I^+ at time t. Since the concentration of ions is much less than the concentration of the neutrals, i.e. $[I^+]<<[A]$, the concentration of the neutrals can be considered as constant. Reaction (4.16) is therefore pseudo-first order and can be described by a pseudo-first order rate constant, ν_f, where

$$\nu_f = k_f[A] \tag{4.18}$$

Therefore

$$\frac{d[I^+]}{dt} = -\nu_f[I^+] \tag{4.19}$$

After rearrangement and integration

$$\ln \frac{[I^+]}{[I^+]_0} = -\nu_f t \qquad (4.20)$$

where $[I^+]_0$ is the concentration of I^+ at time $t = 0$. It is assumed that the measured intensity is proportional to the concentration of ions in the ion source. Therefore the logarithm of the normalized intensity of I^+ plotted versus time gives a straight line whose slope is equal to $-\nu_f/2.303$ or

$$\nu_f = \frac{-2.303 \log(I_2/I_1)}{t_2 - t_1} \qquad (4.21)$$

where I_1 is the intensity of the reactant ion at time t_1 and I_2 is the intensity of the reactant ion at time t_2. This method of calculating rate constants can only be used when the precursor of I^+ has disappeared completely so that I^+ is not being produced from the previous reaction.

The plots of log $I_{CH_5^+}$ versus time are shown in Figures 4.32 to 4.37 and demonstrate that as the ethane concentration is increased the rate of decay of CH_5^+ becomes faster. The pseudo-first order rate constants were calculated from the slopes of the semilogarithmic plots using equation (4.21). A plot of ν_1 measured at various ethane concentrations is shown in Figure 4.38. The plot shows a linear dependence and therefore

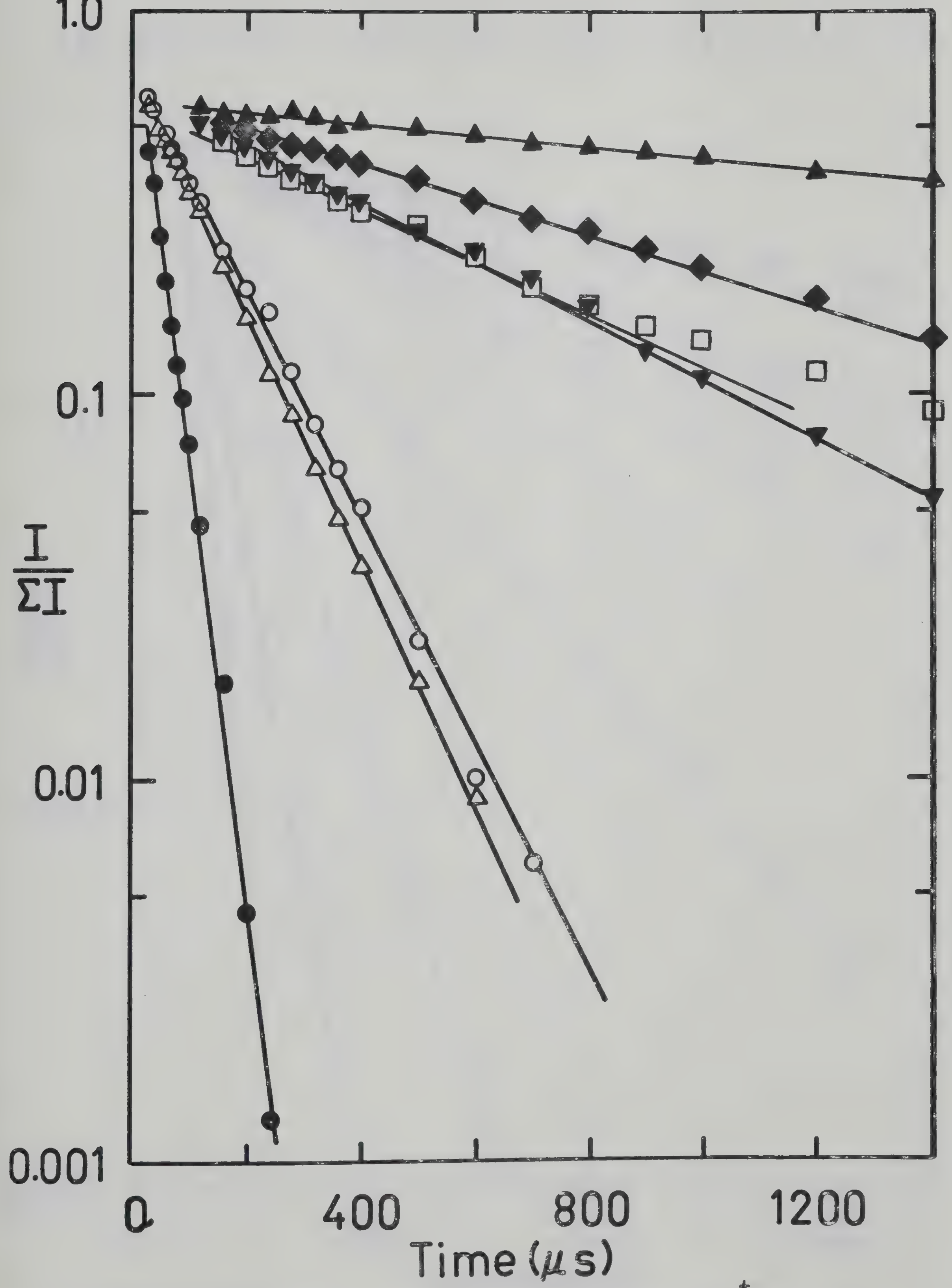

FIGURE 4.32. Logarithmic Plots of the Decay of CH_5^+ at 30°C. $CH_4:C_2H_6$, ● 5000:1, △ 20,000:1, ○ 20,000:1, ▼ 100,000:1, □ 100,000:1, ◆ 200,000:1, ▲ 500,000:1.

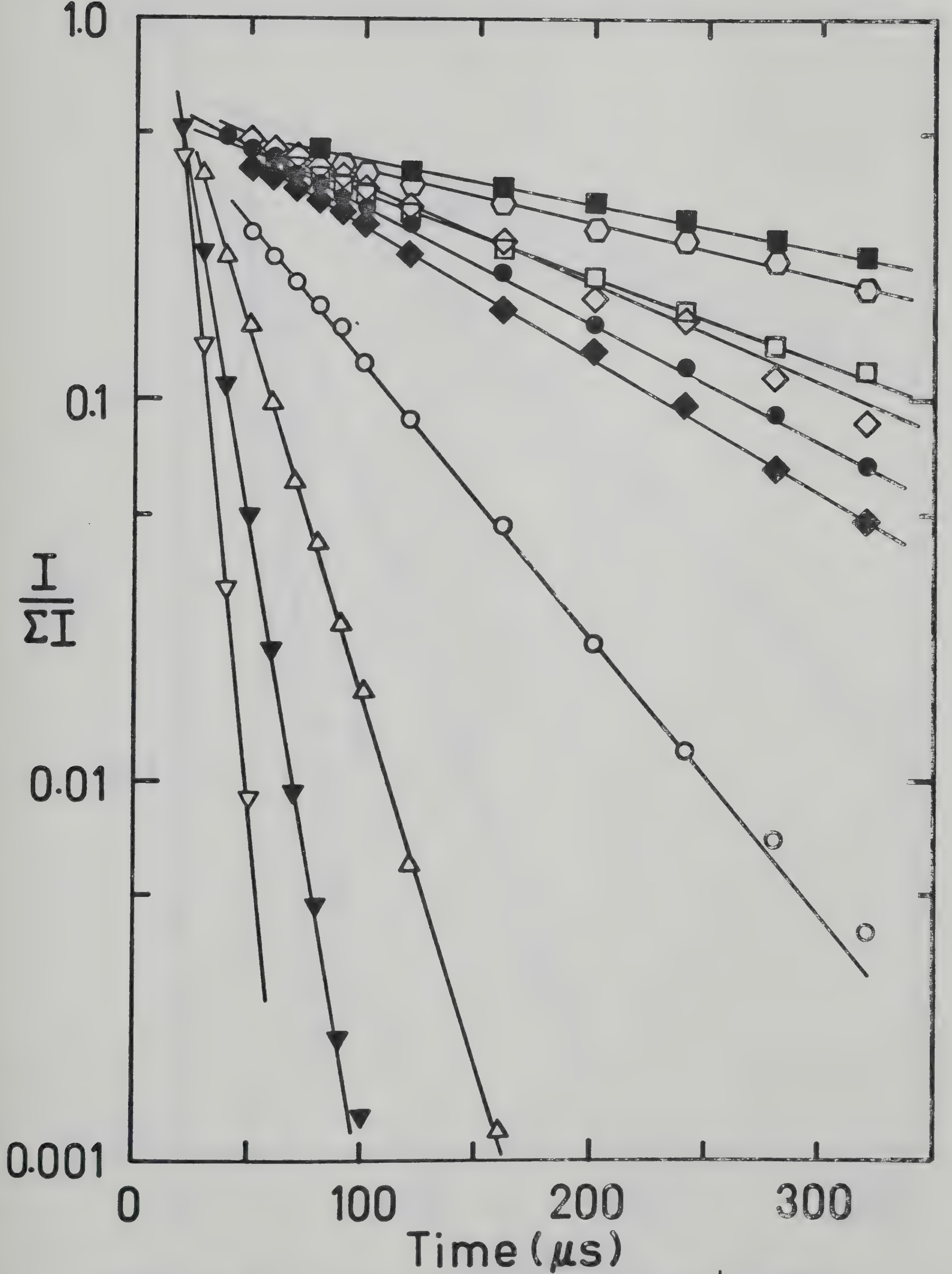

FIGURE 4.33. Logarithmic Plots of the Decay of CH_5^+ at 86°C. $CH_4:C_2H_6$ ▽ 500:1, ▼ 1000:1, △ 2500:1, ○ 5000:1, ◆ 10,000:1, ● 10,000:1, ◇ 20,000:1, ⬡ 50,000:1, ■ 20,000:1.

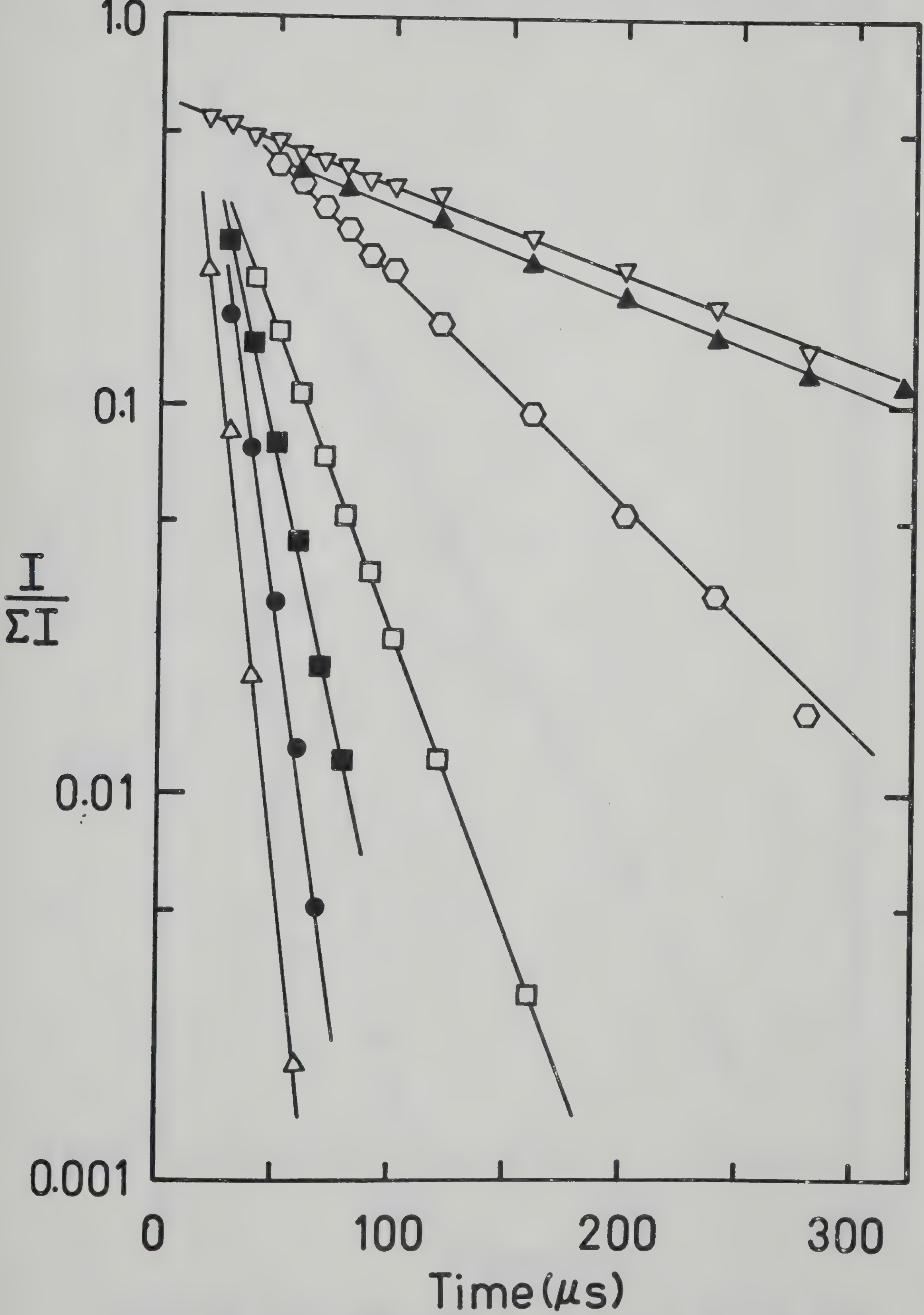

FIGURE 4.34. Logarithmic Plots of the Decay of CH_5^+ at 106°C. $CH_4:C_2H_6$, △ 1000:1, ● 1700:1, ■ 900:1, □ 5000:1, ⬡ 12,000:1, ▲ 800:1, ▽ 10,000:1.

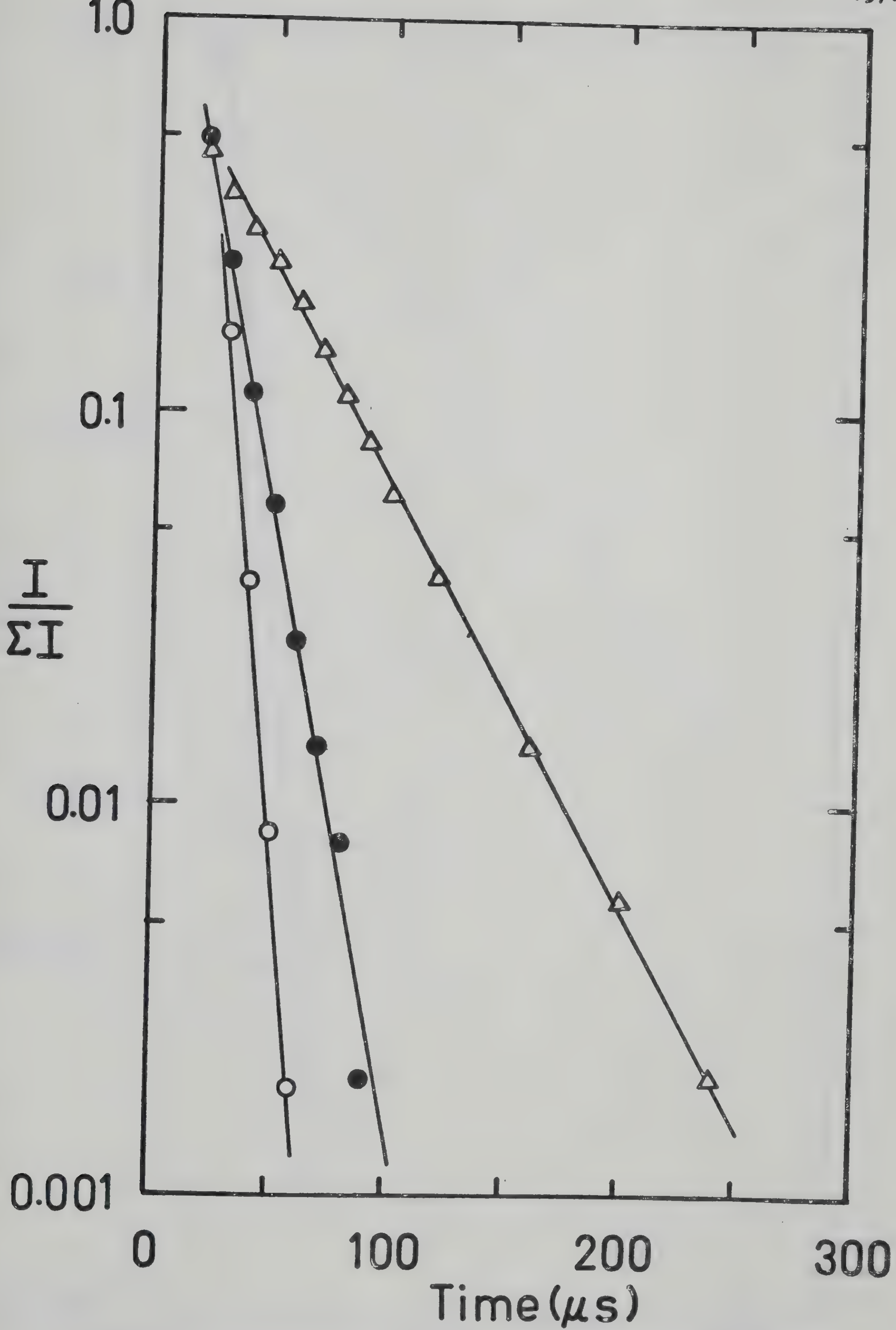

FIGURE 4.35. Logarithmic Plots of the Decay of CH_5^+ at 156°C. $CH_4:C_2H_6$, ○ 500:1, ● 1000:1, △ 2500:1.

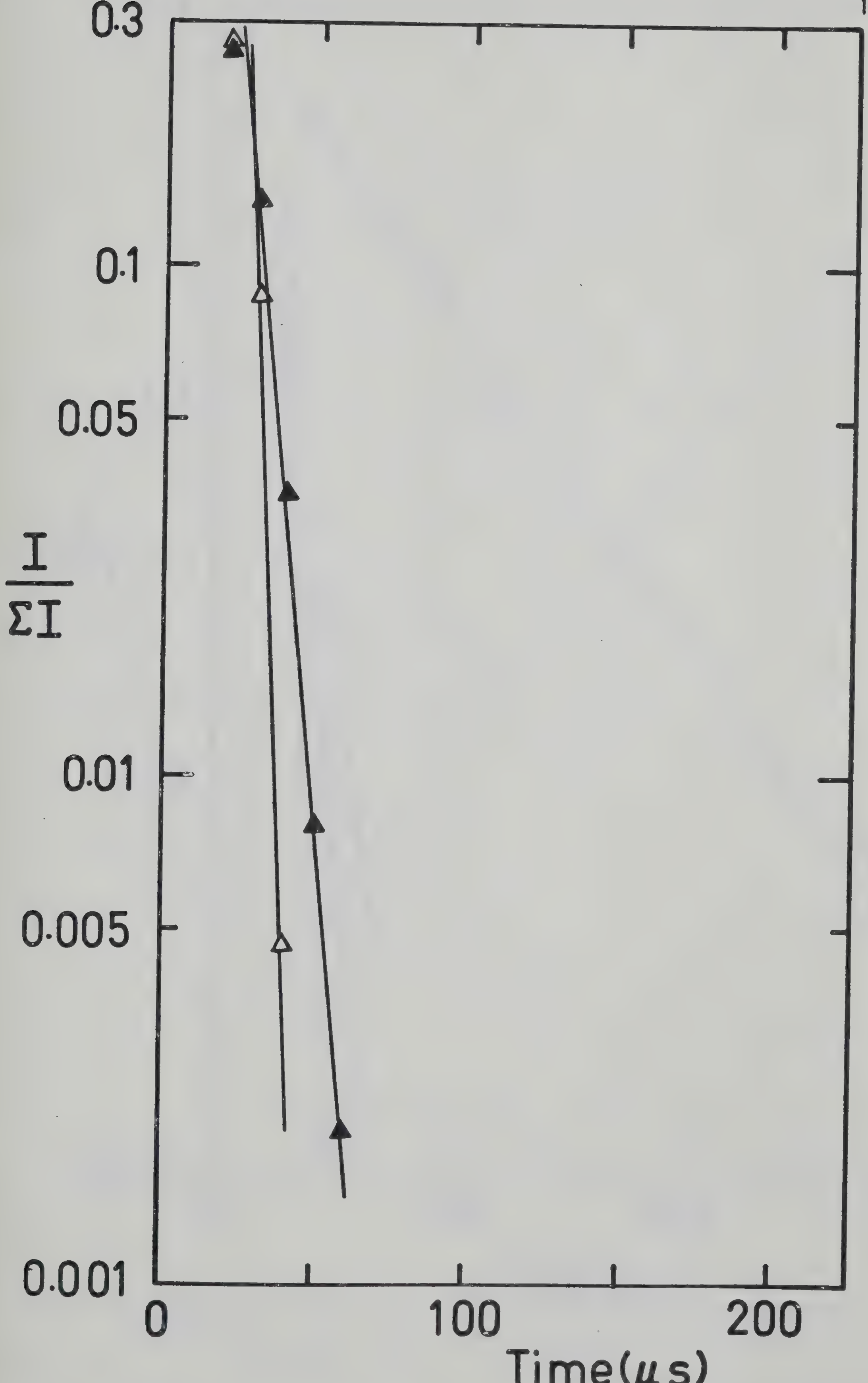

FIGURE 4.36. Logarithmic Plots of the Decay of CH_5^+ at 211°C.

CH_4:C_2H_6, △ 250:1, ▲ 500:1.

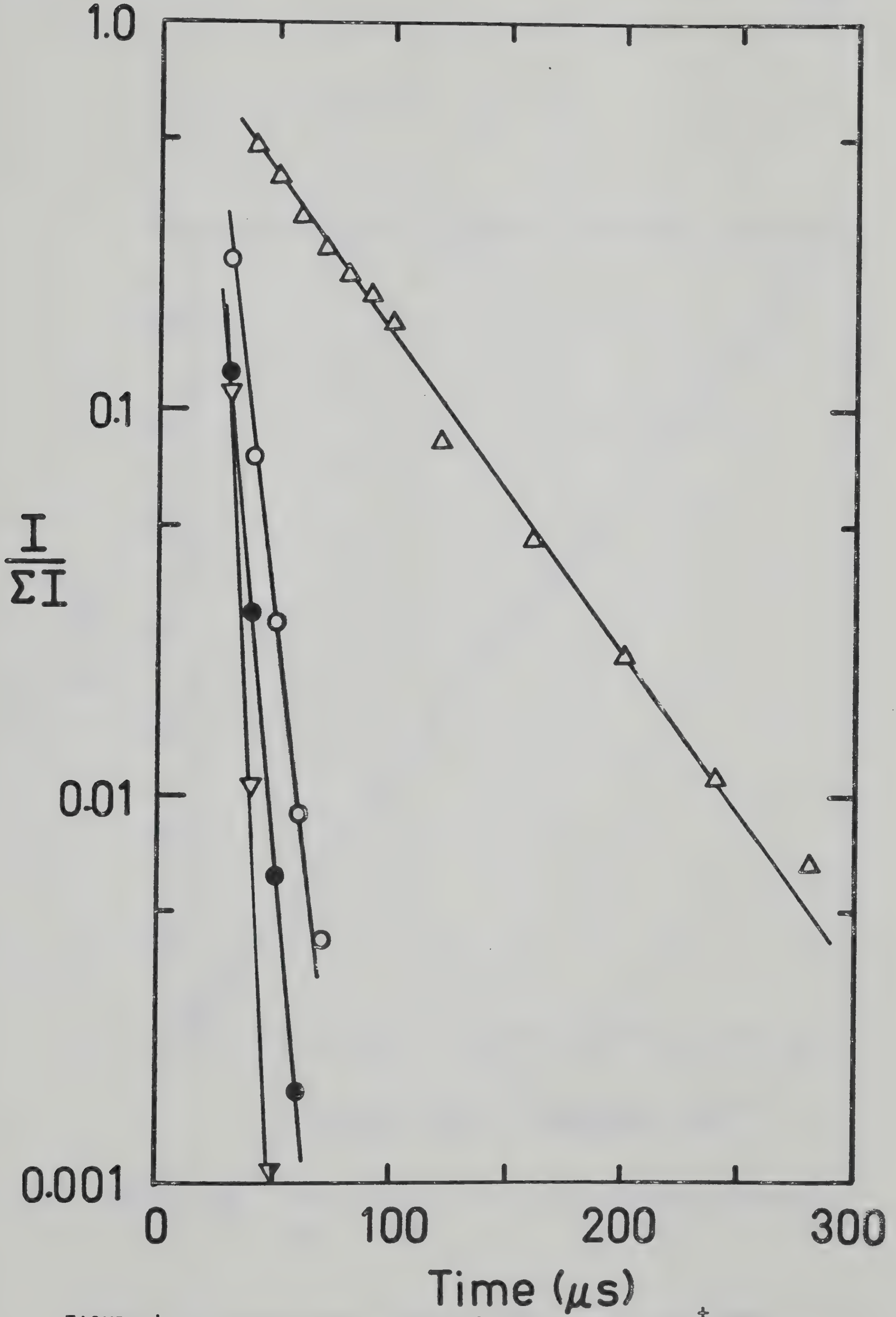

FIGURE 4.37. Logarithmic Plots of the Decay of CH_5^+ When $CH_4:C_2H_6$ = 500:1. T = ● 32°C, ○ 49°C, △ 74°C, ▽ 96°C.

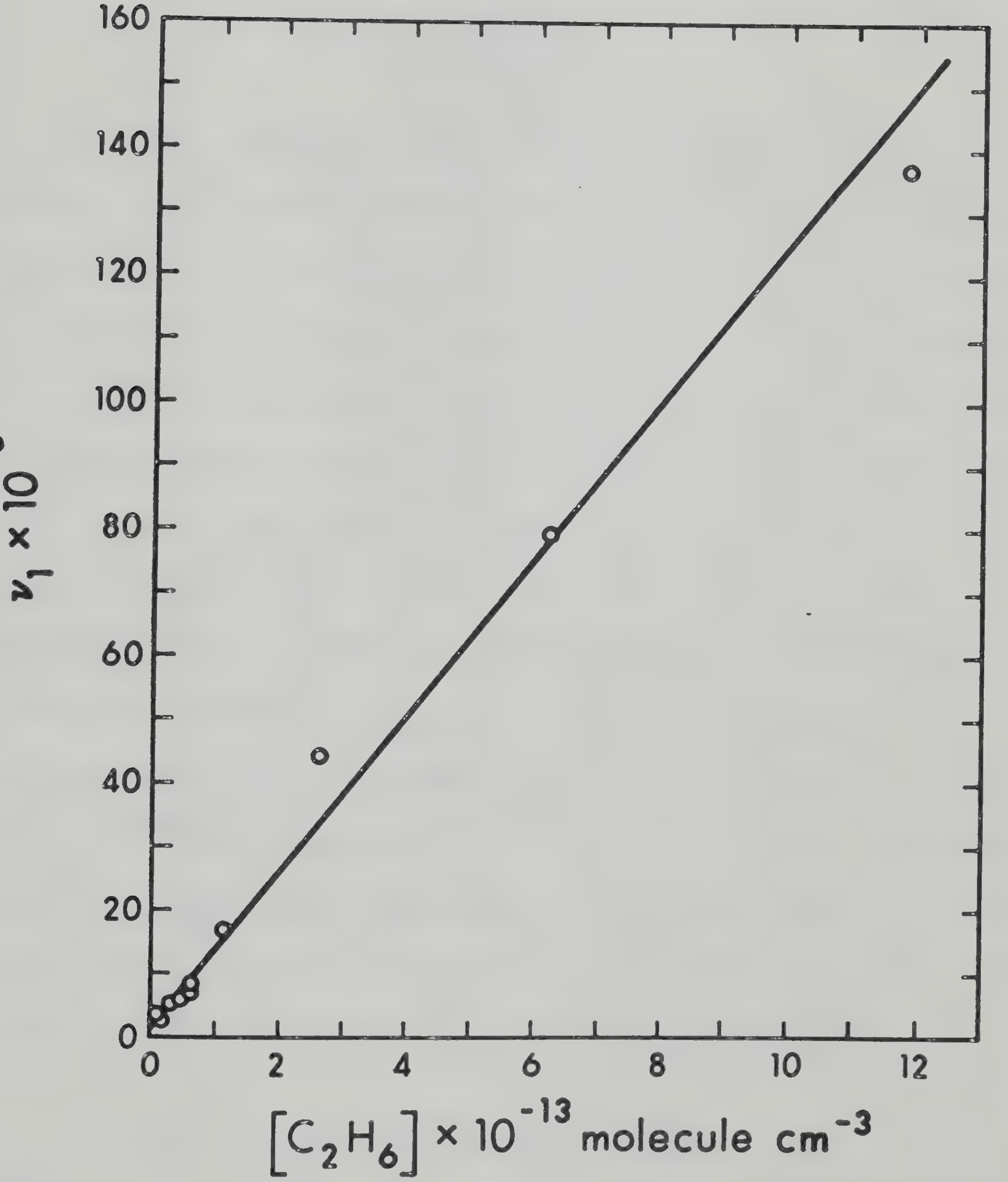

FIGURE 4.38. Plot of ν_1 as a Function of Ethane Concentration.

reaction (4.7) is second order and the rate constant for this reaction is given by

$$k_1 = \frac{\nu_1}{[C_2H_6]} \qquad (4.22)$$

The rate constants for reaction (4.7) were not calculated at high ethane concentration because CH_5^+ disappeared within 40 μsec and therefore the decay of CH_5^+ was too fast to obtain a meaningful rate constant from the slope. Table V summarizes the rate constants calculated under different concentration and temperature conditions. The rate constant k_1 for reaction (4.7) does not appear to be affected by temperature within the error limits of the determination of k_1. Over the temperature range studied, the average value of k_1 was $1.6 \pm 0.4 \times 10^{-9}$ cm^3 molecule^{-1} s^{-1}. Munson and Field (38) estimated the rate constant k_1 to be about 6×10^{-9} cm^3 molecule^{-1} s^{-1} at 210°C. Blair, Heslin and Harrison (129) have measured the rate constant for the deuteron transfer in the similar reaction (4.23) to be 1.1×10^{-9} cm^3 molecule^{-1} s^{-1}. These reported rate

$$CD_5^+ + C_2H_6 \longrightarrow C_2H_6D^+ + CD_4 \qquad (4.23)$$

constants are in good agreement with the present work.

Not many experiments have been reported where the proton transfer rate constants have been measured at different temperatures. The Langevin theory (15) predicts

TABLE V

Summary of Rate Constants Obtained for the Reaction

$CH_5^+ + C_2H_6 = C_2H_7^+ + CH_4$

$\frac{[CH_4]}{[C_2H_6]}$	$k_1 \times 10^9$ cm^3 $molecule^{-1}$ sec^{-1}					
	30°C	86°C	97°C	106°C	156°C	210°C
250				1.1		1.5
500	1.0	1.4(2)[a]	1.6		1.4	1.3
900				1.3(2)		
1000		1.3		1.7(2)		1.2
1250				1.6		
1650				1.8		
2500		1.7			1.3	
5000	1.8	1.5		2.2		
10,000		1.3(2)		0.7		
12,000				2.1		
20,000		1.7(3)				
50,000		2.7				
100,000	2.2					
No. of experiments	3	11	1	10	2	3
Average	1.7 ± 0.6[b]	1.6 ± 0.4	1.6	1.6 ± 0.5	1.4	1.4 ± 0.2

[a] Number in brackets refers to number of experiments conducted at these conditions if greater than 1.

[b] Standard deviation

that there is no activation energy and hence to temperature dependence for ion-molecule reactions. Bohme (54) has reported that the rate constant for reaction (4.24) is independent of temperature. However, Pierce and Porter

$$N_2OH^+ + CO \longrightarrow HCO^+ + N_2O \qquad (4.24)$$

(133) have reported a proton transfer reaction (4.25) where the rate constant depends on T^{-6}.

$$CH_4D^+ + CH_4 \longrightarrow CH_5^+ + CH_3D \qquad (4.25)$$

4.5 The Equilibrium $CH_5^+ + C_2H_6 \rightleftharpoons C_2H_7^+ + CH_4$

The kinetics of reaction (4.7) were relatively simple to calculate, but the measurement and calculation of the equilibrium constant were much more difficult. The ion profiles for a series of experiments at one temperature, e.g. Figures 4.3 to 4.7, show that CH_5^+ disappears very rapidly to give $C_2H_7^+$ when the ethane concentration is high. As the ratio of methane to ethane is increased, CH_5^+ decays more slowly. However, even at the highest dilution ratios of $[CH_4]:[C_2H_6] = 500{,}000:1$, proton transfer from CH_5^+ to C_2H_6 is still occurring over the total period of observation. These ions do not reach equilibrium even at long reaction times. The analog computer fits discussed in Section 4.9 show that for most of

the experiments a very slow forward reaction was sufficient to describe the disappearance of CH_5^+ and that the reverse reaction was negligible.

Since equilibrium could not be achieved in reaction (4.7), several methods were employed to obtain estimates of the equilibrium constant. The equilibrium constant K_1 for reaction (4.7) may be expressed by equation (4.26).

$$CH_5^+ + C_2H_6 \rightleftharpoons C_2H_7^+ + CH_4 \qquad (4.7)$$

$$K_1 = \frac{I_{C_2H_7^+} \cdot P_{CH_4}}{I_{CH_5^+} \cdot P_{C_2H_6}} \qquad (4.26)$$

where $I_{C_2H_7^+}$ and $I_{CH_5^+}$ are the intensities of the ions at equilibrium. Since $I_{C_2H_7^+}/I_{CH_5^+}$ did not reach a constant value, the ratio of the two ions was taken when CH_5 was just approaching zero or at the longest reaction time, which was 1800 μs. The equilibrium constants are shown in Table VI for six experiments at low ethane concentrations. The average value of K_1 was 1.5×10^6. This value for the equilibrium constant represents a lower limit since equilibrium is not yet achieved. The average value of K_1 found by Chong and Franklin (123) was 4.9 at 67°C which corresponds to $K_1 \approx 6$ at 30°C,

TABLE VI

Calculated Equilibrium Constants at 30°C

$\frac{[CH_4]}{[C_2H_6]}$	K_1	K_1'
5000	1.8×10^6	-
20,000	4.8×10^6	6.9×10^5
20,000	3.3×10^5	4.4×10^5
100,000	5.8×10^5	2.8×10^5
200,000	1.0×10^6	1.6×10^6
500,000	2.5×10^5	7.7×10^5
Average	1.5×10^6	6.4×10^5
$-\Delta G^o$(kcalmol)	8.7 ± 1[a]	8.1 ± 1

[a] Standard deviation

assuming $\Delta S \approx 0$. Therefore the lower limit of K_1 from the present work is six orders of magnitude greater than Franklin's value!

From equation (4.27), $\Delta G_1^o = -8.7 \pm 1$ kcal/mol, using

$$\Delta G_1^o = -RT \ln K_1 \qquad (4.27)$$

the average K_1 at 30°C. Assuming $\Delta S_1^o \approx 0$, $\Delta H_1^o = -8.7$ kcal/mol and thus the lower limit of the proton affinity difference between methane and ethane is 8.7 kcal/mol.

The second method that may be used to calculate the equilibrium constant utilizes the measurement of the forward and reverse rate constants of reaction (4.7).

$$CH_5^+ + C_2H_6 \underset{k_{-1}}{\overset{k_1}{\rightleftharpoons}} C_2H_7^+ + CH_4 \qquad (4.7)$$

since

$$K_1' = \frac{k_1}{k_{-1}} \qquad (4.28)$$

The rate constant k_1 was calculated from the semilogarithmic plots shown in Figures 4.32 to 4.37. If reaction (4.7) is reversible, the rate of the reverse reaction only becomes apparent at long reaction times when the product ion has grown appreciably. The reverse reaction can be detected by

a non-linearity at long reaction times in the semilogarithmic plots as the apparent forward rate decreases due to the reverse reaction. For the general first order reaction (4.29)

$$I^+ \underset{\nu_{-1}}{\overset{\nu_1}{\rightleftharpoons}} P^+ \qquad (4.29)$$

the rate equation is

$$\frac{d[I^+]}{dt} = -\nu_1[I^+] + \nu_{-1}[P^+] \qquad (4.30).$$

The solution of equation (4.30) is

$$\ln(I^+ - I_e^+) = -(\nu_1 - \nu_{-1})t + \text{constant} \qquad (4.31)$$

where I^+ is the intensity of the reactant ion at time t and I_e^+ is the intensity of I^+ at equilibrium. Therefore a plot of $\ln(I^+ - I_e^+)$ versus time yields a straight line of slope $-(\nu_1 + \nu_{-1})$. Figure 4.39 shows such plots for the decay of CH_5^+ for five experiments at 30°C. The blank symbols represent the original normalized data points and the deviation from the straight line can be seen at long reaction times. The values of ν_1 for each experiment were calculated from the initial slope in Figure 4.32 before the reverse reaction could cause deviation from the straight line. A value of I_e was then chosen and subtracted from the

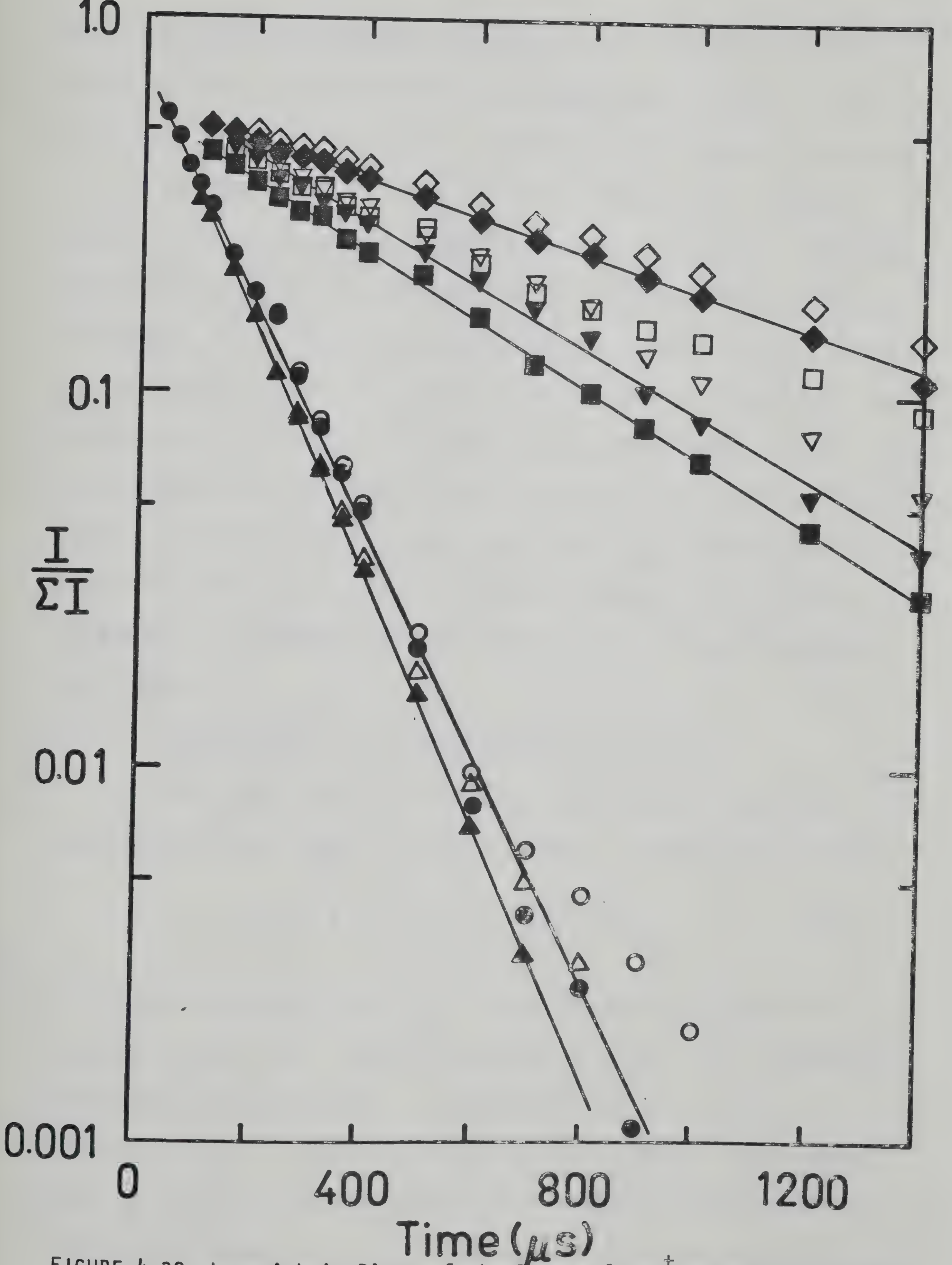

FIGURE 4.39. Logarithmic Plots of the Decay of CH_5^+ at 30°C. ○ Original data, ● data corrected for reverse reaction.

original data such that a straight line fitted all the solid points. The recalculated slope gave $-(\nu_1 + \nu_{-1})$, from which ν_{-1} and thus K_1' could be calculated. The equilibrium constants K_1' found by this method are listed in Table VI. The resultant lower limit of the proton affinity difference using this method was 8.1 ± 1 kcal/mol. The two estimates of K_1 therefore agree within their error limits.

The equilibrium constant of exothermic reactions decreases with increase in temperature, therefore studies at higher temperatures would seem feasible to obtain more accurate estimates of K_1 since the CH_4:C_2H_6 ratio could be lowered. However, as will be shown later, $C_2H_7^+$ slowly disappears by thermal decomposition thus disturbing the equilibrium.

4.6 The Kinetics of the Reactions of $C_2H_5^+$

The $C_2H_5^+$ ion is initially produced by the fast reaction (4.12), which is well known. Figure 4.13 shows

$$CH_3^+ + CH_4 \longrightarrow C_2H_5^+ + H_2 \qquad (4.12)$$

the rapid formation of $C_2H_5^+$, whose intensity reaches a maximum by 30 μsec. The intensity of $C_2H_5^+$ then starts to decay but after 60 μsec it increases again to reach a second maximum. This can only be explained by the production of $C_2H_5^+$ by a slow reaction. Figure 4.15 shows that the rate of decay of $C_2H_5^+$ is similar to that of $C_2H_7^+$.

$C_2H_7^+$ must therefore be the precursor of $C_2H_5^+$ via reaction (4.14). The double maximum of the $C_2H_5^+$ intensity was at

$$C_2H_7^+ \longrightarrow C_2H_5^+ + H_2 \qquad (4.14)$$

first thought to be an artifact of the normalization procedure but it was reproduced by the computer fit and can be explained by the occurrence of reactions (4.12) and (4.14).

If experiments at one temperature are examined, Figures 4.8 to 4.14 at 86°C, for example, it may be seen that as the ethane concentration is changed, the relative intensities of $C_4H_9^+$ and $C_3H_7^+$ also change. At high ethane concentrations, e.g. $[CH_4]:[C_2H_6] = 50:1$, $C_4H_9^+$ is much more abundant at long reaction times than $C_3H_7^+$. However, as the ethane concentration is lowered the amount of $C_4H_9^+$ decreases and $C_3H_7^+$ increases, until at the lowest ethane concentrations $C_3H_7^+$ is much larger than $C_4H_9^+$. The change is illustrated in Table VII, where the intensity ratio $C_3H_7^+/C_4H_9^+$ changes by a factor of 30 as the pressure of ethane varies by a factor of 100. The dependence of the relative intensities of $C_3H_7^+$ and $C_4H_9^+$ on the ethane concentration was also observed by Bennett et al (131) in mixtures of methane and ethane. These workers also found that $C_3H_7^+$ was more abundant than $C_4H_9^+$ at low ethane concentrations.

TABLE VII

Relative Intensities of $C_3H_7^+$ and $C_4H_9^+$ at 86°C

$[CH_4]/[C_2H_6]$	$I_{C_3H_7^+}$ at 1800 µsec
500:1	0.4
1000:1	0.9
2500:1	3.7
5000:1	3.8
10,000:1	8.4
20,000:1	12.6
50,000:1	12.1

If $C_2H_5^+$ reacts only via the intermediate $[C_4H_{11}^+]^*$ then it would be expected that the ratio $I_{C_3H_7^+}/I_{C_4H_9^+}$ would remain approximately the same, independent of the ethane concentration used, since the lifetime of the intermediate would depend on the total pressure in the ion source.

The gradual change in the relative abundance of $C_3H_7^+$ and $C_4H_9^+$ can be explained by a slow reaction of $C_2H_5^+$ with methane to give $C_3H_7^+$. If reaction (4.31) is

$$C_2H_5^+ + CH_4 \xrightarrow{k_4} C_3H_7^+ + H_2 \qquad (4.31)$$

very slow then it will only be observed at low ethane concentrations when reaction (4.15) is negligible. Recently the occurrence of the slow reaction (4.31) was observed in pure methane in our laboratory by Hiraoka and Kebarle (134). The present observation is therefore a confirmation of this finding. The occurrence of reaction (4.31) was not proven conclusively until Hiraoka's report even though ion-molecule reactions in pure methane have been studied extensively. Field and Munson (37) have estimated that $C_2H_5^+$ does not react with methane within 50 to 100 collisions, which was unexpected because reaction (4.31) is exothermic by 9 kcal/mol. Previous work in this laboratory set a lower limit of $k_4 < 10^{-15}$ cm^3 molecule^{-1} s^{-1} (132). The late discovery of reaction (4.31) can be understood when one considers that

most exothermic ion-molecule reactions, whose rates have been measured, proceed with rate constants close to those predicted by the Langevin-Stevenson-Gioumousis equation (16) or the ADO theory (89) where polar molecules are involved. These rate constants are approximately 10^{-9} cm^3 $molecule^{-1}$ s^{-1}. The early apparatus used to measure ion-molecule reaction rate constants was of such design that only the fast reactions ($k \approx 10^{-9}$ cm^3 $molecule^{-1}$ s^{-1}) could be measured and slower reactions were difficult to observe with this apparatus.

The disappearance of $C_2H_5^+$ is therefore described by the two reactions

$$C_2H_5^+ + C_2H_6 \xrightarrow{k_3} C_3H_7^+ \text{ and } C_4H_9^+ \qquad (4.15)$$

$$C_2H_5^+ + CH_4 \xrightarrow{k_4} C_3H_7^+ + H_2 \qquad (4.31)$$

The pseudo-first order rate constant ν_{ov} for the overall disappearance of $C_2H_5^+$ by reactions (4.15) and (4.31) is given by equation (4.32).

$$\nu_{ov} = k_3[C_2H_6] + k_4[CH_4] \qquad (4.32)$$

ν_{ov} can be obtained from the plots of $\log I_{C_2H_5^+}$ versus time shown in Figure 4.40 for different ethane concentrations at 86°C. Dividing equation (4.32) by $[C_2H_6]$ gives

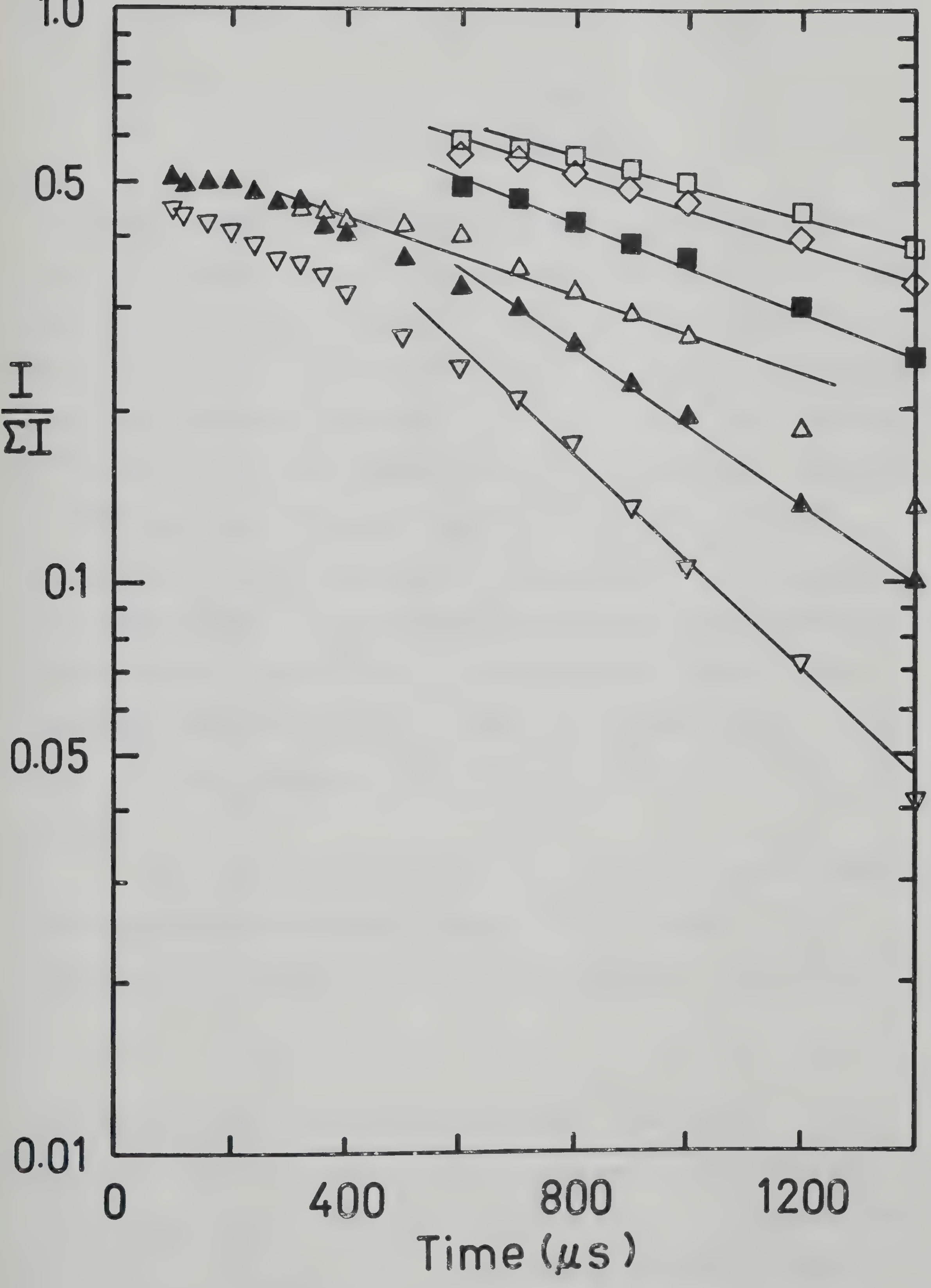

FIGURE 4.40. Logarithmic Plots of the Decay of $C_2H_5^+$ at 86°C

$CH_4:C_2H_6$ = ▽ 500:1, ▲ 1000:1, △ 2500:1, ■ 20,000:1, ◇ 10,000:1, □ 20,000:1.

$$\frac{\nu_{ov}}{[C_2H_6]} = k_3 + k_4\frac{[CH_4]}{[C_2H_6]} \qquad (4.33)$$

Therefore a plot of $\nu_{ov}/[C_2H_6]$ versus $[CH_4]/[C_2H_6]$ should give a straight line with a slope equal to k_4 and a y-intercept equal to k_3. The results obtained from Figure 4.41 lead to $k_4 \approx 1 \times 10^{-14}$ cm^3 molecule^{-1} s^{-1} which is in fair agreement with Hiraoka's value for $k_4 = 1.6 \times 10^{-14}$ cm^3 molecule^{-1} s^{-1} (134) at the same temperature in pure methane. Results at 86°C were used because reaction (4.31) has a positive temperature coefficient and is therefore faster and more noticeable (134). The intercept in Figure 4.41 passes close to the origin, where there is considerable scatter, which makes the plot unsuitable to determine k_3 accurately. However, the plot gives an estimate of $k_3 \approx 1 \times 10^{-11}$ cm^3 molecule^{-1} s^{-1}.

The calculation of k_3 and k_4 is also complicated by the temperature dependent decomposition reaction (4.14). The rate of reaction (4.14) is negligible at room tempera-

$$C_2H_7^+ = C_2H_5^+ + H_2 \qquad (4.14)$$

ture but becomes significant at 86°C. Thus $C_2H_5^+$ is produced by reaction (4.14) while it disappears by reactions (4.15) and (4.31). Thus the apparent rate of disappearance of $C_2H_5^+$ is slowed by the occurrence of reaction (4.14).

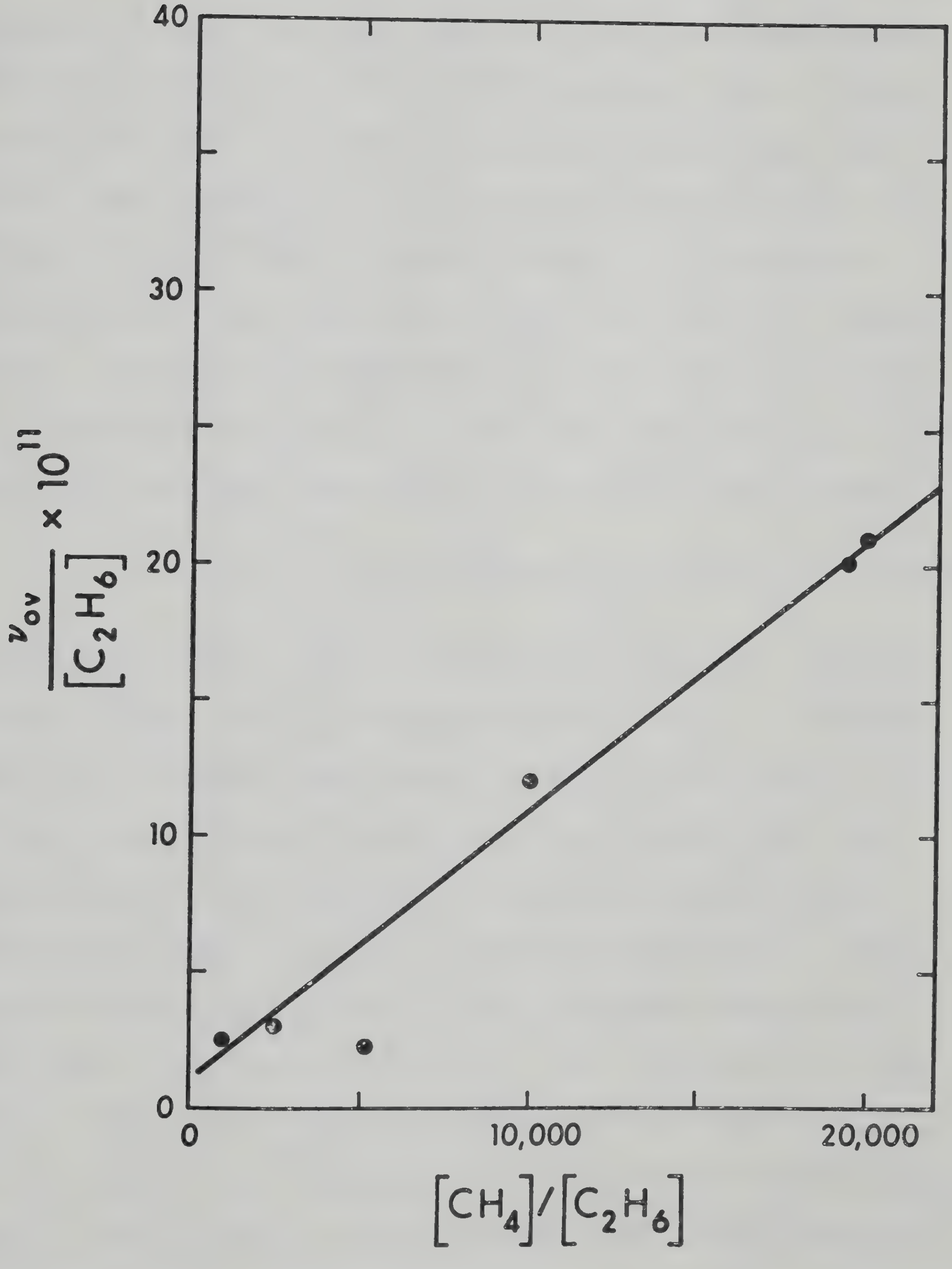

FIGURE 4.41. Plot of $\nu_{ov}/[C_2H_6]$ versus $[CH_4]/[C_2H_6]$ at 86°C.

To determine k_3 more accurately an experiment was conducted at 30°C so that reaction (4.14) was negligible. The lowest methane to ethane ratio used was 50:1. Under these conditions less than 1% of the primary ions would arise from ethane since the ionization cross-section of ethane is twice that of methane (106). At high ethane concentrations the reaction of $C_2H_5^+$ with CH_4, in reaction (4.31), would also be negligible and the disappearance of $C_2H_5^+$ would be due solely to reaction with ethane by (4.15). The experiment was repeated twice at 30°C, one of which

$$C_2H_5^+ + C_2H_6 \xrightarrow{k_3} C_3H_7^+ \text{ and } C_4H_9^+ \qquad (4.15)$$

is shown in Figure 4.27. Figure 4.42 shows the semilogarithmic plots of the two experiments at 30°C. Included also are two experiments under the same concentration conditions but at higher temperatures and demonstrate the interference of the temperature dependent dissociation reaction of $C_2H_7^+$ to $C_2H_5^+$. The rate constant, k_3 was calculated from the slopes of the semilogarithmic plots and gave $k_3 = 5.2$ and 5.3×10^{-11} cm^3 molecule^{-1} s^{-1} at 304°K. This is in close agreement with a value of $k_3 = 5.1 \pm 1 \times 10^{-11}$ cm^3 molecule^{-1} s^{-1} reported by Bohme et al (135). Blair, Heslin and Harrison (129) have reported the rate constant for the reaction

$$C_2D_5^+ + C_2H_6 \longrightarrow C_2D_5H + C_2H_5^+ \qquad (4.34)$$

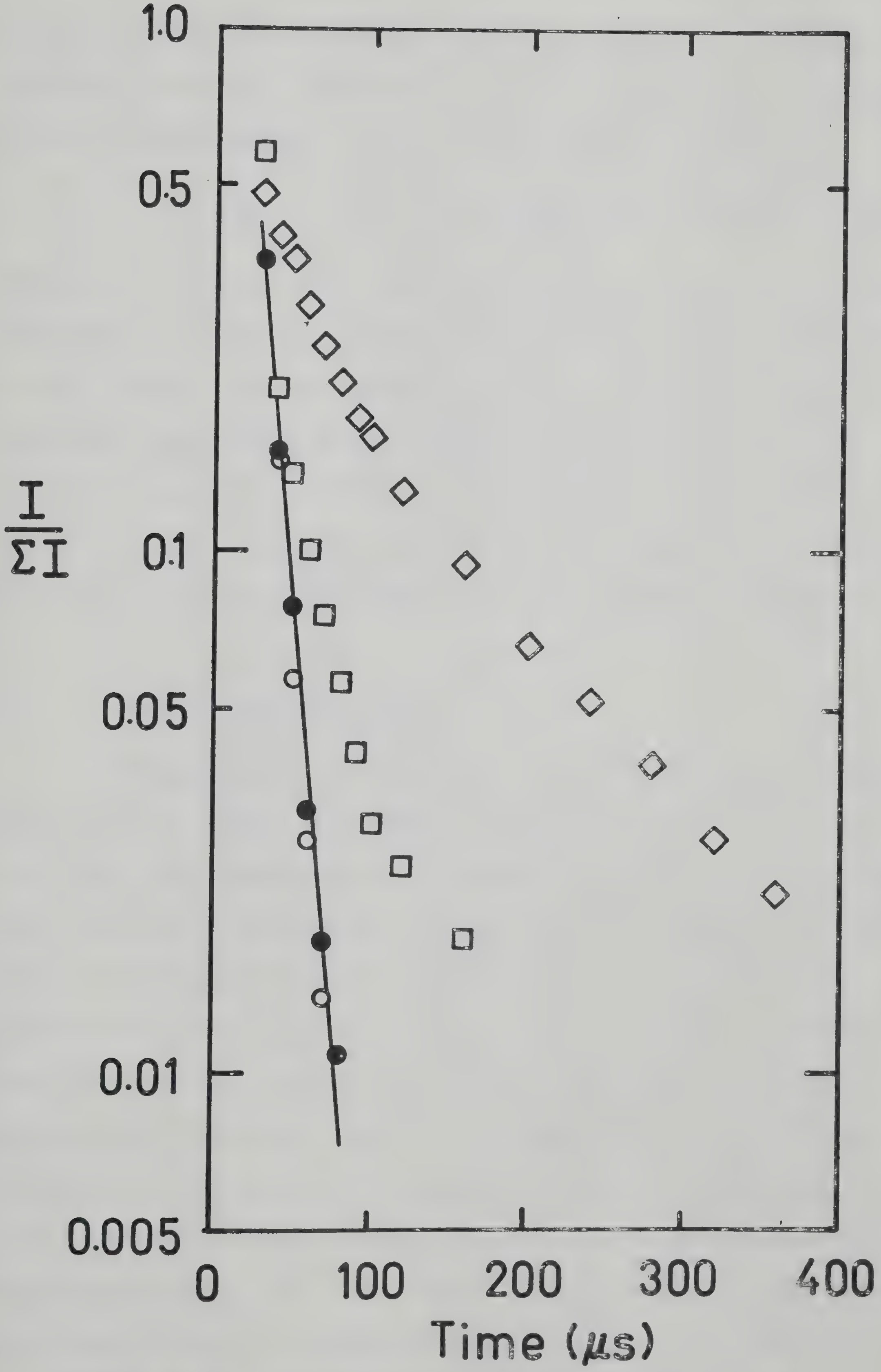

FIGURE 4.42. Logarithmic Plots of the Decay of $C_2H_5^+$ at $[CH_4]:[C_2H_6] = 50:1$, ● 32°C, ○ 30°C, □ 71°C, ◇ 114°C.

to be 2.8×10^{-10}. Reaction 4.34 is, however, a hydride transfer reaction. Harrison (136) estimates that only 15% of the disappearance is due to the adduct ion, $C_4H_6D_5^+$.

$$C_2D_5^+ + C_2H_6 \longrightarrow C_4H_6D_5^+ \longrightarrow \text{products} \quad (4.35)$$

Harrison estimates this rate constant to be 4.2×10^{-11} cm^3 molecule^{-1} s^{-1} which agrees with the rate constant measured in this work. Field has measured k_3 in several different projects. He reported the values of k_3 to be 5×10^{-11} at 410°K (131), 6×10^{-11} at 483°K (38), 5×10^{-11} cm^3 molecule^{-1} s^{-1} at 463°K (122). The rate constant, k_3, obtained in this work is consistent with the reported values.

4.7 The Pyrolysis of $C_2H_7^+$

Inspection of the ion intensity profiles in Figures 4.27 to 4.31, where the ethane concentration is kept constant and the temperature is gradually increased, illustrates the temperature dependence of the rate of disappearance of $C_2H_7^+$. The rapid change of behaviour of $C_2H_7^+$ with temperature is illustrated in Figure 4.43 which is a perspective plot of the intensity of $C_2H_7^+$ as a function of temperature and reaction time. The experiments shown in the perspective plot were all conducted at high ethane concentration where $[CH_4]:[C_2H_6] = 50:1$ and the precursor CH_5^+ decays to zero by 30 μsec. At 32°C $C_2H_7^+$ is very long lived and since the CH_5^+ disappears very rapidly, $C_2H_7^+$ must be

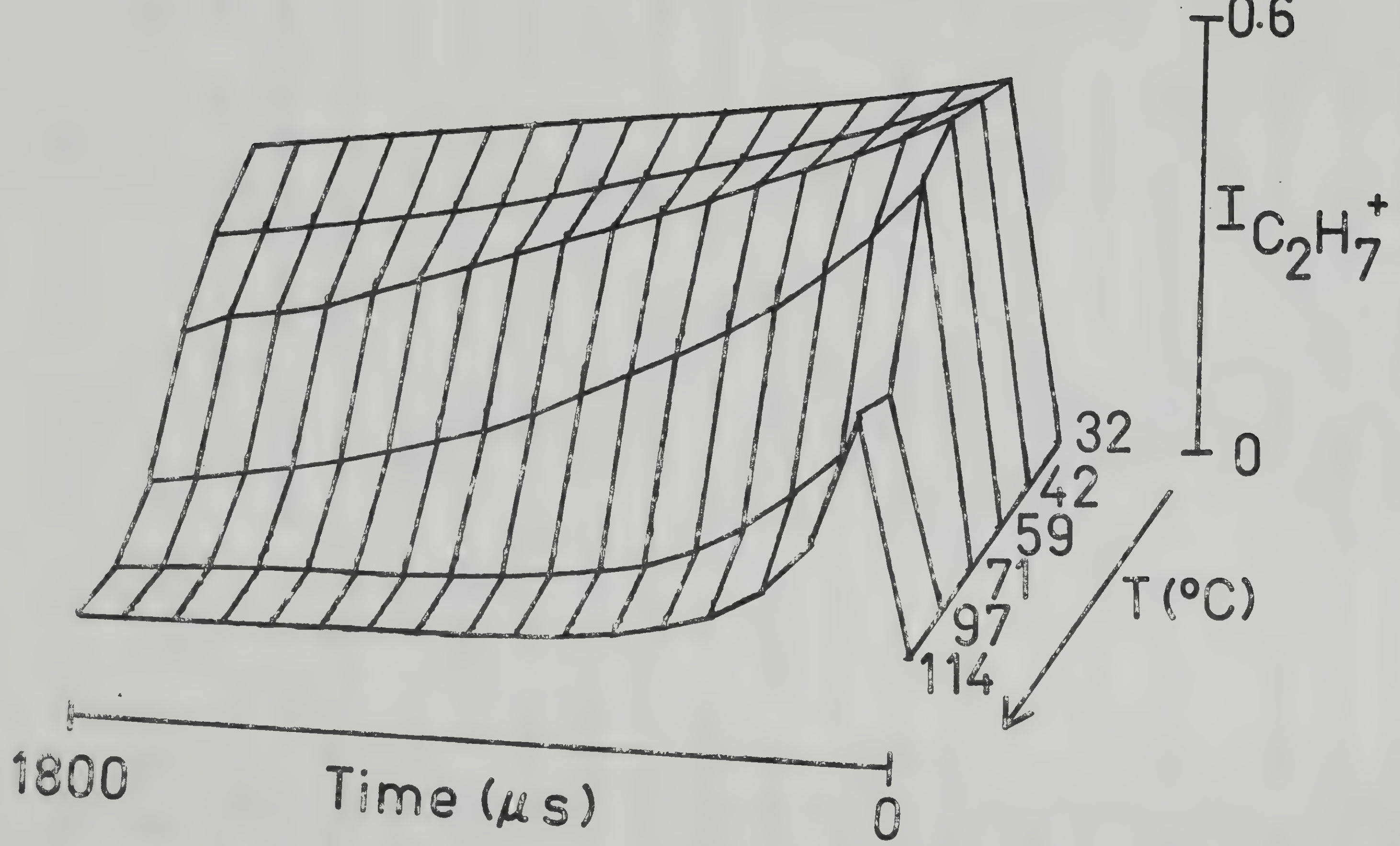

FIGURE 4.43. Perspective Plot of the Intensity of $C_2H_7^+$ as a Function of Temperature and Reaction Time.

reacting very slowly. As the temperature is gradually increased the disappearance of $C_2H_7^+$ becomes more rapid.

The increase in the rate of disappearance of $C_2H_7^+$ with temperature is indicative of an endothermic ion molecule reaction.

The pseudo-first order rate constants ν_2 for reaction (4.14) were calculated from the slopes of the plots of $\log I_{C_2H_7^+}$ *versus* time shown in Figures 4.44 to 4.52. These figures show the effect of changing the ethane concentration whilst staying at one temperature on each graph whereas in the last two figures the ethane concentration is kept constant and the temperature is varied. At constant temperature, the slope does not vary very much with ethane concentration but at constant ethane concentration the slope varies drastically with temperature. To investigate the dependence of the rate of reaction of $C_2H_7^+$ on methane pressure, the ratio of methane to ethane was kept constant but the total ion source pressure was varied (Figure 4.53). Unfortunately the pressure of CH_4 could not be varied over a wide enough pressure range to reach a definite conclusion. It was assumed that $C_2H_7^+$ depended on a collision to initiate thermal activation and reaction (4.14) should be written

$$C_2H_7^+ + CH_4 \xrightarrow{k_{2s}} C_2H_5^+ + H_2 + CH_4 \quad (4.36)$$

Therefore,

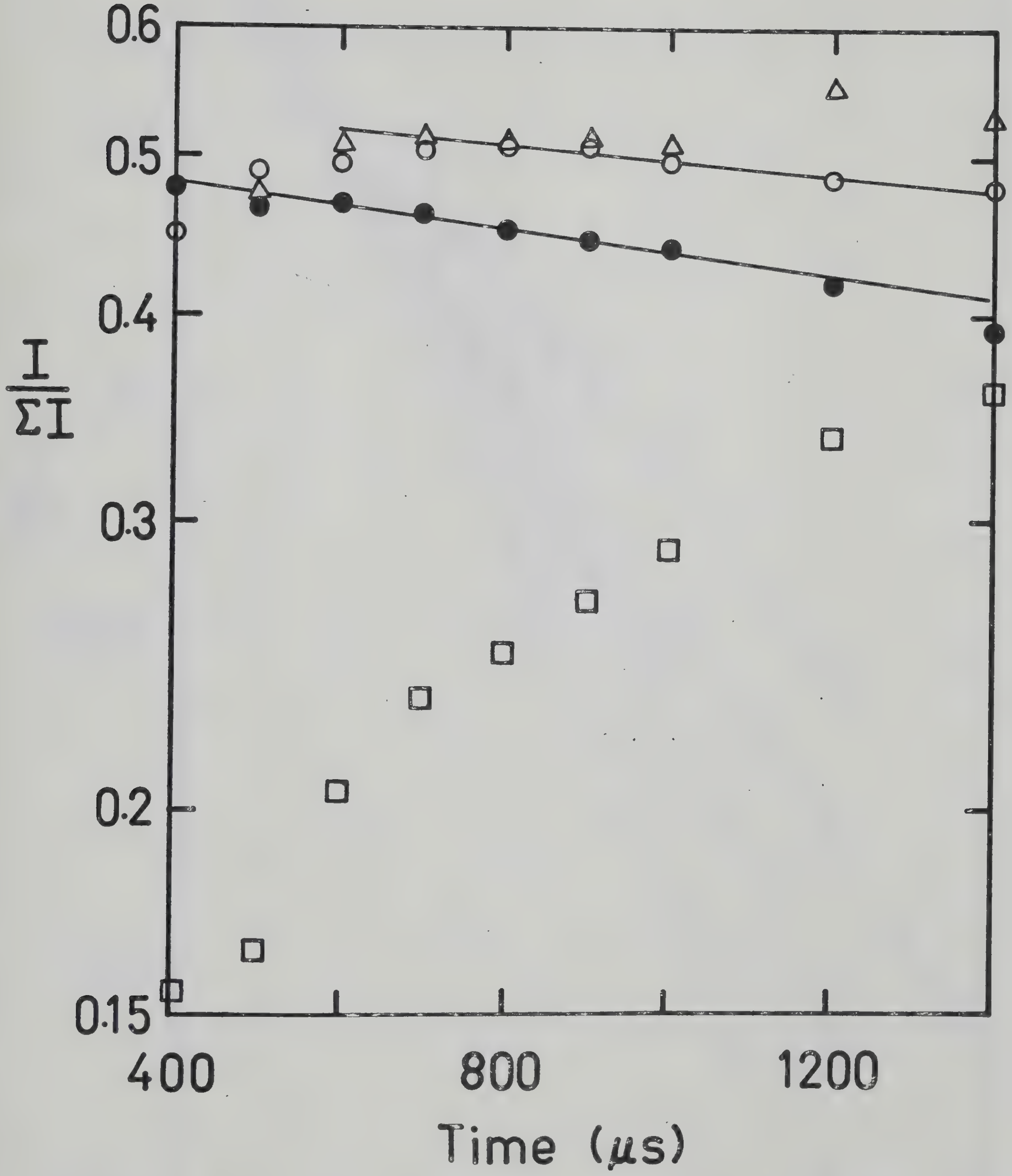

FIGURE 4.44. Logarithmic Plots of the Decay of $C_2H_7^+$ at 30°C. $[CH_4]:[C_2H_6]$ = ● 5000:1, ○ 20,000:1, △ 20,000:1, □ 100,000:1.

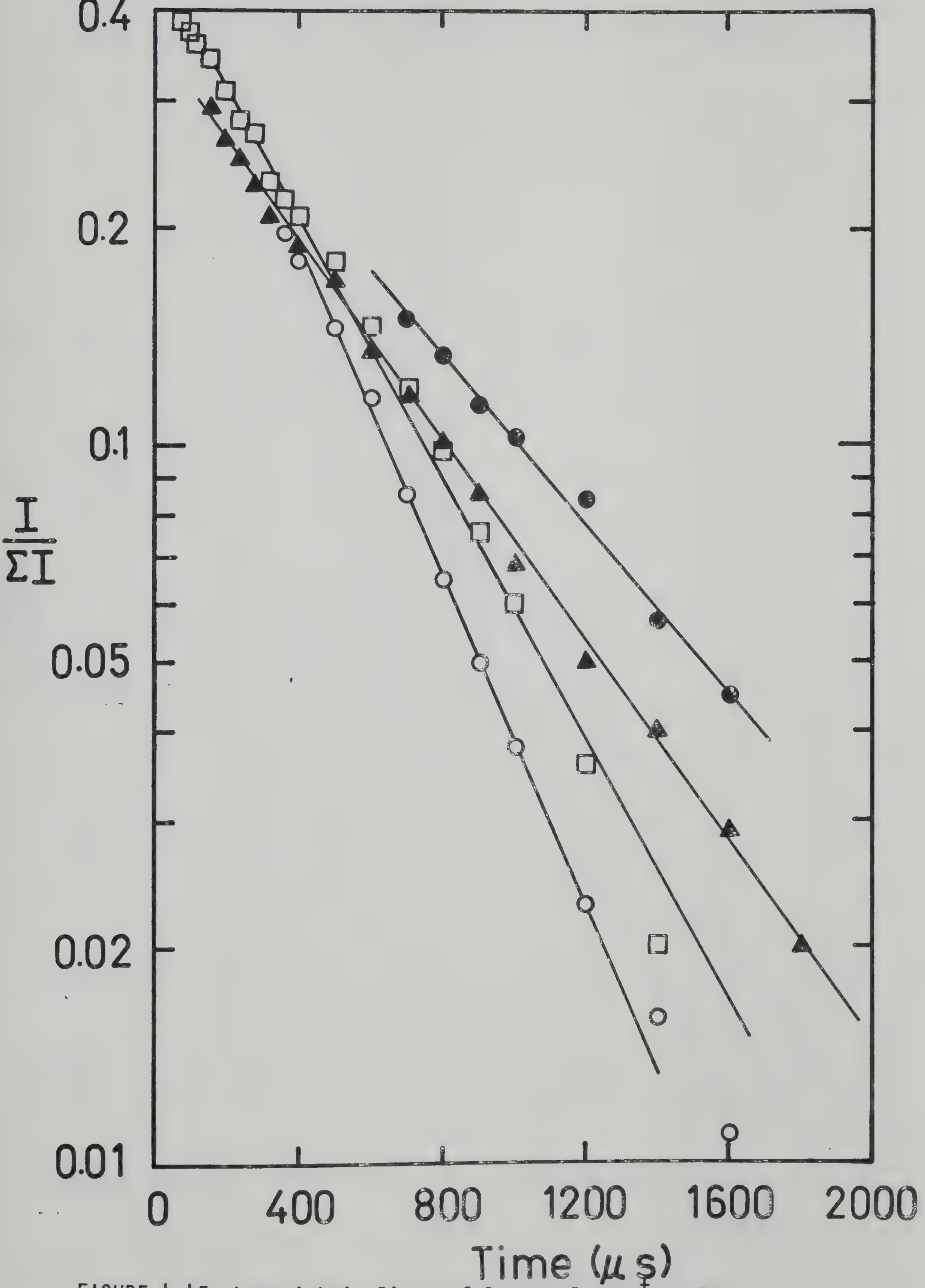

FIGURE 4.45. Logarithmic Plots of Decay of $C_2H_7^+$ at 86°C.

$[CH_4]:[C_2H_6]$ = ○ 20,000:1, ▲ 1000:1, □ 500:1, ● 50,000:1.

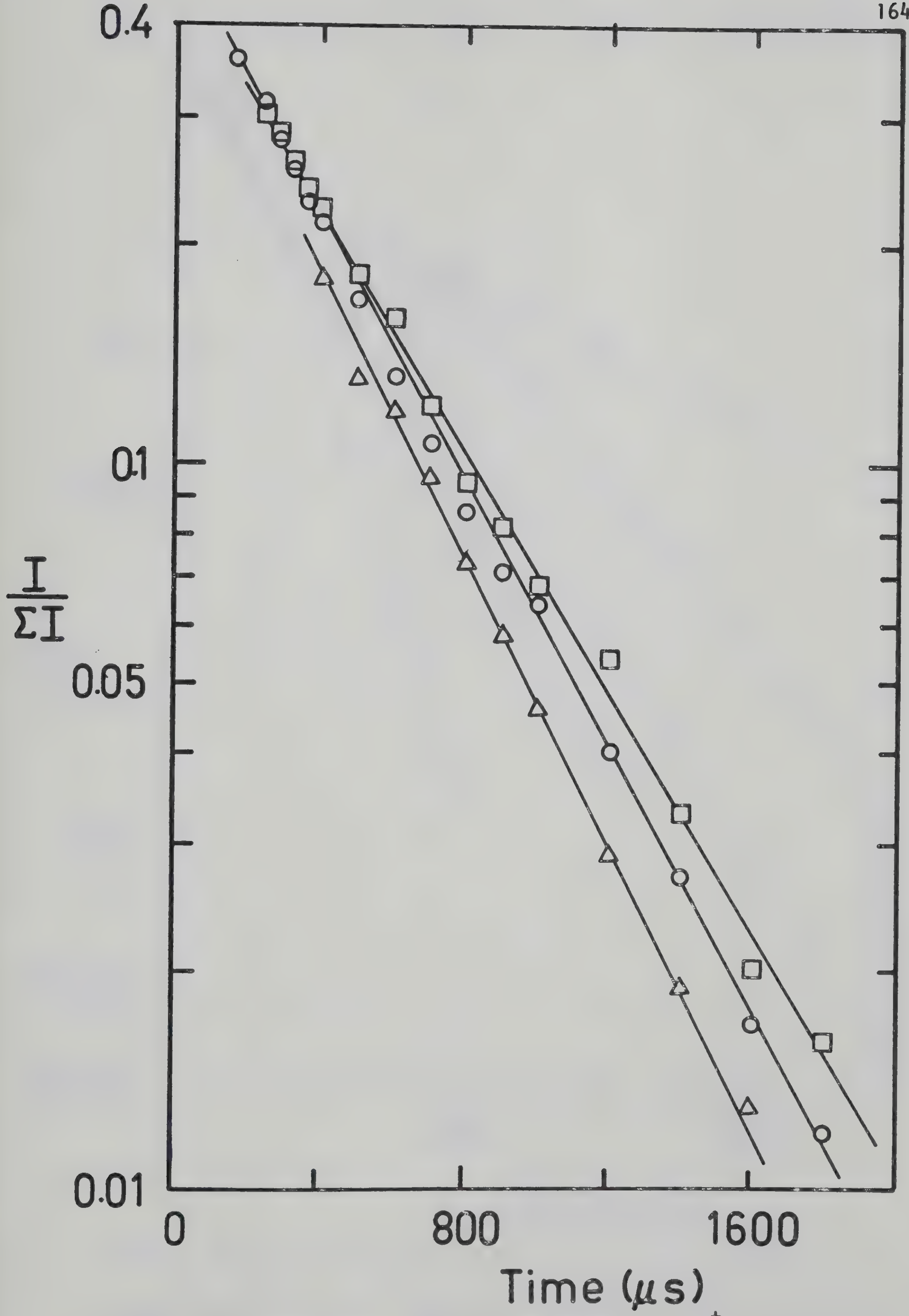

FIGURE 4.46. Logarithmic Plots of the Decay of $C_2H_7^+$ at 86°C.

$[CH_4]:[C_2H_6]$ = △ 5000:1, ○ 2500:1, □ 10,000:1.

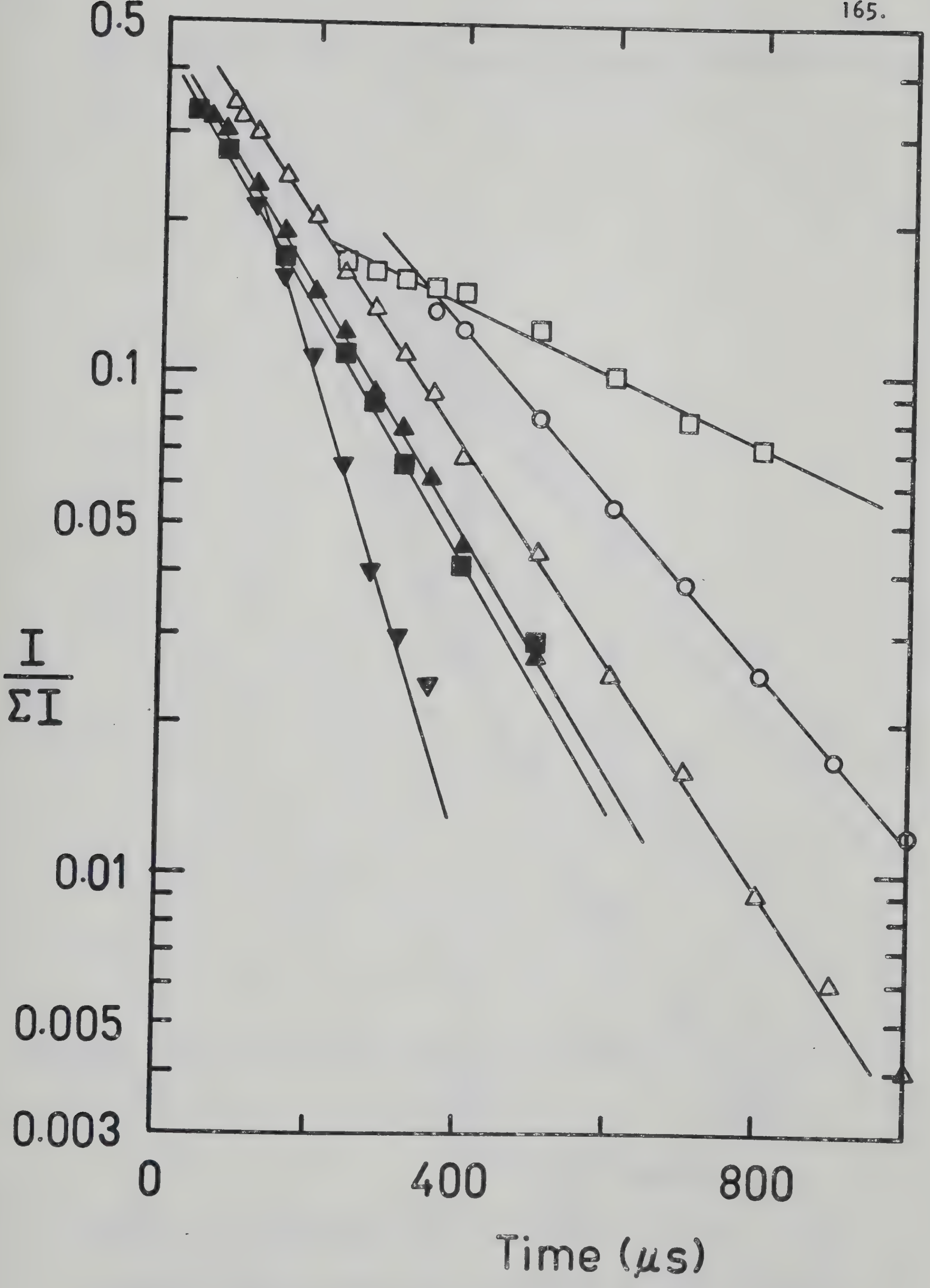

FIGURE 4.47. Logarithmic Plots of the Decay of $C_2H_7^+$ at 106°C.

$CH_4:C_2H_6$ = ▼ 800:1, ■ 1000:1, ▲ 900:1, △ 250:1, ○ 10,000:1

□ 800:1.

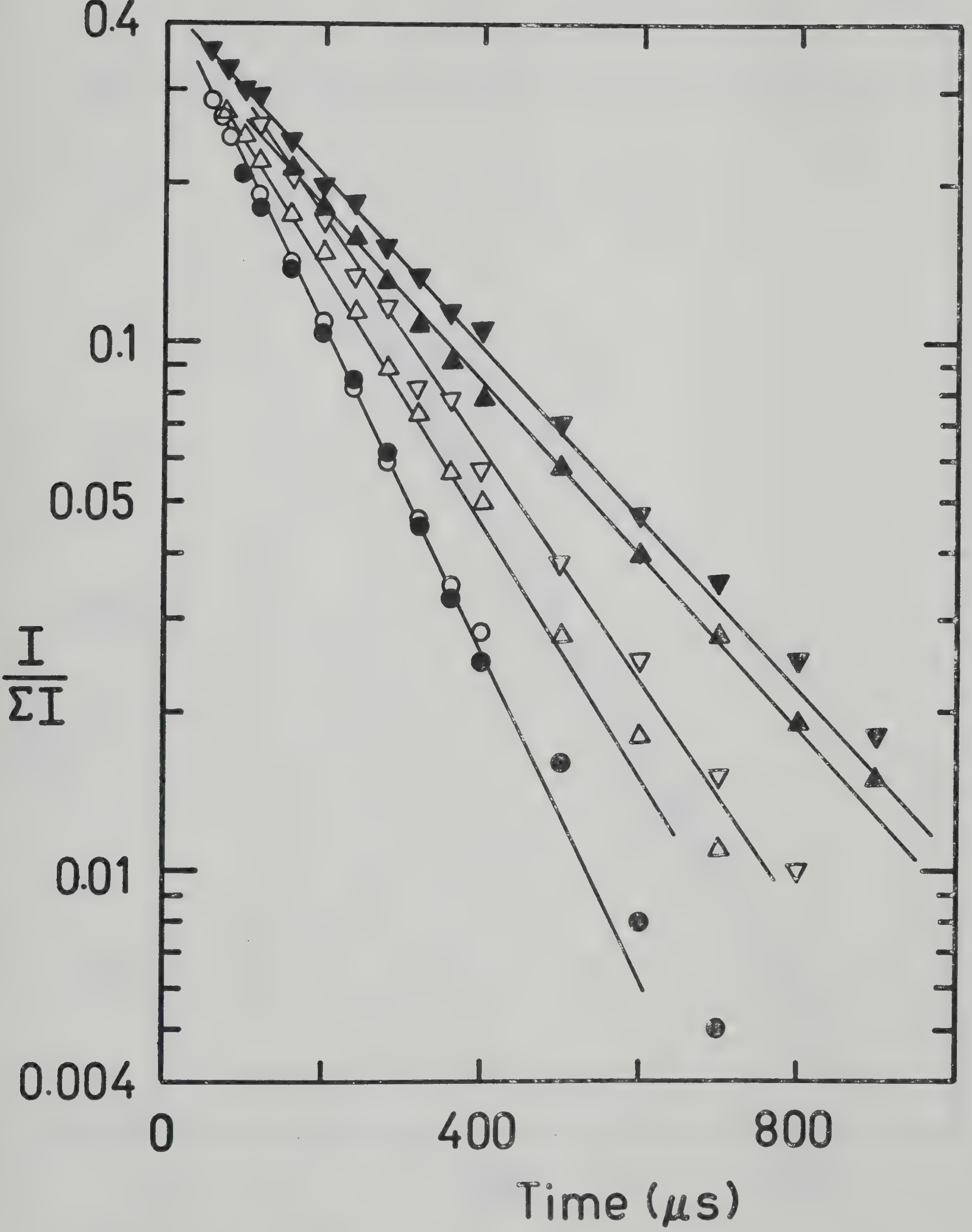

FIGURE 4.48. Logarithmic Plots of the Decay of $C_2H_7^+$ at 106°C. $[CH_4]:[C_2H_6]$ = ● 5000:1, ○ 1700:1, △ 1200:1, ▽ 1000:1, ▲ 12,000:1, ▼ 250:1.

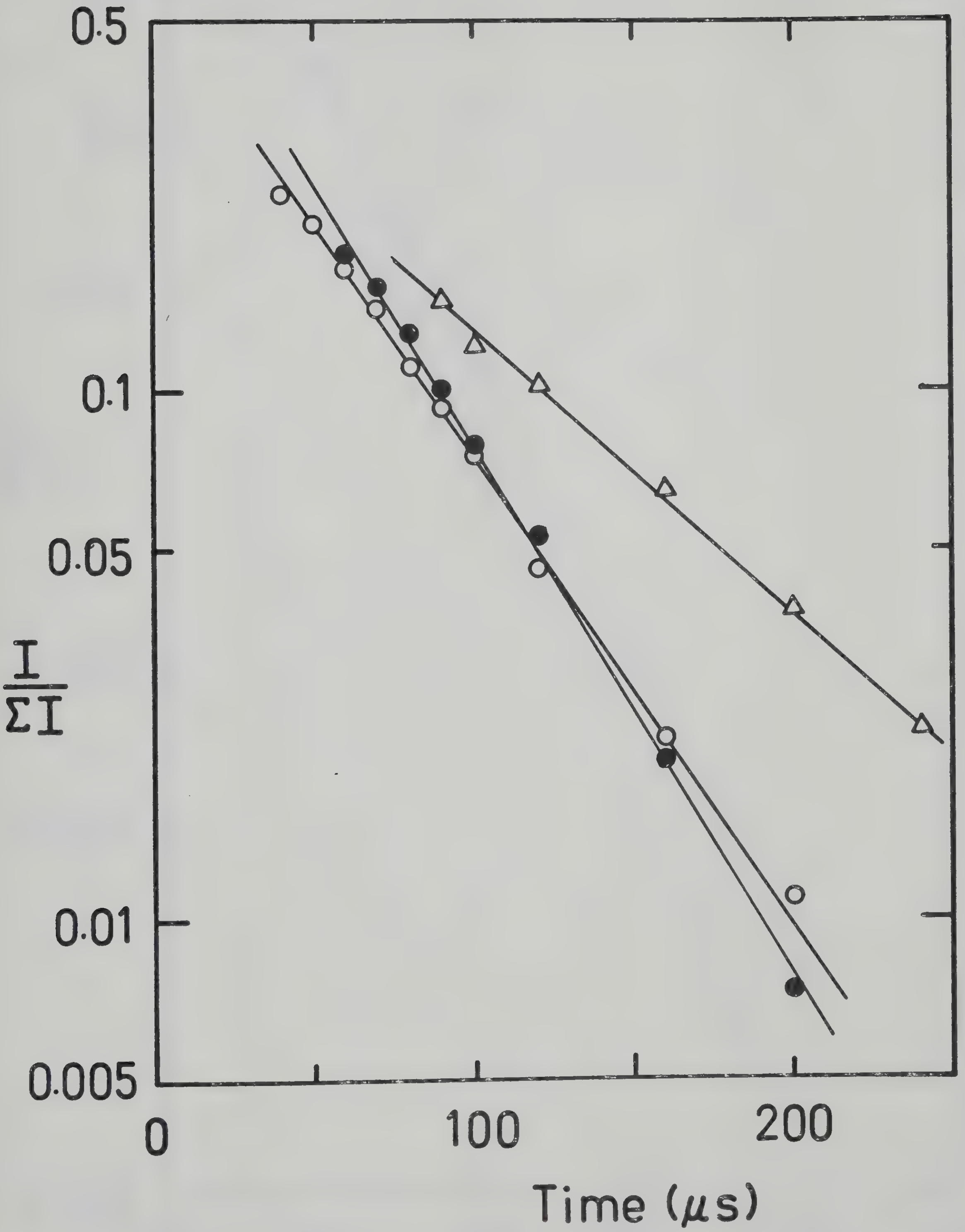

FIGURE 4.49. Logarithmic Plots of the Decay of $C_2H_7^+$ at 156°C.

$CH_4:C_2H_6$ = ● 500:1, ○ 1000:1, △ 2500:1.

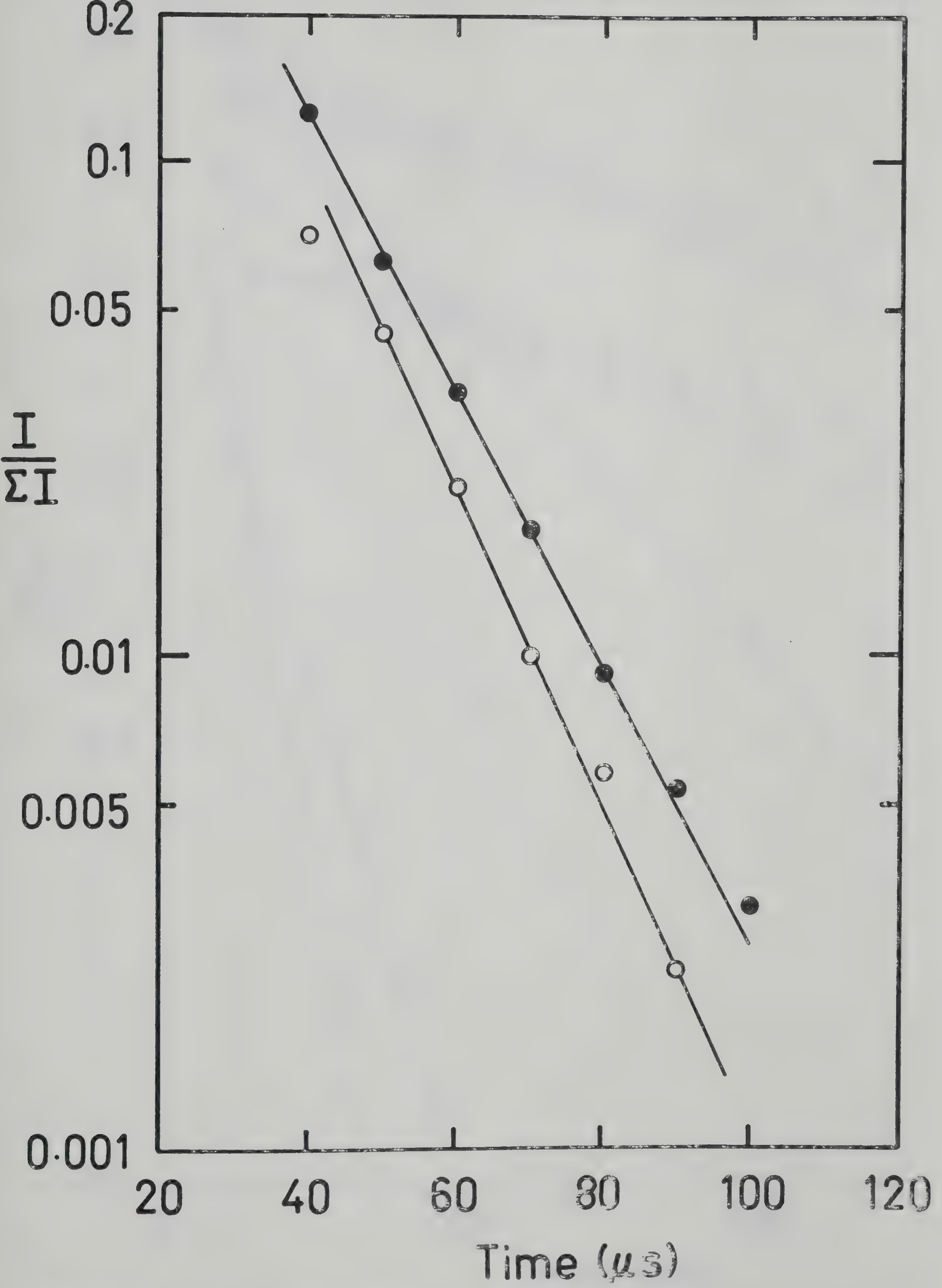

FIGURE 4.50. Logarithmic Plots of the Decay of $C_2H_7^+$ at 210°C.

$[CH_4]:[C_2H_6]$ = ● 250:1, ○ 500:1.

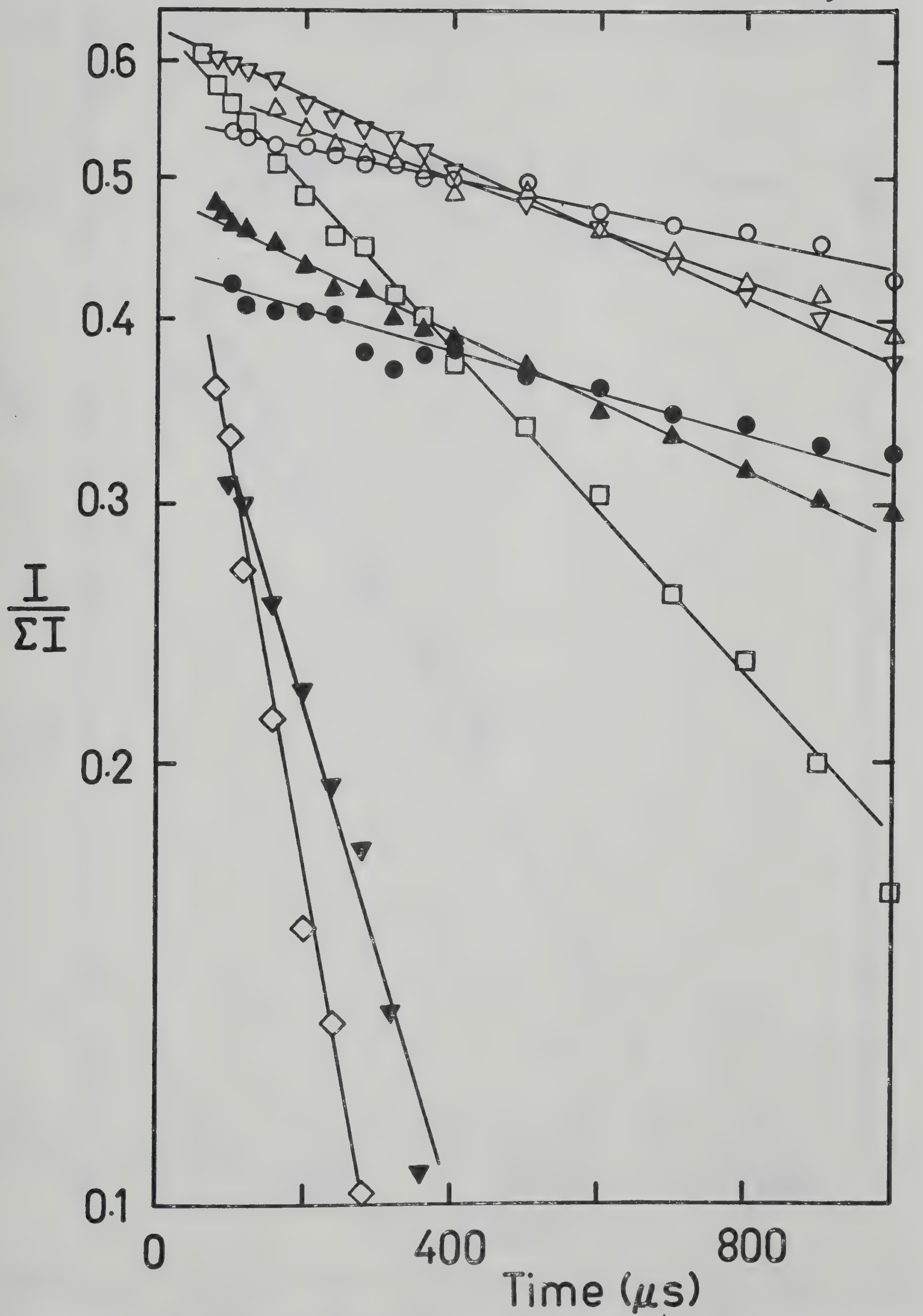

FIGURE 4.51. Logarithmic Plots of the Decay of $C_2H_7^+$ at $[CH_4]:[C_2H_6]$ = 50:1 ● 30°C, ○ 32°C, △ 42°C, ▲ 51°C, ▽ 59°C, □ 71°C, ▼ 97°C, ◇ 114°C.

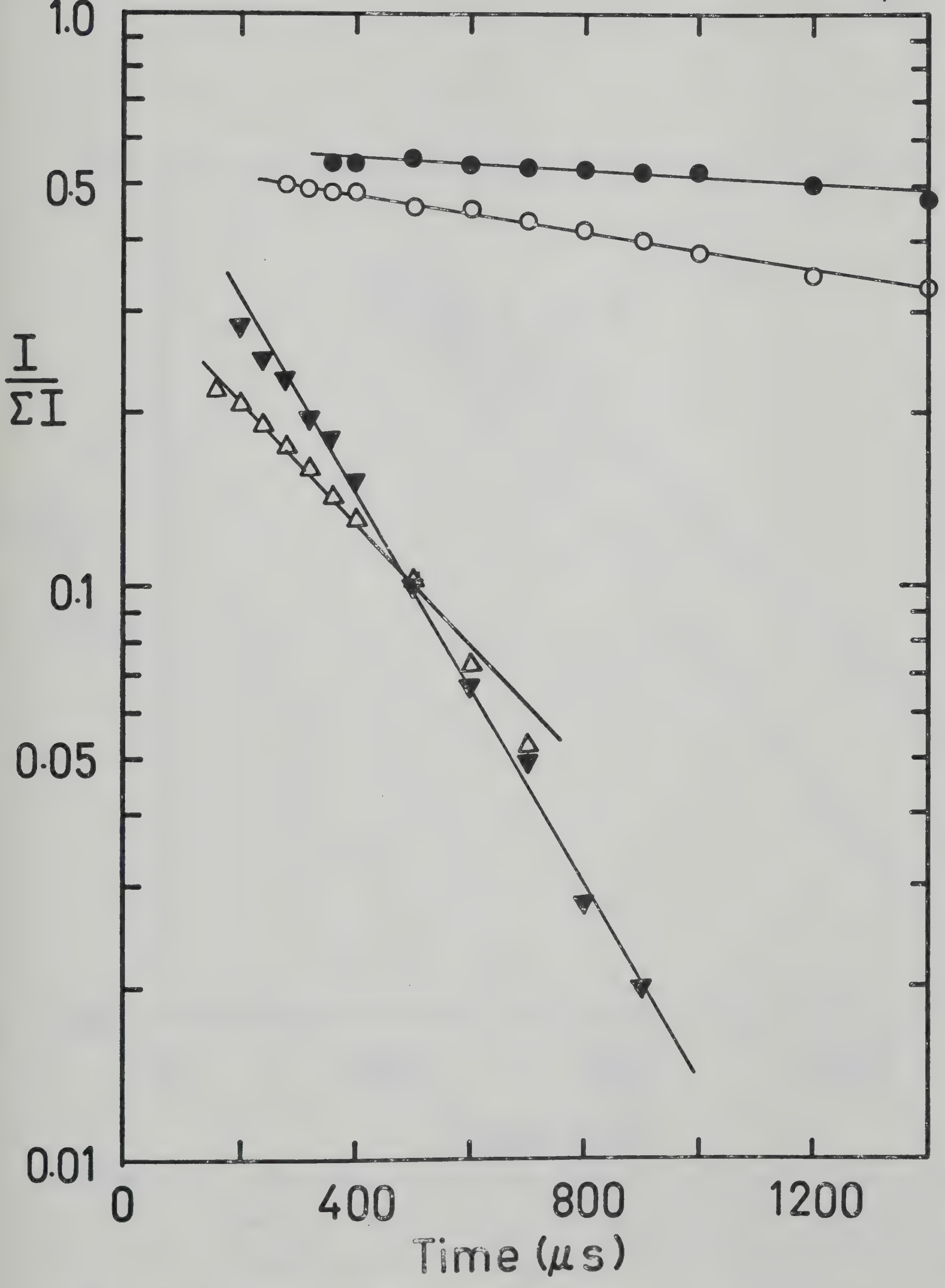

FIGURE 4.52. Logarithmic Plots of the Decay of $C_2H_7^+$ at $[CH_4]:[C_2H_6] = 500:1$
● 32°C, ○ 49°C, △ 74°C, ▼ 96°C.

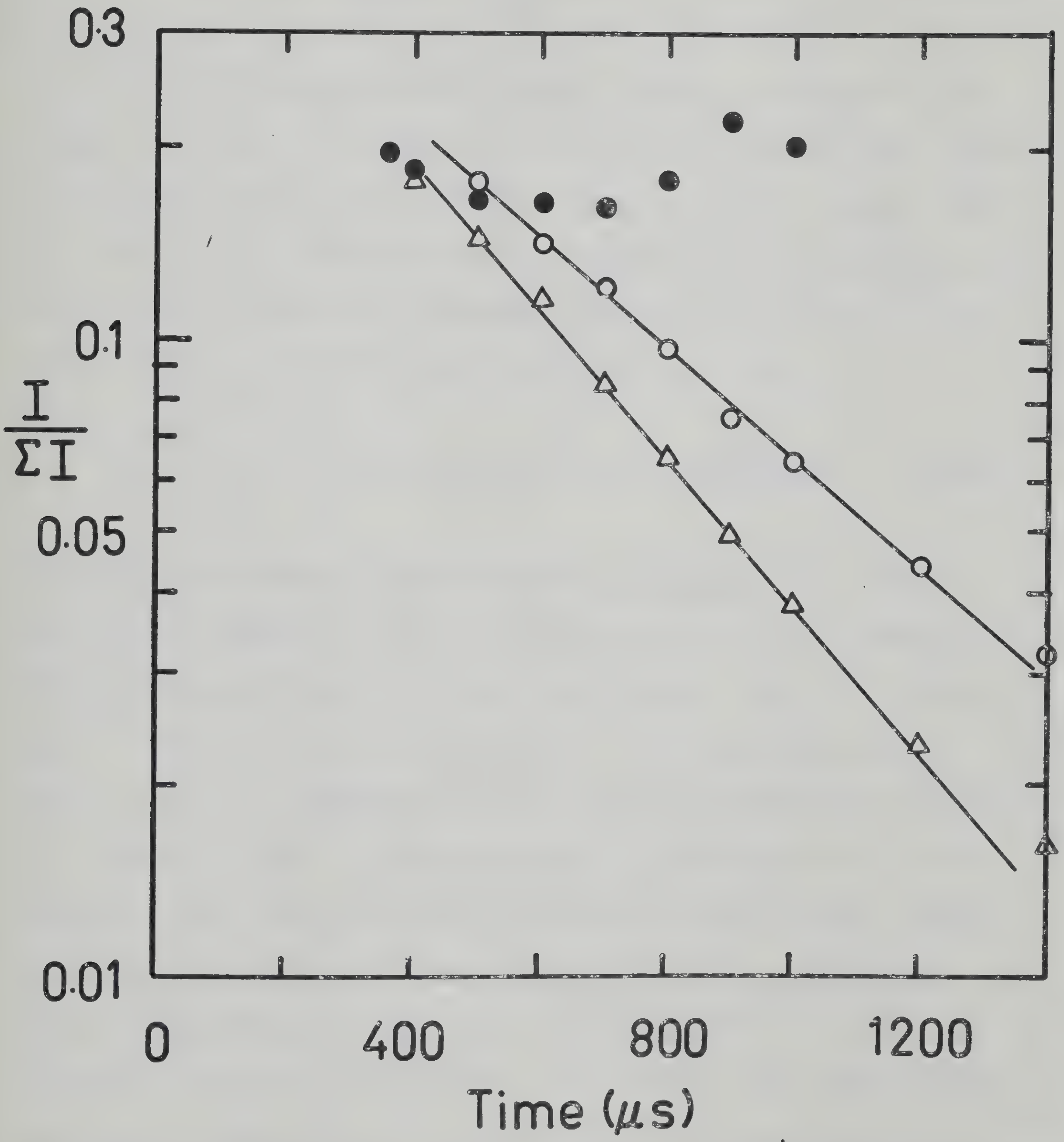

FIGURE 4.53. Logarithmic Plots of the Decay of $C_2H_7^+$ at 86°C with Varying Methane Pressure. ○ 2.3 torr CH_4, 0.12 mtorr C_2H_6, ● 1.0 torr CH_4, 0.05 mtorr C_2H_6, △ 3.2 torr CH_4, 0.16 mtorr C_2H_6.

$$k_{2s} = \frac{\nu_2}{[CH_4]} \tag{4.37}$$

A plot of $\nu_2/[CH_4]$ plotted versus $[C_2H_6]$ in Figure 4.54 shows that k_{2s} is independent of ethane concentration. The rate constants, k_{2s} at various temperatures are summarized in Table VIII. The temperature range of the experiments is only 180° but the rate constant changes by a factor of almost 1000. A form of the Arrhenius equation is

$$\log k_{2s} = \log A - \frac{E_a}{2.303RT} \tag{4.38}$$

Figure 4.55 shows a plot of log k_{2s} versus 1/T. The activation energy, E_a may be calculated from the slope of the Arrhenius plot. E_a was found to be 10.5 ± 0.3 kcal/mol. The value of A obtained from the intercept was 8.3×10^{-8} cm^3 molecule^{-1} s^{-1}. The pre-exponential factor is almost 10^{-7} and is therefore much larger than the normal Langevin rate constant for ion-molecule collisions, whose magnitude is about 10^{-9} cm^3 molecule^{-1} s^{-1}. Large pre-exponential factors have been found for other bimolecular thermal activation reactions. For example the temperature dependence for reaction (4.39) led to a pre-exponential

$$H_5^+ + H_2 \longrightarrow H_3^+ + 2H_2 \tag{4.39}$$

factor of 9×10^{-6} (137) which is even larger than the

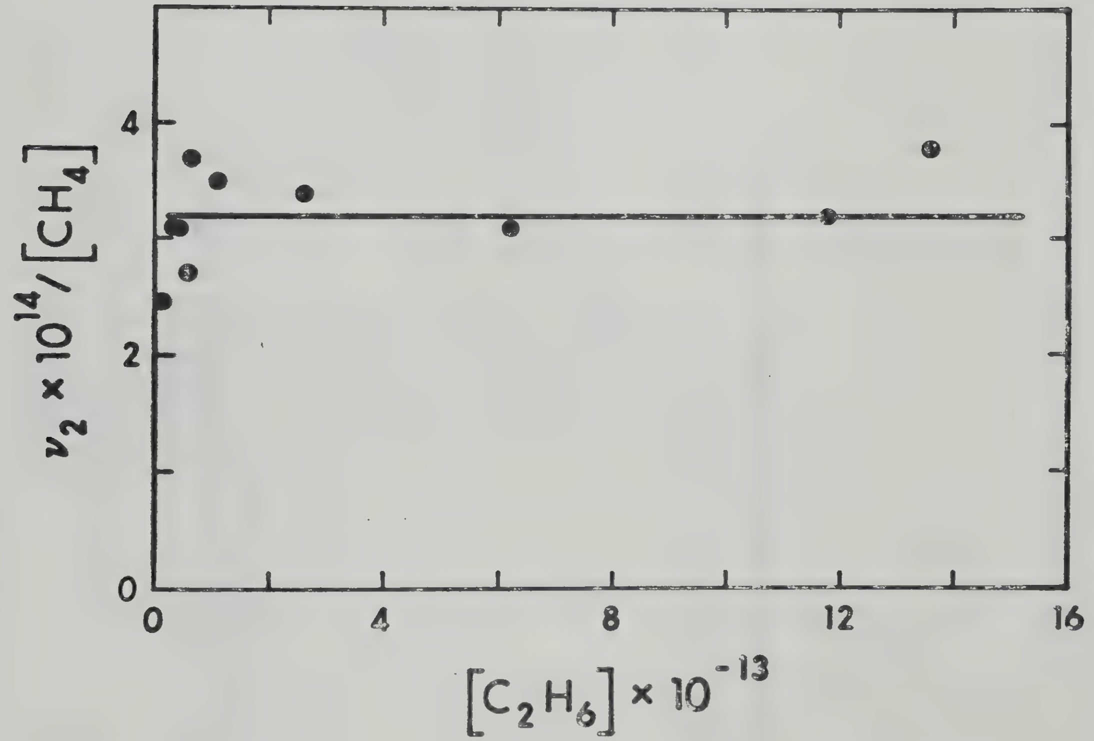

FIGURE 4.54. Plot of $\nu_2/[CH_4]$ *versus* Ethane Pressure at 86°C.

TABLE VIII

Summary of Rate Constants, k_{2s}, for Decay of $C_2H_7^+$

$\frac{CH_4}{C_2H_6}$	Temperature										
	30°C	42°C	51°C	59°C	71°C	86°C	97°C	106°C	114°C	156°C	210°C
50:1	3.6×10^{-15}(2)	4.9×10^{-15}	7.5×10^{-15}	7.4×10^{-15}	1.8×10^{-14}		5.7×10^{-14}		1.1×10^{-13}		
250:1								6.6×10^{-14}(2)			1.3×10^{-12}
500:1	1.8×10^{-15}		5.4×10^{-15}		3.6×10^{-14}	3.5×10^{-14}(2)	5.8×10^{-14}			4.6×10^{-13}	1.4×10^{-12}
900:1								8.4×10^{-14}(3)			
1000:1						3.1×10^{-14}		7.4×10^{-14}(2)		4.2×10^{-13}	
1250:1								7.5×10^{-14}			
1650:1								8.3×10^{-14}			
2500:1						3.4×10^{-14}				2.5×10^{-13}	
5000:1	2.0×10^{-15}					3.5×10^{-14}		9.0×10^{-14}			
10,000:1						3.2×10^{-14}		7.0×10^{-14}			
12,000:1								5.0×10^{-14}			
20,000:1	1.4×10^{-15}					3.2×10^{-14}(2)					
50,000:1						2.4×10^{-14}					
100,000:1											
Average	2.2×10^{-15}	4.9×10^{-15}	6.5×10^{-15}	7.4×10^{-15}	2.7×10^{-14}	3.2×10^{-14}	5.8×10^{-14}	8.8×10^{-14}	1.1×10^{-13}	3.7×10^{-13}	1.34×10^{-12}

a. Number in brackets refers to number of experiments conducted at these conditions if greater than 1.

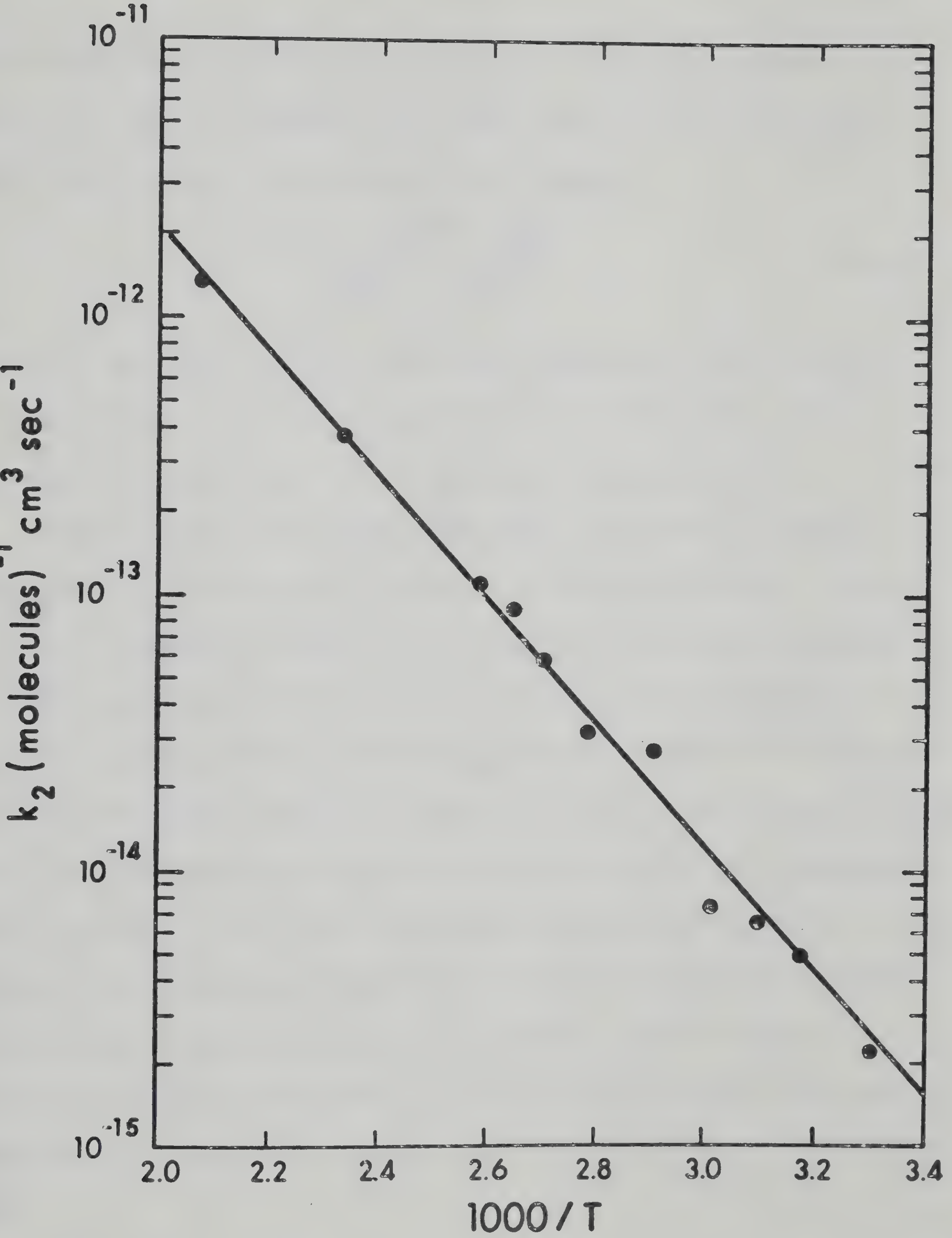

FIGURE 4.55. Arrhenius Plot for the Rate Constant k_2 at various Temperatures.

value obtained for reaction (4.36). The pre-exponential factor A, can be equated with the bimolecular collision rate (138) using simple collision theory.

$$A = \frac{(\sigma_A + \sigma_B)^2 N}{1000} \sqrt{\frac{\pi RT}{2\mu}} \tag{4.40}$$

where σ_A and σ_B are the collision diameters of A and B in a bimolecular reaction between the two molecules, N is Avogadro's number and μ is the molar reduced mass of A and B. Simple collision theory neglects any steric factors, which may be introduced if two colliding molecules have to be in a suitable orientation. Another difficulty arises because collision theory assumes that only 2 degrees of freedom can contribute the energy that is used in surmounting the activated complex energy barrier. Hinshelwood (139) first suggested that there is no reason to ignore energy contributions from their internal degrees of freedom. If energy from rotational and vibrational degrees of freedom contribute to the energy of activation then a larger fraction of the collisions will be effective and the pre-exponential factor is larger than the bimolecular collision rate.

4.8 Thermochemical Calculations

According to theoretical calculations by Lathan, Hehre and Pople (128,140) using STO-3G Molecular Orbital

basis and others (141) the most stable structure of CH_5^+ is the two-electron three centre bonded species I which has C_s symmetry. Two stable isomers of $C_2H_7^+$ have been predicted

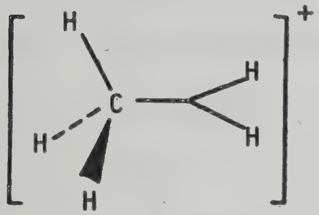

I

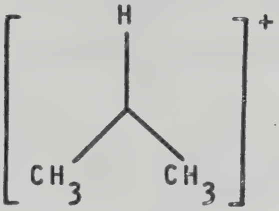

II

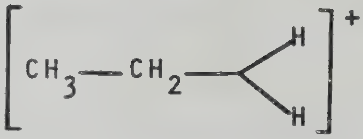

III

by ab initio calculations by Lathan et al (128,140). These workers calculated that the C-C protonated structure, II is about 11 kcal/mol more stable than the C-H protonated structure III. However, recent results obtained by Bischof and Dewar (142) using a simpler semi-empirical method, MINDO/3 yielded the opposite result: that structure III is more stable than II by 15 kcal/mol although the geometry and the dimensions of the two structures agreed closely with those of Pople. Recent experiments in our laboratory have indicated that structure II is the more stable (143).

The dehydrogenation of $C_2H_7^+$ in reaction (4.14) can therefore be visualized as a rearrangement from II to III followed by a dissociation of the bond. Since

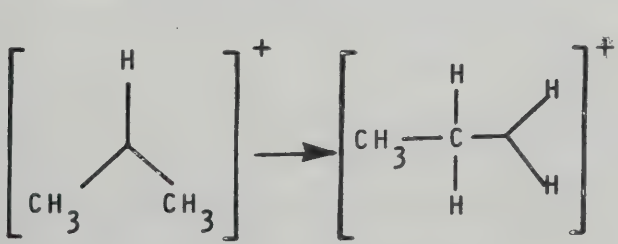

$$\longrightarrow C_2H_5^+ + H_2 \qquad (4.41)$$

II III

structure III has been calculated as 11 kcal/mol less stable, then the activation energy measured in this work, 10.5 kcal/mol appears of the right magnitude if the dissociation of III to $C_2H_5^+$ and H_2 is thermoneutral. The energy diagram that can be envisaged for the reaction scheme (4.41) is shown in Figure 4.56.

If it is assumed that the reverse of reaction (4.14) proceeds without any activation energy then $E_2 \approx \Delta H_{-2} = -10.5$

$$C_2H_5^+ + H_2 \xrightarrow{k_{-2}} C_2H_7^+ \qquad (4.42)$$

kcal/mol. Since $\Delta H_f(H_2) = 0$ and $\Delta H_f(C_2H_5^+) = 219$ kcal/mol

$$\Delta H_{-2} = \Delta H_f(C_2H_7^+) - \Delta H_f(C_2H_5^+) - \Delta H_f(H_2) \qquad (4.43)$$

(127) then $\Delta H_f(C_2H_7^+)$ from equation (4.43) equals 208.5 kcal/mol. The proton affinity of C_2H_6 is given by

$$C_2H_6 + H^+ \longrightarrow C_2H_7^+ \qquad \Delta H = -PA(C_2H_6) \qquad (4.44)$$

therefore the proton affinity of C_2H_6 predicted by the activation energy E_2 is:

$$\begin{aligned} PA(C_2H_6) &= \Delta H_f(C_2H_6) + \Delta H_f(H^+) - \Delta H_f(C_2H_7^+) \\ &= -20.2 + 366 - 208.5 \qquad (4.45) \\ &= 137.3 \text{ kcal/mol} \end{aligned}$$

This value is close to $PA(C_2H_6) = 139 \pm 2$ kcal/mol deduced

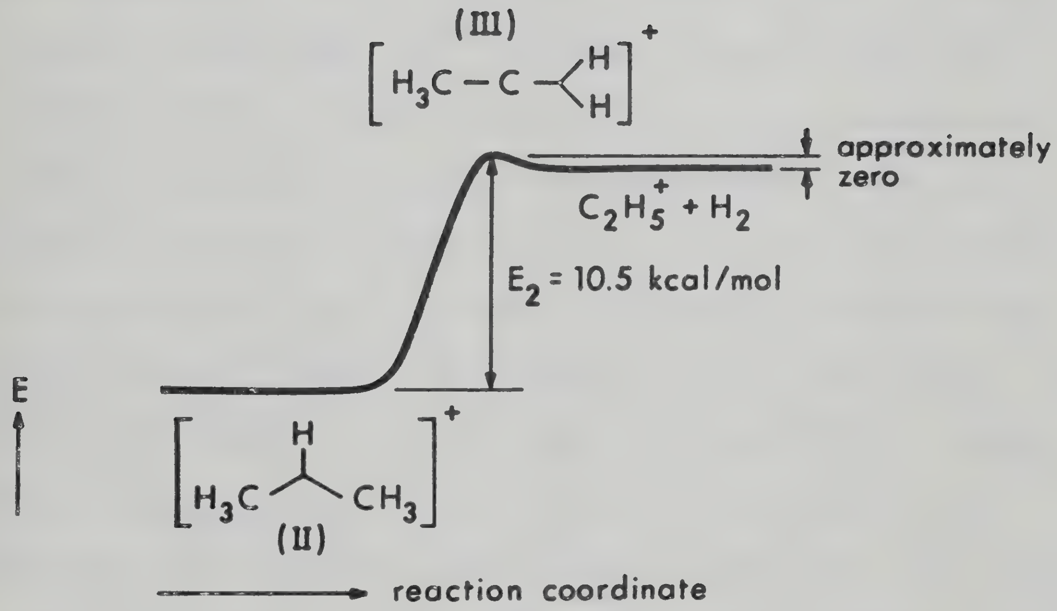
(III)
$[H_3C-C\langle^H_H]^+$
approximately zero
$C_2H_5^+ + H_2$
E_2 = 10.5 kcal/mol
E
$[H_3C\overset{H}{\wedge}CH_3]^+$
(II)
reaction coordinate

FIGURE 4.56. Schematic Potential Energy Diagram for the Reaction $C_2H_7^+ \longrightarrow C_2H_5^+ + H_2$.

from recent measurements by Bohme (42). From the proton affinity of ethane calculated here and from the known value of PA(CH_4) = 127 kcal/mol (144), the proton affinity difference between the two compounds is 10.3 kcal/mol.

The treatment of the data in three different ways shows that the proton affinity difference between methane and ethane is 9.0 ± 1.2 kcal/mol, which agrees with Bohme's results rather than the 1 kcal/mol found by Chong and Granklin (123). This work supports Bohme's suggestion (124), that equilibrium was not achieved in Chong and Frahklin's system. These workers conducted their experiments at 67°C, where we have shown the dissociation of $C_2H_7^+$ to $C_2H_5^+$ and H_2 to be appreciable. Therefore, under Chong and Franklin's conditions, the equilibrium between CH_5^+ and $C_2H_7^+$ was disturbed by the "leakage" of $C_2H_7^+$ through dissociation. This example emphasizes the importance of being able to observe the temporal behaviour of the ions being studied so that the achievement of equilibrium can also be observed.

4.9 Analog Computer Analysis of Results

The validity of a reaction sequence may be tested by simulating the change of ion intensity with time on an analog computer. The values of the rate constants are adjusted until an optimum fit to the experimental points is obtained. The rate constants used in the fitting are the

pseudo-first order rate constants ν_i, where $i = \pm 1$ to ± 3 in this system.

The reaction sequence used was

$$CH_5^+ + C_2H_6 \underset{k_{-1}}{\overset{k_1}{\rightleftharpoons}} C_2H_7^+ + CH_4 \tag{4.7}$$

$$C_2H_7^+ + CH_4 \underset{k_{-2}}{\overset{k_2}{\rightleftharpoons}} C_2H_5^+ + H_2 + CH_4 \tag{4.36}$$

$$C_2H_5^+ + \begin{matrix} CH_4 \\ C_2H_6 \end{matrix} \xrightarrow{k_{ov}} C_4H_9^+ \text{ and } C_3H_7^+ \tag{4.46}$$

A set of differential equations may be written to describe the system.

$$\frac{d[CH_5^+]}{dt} = \nu_{-1}[C_2H_7^+] - \nu_1[CH_5^+] \tag{4.47}$$

$$\frac{d[C_2H_7^+]}{dt} = \nu_1[CH_5^+] - \nu_{-1}[C_2H_7^+] - \nu_2[C_2H_7^+] + \nu_{-2}[C_2H_5^+] \tag{4.48}$$

$$\frac{d[C_2H_5^+]}{dt} = \nu_2[C_2H_7^+] - \nu_{-2}[C_2H_5^+] - \nu_{ov}[C_2H_5^+] \tag{4.49}$$

$$\frac{d[\text{product}]}{dt} = \nu_{ov}[C_2H_5^+] \tag{4.50}$$

where ν_{ov} represents the overall disappearance of $C_2H_5^+$ to $C_3H_7^+$ and $C_4H_9^+$.

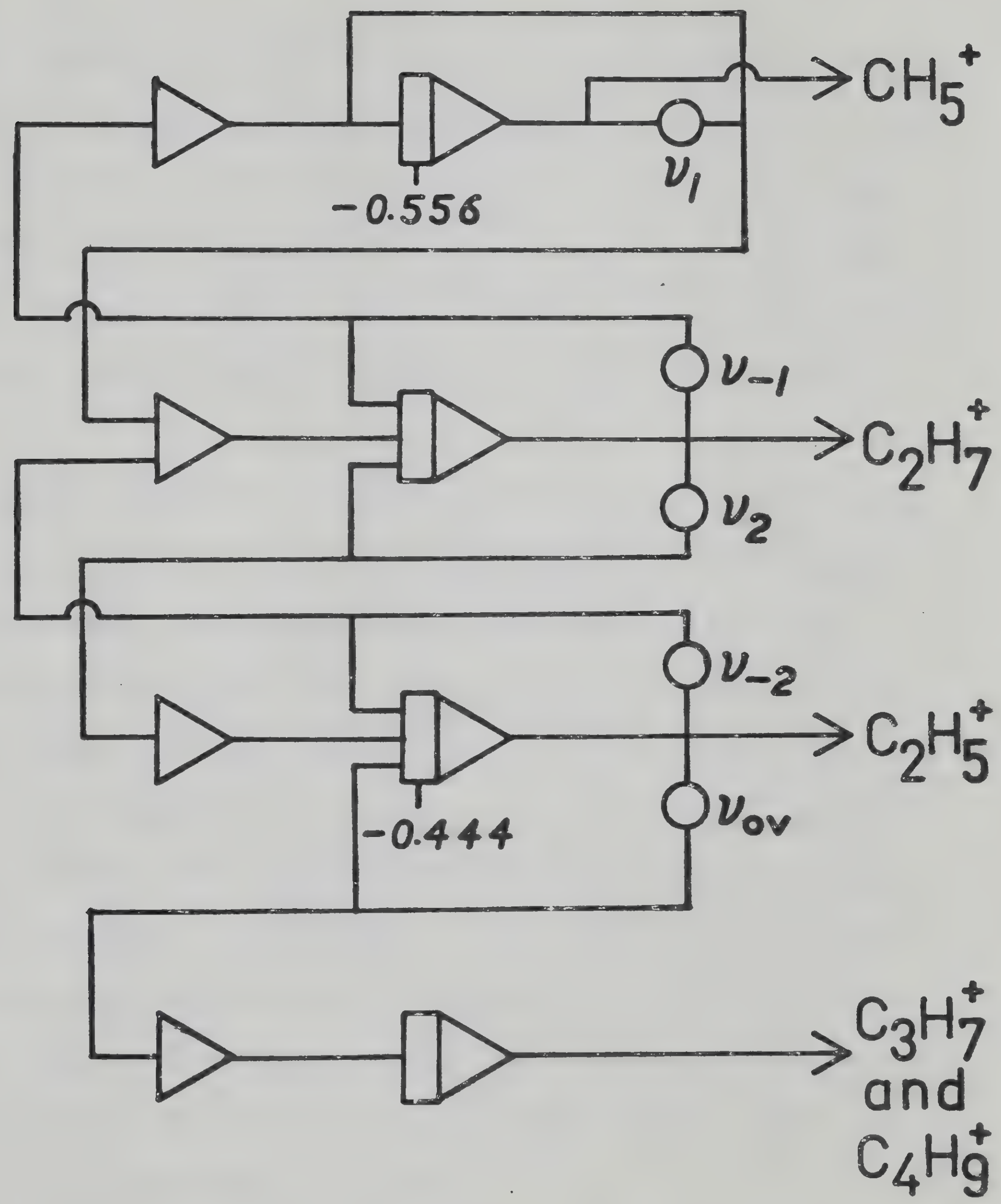
CH_5^+
-0.556
ν_1
ν_{-1}
$C_2H_7^+$
ν_2
ν_{-2}
$C_2H_5^+$
-0.444
ν_{ov}
$C_3H_7^+$ and $C_4H_9^+$

FIGURE 4.57. Analog Computer Program to Produce Best Fit for the Normalized Intensity Curves.

The reactions of CH_4^+ and CH_3^+ to CH_5^+ and $C_2H_5^+$, respectively, were too rapid to be explicitly included in the computer analysis. Since CH_4^+ and CH_3^+ are formed in the ratio of 5:4 and the abundance ratio of their product ions $CH_5^+:C_2H_5^+$ is very similar (37) at 2 torr, the initial conditions were set at $[CH_5^+] = 0.556$ and $[C_2H_5^+] = 0.444$ at $t = 0$.

Equations (4.47) to (4.50) can be solved analytically (145), or more readily with an analog computer. The analog computer used was a Yokogawa Electronic Works Type 3302 whose accuracy was about 1%. The computer program used is shown in Figure 4.57 and the fitted curves are shown by the solid lines in Figures 4.3 to 4.31. It was found that the agreement between the calculated and experimental rate constants was generally within 20%. Since the final rate constants in the reaction sequence depend on those that preceed them, the error increases for the rate constants of later reactions. The calculated and experimental rate constants are summarized in Table IX.

Since the analog program takes into account the fact that $C_2H_7^+$ is still producing $C_2H_5^+$ as the $C_2H_5^+$ is reacting further with methane and ethane, the ν_{ov}' values obtained from the analog fit may be used to find a more accurate value of k_4 by plotting $\nu_{ov}/[C_2H_6]$ versus $[CH_4]/[C_2H_6]$ as in Figure 4.41 using equation (4.32). Figures 4.58 and 4.59 show these plots at 30°C and 86°C, the points for 106°C

TABLE IX

Average Rate Constants

		$k_1 \times 10^9$		k_{-1}		$k_2 \times 10^{14}$		$K_2 = k_2/k_{-2}$		$k_3 \times 10^{11}$		$k_4 \times 10^{14}$	
		cm^3 $molecule^{-1}$ s^{-1}											
Temp.	# expts.	exp	calc	exp[a]	calc	exp	calc	calc	b	exp	calc	exp	calc
30°C	9	1.7	1.9	1.1×10^{-15}	3.9×10^{-15}	0.22	0.17	11	1.1	5.3	2.2	-	0.7
86°C	10	1.6	1.8		4.4×10^{-14}	3.2	2.4	5.8	13.3	1	-	1	1.6
97°C	1	1.6	0.6		-	5.8	5.7	2	23	-	-	-	-
106°C	11	1.6	1.4		1.6×10^{-14}	8.8	6.9	11.7	35.7	-	-	-	-
156°C	3	1.4	1.3		-	37	38	-	-	-	-	-	-
210°C	3	1.4	1.1		-	134	134	-	-	-	-	-	-

a. k_{-1} calculated from k_1/K_1

b. From reference 143.

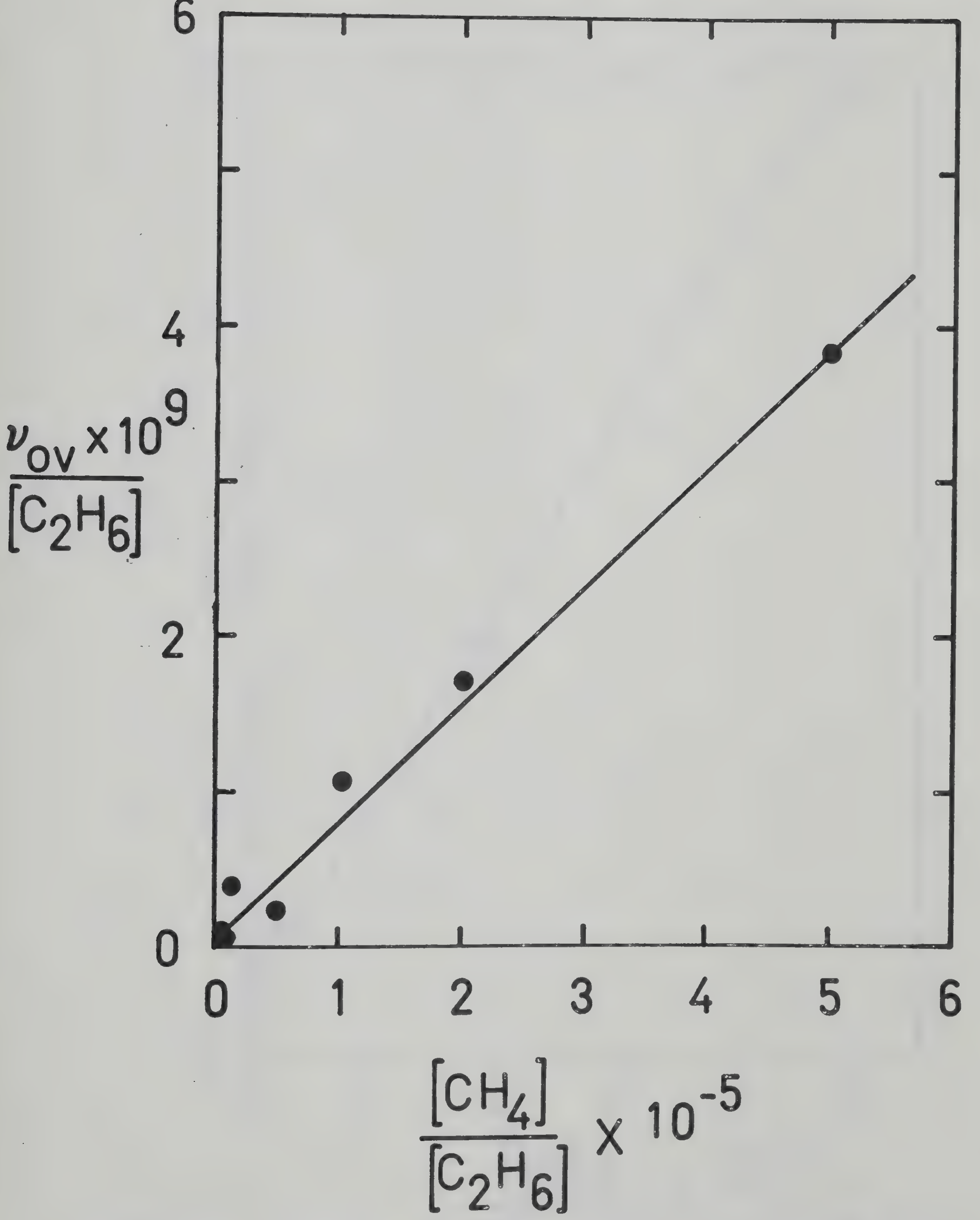

FIGURE 4.58. Plot of $\nu_{ov}/[C_2H_6]$ versus $[CH_4]/[C_2H_6]$ at 30°C Using Values of ν_{ov} Calculated from Best Computer Fit.

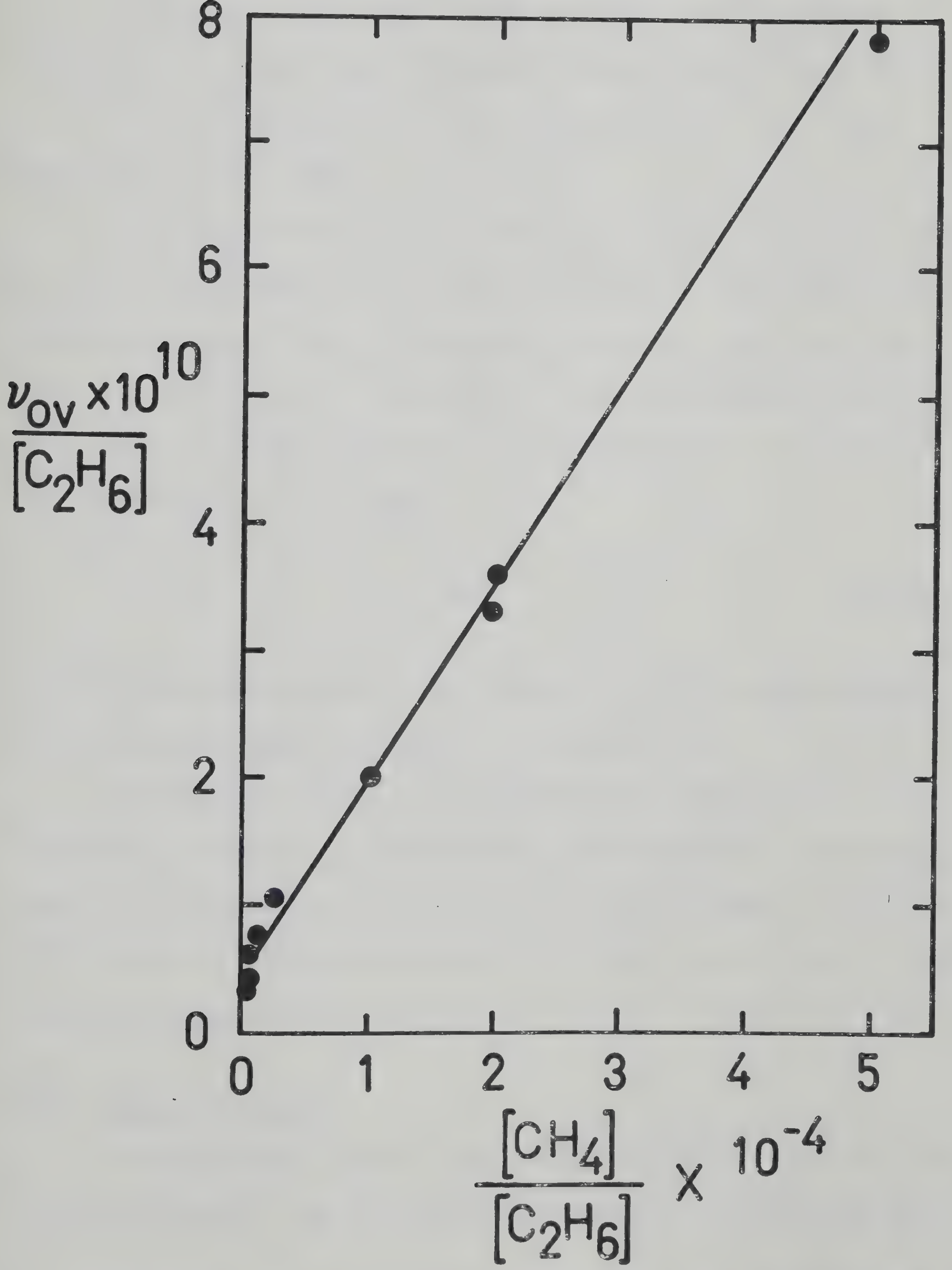

FIGURE 4.59. Plot of $\nu_{ov}/[C_2H_6]$ versus $[CH_4]/C_2H_6]$ at 86°C Using Values Calculated from Best Computer Fit.

were too scattered to obtain a meaningful slope. k_4 from the slopes of these graphs was 6.9 x 10^{-15} cm^3 $molecule^{-1}$ s^{-1} at 30°C and 1.6 x 10^{-14} cm^3 $molecule^{-1}$ s^{-1} at 86°C, these values agree with Hiraoka's values of k_4 (134) of 9 x 10^{-15} cm^3 $molecule^{-1}$ s^{-1} at 30°C and 1.7 x 10^{-14} cm^3 $molecule^{-1}$ s^{-1} at 86°C.

The magnitude of K_1 is also predicted to be very large by the analog computer program. Out of 50 experiments only three were found with a measurable reverse reaction rate for reaction (4.7). The average calculated value for k_1 was 1.9 x 10^{-9} cm^3 $molecule^{-1}$ s^{-1} and k_{-1} was 1.9 x 10^{-14} cm^3 $molecule^{-1}$ s^{-1}. Since

$$K_1 = \frac{k_1}{k_{-1}} \qquad (4.28)$$

K_1 is predicted to be of the order of 10^5, the same magnitude as calculated previously in section 4.5.

The analog computer is therefore a useful tool in verifying a reaction sequence but its accuracy in predicting the rate constants in a long reaction scheme is only sufficient to indicate the order of magnitude of the various rate constants.

4.10 Recent Results

Although the project was terminated at this point, the investigation of the energetics of reaction (4.14) was con-

tinued on another instrument by Dr. K. Hiraoka and a summary

$$C_2H_7^+ \longrightarrow C_2H_5^+ + H_2 \qquad (4.14)$$

of his findings is included here where they are pertinent to the project under discussion.

The apparatus of Hiraoka and Kebarle (62,146) could be used with two ion sources, one for use with experiments below room temperature and another for room temperature and above.

Hiraoka (143) studied the reverse of reaction (4.14).

$$C_2H_5^+ + H_2 \xrightarrow{k_{-2}} C_2H_7^+ \qquad (4.42)$$

He found that two different isomers of $C_2H_7^+$ could be observed experimentally each with different energetic properties. The structures II (C-C protonated ethane) and III (C-H protonated ethane) were attributed to the two isomers.

At temperatures between -100°C and +40°C, reaction (4.42) was observed and the structure of $C_2H_7^+$ was assumed to be II. The rate constant, k_{-2}, was measured at various

$$C_2H_5^+ + H_2 \xrightarrow{k_{-2}} C_2H_7^+(\mathrm{II}) \qquad (4.42)$$

temperatures in this range and the Arrhenius plot defined the relationship (4.51)

$$k_{-2\mathrm{II}} = 7.3 \times 10^{-14} \exp\left(\frac{-1175 \text{ cal/mol}}{RT}\right) \qquad (4.51)$$

$$\mathrm{cm^3\ molecule^{-1}\ s^{-1}}$$

The activation energy, E_{-2}, for reaction (4.42) is therefore very small, 1.2 kcal/mol as was assumed in the thermochemical calculations in section 4.8. The results also showed that reaction (4.42) was second order, whereas in section 4.7 it was assumed to be third order. The evidence presented there however was not conclusive enough to prove second or third order. Reaction (4.42) is an association reaction and this type of reaction is normally third order (9,146).

Third order reactions generally have no activation energy barrier for the formation of the ion-molecule complex. These types of reactions normally have a negative temperature dependence because as the temperature increases the lifetime of the adduct ion decreases. Hiraoka observed a second order dependence for reaction (4.42) and a positive temperature dependence. Hiraoka and Kebarlė proposed that the observed temperature dependence may arise from the fact that only a small fraction of reactants, i.e. those on the high energy end of the Maxwell distribution, surmount the activation barrier to form the associated excited complex. The complex contains excess energy approximately equal to the potential energy difference between the zero point energy of the complex and the top of the energy barrier. The complex is therefore long-lived and efficiently stabilized by third body collisions. When excited complexes are formed without having to pass an activation barrier, all of

the reactant molecules are able to participate. The resultant complex contains excess thermal energy and is much shorter lived. The rate of formation therefore remains third order up to higher pressures.

Within the temperature range 85° to 200°C the reverse reaction rate of reaction (4.42) becomes comparable to the forward reaction rate and measurements of the equilibrium constant, K_{-2} were possible. The van't Hoff plot is shown

$$C_2H_5^+ + H_2 \overset{K_{-2}}{\rightleftarrows} C_2H_7^+(II) \qquad (4.42)$$

on the left hand side of Figure 4.60 and led to $\Delta H^o_{-2} = -11.8$ kcal/mol and $\Delta S^o_{-2} = -25$ e.u. The point at the low temperature end of this line, represented by a closed square was not obtained by direct equilibrium measurement but from the ratio $K_{-2} = k_{-2}/k_2$ where k_{-2} was obtained from Hiraoka's measurements and k_2 was the rate constant at room temperature measured in this work (Figure 4.55). The points fit the extrapolated results of Hiraoka's very well.

Below -100°C the rate of production of $C_2H_7^+$ by reaction (4.42) was too slow to observe. However, as the temperature was lowered further the formation of $C_2H_7^+$ could be observed again. Hiraoka found that the formation of $C_2H_7^+$ below -130°C had a negative temperature dependence, which was indicative of an exothermic association reaction, in which the adduct ion is formed without passing over an

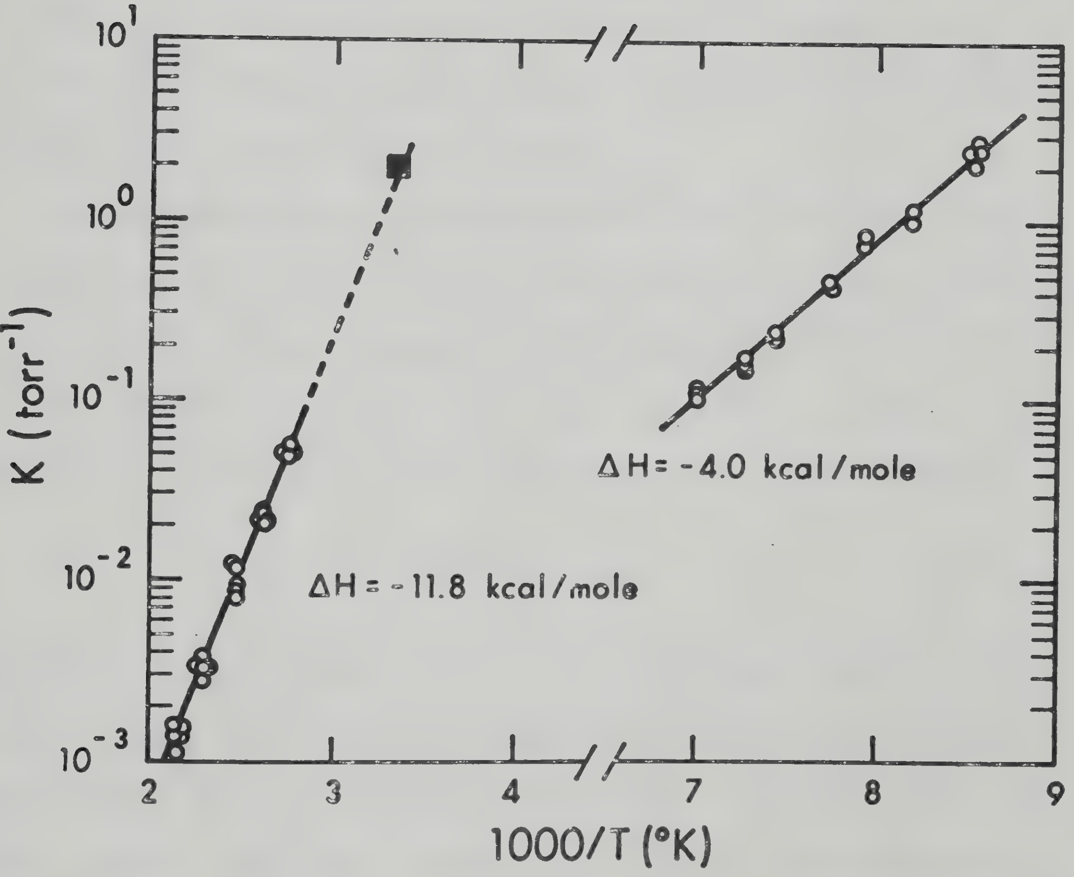

FIGURE 4.60. van't Hoff Plot for the Equilibrium $C_2H_5^+ + H_2 \rightleftarrows C_2H_7^+$ Studied at Two Different Temperature Ranges.

activation energy barrier. Such reactions generally depend on a third body. The equilibrium (4.42) was studied over the temperature range -130°C to -160°C. The van't Hoff plot obtained is shown on the right hand side of Figure 4.60. ΔH^{o}_{-2} for this reaction was -4.0 and ΔS^{o}_{-2} was -19.6 e.u. Therefore the $C_2H_7^+$ ion observed at high and low temperatures have different thermochemical properties and must therefore be a result of two different isomers.

The thermochemical data obtained from Hiraoka's work is summarized in the energy diagram shown in Figure 4.61. The activation energy measurement of reaction (4.14) described in section 4.7 gave E_2 = 10.5 kcal/mol. From Figure 4.61 $E_2 = 1.2 + 11.8 = 13$ kcal/mol. The smaller

$$C_2H_7^+ \xrightarrow{k_2} C_2H_5^+ + H_2 \qquad (4.14)$$

value of E_2 found by measuring k_2 in this work may be due to the reverse reaction rate becoming important at higher temperatures, making the apparent forward rate smaller. The overall effect would be to make the slope of the Arrhenius plot smaller and thus E_2 would be smaller.

An earlier paper by Lathan, Hehre and Pople (128), using STO-3G basis, suggested that the classical structure of $C_2H_5^+$ (IV) was 11 kcal/mol more stable than the bridged structure V.

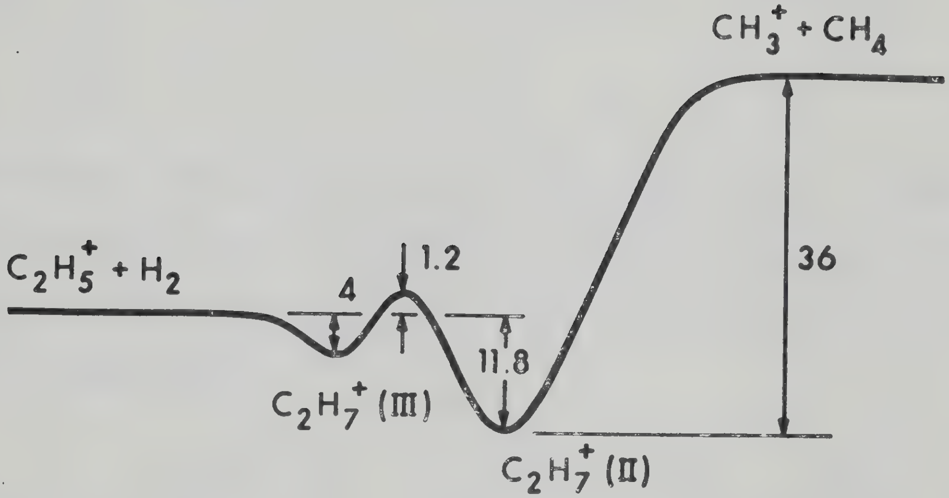
$CH_3^+ + CH_4$
$C_2H_5^+ + H_2$
1.2
4
36
11.8
$C_2H_7^+$ (III)
$C_2H_7^+$ (II)

FIGURE 4.61. Schematic Potential Energy Diagram for the Reaction of Protonated Ethane.

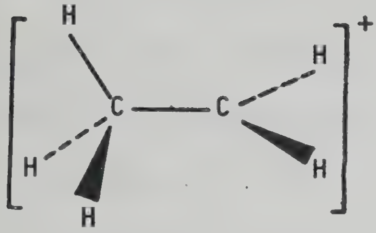

IV

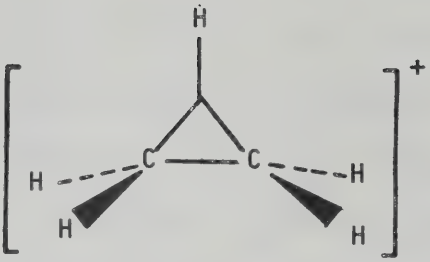

V

Therefore as a hydrogen molecule approaches $C_2H_5^+$, assumed to have the most stable structure IV, the initial formation of $C_2H_7^+$ is most likely to be structure III as visualized in the scheme (4.52).

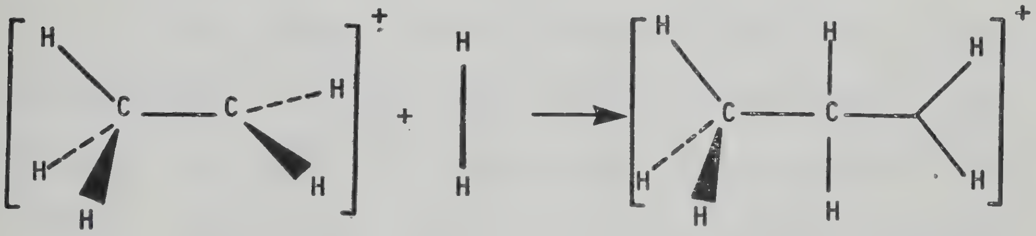

(4.52)

IV III

At the high temperatures used in this work, 30°C to 230°C, the thermal energy of the reactants is sufficient to surmount the 5.2 kcal/mol barrier to rearrange and form the more stable structure II. At the low temperatures used by Hiraoka, below -130°C, the thermal energy of the reactants is not enough to pass over the barrier and the ion observed has the structure III under these temperature conditions. This scheme is reasonable as structure III consists of a $C_2H_5^+$ ion weakly interacting with the electron pair of a hydrogen molecule. The fact that $\Delta H_{-2} = -4$ kcal/mol for

reaction (4.42) at low temperatures is small, is a measure of the bond energy in the $C_2H_5^+.H_2$ complex. The thermochemical measurements obtained by Hiraoka therefore support the assumptions made in section 4.8 concerning the isomeric structures of $C_2H_7^+$ as it participates in reaction (4.14).

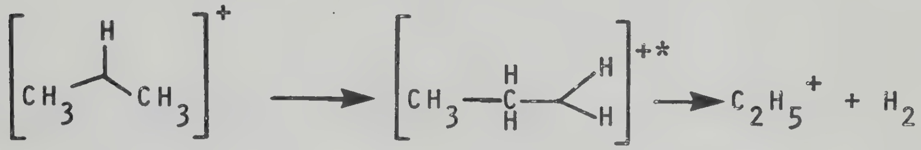

(4.14)

II III IV

A very recent report by Pople (147) has extended the calculations of $C_2H_5^+$. The first improvement (4-31G) doubled the number of basis sets in the valence shell. A further improvement ($6\text{-}31G^*$) included the d-functions on the carbon atoms and finally included a set of p-functions on each hydrogen ($6\text{-}31G^{**}$). Table X shows that as more functions are taken into account, the bridged structure of $C_2H_5^+$ becomes favoured compared to the classical structure. This trend had also been found by Zurawski et al (148).

If the favoured structure of $C_2H_5^+$ is the bridged structure then the hydrogen molecule must approach broadside to the C-C bond in $C_2H_5^+$ and the transition state can be represented by structure VI.

TABLE X

Theoretical Calculations by J. A. Pople (147) of the Relative Energies of $C_2H_5^+$ Isomers Using Different Basis Sets

	STO-3G	UHF/4-31G	UHF/6-31G*	UHF/6-31G**	UMP2/31-G*
$C_2H_5^+$ (classical, IV)	-11.4	-7.3	-0.1	-0.4	6.3
$C_2H_5^+$ (bridged, V)	0	0	0	0	0

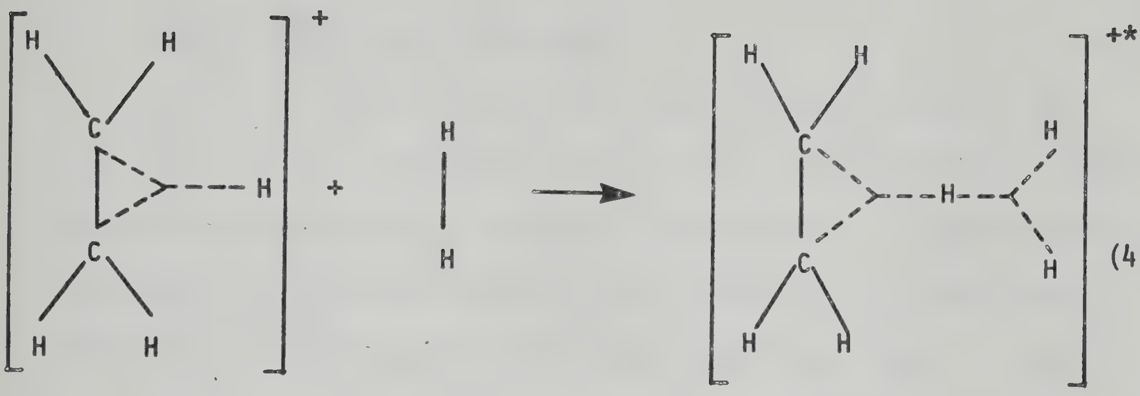

VI

(4.53)

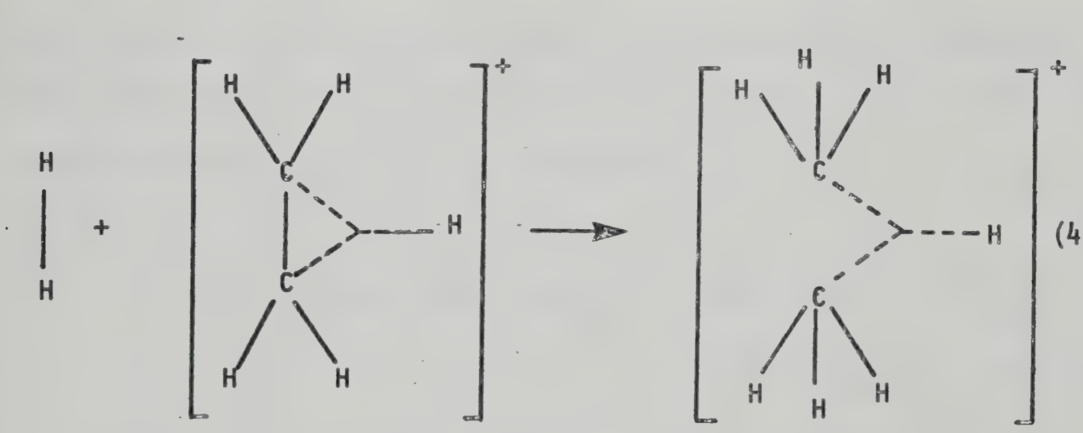

II

(4.54)

The occurrence of an excited intermediate such as VI is difficult to understand but attack from the rear as in reaction (4.54) may conceivably lead to the stable isomer of $C_2H_7^+$(II). It then becomes difficult to explain the potential energy curve in Figure 4.61 in terms of the number of maxima and minima if structure II is to remain the most stable structure of $C_2H_7^+$.

4.11 Other Reactions Observed

Other ions observed were $C_2H_4^+$, $C_3H_5^+$, $C_4H_{10}^+$ and $C_5H_{11}^+$. $C_2H_4^+$ is formed by the primary and secondary fragmentation processes of methane and ethane. It was assumed that $C_2H_4^+$ originates mostly from the major constituent, methane, by reaction (4.55) (37). The reaction of $C_2H_4^+$

$$CH_2^+ + CH_4 \longrightarrow C_2H_4^+ + H_2 \qquad (4.55)$$

with ethane is well known, (112,114,129,149) but Bennett, Lias and Field (131) were the first to report the stabilized intermediate $C_4H_{10}^+$ in the reaction

$$\begin{aligned} C_2H_4^+ + C_2H_6 \longrightarrow [C_4H_{10}^+]^* &\longrightarrow C_3H_7^+ + CH_3 \\ &\xrightarrow{M} C_4H_{10}^+ \qquad (4.56) \end{aligned}$$

The ion $C_4H_{10}^+$ was also observed in the present work, as a minor product, when the ethane concentration was high. The formation of $C_3H_7^+$ by reaction (4.56) was thought not to interfere with the kinetic analysis of the reaction of $C_2H_5^+$ described in section 4.6 since the reaction of $C_2H_4^+$ was extremely slow and the concentration of ethane was low.

The $C_3H_5^+$ ion is also a product of a secondary reaction (4.57) in methane (37). The precursor $C_2H_3^+$ was

$$C_2H_3^+ + CH_4 \longrightarrow C_3H_5^+ + H_2 \qquad (4.57)$$

not observed in these experiments. $C_3H_5^+$ was found to be essentially unreactive in the methane/ethane system.

The $C_5H_{11}^+$ ion was only observed during the experiments with a methane to ethane ratio of 50:1 at temperatures below 80°C. The intensity of $C_5H_{11}^+$ was very small, only about 0.5% of the total ionization. $C_5H_{11}^+$ must be formed from an ion association reaction with ethane, for example (4.58). $C_5H_{11}^+$ has been observed in pure methane

$$C_3H_7^+ + C_2H_6 \longrightarrow C_5H_{11}^+ + H_2 \qquad (4.58)$$

(37) but there are no reports of the ion being observed in ethane or methane/ethane mixtures.

4.12 Conclusion

The study of the methane-ethane system has brought to light some interesting information. The measurement of the proton affinity difference between these two compounds proved that this difference was at least 10 kcal/mol. A recent measurement (44) has estimated that the proton affinities of higher alkanes show similar differences to their lower homologues. For example the proton affinity of propane was calculated to be 148 kcal/mol, almost 10 kcal/mol above that of ethane. Similarly the proton affinity of iso-butane was estimated to be 164 kcal/mol, a difference of 16 kcal/mol from its lower homologue.

The independent observation of the reaction of $C_2H_5^+$ with methane in reaction (4.31) substantiated the previous

$$C_2H_5^+ + CH_4 \longrightarrow C_3H_7^+ + H_2 \qquad (4.31)$$

report from this laboratory that this reaction was very slow but observable and the rate constant could be measured.

The dissociation of $C_2H_7^+$ to $C_2H_5^+$ and H_2 had been observed by several workers but no rate constants had been measured before and no investigations into the temperature dependence of the reaction had been reported. The pyrolysis of $C_2H_7^+$ explains some anomalies of previous work done on the methane-ethane system and also initiated further investigations of the reaction which led to the observation and thermochemical measurements of two different isomers of $C_2H_7^+$ and higher homologues.

CHAPTER 5

SOLVATION OF Cl^- BY VARIOUS SOLVENT MOLECULES

5.1 Introduction

The recent application of ion-molecule reactions to acid-base measurements has created great interest and the field has expanded rapidly. The measurement of gas phase acidity and basicity using ion-molecule reactions is important because it enables the intrinsic acidic or basic behaviour of the molecule to be investigated without the interference of a solvent. This type of measurement also eliminates ions of the opposite charge which complicate the interpretation of data obtained from solution studies. Gas phase measurements are therefore useful to the physical organic chemist who is well versed in the acidic and basic behaviour of organic compounds in solution and can interpret the gas phase measurements to estimate the effect of solvents and other ions.

A measure of the gas phase acidity of a compound RH is the enthalpy for reaction (5.1), which is also the

$$R\text{-}H \longrightarrow R^- + H^+ \qquad (5.1)$$

proton affinity of R^-. The enthalpy for reaction (5.1) can be regarded as the heterolytic bond energy $D(R^- - H^+)$, which can also be expressed using the homolytic bond energy, D(R-H):

$$\text{Gas phase acidity} = D(R^- - H^+)$$
$$= D(R - H) + IP(H) - EA(R) \qquad (5.2)$$

where IP(H) is the ionization potential of the hydrogen atom and EA(R) is the electron affinity of the radical, R. Since IP(H) is common to expression (5.2) for all compounds RH, it can be omitted from calculations of the gas phase acidity. The relative measure of acidity is therefore the enthalpy for the reaction

$$e + RH \longrightarrow R^- + H \qquad (5.3)$$

Therefore,

$$\Delta H = D(R - H) - EA(R) \qquad (5.4)$$

Therefore as the gas phase acidity increases, the quantity D(R - H) - EA(R) decreases.

In a solution, the proton is always accepted by a base. Acid dissociation is therefore more accurately related to the gas phase analog of the Brönsted acid-base reaction

$$R_1H + R_2^- \rightleftharpoons R_1^- + R_2H \qquad (5.5)$$

The enthalpy for reaction (5.5) is

$$\Delta H = D(R_1 - H) - EA(R_1) - (D(R_2 - H) - EA(R_2)) \qquad (5.6)$$

In the investigation of ionic solutions, the nature of the interactions of the ions in solution, such as R^-, with their adjacent solvating molecules is of fundamental importance and has been the subject of numerous studies (150). Ion-solvent interactions can also be studied in the gas phase by first observing the isolated ion, then adding solvent molecules one at a time and examining the effect of each addition. This approach has been used in experimental and theoretical studies (151-155).

Ion-solvent interactions have traditionally been investigated in terms of electrostatic forces such as ion-dipole and ion-induced dipole forces. If a solvent molecule RH is considered, which has a dipole moment with the hydrogen carrying the partial positive charge, as RH approaches a negative ion X^-, the acidic hydrogen will be oriented towards X^-. The presence of the negative ion will induce a further shift of electrons away from the hydrogen atom. The complex $R^-H^+---X^-$ can be considered as resulting from a partial proton donation to the negative ion i.e. a partial neutralization of a Brönsted base, X^- by the acid RH. Kebarle et al (156) proposed that the interaction of RH with X^- should follow the gas phase acidity of RH i.e. the bond energies of the RHX^- complexes should increase as the gas phase acidity of RH increases.

Examination of gaseous ionic equilibria such as (5.7)

$$X^-(RH)_{n-1} + RH \underset{}{\overset{K_{n-1,n}}{\rightleftarrows}} X^-(RH)_n \qquad (5.7)$$

allows the equilibrium constant $K_{n-1,n}$ to be measured where

$$K_{n-1,n} = \frac{I_{X^-(RH)_n}}{I_{X^-(RH)_{n-1}} . P_{RH}} \qquad (5.8)$$

The measurement of $K_{n-1,n}$ at different temperatures yields $\Delta H^o_{n-1,n}$, $\Delta G^o_{n-1,n}$ and $\Delta S^o_{n-1,n}$ for the addition of a solvent molecule, RH to the ion cluster $X^-(RH)_{n-1}$. When $n = 1$, the equilibrium studied gives the thermodynamic parameters for the addition of the first solvent molecule to the isolated ion and is described by $K_{0,1}$, $\Delta G^o_{0,1}$ and $\Delta H^o_{0,1}$. Therefore if the above mentioned relationship holds it would be expected that the interaction between RH and X^- will increase as the gas phase acidity of RH increases. Quantitatively, one would expect $-\Delta H^o_{0,1}$ and $-\Delta G^o_{0,1}$ to increase as D(R - H) - EA(R) decreases.

5.2 Previous Work on Gas Phase Acidities

As discussed in the previous section a correlation between the gas phase acidities of compounds RH and the bonding in $RHCl^-$ complexes could exist. The present section provides an overview of the studies of gas phase acidities since this property will be needed in the subsequent treatment.

The first qualitative measurements of gas phase

acidities were reported by Brauman et al (30) in 1968. This study was the first direct measurement of relative acidities of neutral compounds in the gas phase.

Brauman and Blair (30) used Ion Cyclotron Resonance Spectroscopy (27,157,158) to measure the relative acidities: acetyl acetone > acetyl cyanide > hydrogen cyanide. Brauman determined the acidity order by observing in which direction proton transfer occurred between two of the compounds. For example, reaction (5.9) was observed to

$$CH_3COCN + CN^- \longrightarrow {}^-CH_2COCN + HCN \qquad (5.9)$$

occur in the direction shown, whereas the reverse reaction was not seen, indicating that it was endothermic. Acetyl cyanide is therefore a stronger acid than hydrogen cyanide in the gas phase. The relative acidities of acetyl acetone ($pK_a = 9.0$) and hydrogen cyanide ($pK_a = 9.2$) are in the same order in water (159,160) as in the gas phase at room temperature.

Brauman and Blair continued their study of gas phase acidities by investigating the relative acidities of a series of simple aliphatic alcohols (31,161) by proton transfer reactions of the type (5.10). If the reaction

$$R_1OH + R_2O^- \longrightarrow R_1O^- + R_2OH \qquad (5.10)$$

proceeds in the direction shown then the gas phase acidity of R_1OH is greater than that of R_2OH.

Brauman concluded from his results that all of the simple aliphatic alcohols were stronger acids than water in the gas phase. He also found that the larger the alkyl group the stronger the gas phase acidity. For example: $(CH_3)_3CCH_2OH > (CH_3)_3COH > (CH_3)_2CHOH > C_2H_5OH > CH_3OH > H_2O$. This is the opposite order expected from consideration of the electron releasing inductive effect of the alkyl groups, since substituents which are electron releasing will destabilize the negative charge in the alkoxide ion. Therefore the formation of the t-butoxide ion should be more unfavourable than the methoxide ion. The order of acidity in solution is $CH_3OH > C_2H_5OH > (CH_3)_3COH$, which is the reverse of the gas phase acidity order. Brauman suggested that the acidity order in solution includes solvation effects and does not represent the intrinsic molecular property.

Munson (162) has shown that the gas phase basicity order of methylamines followed the normal inductive order: $(CH_3)_3N > (CH_3)_2NH > CH_3NH_2 > NH_3$. Increase of amine basicity was expected with increased methyl substitution because methyl groups are electron releasing and stabilize the positive ion.

Therefore, according to Brauman's acidity measurements (161) and Munson's basicity measurements (162), increasing the number of alkyl groups stabilizes both anions and cations in the gas phase. To explain these results, Brauman

postulated (31) that in the gas phase the ability of the alkyl groups to stabilize both positive and negative saturated ions arises from the polarizability of the alkyl group. Some of the charge is spread over the alkyl group thus stabilizing positive or negative ions.

Further investigations by Brauman and Blair (32,163) indicated that in the measurement of gas phase acidities of amines, the same stabilizing effect of the amide ions by increasing alkyl substitution is observed, as in reaction (5.11). Comparison of solution and gas phase acidities was

$$R_1NH_2 + R_2NH^- \rightleftharpoons R_1NH^- + R_2NH_2 \qquad (5.11)$$

impossible in this case because of the difficulty of forming the amide ion in solution and is also complicated by the formation of ion pairs.

Brauman and Blair next investigated the stabilization effect of alkyl groups attached to an unsaturated carbon (164). It was found that in systems involving bonding to an unsaturated carbon, alkyl groups destabilized anions relative to hydrogen. However, larger alkyl groups stabilized anions relative to smaller ones.

Bohme et al (165) used the flowing afterglow technique to measure the forward and reverse rate constants of reactions of the type (5.12) to determine the equilibrium constant. By changing the nature of A and B the ΔpK_a

$$AH + B^- \underset{k_r}{\overset{k_f}{\rightleftharpoons}} BH + A^- \qquad (5.12)$$

can be calculated and an acidity scale can be built. Bohme has measured the gas phase acidities of various oxygen and carbon acids using this technique (166) and his results are in good agreement with the acidity order of Brauman's.

Neither the early experiments with the flowing afterglow technique (165) nor the ion cyclotron experiments by Brauman actually represented measurements of ionic equilibria. Yamdagni and Kebarle (167) were the first to observe ionic equilibria of the type (5.13) directly in order to determine the relative acidities of the two compounds A_1H

$$A_1H + A_2^- \rightleftharpoons A_2H + A_1^- \qquad (5.13)$$

and A_2H. The measurement of equilibria (5.13) enables ΔG^o to be calculated which is equal to the difference in gas phase acidities of A_1H and A_2H.

Kebarle et al (167) have measured the gas phase acidity of carboxylic acids. The order of acidity increase was acetic, propionic, butyric, formic acid. The former three acids follow the order Brauman found with the alcohols but formic acid is stronger than butyric acid which is analogous to the order of substituted acetylenes investigated by Brauman (164). Kebarle and coworkers further investigated the effect of halogen substituents on the

acidity of acetic acids (168). They found that, as observed in solution, introduction of a halogen substituent results in a large increase in acidity. The increased acidity has been ascribed to the stabilization of the negative charge by the electron withdrawing effect of the halogen substituent. A comparison of the ΔG^o values for proton transfer from acetic acid to the haloacetic acid in the gas phase and in solution shows that the ΔG^o values for the gas phase are on average about four times larger than those in solution. Kebarle et al also found that the order of acidities in the gas phase was Br > Cl > F which was the opposite to that found in aqueous solution.

Investigation of the gas phase acidities of many substituted benzoic acids by Kebarle and coworkers (71) enabled correlations to be drawn with the σ values of McDaniel and Brown (169) and the σ^o values of Taft (170). The correlation was better when σ^o values were used. The effect of substituents was again found to be larger in the gas phase than in solution. For this series of compounds the effect was ten times larger in the gas phase. Attenuation of the effects of substituents in aqueous solution has been observed by Taft (171) and Lossing (172) and has been attributed to a decrease in solvation for the stabilized ions.

Carbon acids have not been studied extensively in the gas phase. McMahon and Kebarle (72) have studied the

effect of substituents on methane. The acidity of the substituted methane increase in the order phenyl ≈ vinyl < acetyl < CN < benzoyl. The introduction of a second group of the same type increases the acidity by 60% of the first addition. A more recent study (173) has extended the measurement of the acidities of carbon and nitrogen acids and the effects of substituents upon the stabilities of the carbanions and nitrogen anions in the gas phase. The latter are seldom postulated in the mechanisms of organic reactions in solution.

The gas phase acidities of various substituted phenols (174) have been measured by McMahon and Kebarle and they found that the order of acidity in the gas phase and aqueous solution are the same. McIver and Silvers (175) have also measured the relative gas phase acidities of some substituted phenols. The agreement between McIver's and Kebarle's measurements is good. Theoretical calculations by Radom (176) predicted the same relative order of acidity of the substituted phenols as that found experimentally.

5.3 Previous Work on Chloride Affinities and Other Related Complexes

Yamdagni and Kebarle's proposal (156) that the order of increasing gas phase acidity of RH follows the order of hydrogen-bond energy of the complex $RH-X^-$ was tested on a series of alcohols and carboxylic acids. The chloride ion

was chosen as the negative ion because of the ease of producing it in the ion source.

The proposal of Yamdagni and Kebarle was based on studies of the ionic equilibria (5.14) and measurements of $\Delta H^o_{0,1}$ for various compounds RH. The $\Delta H^o_{0,1}$ measured is

$$RH + Cl^- \underset{}{\overset{K_{0,1}}{\rightleftarrows}} RHCl^- \qquad (5.14)$$

the hydrogen-bond energy in the complex $RH\text{-}Cl^-$. The order of $\Delta H^o_{0,1}$ observed was: $HCOOH > CH_3COOH > C_6H_5OH > CHCl_3 > (CH_3)_3COH > CH_3OH > H_2O$. Brauman had previously established (31) the order of the gas phase acidities to be $C_6H_5OH > (CH_3)_3COH > CH_3OH > H_2O$ which is in the same order as the hydrogen-bond energy in clusters with Cl^-. Kebarle _et al_ (167) had previously found that the gas phase acidity of formic acid was greater than that of acetic acid. The same order as the hydrogen-bond energy or chloride affinity.

The correlation between gas phase acidities and chloride ion affinities measured by Yamdagni and Kebarle is based on a small number of RH compounds nearly all of which were oxygen acids. It was felt that the range of compounds was too narrow to assume that the rule held universally. By studying different compounds the nature of the interaction between RH and Cl^- may be better understood. The recent studies of McMahon and Kebarle (173-174), which measured the gas phase acidities of many carbon and

nitrogen acids, provided a wide series of compounds with different functional groups to test the correspondence of acidity order and chloride ion affinity.

Before describing the results of the $RHCl^-$ equilibria measurements, a brief discussion of the theoretical work relative to complexes of this type is given.

To explain the interaction between RH and X^-, information on the detailed electronic structure of the solvated ion and the nature of the binding forces is required. Several groups have calculated the energy surfaces for the case where RH = HOH (154,177-179).

Diercksen and Kraemer performed ab initio SCF-MO calculations on $Li^+.H_2O$, $Na^+.H_2O$, $F^-.H_2O$ and $Cl^-.H_2O$ (177). Two stable structures of the anion-water complex are possible. The first is structure I which has C_{2v} symmetry. Structure II shows the other configuration which contains a hydrogen bond where F^- or Cl^- is in line with one of the O-H bonds. Diercksen and Kraemer found structure II to have the lowest energy with a hydrogen bond strength for $F^-.H_2O$ of 24.07 kcal/mol. This is in good agreement with the experimentally determined value of 23.3 kcal/mol (180) by Arshadi et al.

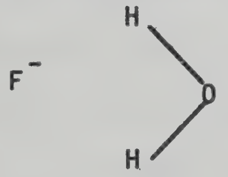

I

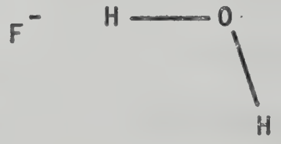

II

Clementi, also on the basis of ab initio SCF-MO calculations (178), noted that as the size of the anions increases, the distinction between the two limiting structures I and II becomes less important. Thus the energy minimum in the $Cl^-.H_2O$ complex corresponds to a $Cl^-.HOH$ angle of 165.4° instead of 180° for structure II. The angle in the $F^-.H_2O$ complex obtained by Clementi was 175.4°, nearer to a linear hydrogen bond and in substantial agreement with Diercksen's results. The calculated binding energy for the $Cl^-.H_2O$ complex obtained by Clementi was 11.24 kcal/mol for structure I and 11.30 kcal/mol for structure II. Arshadi's (180) experimental results for the $Cl^-.H_2O$ complex were 13.1 kcal/mol which does not agree so closely as the fluoride results.

Clementi and coworkers' work on cation-water complexes showed that there was no appreciable charge transfer from the water molecule to the cation (154). They found that the interaction was mainly electrostatic in origin i.e. from ion-dipole and ion-induced dipole interactions, the latter being due to a shift of electrons within the water molecule. In the anion-water complexes, Clementi et al (178) found that the interaction was also essentially electrostatic and that an appreciable electron shift or polarization occurred within the water molecule. These conclusions were based on the electron distribution in structures I and II for the $F^-.H_2O$ complex where the F-O

separation is 5.15 a.u. The gross Mulliken electron population

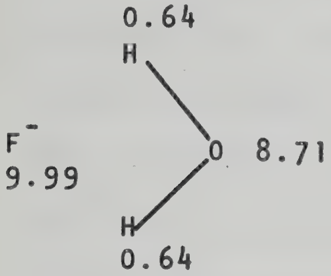

I

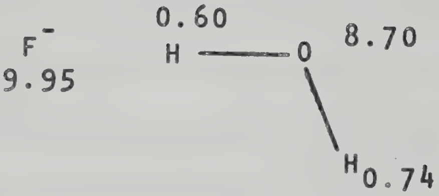

II

shows that there is a small amount of charge transfer from the fluoride ion to the water molecule in the hydrogen bond configuration whereas the amount of charge transfer is negligible in the C_{2v} structure. There is considerable charge transfer within the molecule for both structures. No data is given for the $Cl^-.H_2O$ complex but the charge transfer within the molecule will be less than for $F^-.H_2O$.

Since the theoretical calculations of Clementi and Diercksen show that the interaction in the anion-water complexes is mainly electrostatic there is some justification for doing electrostatic calculations which are more easily performed.

Electrostatic calculations have been performed by Eliezer and Krindel (181) and Spears (182) on ion hydrates. Spears (182) has also investigated complexes of anions and cations with such molecules as O_2, N_2 and CO_2 and found that the bonding energy between these compounds and the alkali and halide ions was about ten times less than

for a water molecule. This result may have been expected since O_2 and N_2 have no permanent dipole moments. Spears also pointed out that the ion-quadrupole interaction dominates the bond energies of complexes involving O_2, N_2 and CO_2 whereas they are negligible in complexes with water. Davidson and Kebarle (183) have carried out electrostatic calculations on complexes involving the solvation of positive and negative ions by water and acetonitrile.

The total stabilization energy, E_t between an ion and a single solvent molecule can be expressed as a sum of four terms shown in equation (5.15).

$$E_t = E_{dip} + E_{ind} + E_{dis} + E_{rep} \qquad (5.15)$$

E_{dip} is the ion-dipole attraction, E_{ind} is the ion-induced dipole interaction, E_{dis} is the energy due to attractive van der Waals or dispersion forces between the ion and the molecule and E_{rep} is the energy term representing the electronic repulsion between the ion and solvent molecule. Davidson and Kebarle (183) found experimentally that acetonitrile solvated positive ions better than negative ions. Electrostatic calculations using point dipoles predict equal solvation of positive and negative ions. By using the charge distribution over the whole molecule, Davidson's calculations of E_t agreed well with the experimentally measured $\Delta H^o_{0,1}$ values. The computations also showed that $E_{ind} + E_{dis}$ almost cancelled

E_{rep} so that $E_t \approx E_{dip}$. Therefore the major contribution to the total stabilization energy is the ion-dipole interaction. By calculating E_t for different orientations of the solvent molecule and comparing the different E_t's obtained to the measured $\Delta H^o_{0,1}$ the preferred orientation of the solvent molecule can be determined.

5.4 Experimental

The experiments carried out in this investigation were conducted on the instrument described in section 2.9.

Gas mixtures were made in a 5-litre bulb that was part of the gas handling system. The system was enclosed in a box that could be heated to 200°C. The temperature inside the box was generally maintained at 100-105°C, or a temperature which was sufficient to vaporize the compounds used. The gas handling plant was periodically baked at 200°C.

Gas mixtures were made by filling the bulb with one atmosphere of ultra high purity methane and then injecting the required amount of the liquids through an injection port. The gases were then allowed to mix for thirty minutes before performing the experiment. To ensure that thirty minutes was a sufficient time for the gases to be completely mixed, an experiment was performed at various intervals up to 20 hours from the time the gases were mixed. The equilibrium constant measured at

different times is shown in Figure 5.1. The equilibrium constant measured over the total time period was the same. Half an hour was therefore considered a sufficient period for the gases to be well mixed.

The reactant Cl^- ions were produced by adding traces (1.5 torr) of carbon tetrachloride to the bulb. Chloride ions were probably generated by dissociative electron capture of near thermal electrons by reaction (5.16). The chloride ions then reacted with RH forming $Cl^-(RH)_n$

$$e + CCl_4 \longrightarrow Cl^- + CCl_3 \qquad (5.16)$$

clusters by reaction (5.14). Suitable temperatures and pressures were chosen such that n was equal to 1.

If the compound, RH was a solid at room temperature, the substance was dissolved in methanol, which would not interfere with the cluster formation under study since methanol is a much weaker acid than any of the compounds investigated. Initially, carbon tetrachloride was thought to be a suitable solvent since it was added to the system anyway. However, the amount of carbon tetrachloride required to dissolve the acid was large and exerted 30 torr pressure in the bulb. Large peaks were found at the masses 160,162,164 and 166 with ratios of approximately 28:28:9:1 which is indicative of a compound containing three chlorine atoms (184). These peaks were broad and

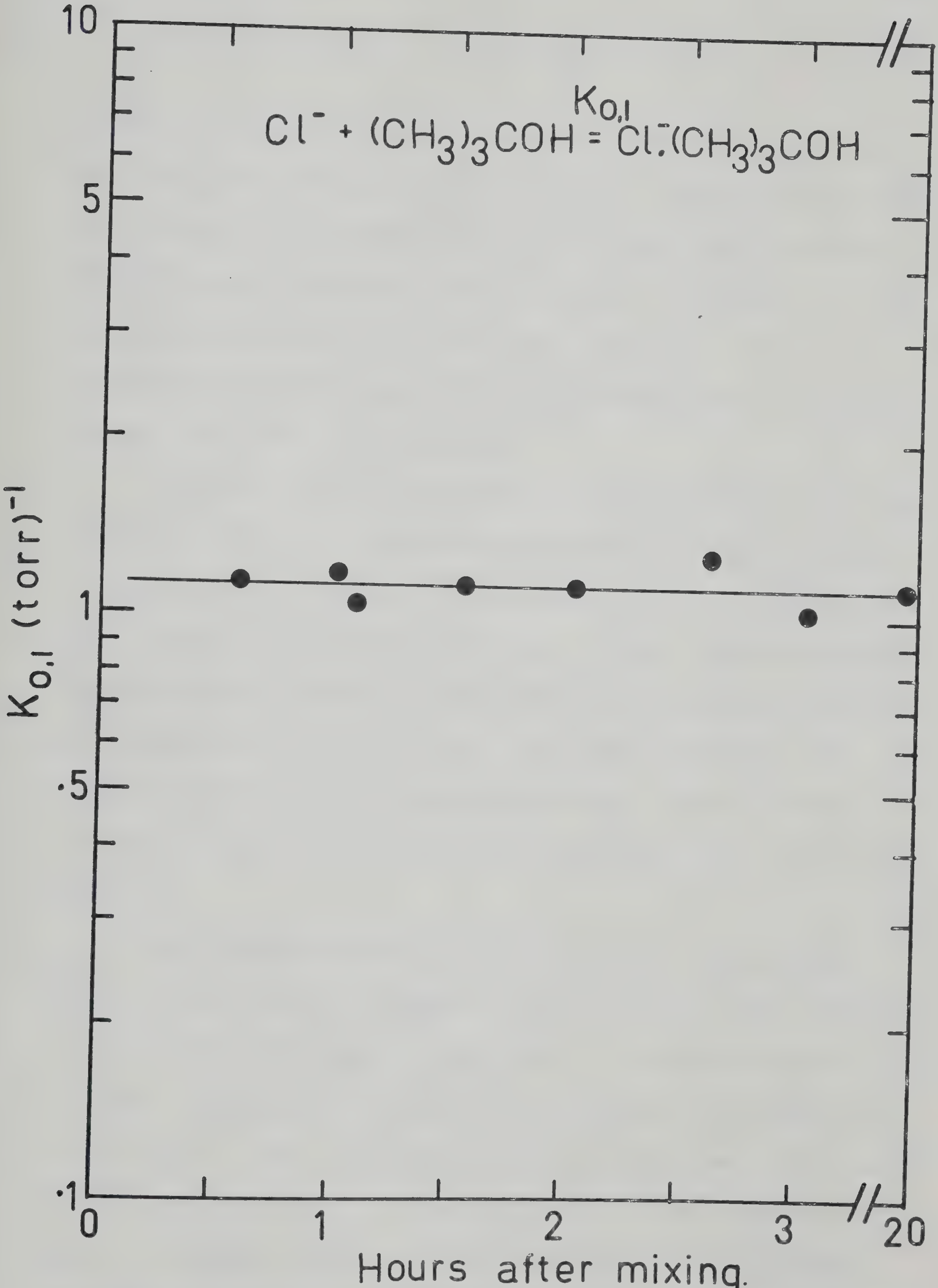

FIGURE 5.1 Plot of Equilibrium Constant $K_{0,1}$ for the Reaction $Cl^- + (CH_3)_3COH \rightleftarrows (CH_3)_3COH.Cl^-$ *versus* the Time After the Reactants Were Mixed in the Bulb.

diffuse and persisted even when the electron gun filament and gas supply were turned off. These spurious peaks were thought to be CCl_3^- which were generated by thermionic emission outside the ion source. The walls of the mass spectrometer must have been saturated with carbon tetrachloride as several days of pumping were necessary before the peaks disappeared.

Typical partial pressures in the bulb were 700 torr methane, 1.5 torr carbon tetrachloride, 10 to 50 mtorr of the acid and 50 torr of methanol, if the substance was a solid. The pressure of gas in the ion source was controlled by carefully adjusting the valve between the bulb and manifold to achieve the required flow. The temperature of the ion source could be varied between 25-435°C. Total ion source pressures of 1-5 torr were used.

The electron beam was pulsed on for 10-20 μsec every 3 msec and the temporal profile of the ion intensities were collected and stored in the multichannel scaler. Examples of typical ion profiles are shown in Figure 5.2. After 100 μsec, the ion profiles of Cl^- and $RHCl^-$ are parallel, indicating that the ion abundances are in a steady state and the two ions are in thermodynamic equilibrium. To eliminate the effect of any signal drift the chloride ion was collected for 30 seconds, for example, then the cluster ion $RHCl^-$ for 60

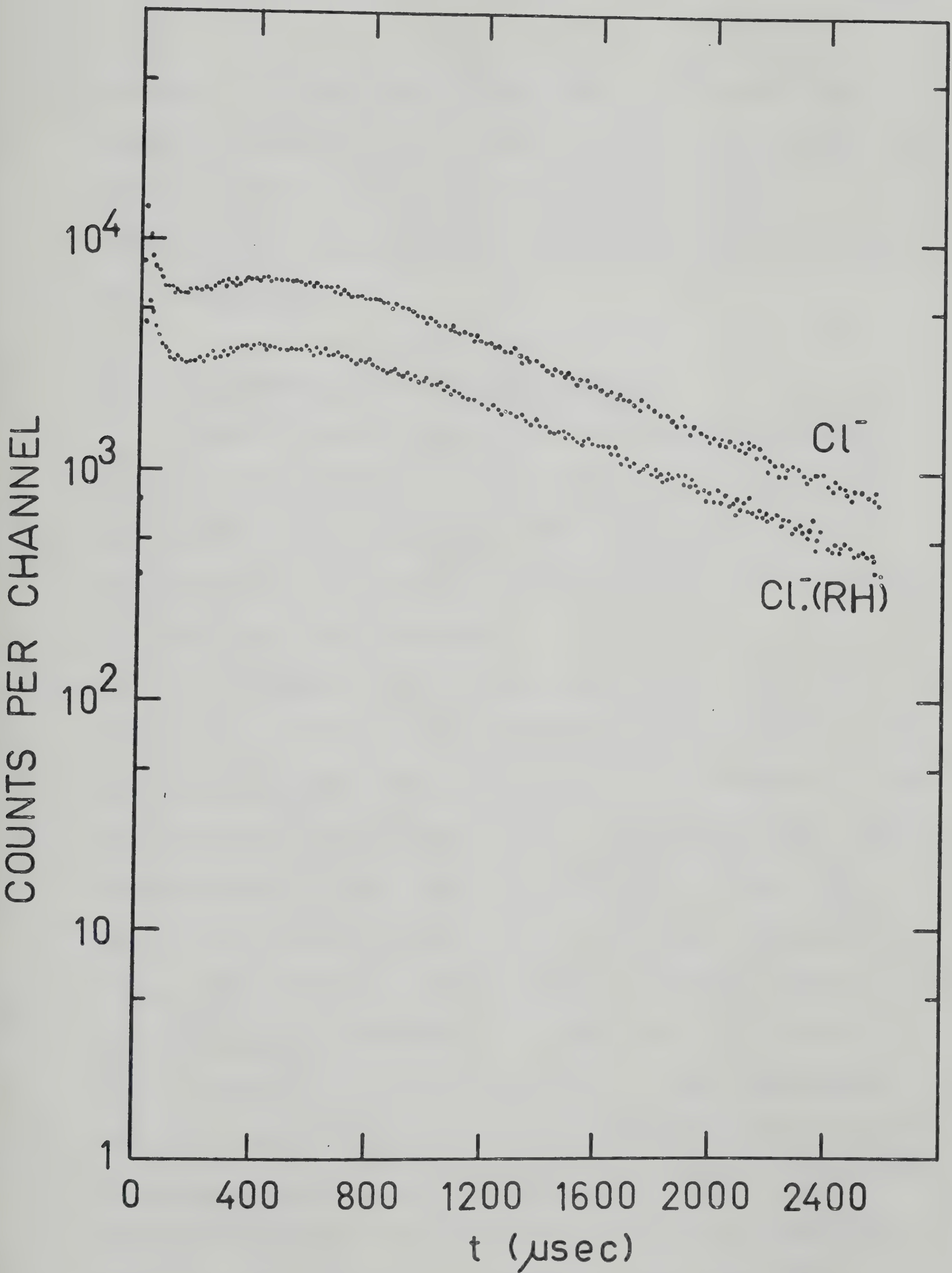

FIGURE 5.2. Time Dependence of Cl^- and $CH_3COCH_3.Cl^-$ Ions in 2.75 torr CH_4 Containing 0.15 torr Acetone at 114°C.

seconds. The chloride ion was again collected for a futher 30 seconds and accumulated with the previous collection of Cl^-. Thus each ion was collected for the same amount of time but any consistent drift in signal was eliminated.

5.5 Measurement of Ionic Equilibria

Special precautions have to be taken when measuring ionic equilibria to ensure that the measured ion intensities are an accurate reflection of the ionic concentrations in the ion source and that the ions are in true ionic equilibrium.

The largest error in the measurement of ionic equilibria is due to the problem of stripping (74). The region of highest pressure in the vacuum chamber is that just outside the ion exit slit. Stripping occurs when the pressure in this zone is sufficiently high that there is a probability of an ion emerging from the ion source and colliding with a neutral molecule before it reaches the mass analyzer. If the ion is a cluster $RHCl^-$, there is a possibility that it may dissociate into Cl^- and RH. Therefore the detected intensity of Cl^- is larger than it is inside the ion source and the observed intensity of the cluster ion is correspondingly smaller. The equilibrium constant, $K_{0,1}$ for reaction (5.14) is given by equation (5.17).

TABLE XI

The Effect of the Relative Intensity of Ions if 10% Collisional Dissociation Occurs

$P_{RH} = 0.1$ torr

		I_{RHCl^-}	I_{Cl^-}	$K_{0,1}$ (torr^{-1})
(a)	Inside Ion Source	10	1	100
	Outside Ion Source	9	2	45
(b)	Inside Ion Source	1	10	1
	Outside Ion Source	0.9	10.1	0.89

$$Cl^- + RH \xrightarrow{K_{0,1}} RHCl^- \qquad (5.14)$$

$$K_{0,1} = \frac{I_{RHCl^-}}{I_{Cl^-} \cdot P_{RH}} \qquad (5.17)$$

Therefore the stripping effect will result in a lower measured $K_{0,1}$ than the actual value. As the pressure in the ion source is increased, the pressure outside the ion source is increased and the number of collisions in this region increases. The effect of collisions outside the ion source can therefore be detected by measuring the equilibrium constant at different ion source pressures. If no stripping occurs the equilibrium constant will be independent of increasing pressure. If stripping occurs the equilibrium constant will decrease with increasing pressure. Normally the partial pressure of RH is varied by a factor of ten to test if such collisions occur.

The relative intensity of the ions is also important. If the pressure of RH is 100 mtorr, for example, and the ratio of $I_{RHCl^-}/I_{Cl^-} = 10$, then the equilibrium constant, $K_{0,1} = 100$ torr^{-1} (Table XI, case (a)). However, if 10% dissociation of the cluster $RHCl^-$ occurs then the intensities of both ions are changed and $K_{0,1}$ is now 45 torr^{-1}, a decrease of over 50%. If the ratio of I_{RHCl^-}/I_{Cl^-} is 0.1, then a dissociation loss of 10% means only

an 11% decrease in the equilibrium constant (case (b)). The pressure of the neutral, RH and the temperature of the ion source were therefore chosen such that the intensity of the chloride ion was at least twice that of the cluster ion under the worst conditions i.e. when the pressure of RH was highest.

The gas mixture in the 5-litre bulb could be flowed for over an hour before the rate of pressure drop was appreciable. This was sufficient time for four or five different ion source pressures to be used in an experiment with one mixture. A new mixture was then made containing a different partial pressure of the compound, RH. Using this method the partial pressure of RH could be varied over a factor of ten using two or three different mixtures.

5.6 Results

The compounds used in the clustering reaction with Cl^- varied from strong acids, such as substituted phenols to weak carbon acids such as ketones and substituted benzenes.

The equilibrium constant, $K_{0,1}$ was obtained from equation (5.17). If $K_{0,1}$ is measured at various tempera-

$$K_{0,1} = \frac{I_{RHCl^-}}{I_{Cl^-} . P_{RH}} \qquad (5.17)$$

tures a plot of $K_{0,1}$ *versus* 1/T gives $\Delta G^o_{0,1}$, $\Delta H^o_{0,1}$ and

$\Delta S^o_{0,1}$. The variation of $K_{0,1}$ as a function of temperature was measured for substituted phenols, phenol, acetone, formic acid and t-butanol. Clusters of Cl^- with formic acid and t-butanol had previously been measured in this laboratory (156) but were re-examined because Yamdagni's value of $\Delta S^o_{0,1}$ for HCOOH was -39.6 e.u. which is very large for an association reaction. On the other hand, the $S^o_{0,1}$ value obtained for t-butanol was only -10.3 e.u. which is very low for the same type of reaction. In Yamdagni's experiments the pure solvent was flowed through the ion source instead of being diluted as in this work. Figures 5.3 to 5.11 show the individual measurements on each compound. The equilibrium constant is measured at different pressures to check that true equilibrium is established and no collisional dissociation outside the ion source is occurring. Different bulb mixtures at the same temperature are shown by shaded and unshaded points. At low temperatures where I_{RHCl^-}/I_{Cl^-} approaches 100, the stripping becomes appreciable and $K_{0,1}$ decreases with increasing pressure, this is illustrated in Figure 5.4. The van't Hoff plots are shown in Figures 5.12 and 5.13 for RH = t-butanol, formic acid, acetone, phenol, p-cresol, p-chlorophenol, p-fluorophenol, p-cyanophenol using the average equilibrium constant determined at

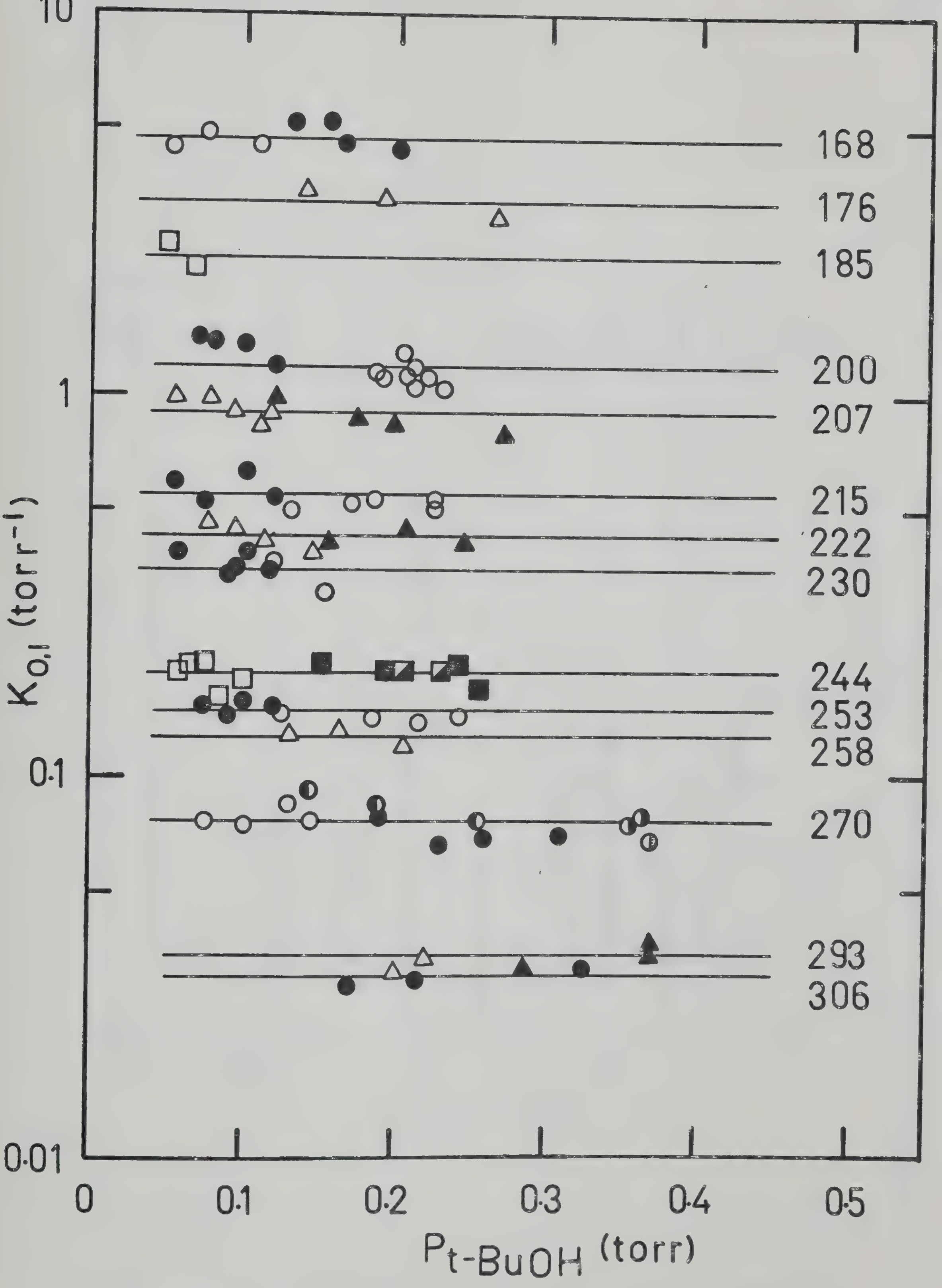

FIGURE 5.3. Measured Equilibrium Constants for the Reaction $Cl^- + (CH_3)_3COH \rightleftharpoons (CH_3)_3COH.Cl^-$ at Various Temperatures. Shaded and Unshaded Points at the Same Temperature Represent Different Mixtures.

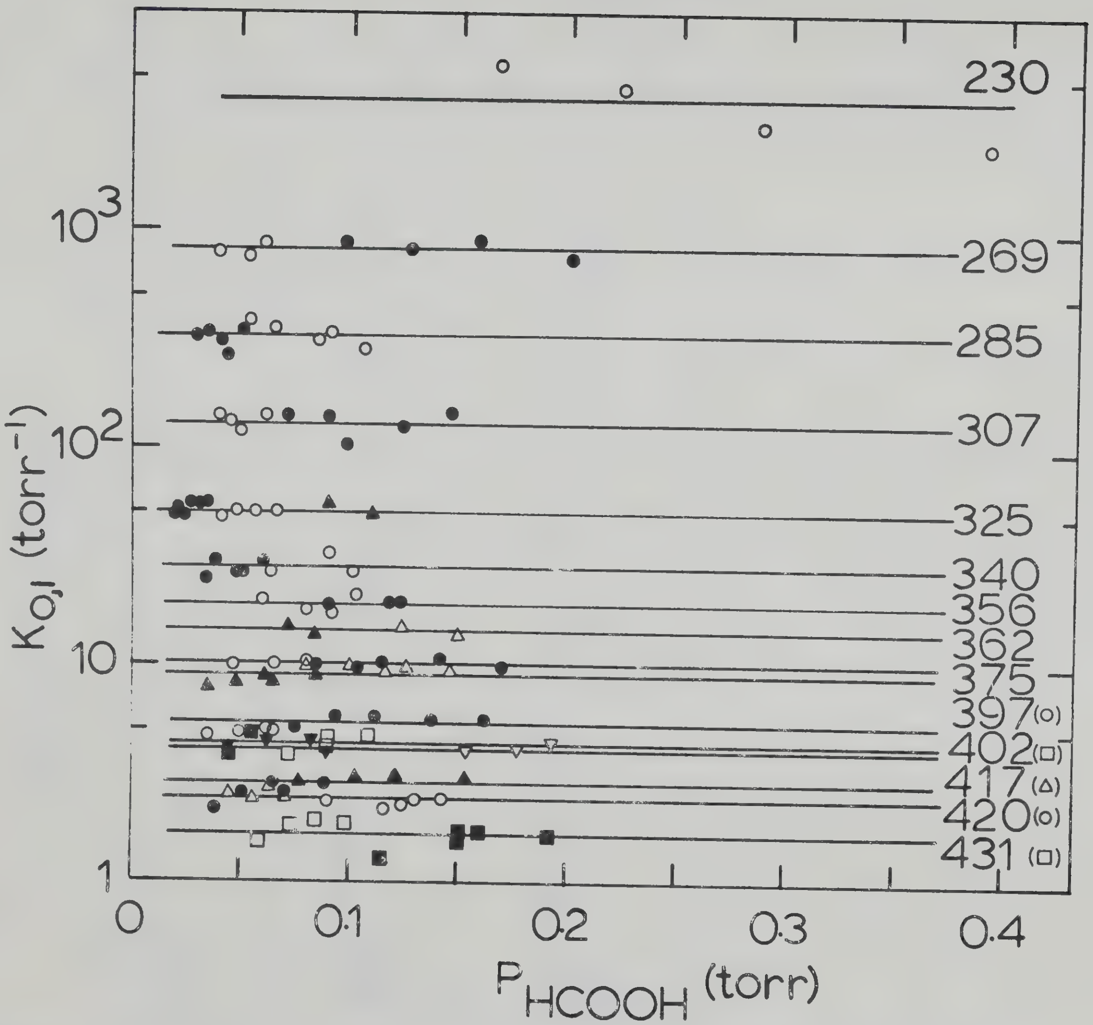

FIGURE 5.4. Measured Equilibrium Constants for the Reaction $Cl^- + HCOOH \rightleftarrows HCOOH.Cl^-$ at Various Temperatures.

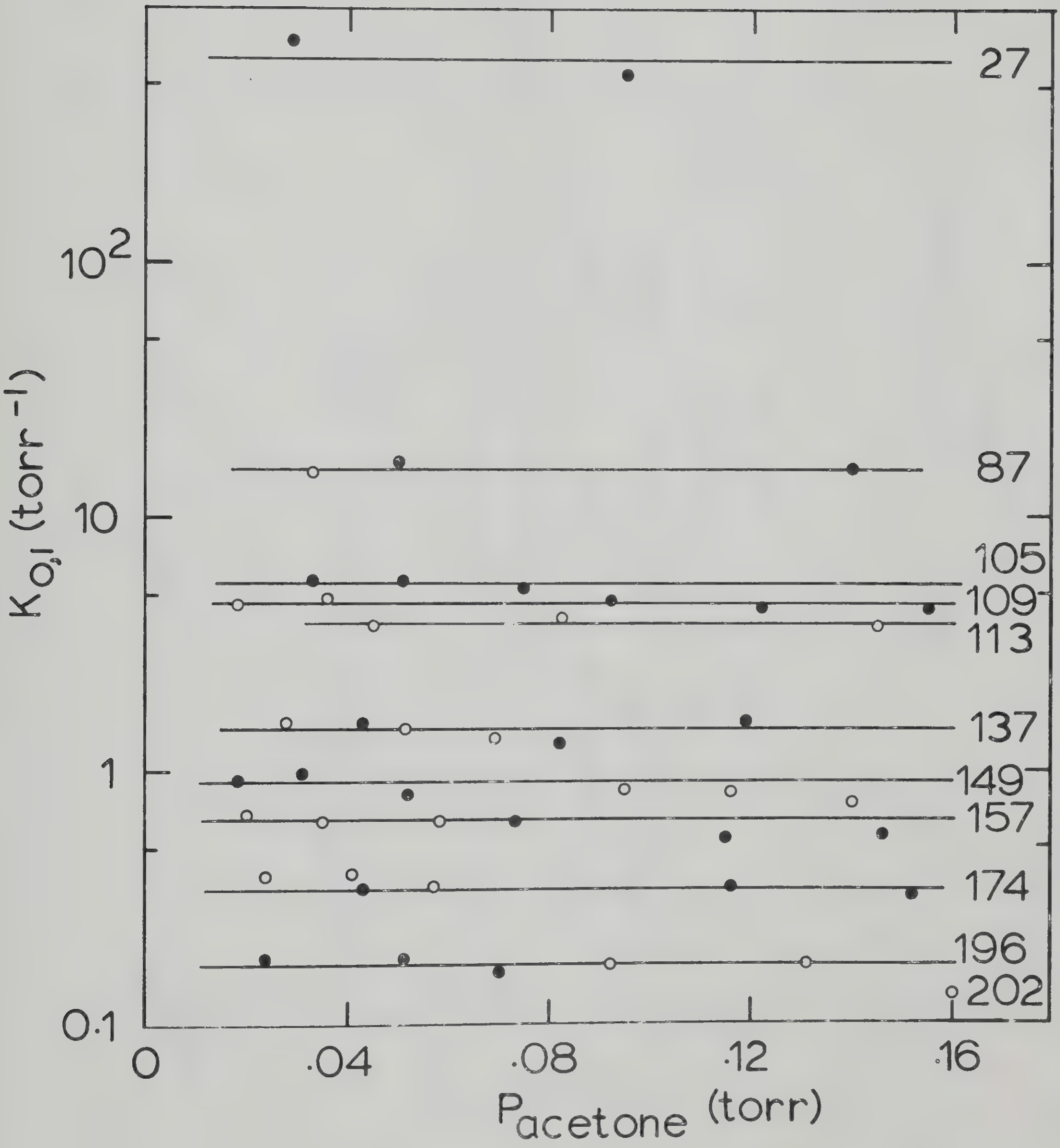

FIGURE 5.5. Measured Equilibrium Constants for the Reaction $Cl^- + CH_3COCH_3 \rightleftarrows CH_3COCH_3.Cl^-$ at Various Temperatures.

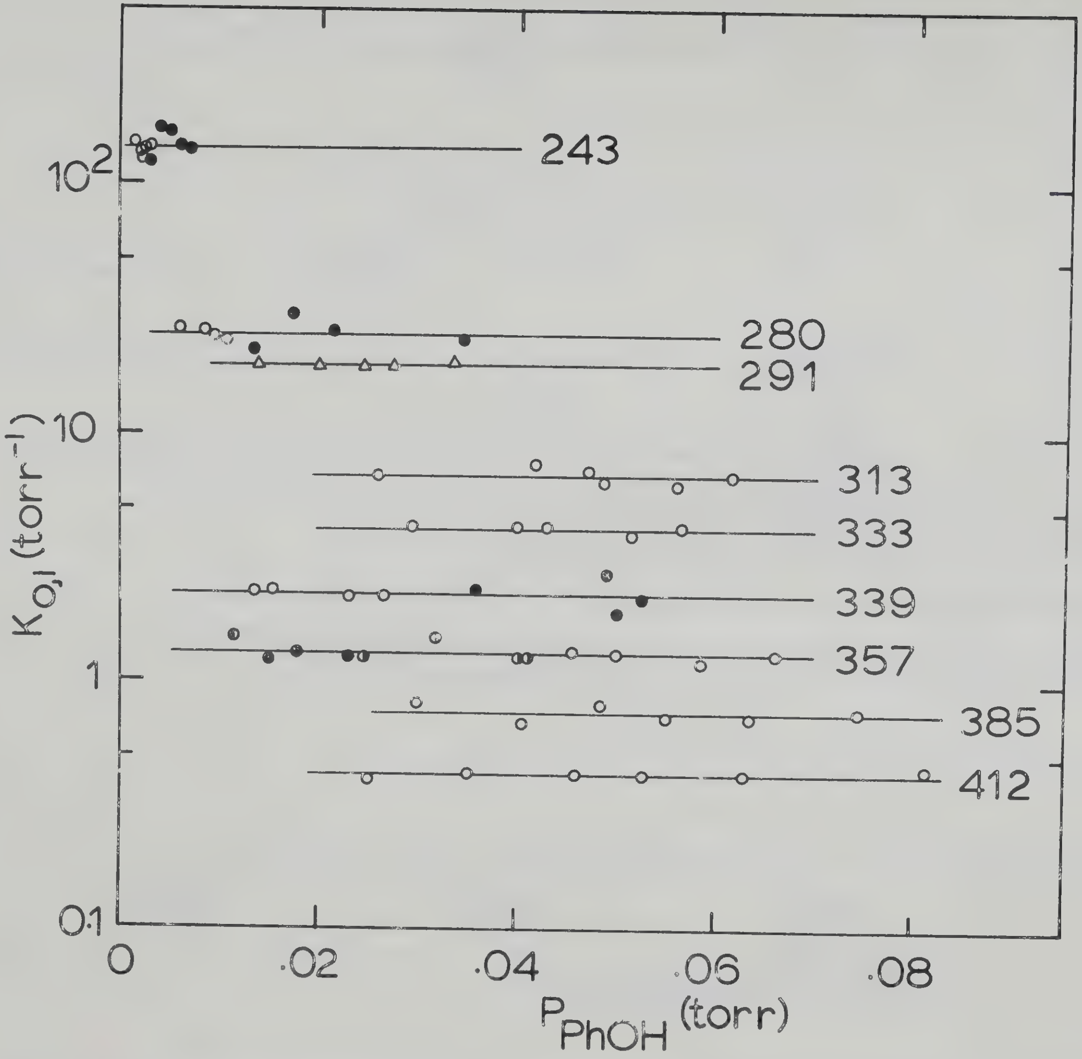

FIGURE 5.6. Measured Equilibrium Constants for the Reaction $Cl^- + C_6H_5OH \rightleftarrows C_6H_5OH.Cl^-$ at Various Temperatures.

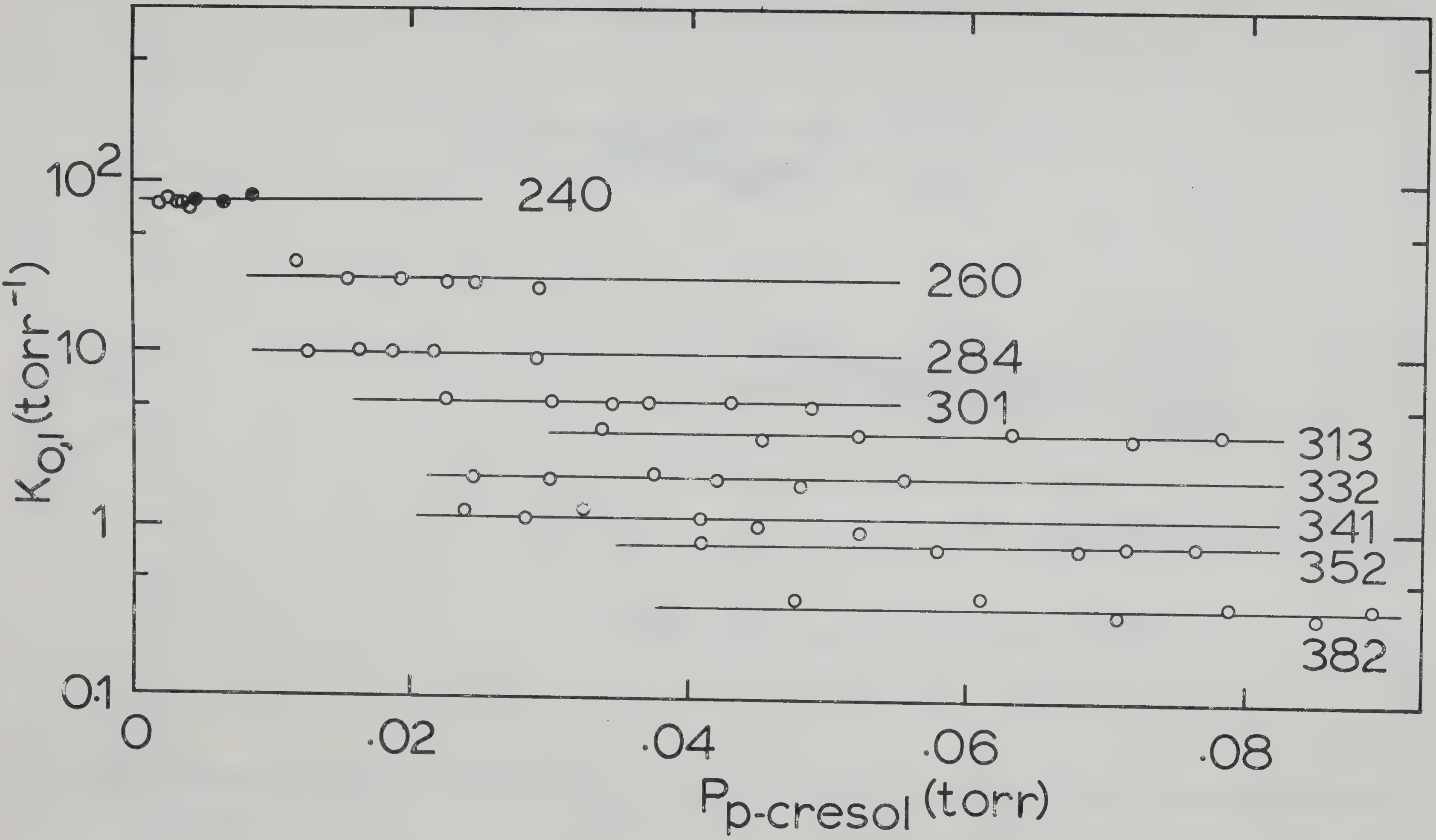

FIGURE 5.7. Measured Equilibrium Constants for the Reaction $Cl^- + p\text{-}CH_3.C_6H_4OH \rightleftharpoons p\text{-}CH_3C_6H_4OH.Cl^-$ at Various Temperatures.

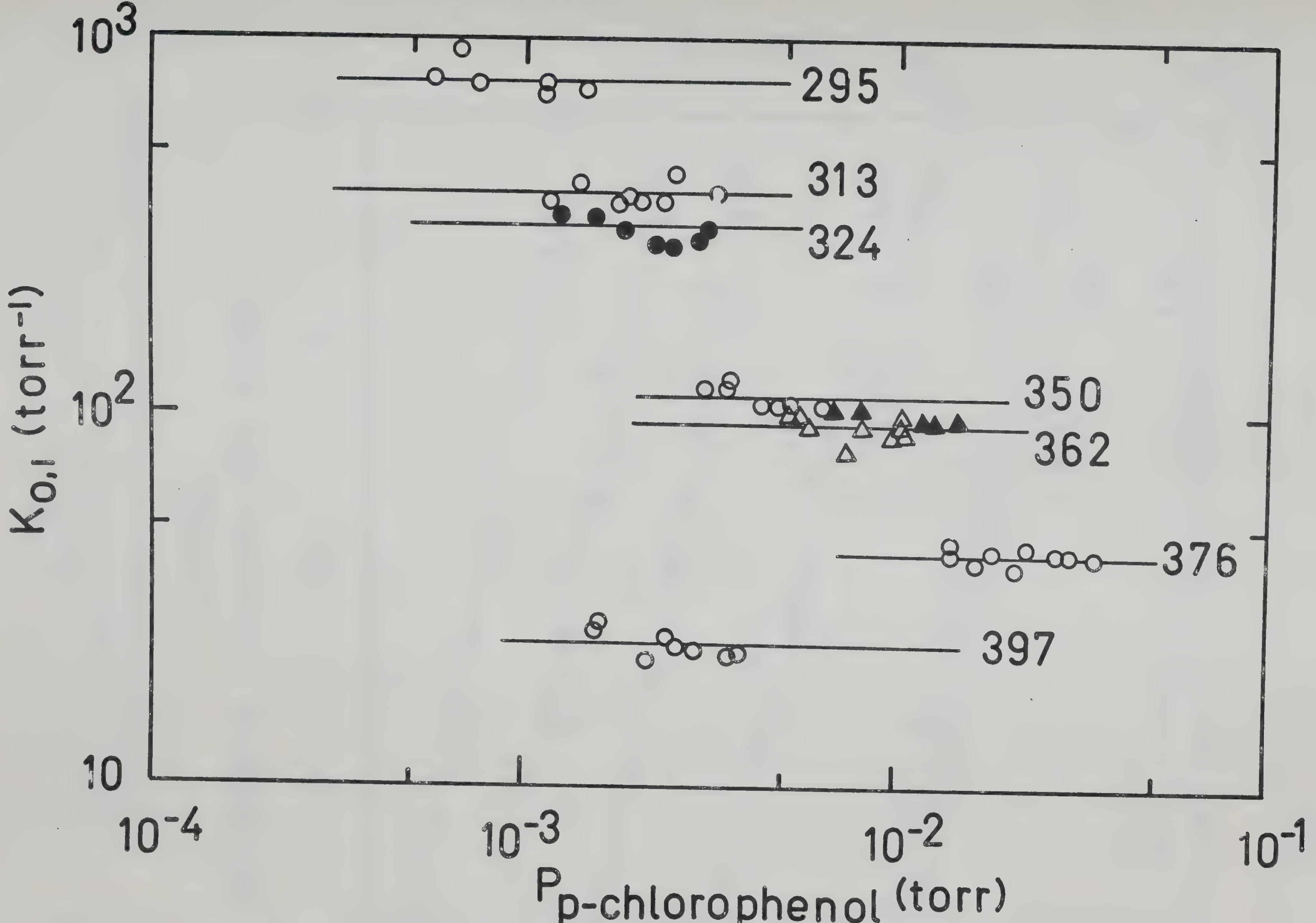

FIGURE 5.8. Measured Equilibrium Constants for the Reaction $Cl^- + p\text{-}Cl.C_6H_4OH \rightleftarrows p\text{-}Cl.C_6H_4OH.Cl^-$ at Various Temperatures

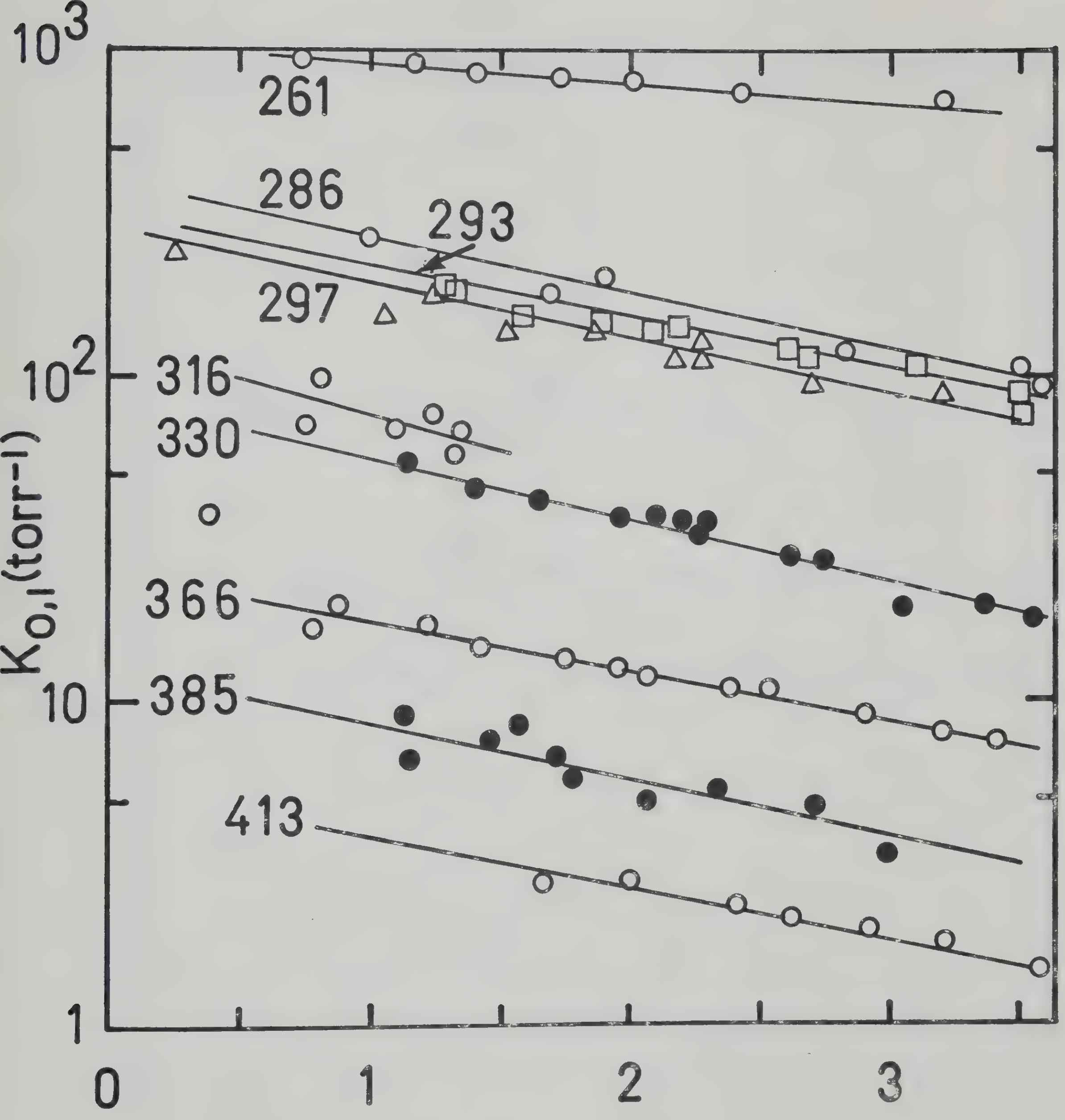

FIGURE 5.9. Measured Equilibrium Constants for the Reaction $Cl^- + p\text{-}F.C_6H_4OH \rightleftharpoons p\text{-}F.C_6H_4OH.Cl^-$ as a Function of Total Ion Source Pressure.

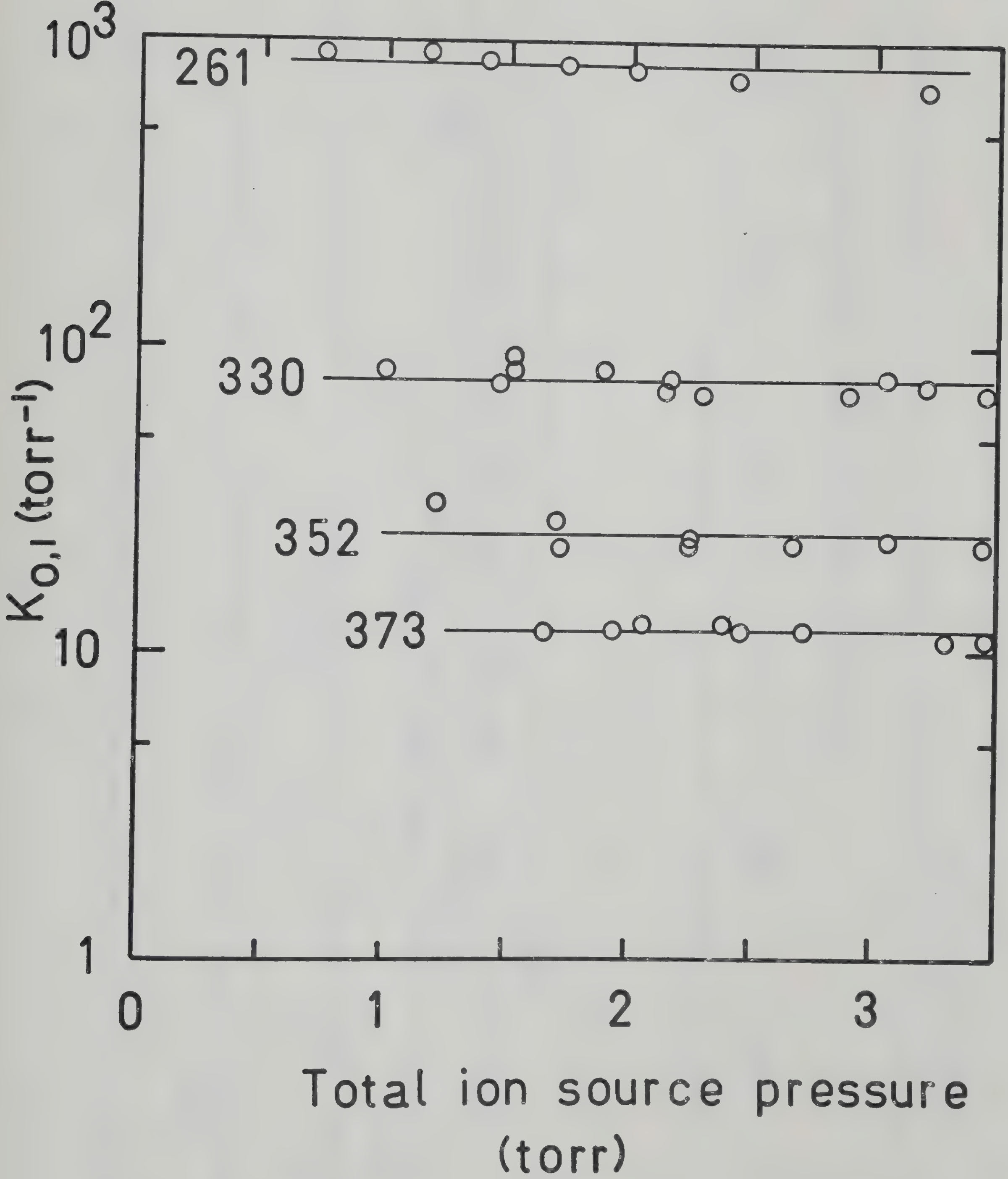

FIGURE 5.10. Measured Equilibrium Constants for the Reaction $Cl^- + p\text{-}F.C_6H_4OH \rightleftarrows p\text{-}F.C_6H_4OH.Cl^-$ as a Function of Total Ion Source Pressure After Changing the Ion Source Slits.

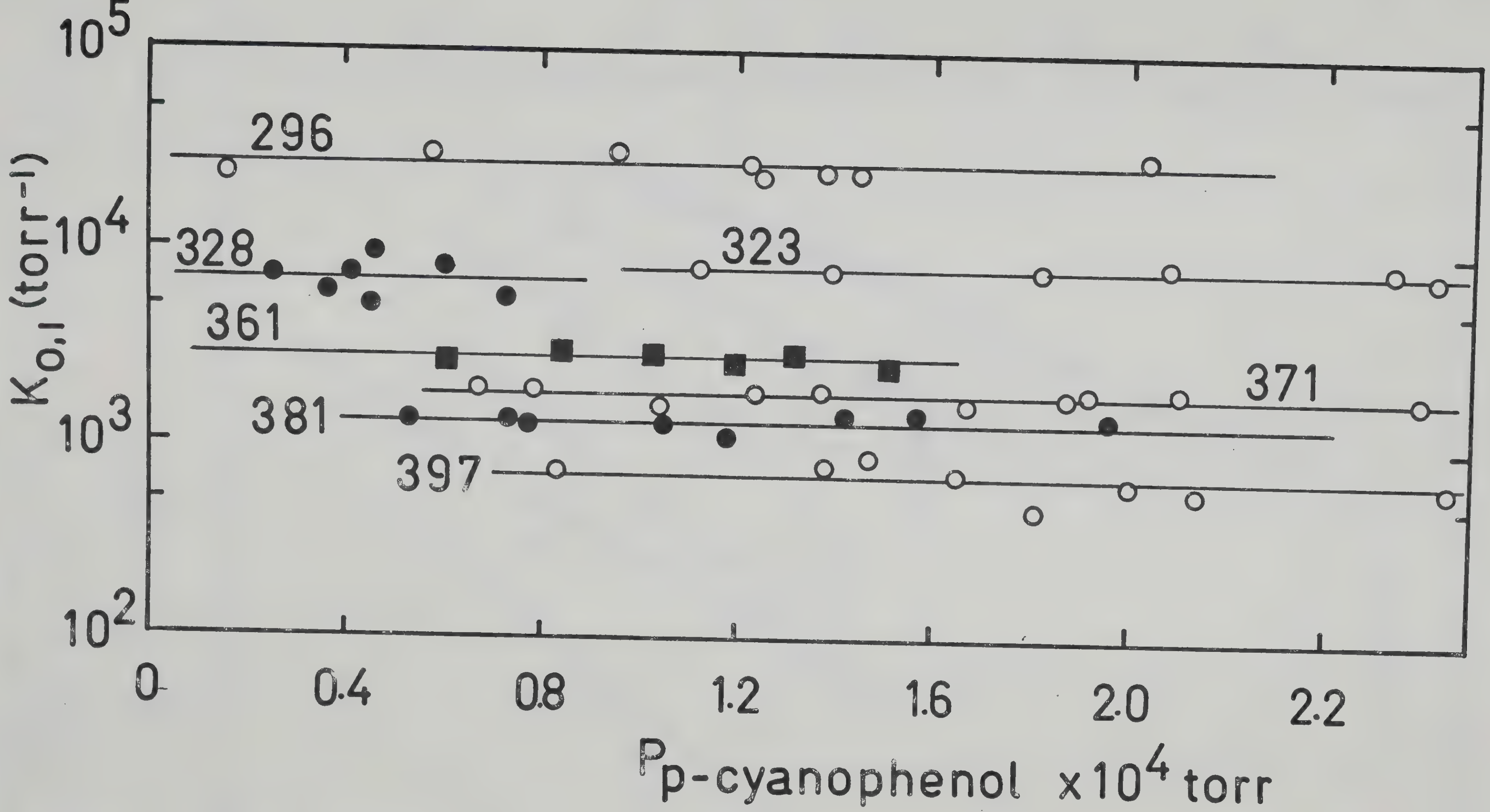

FIGURE 5.11. Measured Equilibrium Constants for the Reaction $Cl^- + p\text{-}CN.C_6H_4OH \rightleftharpoons p\text{-}CN.C_6H_4OH.Cl^-$ at Various Temperatures.

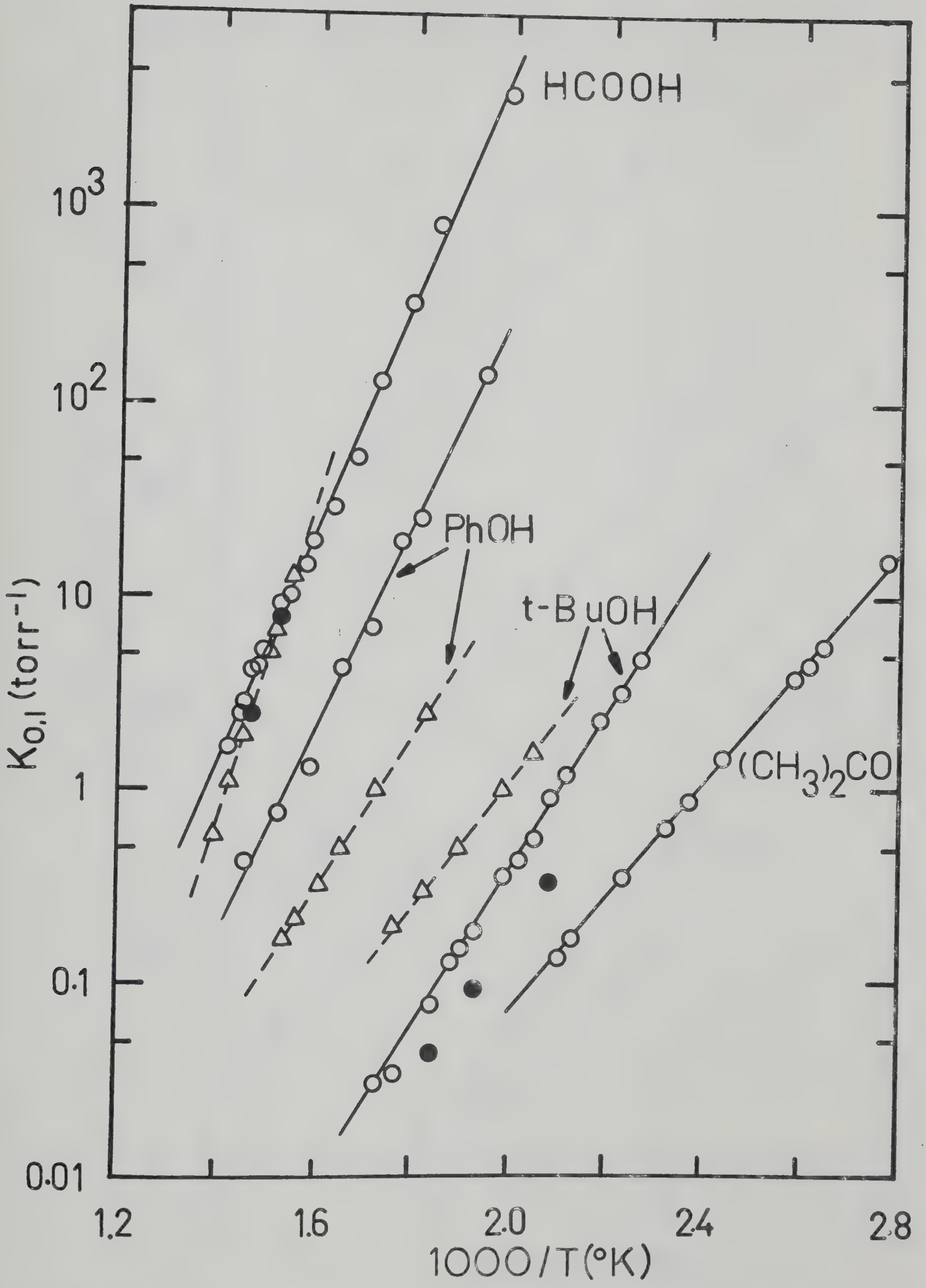

FIGURE 5.12. van't Hoff Plots for the Reaction $Cl^- + RH \rightleftarrows RHCl^-$ where RH = Acetone, Formic Acid, t-Butanol and Phenol. ○ This work, ●, This Work Using Pure RH, △ Yamdagni and Kebarle Reference (156) Using Pure RH.

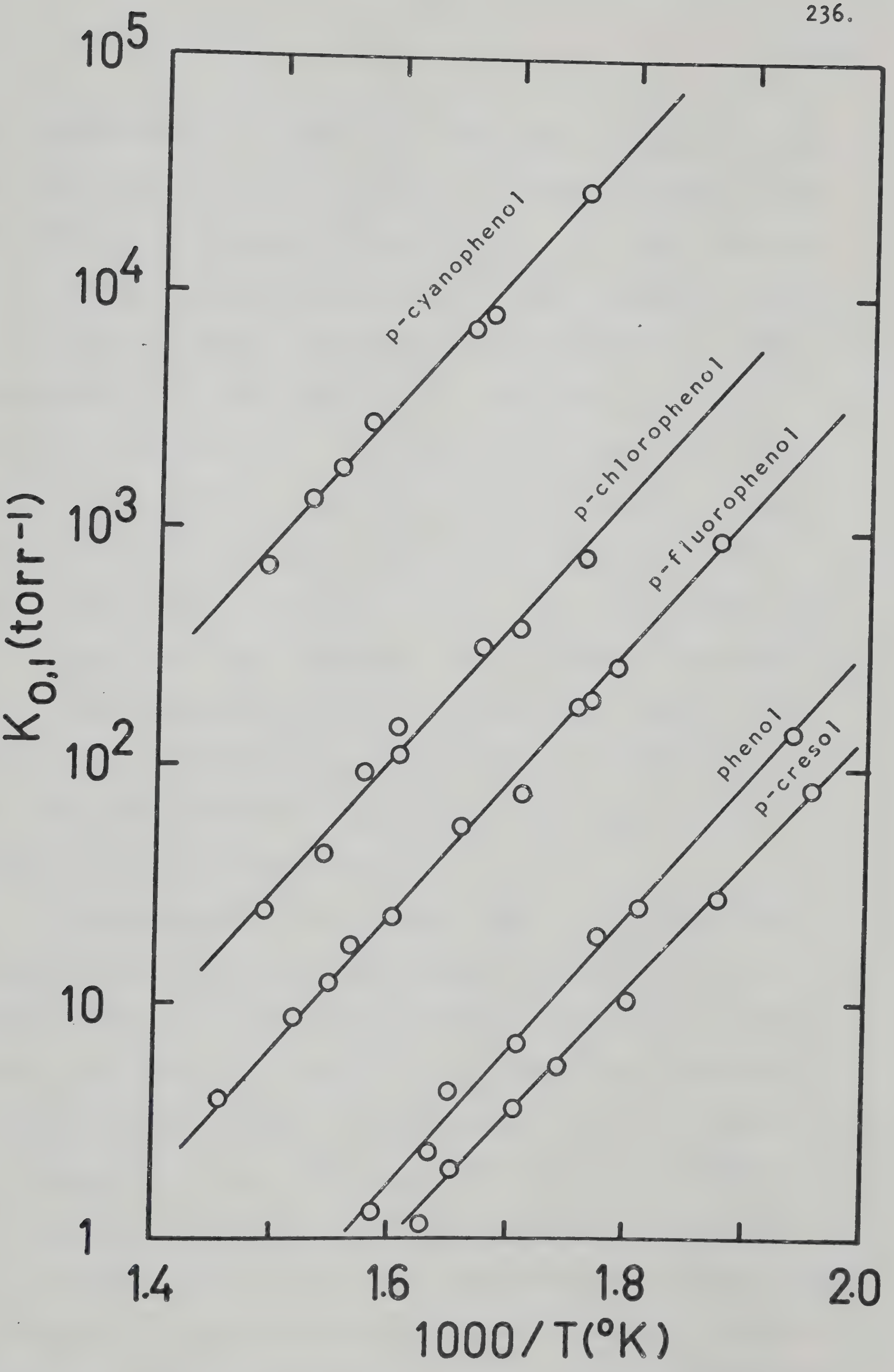

FIGURE 5.13. van't HoffPlots for Phenol and Substituted Phenols for the Reaction $Cl^- + RH \rightleftharpoons RHCl^-$.

each temperature. Figure 5.12 also shows Yamdagni's results by the triangular symbols. A few experiments were repeated using the pure solvent only. This was achieved by injecting a sufficient volume of the compound into the bulb to give a vapour pressure of about 700 torr. The experiments with the pure solvent are shown by solid circles in Figure 5.12. In the case of formic acid the measurements made in this work are very close to those obtained previously. The two experiments repeated in pure formic acid lie exactly on the line of Yamdagni *et al*. However for the t-butanol, the previously measured equilibrium constants are about three times larger than the present measurements and for phenol the direction is reversed and Yamdagni's results are about ten times smaller than the present work.

Determinations of $K_{0,1}$ done under different conditions and by different experimenters that are within a factor of two are considered acceptable, but the discrepancies observed in Figure 5.12 are much larger and must be due to other factors. Experiments with pure t-butanol were repeated and are shown as solid circles in Figure 5.12 and they lie below those performed in diluted mixtures with methane. To examine the effect of the pressure of t-butanol, two experiments were performed at the same temperature. One was performed using pure t-butanol and the other with t-butanol diluted with methane in the

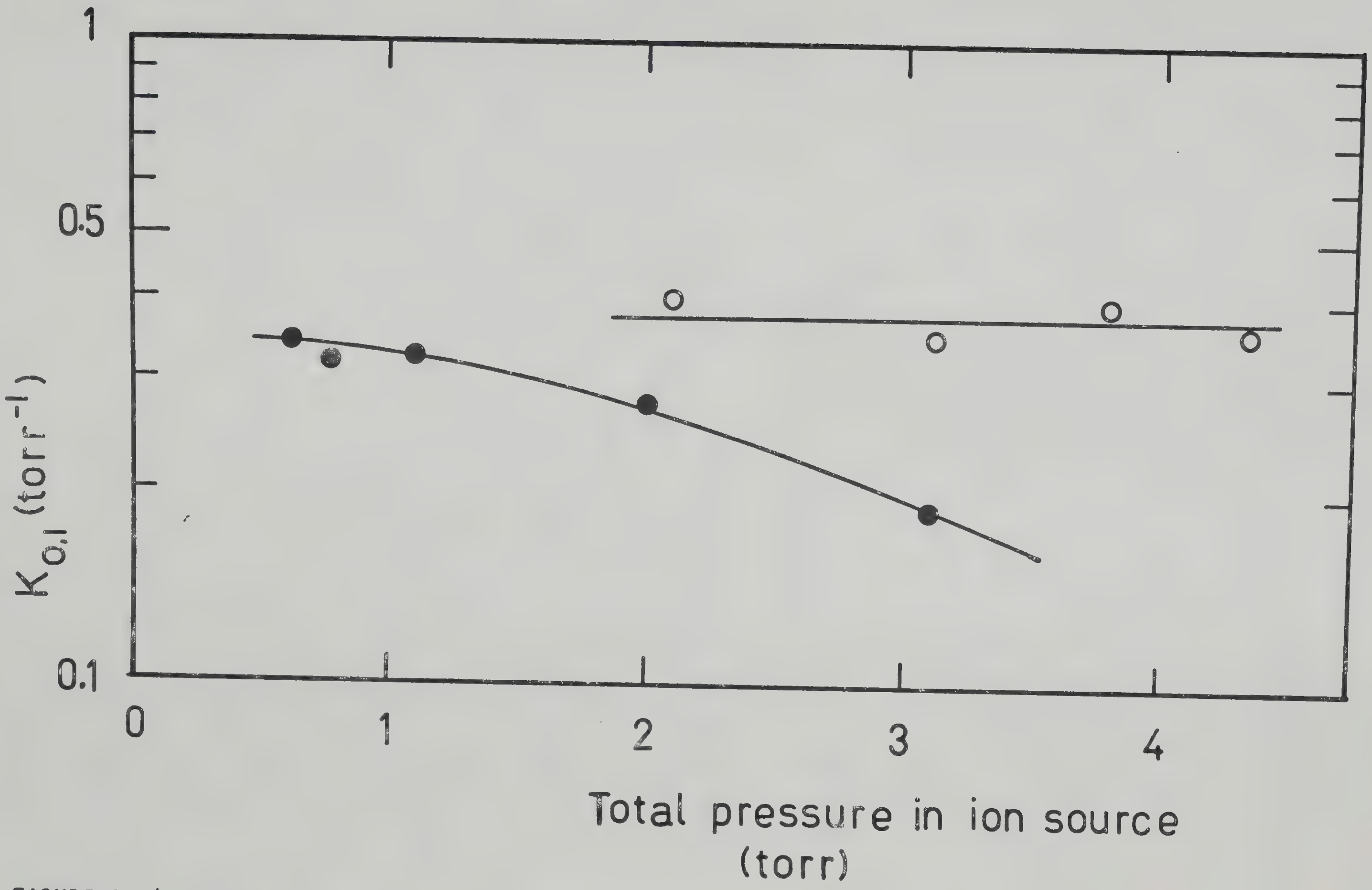

FIGURE 5.14. Measured Equilibrium Constants for the Reaction $Cl^- + t\text{-}BuOH \rightleftarrows t\text{-}BuOH.Cl^-$ at 231°C for a Mixture of t-BuOH in CH_4 (○) and pure t-BuOH (●).

normal manner. Figure 5.14 shows that the equilibrium constant measured in the diluted mixture remains constant with increasing total ion source pressure, (shown by open circles). However, the experiment using pure t-butanol displays a decrease of $K_{0,1}$ with increasing pressure. In the diluted mixture the partial pressure of t-butanol at total ion source pressure of 4 torr was 110 mtorr. The ratio of Cl^- and $RHCl^-$ can be calculated from

$$\frac{I_{Cl^-}}{I_{RHCl^-}} = \frac{1}{K_{0,1} \cdot P_{RH}} \qquad (5.18)$$

at 231°C, $K_{0,1} = 0.39$ torr^{-1} and $I_{Cl^-}:I_{RHCl^-} \approx 25:1$ and stripping is minimized. However, when pure t-butanol is present at an ion source pressure of 4 torr, the ratio of I_{Cl^-}/I_{RHCl^-} from equation (5.18) is $\approx 1:2$. Under these conditions the cluster ion is twice as large as Cl^- and collisional dissociation outside the ion source leads to a larger error in $K_{0,1}$. This effect explains the difference in the two separate measurements of phenol.

The above explanation cannot be valid for t-butanol where Yamdagni's values are higher than the present measurements. Yamdagni controlled the pressure of the pure solvent by surrounding a glass bulb containing the solvent with a controlled temperature water bath. The ion source pressure was varied by changing the temperature of the vapour then passed through a calibrated capillary and

entered the flow system. A trace of CCl_4 was added to the flow by a second capillary. Dissolved air in the solvent or an error in the estimation of the fraction of CCl_4 added could lead to inaccuracies.

Table XII summarizes the thermodynamic parameters obtainted from the van't Hoff plots shown in Figure 5.12.

The equilibrium constants, $K_{0,1}$, are shown for a series of para substituted phenols in Figures 5.6 to 5.11. Para substituted phenols were chosen because there is maximum opportunity for conjugation but without the interference of steric effects which may occur with ortho substituents.

It can be seen in Figure 5.9 that the equilibrium constants were not constant with ion source pressure for p-fluorophenol. Initially it was believed that some effect other than stripping was causing the behaviour since a curved decrease in $K_{0,1}$ (see Figure 5.14) and not a linear variation is normally observed when stripping occurs. The system was examined to make sure that no deposition was occurring in the glass tubes to and from the ion source or in the metal valves. The valves protruded through the front of the heated box for accessability, and were thus cooler than the bulb. As gas leaked from the bulb through the valve the phenol may have condensed on the cooler surface. Heating tape was wrapped around the valve to ensure that the valve was at the same tem-

TABLE XII

Thermodynamic Data Obtained for the Reaction $Cl^- + RH = RHCl^-$

Acid RH	$-\Delta H_{0,1}$ kcal/mol		$-\Delta S_{0,1}$ e.u.		$-\Delta G_{0,1}$ kcal/mol		D-EA
	This Work	Previous Work[a]	This Work	Previous Work	This Work	Previous Work	kcal/mol
HCOOH	27.4 ± 0.4[d]	37.2	24.5 ± 0.5	39.6	20.1 ± 0.4	25.4	28.6[a]
Phenol	27.4 ± 0.9	19.4	25.0 ± 1.4	15.5	17.2 ± 0.9	14.8	33.3[c]
t-BuOH	19.2 ± 0.3	14.2	27.2 ± 0.5	10.3	11.1 ± 0.3	11.1	-
Acetone	13.7 ± 0.1	-	19.6 ± 0.2	-	7.9 ± 0.1	-	50.1[b]

a. Reference 156

b. Reference 72

c. Reference 174

d. Standard deviation from least squares analysis

perature, as the bulb, but the same effect was still observed. When the ion source exit and entrance slits were replaced the effect disappeared and Figure 5.10 was obtained. It was found that the measured equilibrium constants were the same as the equilibrium constants in Figure 5.9 at an ion source pressure of 1.0 torr and these results were used in the van't Hoff plot.

Para-cyanophenol is a stronger acid than HCl in the gas phase and thus reaction (5.19) occurs in addition to the clustering reaction with Cl^-. To suppress reaction

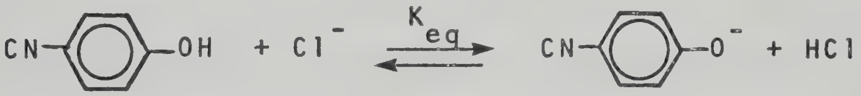

(5.19)

(5.19) 10 torr of HCl gas was added to the bulb mixture. The three ions Cl^-, 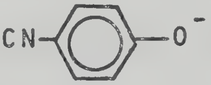 and 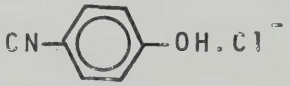 were found to be in equilibrium. The measurement of the equilibrium constant, K_{eq}, for reaction (5.19) was obtained using

$$K_{eq} = \frac{I_{CNPhO^-} \cdot P_{HCl}}{I_{Cl^-} \cdot P_{CNPhOH}} \qquad (5.20)$$

The ΔG^o calculated from $RT \ln K_{eq}$ is equal to the difference in the gas phase acidity between HCl and p-cyanophenol. The calculated ΔG^o was -4.0 kcal/mol which is in agreement with the previously measured -4.4 kcal/mol (174).

The van't Hoff plots shown in Figure 5.13 for the different phenols are virtually parallel which indicates

that the $\Delta H^o_{0,1}$ values are very similar. These results were surprising since it was expected that the $\Delta H^o_{0,1}$ values would be different. Since $\Delta S^o_{0,1}$ is calculated from the intercept for the present plots, the $\Delta S^o_{0,1}$ values will be different for each phenol and not the $\Delta H^o_{0,1}$ values.

In order to examine whether the van't Hoff plots of the phenols were affected by some systematic error, experiments were conducted at several temperatures for mixtures of two or more of the compounds. The phenols were dissolved in methanol and their partial pressures in the ion source were between 1 and 10 mtorr. By studying the two compounds at the same time as well as the clustering reaction with Cl^-, the Cl^- transfer from one phenol to another could be investigated.

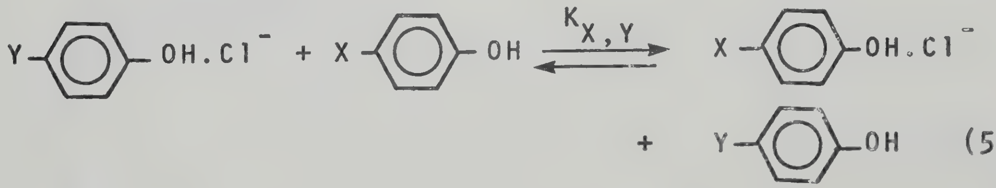

(5.21)

The equilibrium constant $K_{X,Y}$ was measured at different temperatures for different X and Y. The resultant van't Hoff plots are shown in Figure 5.15 where X and Y are H, CH_3, F, Cl and CN. The $\Delta H^o_{X,Y}$ values calculated should be equal to the difference of the two $\Delta H^o_{0,1}$ values. This follows from the thermodynamic cycle (5.22).

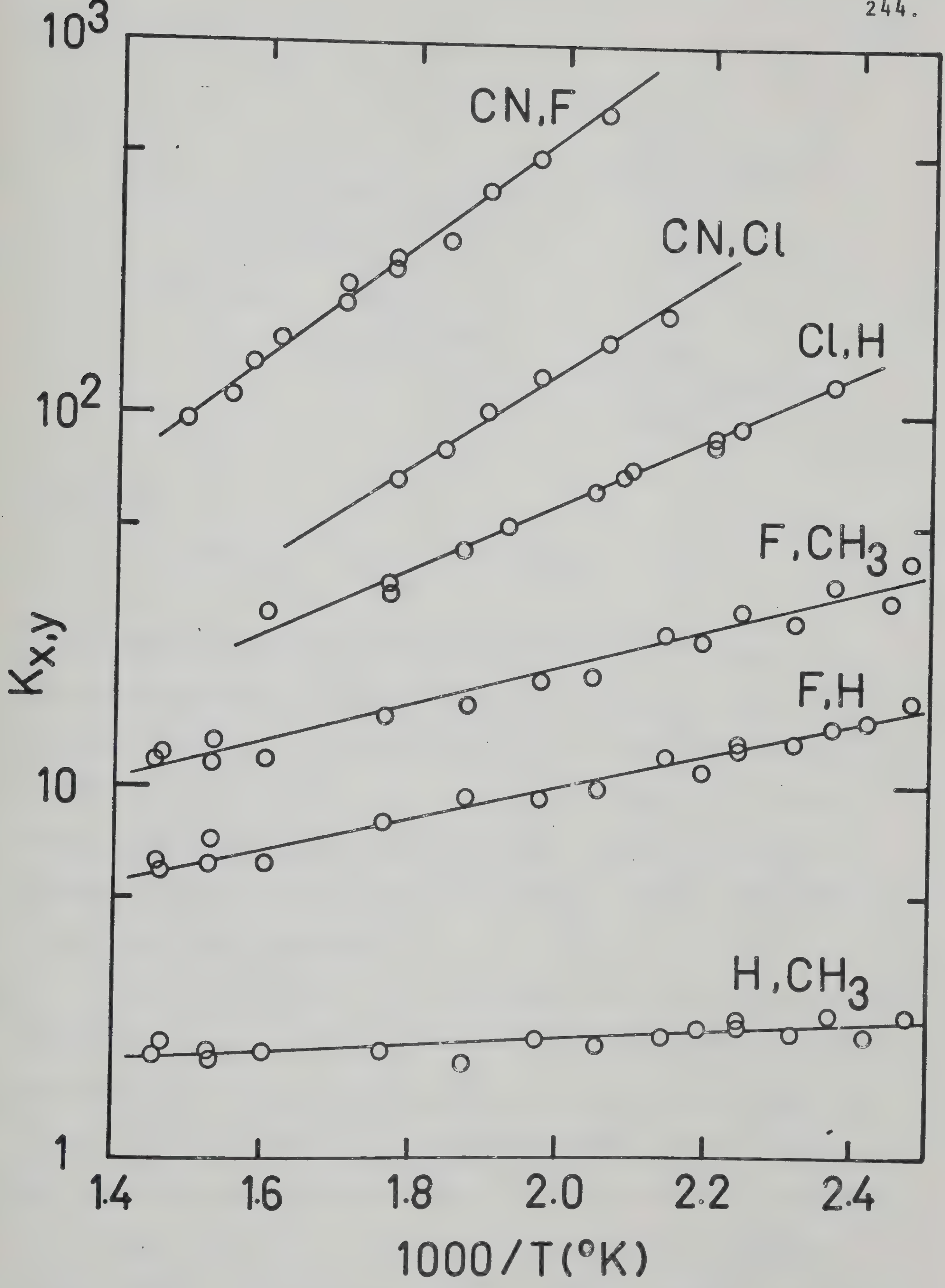

FIGURE 5.15. van't Hoff Plot for the Reaction $Y\text{-}C_6H_4\text{-}OH.Cl^- + X\text{-}C_6H_4OH \rightleftarrows X\text{-}C_6H_4OH.Cl^- + Y\text{-}C_6H_4OH$ for Various X and Y.

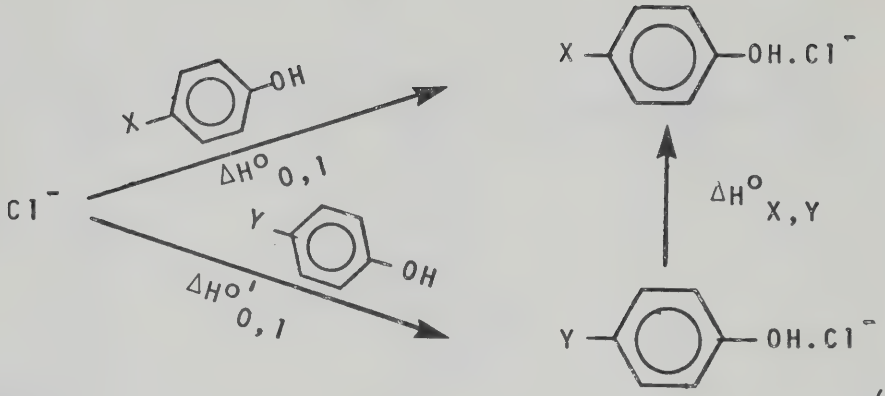

(5.22)

Therefore

$$\Delta H^{o}_{X,Y} = \Delta H^{o}_{0,1} - \Delta H^{o\prime}_{0,1} \qquad (5.23)$$

The thermochemical values from the Van't Hoff plots in Figures 5.13 and 5.15 are shown in Table XIII. The $\Delta H_{X,Y}$ values relative to phenol are shown in Figure 5.16 and tabulated in Table XIII. The agreement between the various measurements of $\Delta H^{o}_{X,Y}$ is quite good except for p-cyanophenol, but the error limits are large for the measurements involving this compound.

From Table XIII it is obvious that this second set of experiments does predict differences in the $\Delta H^{o}_{0,1}$ values and similar values of $\Delta S^{o}_{0,1}$ which is opposite to the results from the direct $K_{0,1}$ determinations. The results obtained from the study of the chloride transfer reaction (5.21) are believed to be more accurate for two reasons. First, higher concentrations of the phenols may be used in the chloride transfer reaction than in the direct addition

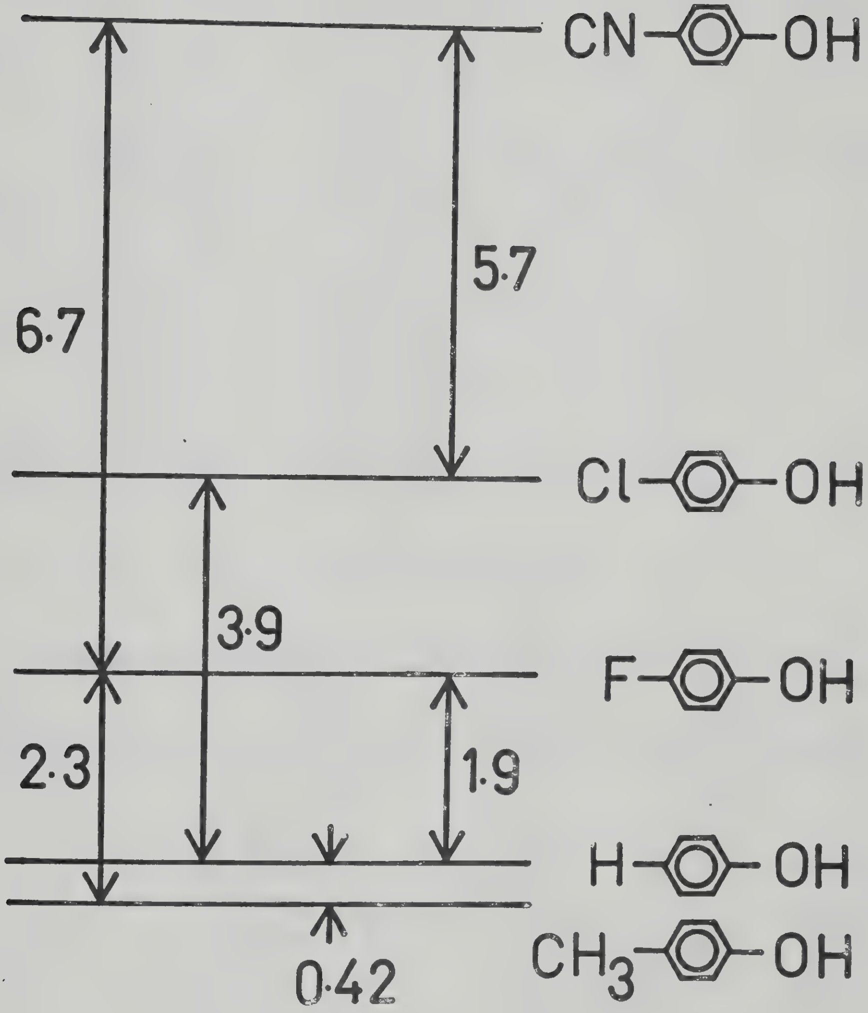
CN-⌬-OH
Cl-⌬-OH
F-⌬-OH
H-⌬-OH
CH3-⌬-OH
6·7
5·7
3·9
2·3
1·9
0·42

FIGURE 5.16. Relative Hydrogen-bond Strengths to Cl^- for Various Phenols. Numbers Beside Arrows Correspond to Directly Measured $\Delta H^o_{X,Y}$ values

TABLE XIII

Thermochemical Data for the Reaction $Cl^- + RH \rightleftharpoons RHCl^-$

Compound	$-\Delta H^o_{0,1}$ kcal/mol	$-\Delta S^o_{0,1}$ e.u.	$-\Delta G^o_{0,1}$ kcal/mol	D-EA kcal/mol
p-CN phenol	26.3 ± 1.0[a]	12.8 ± 1.6	22.5 ± 1.0	15.6
p-Cl phenol	25.8 ± 1.3	19.7 ± 2.0	20.0 ± 1.3	26.65
p-F phenol	25.6 ± 0.5	21.5 ± 0.9	19.2 ± 0.5	30.65
phenol	24.7 ± 0.9	25.0 ± 1.4	17.2 ± 0.9	33.30
p-CH_3 phenol	25.2 ± 0.4	27.4 ± 0.7	17.1 ± 0.4	34.55

Calculated Thermodynamic Quantities for the Reaction

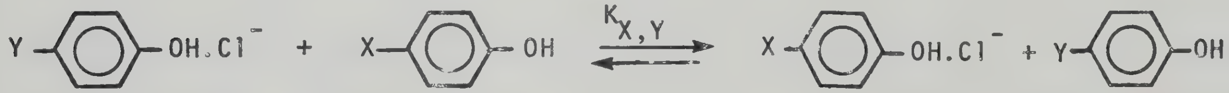

X	Y	$-\Delta H^o_{X,Y}$ kcal/mol	$\Delta S^o_{X,Y}$ e.u.	$-\Delta G^o_{X,Y}$ kcal/mol
CH_3	H	0.42 ± 0.08	0.6 ± 0.2	0.61 ± 0.09
H	F	1.9 ± 0.1	0.8 ± 0.2	2.1 ± 0.1
CH_3	F	2.3 ± 0.1	1.4 ± 0.2	2.7 ± 0.1
Cl	H	3.9 ± 0.1	0.34 ± 0.2	3.8 ± 0.1
CN	Cl	5.7 ± 0.4	-1.8 ± 0.7	5.2 ± 0.4
CN	F	6.7 ± 0.3	0.86 ± 0.5	6.5 ± 0.3

a. Standard deviation from least squares analysis.

of Cl^-, reducing errors due to absorption on to or desorption from the walls. Second, any collisional dissociation of the cluster ion that may occur outside the ion source will have less of an adverse effect since the Cl^- formed does not enter the equilibrium constant whereas serious error is introduced in the clustering reaction by non-equilibrium Cl^-.

The upper part of Table XIII shows that instead of $\Delta H^o_{0,1}$ changing with the nature of the phenol, the change is reflected in the $\Delta S^o_{0,1}$ values. As the interaction with Cl^- increases, the entropy of $RHCl^-$ should decrease. For reaction (5.14)

$$Cl^- + RH \rightleftarrows RHCl^- \qquad (5.14)$$

$\Delta S^o_{0,1}$ is given by

$$\Delta S^o_{0,1} = S^o_{RHCl^-} - S^o_{Cl^-} - S^o_{RH} \qquad (5.24)$$

As the hydrogen bond energy increases $S^o_{RHCl^-}$ should decrease, therefore $\Delta S^o_{0,1}$ should decrease or become more negative assuming S^o_{RH} values are similar for the different phenols. However, Table XIII shows the opposite trend. The $\Delta S^o_{0,1}$ value for p-cyanophenol is -12.8 e.u. which is quite low for an association reaction.

The discrepancy between the two sets of results which measure $K_{0,1}$ and $K_{X,Y}$ may be explained if the straight lines shown in the van't Hoff plot in Figure 5.13 are

actually part of a slight curve which, over a narrow temperature range appears to be a straight line.

A curve in the van't Hoff plot may be explained by several factors. The actual van't Hoff plot is represented by line AEC in Figure 5.17. If decomposition of the phenols occurs at high temperatures, the calculated value of $K_{0,1}$ is smaller than the true value and curve BEC would be obtained over a wide temperature range since

$$K_{0,1} = \frac{I_{RHCl^-}}{I_{Cl^-} \cdot P_{RH}} \qquad (5.17)$$

and the true pressure of RH is smaller than is believed. The partial pressures of the phenols used had to be very low. Partial pressures of the phenols down to 10^{-4} torr were used. The strongest acid used was p-cyanophenol. When partial pressures of less than 10^{-4} torr of p-cyanophenol were admitted to the ion source, the ratio of I_{RHCl^-}/I_{Cl^-} did not change for different ion source pressures. Therefore the partial pressure of p-cyanophenol was not changing due to the compound being desorbed from the walls. In this case line FEC would be obtained in the van't Hoff plot. As mentioned in section 5.5 collisional dissociation outside the ion source causes reduction of the equilibrium constant with increasing ion source pressure. If collisional dissociation occurs the effect is more pronounced at lower temperatures and the van't Hoff plot would resemble curve AED. Therefore

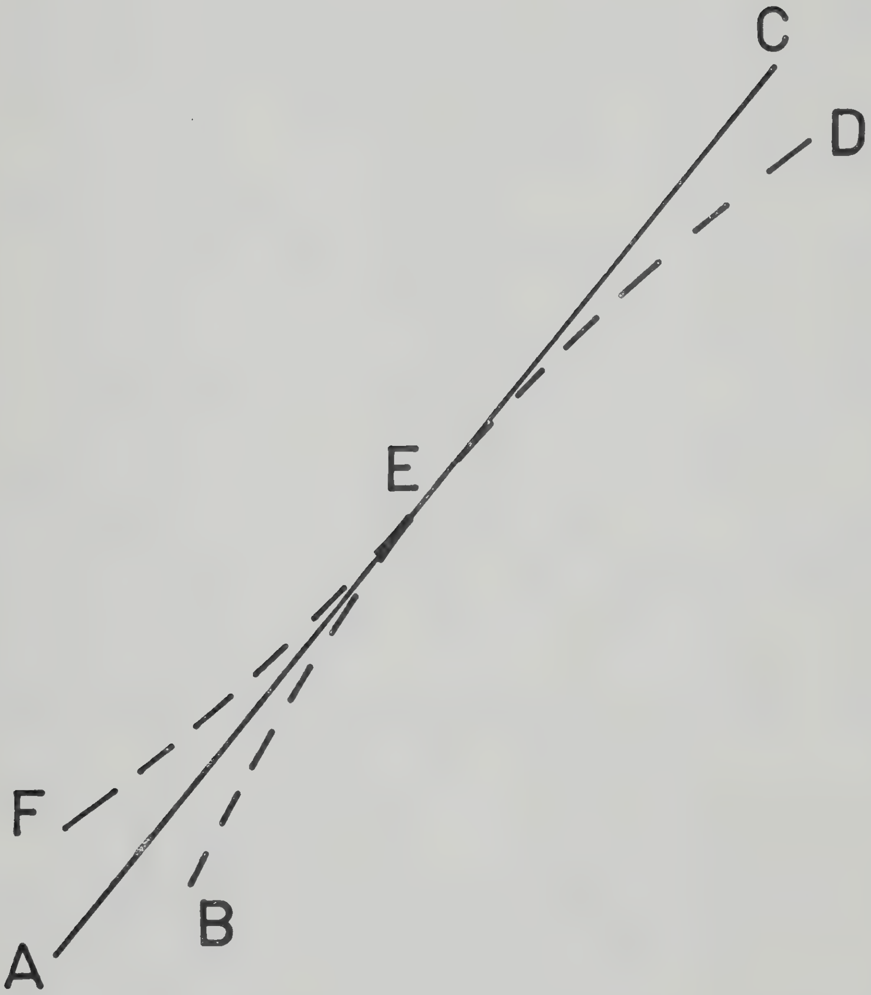

FIGURE 5.17. Possible Deviations from the True van't Hoff Plot, Line AEC.

stripping and desorption from the walls have the effect of making the slope and hence $-\Delta H_{0,1}$ smaller than the true value and $\Delta S_{0,1}$ would become more positive. Decomposition would result in a steeper slope and a more negative value of $\Delta H_{0,1}$ and $\Delta S_{0,1}$.

A further source of error may be the formation of Cl^- from other sources besides production by electron impact inside the ion source. For example, if pressures of CCl_4 greater than 10 mtorr were admitted to the ion source, the intensity of Cl^- increased when the ion gauge filament was turned on. If Cl^- from spurious sources is detected as well as Cl^- from the ion source then the measured equilibrium constant will be smaller than the true $K_{0,1}$ and line BEC will be obtained.

It is apparent that stripping or desorption from the walls causes the inaccurate results of the 0,1 addition of phenols to Cl^-. By studying reactions of the type (5.21), collisional dissociation of the complexes with Cl^- cancels out, if they dissociate at similar rates, and the results are much more accurate.

A clustering reaction (5.14) was also studied using various nitrogen and carbon acids. Figure 5.18 shows the effect of various substituents on benzene at 27°C and Figure 5.19 shows the measured equilibrium constants, $K_{0,1}$ of several ketones and pyrrole at

FIGURE 5.18. Measured Equilibrium Constants for the Reaction $Cl^- + RH = Cl^-.RH$ at 26°C Where RH is

○	Acetone
●	m-difluorobenzene
⊗	p-nitrotoluene
△	diphenylmethane
◐	iodobenzene
□	nitrobenzene
⬡	bromobenzene
◆	chlorobenzene
▼	fluorobenzene
◇	cumene
⎔	n-propylbenzene
⬣	ethylbenzene
■	mesitylene
▯	m-xylene
▲	toluene
◑	p-xylene
⬢	benzene
▽	1,4-pentadiene

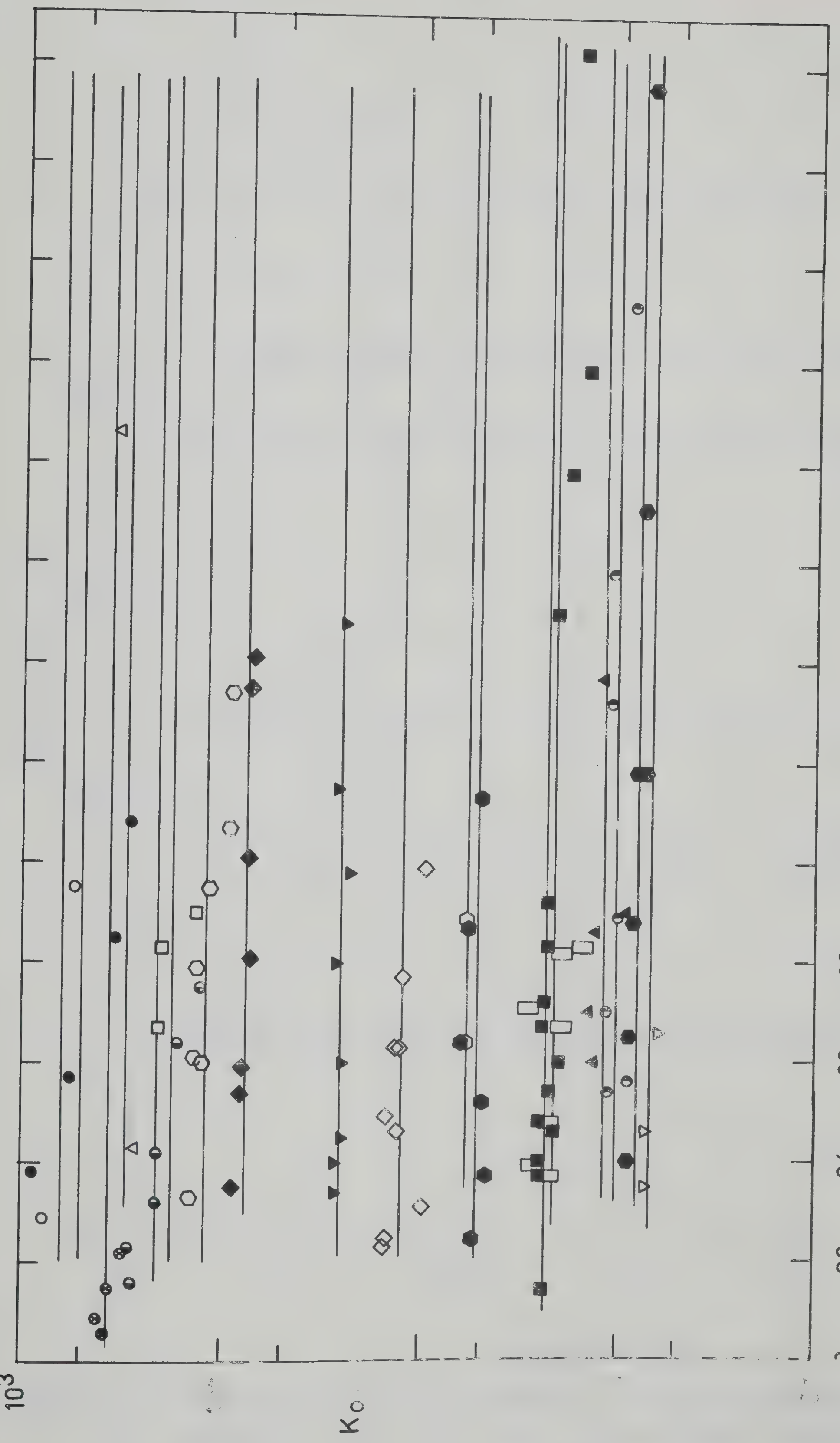
10^3
K_0
0
.02
.04
.06
.08
.10
.12
.14
.16
.18
.20
.22
.24
.26
P_{RH} (torr)

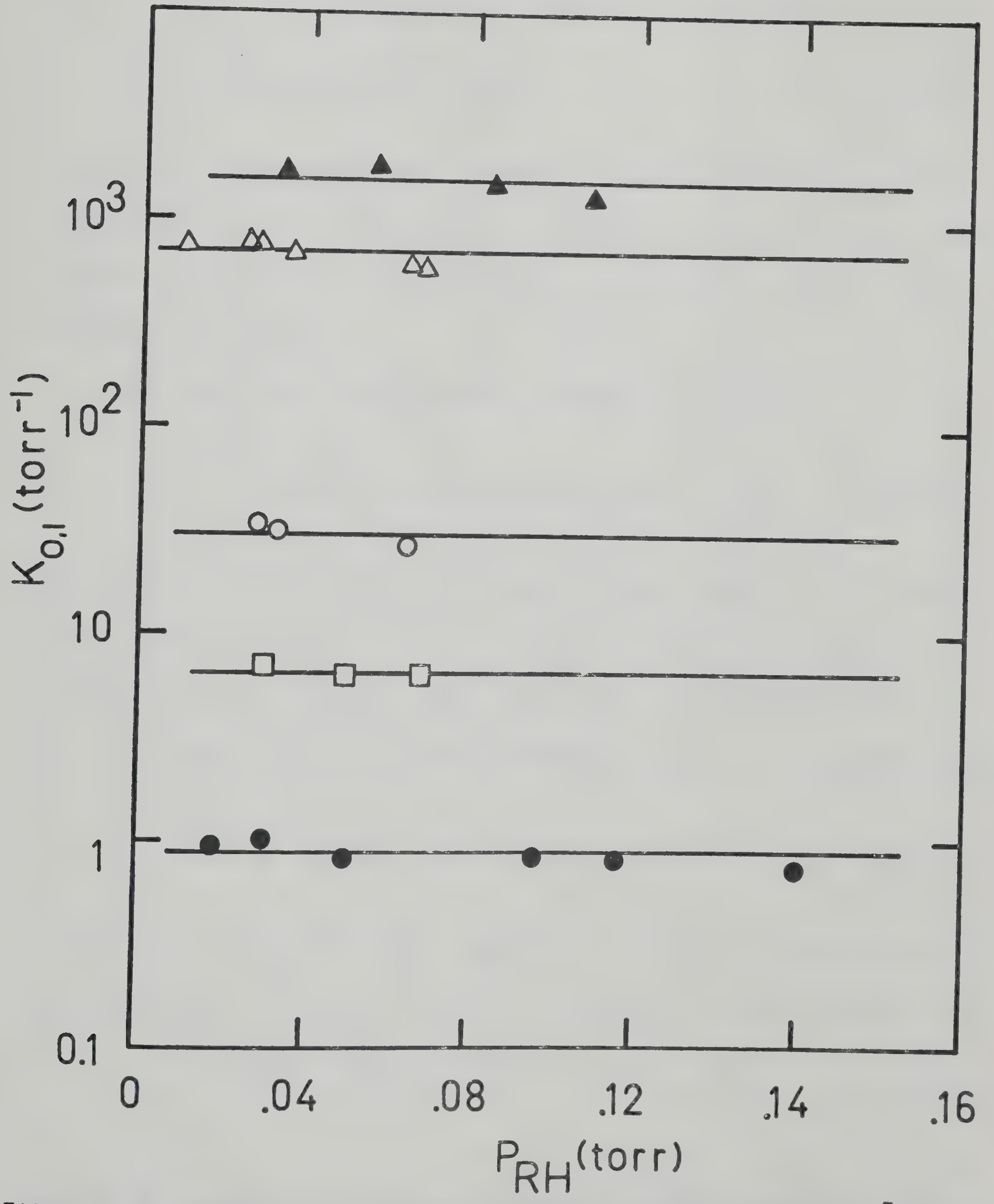

FIGURE 5.19. Measured Equilibrium Constants for the Reaction $Cl^- + RH \rightleftarrows RHCl^-$ at 148°C where RH is pyrrole (▲), acetyl acetone (△), phenylacetone (○), acetophenone (□) and acetone (●).

148°C. The free energy $\Delta G^{o}_{0,1}$ for reaction (5.14) may be calculated using the expression

$$\Delta G^{o}_{0,1} = -RT \ln K_{0,1} \qquad (5.25)$$

where $K_{0,1}$ is expressed in atm^{-1}. However, since some experiments were conducted at 148°C the $\Delta G^{o}_{0,1}$, calculated from equation (5.25) cannot be compared with $\Delta G^{o}_{0,1}$ calculated at 27°C.

In the chloride transfer reaction (5.26),

$$R_1H.Cl^- + R_2H \rightleftharpoons R_2H.Cl^- + R_1H \qquad (5.26)$$

the entropy change for the reaction was found to be zero $\pm$ 2 e.u. (see Table XIII). Therefore ΔG^{o}_{T} for reaction (5.26) will not change very much with temperature since the $T\Delta S^{o}$ term will be approximately zero in the expression

$$\Delta G^{o} = \Delta H^{o} - T\Delta S^{o} \qquad (5.27)$$

Therefore, $\Delta G^{o} \approx \Delta H^{o}$ for reaction (5.26). Using relationship (5.28) a relative order of ΔG^{o}_{T} may be constructed,

$$\Delta G^{o}_{T} = \Delta G^{o}_{0,1}(R_1H) - \Delta G^{o}_{0,1}(R_2H) \qquad (5.28)$$

where $\Delta G^{o}_{0,1}(R_1H)$ and $\Delta G^{o}_{0,1}(R_2H)$ are the free energies for the clustering reaction for compounds R_1H and R_2H.

The compound with the weakest interaction with Cl^- was 1,4 pentadiene. For convenience this compound was taken as the reference compound and $\Delta G^o_{0,1}$ was set equal to zero and the remaining ΔG^o_T values calculated accordingly. Table XIV summarizes the ΔG^o_T values for the chloride ion transfer from 1,4 pentadiene to RH. Previous measurements of chloride affinities in this laborabory are also included in Table XIV.

It is interesting to note the compounds where the clusters with Cl^- could not be observed. No cluster was observed with cyclopentadiene. Cyclopentadiene exists as a dimer after standing at room temperature for some time. The dimer reverts to the monomer above 165°C. Initial experiments used dicyclopentadiene and the temperature of the gas handling plant was maintained about 175°C to initiate monomerization but no cluster with Cl^- was observed. The dicyclopentadiene was then fractionally distilled and kept in ice to ensure that the monomer was injected into the bulb and thus flowed through the ion source but no cluster with Cl^- could be detected. Since the complex could not be observed only an upper limit of $K_{0,1}$ could be calculated. The maximum ion ratio that could be detected on the instrument was 1000:1. Therefore if $I_{Cl^-}:I_{CpCl^-} > 1000:1$, then for a partial pressure of .137 torr cyclopentadiene, $K_{0,1}$ must be less than .0073 $torr^{-1}$. Therefore $+\Delta G^o_{0,1} < 1.6$ kcal/mol. When

TABLE XIV

Choride Affinities, ΔG^{0}_{T} with Respect to 1,4 pentadiene

Compound	$-\Delta G^{o}_{T}$	T°C[a]	D-EA
p-CN phenol	19.6	296-397	15.6[b]
p-chlorophenol	17.3	295-397	26.7[b], 30.4[k]
HCOOH	16.3	230-431	28.6[c]
p-F phenol	15.3	261-413	30.7[b], 31.2[k]
phenol	13.4	280-412	33.3[b], 33.3[k]
p-cresol	13.0	240-382	34.7[b], 34.5[k]
acetic acid	12.0[i]	309-428	31.8[c]
pyrrole	10.3	148	41.9[d]
acetylacetone	9.65	148	28.0[d]
t-butanol	7.29	168-306	59.1[e]
phenyl acetone	7.02	148	36.2[d]
acetophenone	5.74	148	45.6[d]
chloroform	5.59[i]	255-373	67.6[f]
methanol	4.49	107-203	63.2[e]
acetone	4.09	87-202	50.1[d]
n-difluorobenzene	3.95	27	
acetonitrile	3.79[g]	144-256	52.9[g]
p-nitrotoluene	3.73	27	37.0[d]
diphenyl methane	3.64	27	47.0[h]
anisole	3.55	27	
iodobenzene	3.43	27	
nitrobenzene	3.33	27	
bromobenzene	3.09	27	
chlorobenzene	2.82	27	
fluorobenzene	2.16	27	
cumene	1.75	27	
n-propylbenzene	1.28	27	
ethylbenzene	1.23	27	
mesitylene	0.74	27	

(continued)

Table XIV (continued)

m-xylene	0.69	27	
triphenylmethane	0.40	27	
toluene	0.26	27	66.9[h]
p-xylene	0.19	27	
benzene	0.06	27	79.8[f]
1,4 pentadiene	0	27	46.1[h]
cyclopentadiene	<-1.6	27	39.1[h]

a. Temperature at which $K_{0,1}$ was measured. Since ΔS^o_T is small, ΔG^o_T changes little with temperature such that the values obtained at different temperatures are directly comparable.

Energy changes in kcal/mol.

b. McMahon and Kebarle, reference 174.

c. Yamdagni and Kebarle, reference 167.

d. McMahon and Kebarle, reference 173

e. McIver and Miller, reference 185

f. Bohme _et al_, reference 165

g. Remeasured by M.F. See Chapter 6

h. McMahon and Kebarle, reference 72

i. Yamdagni and Kebarle, reference 156

j. Yamdagni, Payzant and Kebarle, reference 68

k. McIver and Silvers, measured relative acidities.

Values quoted are calculated from McMahon's D-EA phenol = 33.3, reference 175.

this is placed relative to 1,4 pentadiene, $\Delta G^{o}_{T} > +1.6$ kcal/mol.

Trifluoroacetone would not cluster with Cl^- but a large peak was observed at m/e 113 which may correspond to CF_3COO^-. CF_3COOH is a very strong acid (167) and would proton transfer to Cl^- to give HCl. Therefore no Cl^- would be available for clustering with trifluoroacetone. The source of CF_3COOH in the ion source is not very clear. Some CF_3COOH might have been present in the trifluoroacetone used. Alternatively the CF_3COOH might have been produced in the ion source by some reaction.

5.7 Discussion

(a) General Inspection of the Data Obtained

Examination of Table XIV reveals that there is only a very rough correlation of chloride affinity increase with (D-EA) decrease i.e. with gas phase acidity increase. There are three notable exceptions to the correlation. First, 1,4 pentadiene interacts very weakly with Cl^- but has a gas phase acidity comparable to acetophenone whose chloride affinity is 6 kcal/mol stronger. Second, cyclopentadiene has quite a strong gas phase acidity due to the aromatic character it gains when the anion is formed. However, the cluster with Cl^- could not be observed even at the lowest temperature obtainable i.e. room temperature. Another exception is t-butanol which has quite a

strong interaction with Cl^- but its gas phase acidity is weak.

Since the general correlation with gas phase acidity fails it is only meaningful to examine the separate classes of compounds individually i.e. oxygen acids, ketones, hydrocarbon acids and substituted benzenes.

(b) Chloride Affinities of Oxygen Acids: Substituted Phenols and Others

Figure 5.20 shows the correlation between chloride affinities and the gas phase acidities for several oxygen acids. The solid line indicates that for a series of similar compounds i.e. substituted phenols, the correlation between acidity and chloride affinity is very good. The line also passes through the point for formic acid. The broken line indicates the best fit of all the oxygen acids measured and shows that there is a good correlation except for acetic acid which is out of order.

For the series of phenols studied, the order of their interaction with Cl^- is that expected from consideration of the inductive or resonance effects. The resonance effect in phenol promotes the formation of clusters with Cl^- by contributions from structures such as VII to IX. These resonance structures show the ability of phenol to support charge separation within the molecule which makes the hydroxyl hydrogen more positive

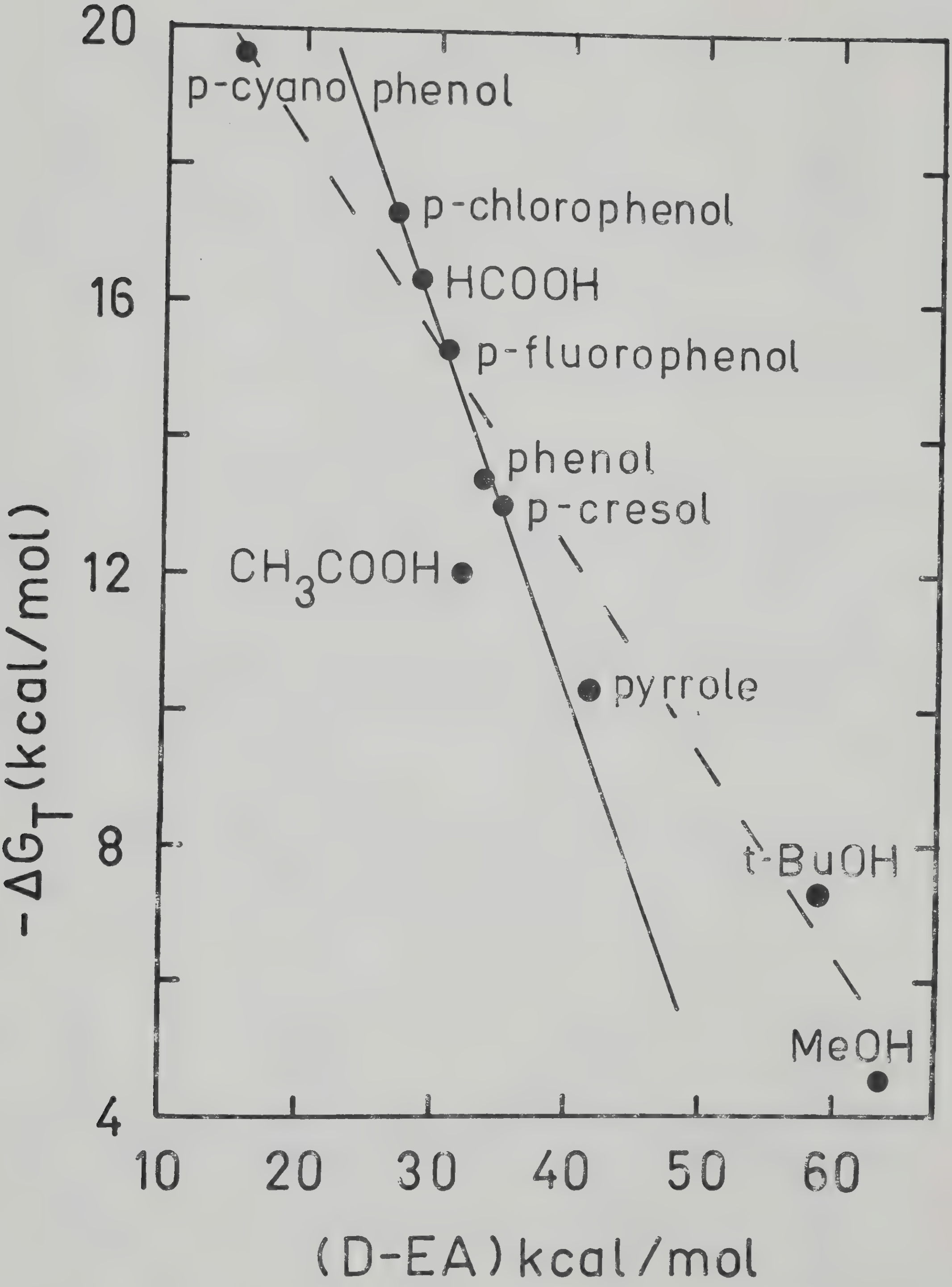

FIGURE 5.20. Correlation of Gas Phase Acidities *versus* Chloride Affinities Relative to 1,4-pentadiene for Various Oxygen Acids and Pyrrole.

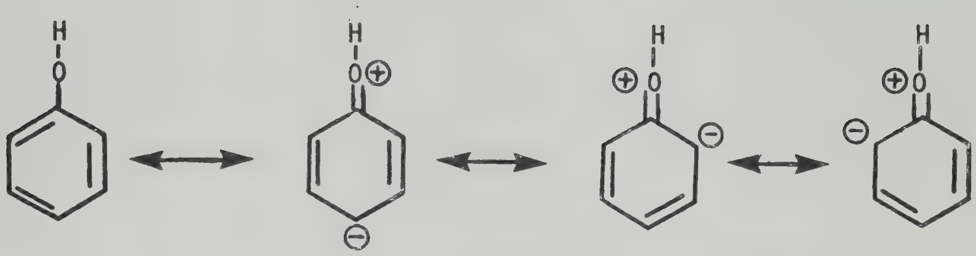

VII VIII IX

and thus able to interact more strongly with a chloride ion. When various functional groups are substituted, their inductive and resonance effects will modify the charge distribution on the ring and hydroxyl group so that the magnitude of the interaction with Cl^- will change.

In p-cresol, resonance structures X to XII contribute to the stability of the cluster with Cl^-.

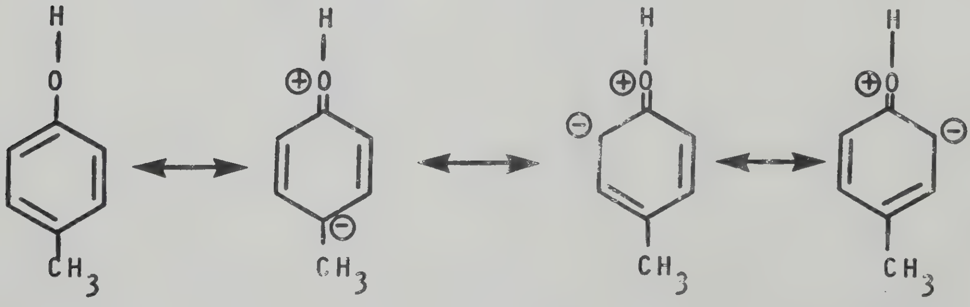

X XI XII

Structure X will not be as important as XI and XII since the negative charge is situated in a region where there

is a concentration of negative charge due to the electron donating properties of the methyl group. This effect of the methyl group makes hydrogen bonding to Cl^- less favourable than the bonding observed with phenol.

The addition of strongly electron withdrawing substituents favours hydrogen bonding relative to phenol and the interaction is much stronger. Chlorophenol has a larger chloride affinity than fluorophenol which is the same order as the gas phase acidity. The electron withdrawing effect of halogen substituents favours resonance structures such as XIII where the negative charge is situated at the carbon adjacent to the halogen. The strongest interaction was found with p-cyanophenol. The cyano group is one of the strongest electron withdrawing groups because of charge separated resonance structures of the type XIV.

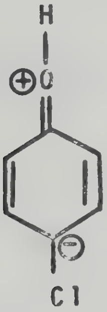
XIII

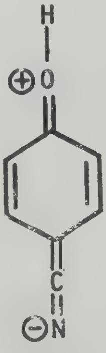
XIV

Since the gas phase acidities correlate very well with hydrogen-bond energy, factors that affect the gas

phase acidity must also affect the hydrogen bonding. In the consideration of the substituted phenols it is the ability to delocalize the negative charge in the case of the anion and to stabilize charge separation in the cluster that affects acidity and chloride affinity respectively. In both cases this is achieved because the oxygen possesses lone pairs which can take part in resonance shifts. An interesting comparison to the oxygen acids is pyrrole which is also included in Figure 5.20 but possesses only one lone pair. It lies very close to the line of the oxygen acids. The hydrogen attached to the nitrogen is acidic due to the resonance structures XV to XVI and the chloride ion will attach *via* a hydrogen bond to the acidic hydrogen.

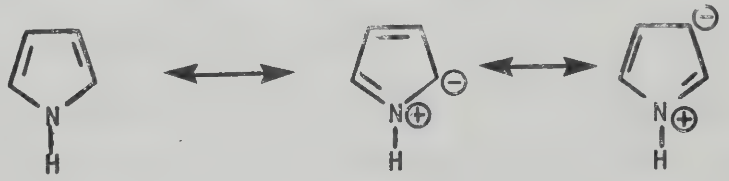

XV XVI

Kolthoff and Chantooni have studied the hydrogen-bonding to Cl^- to substituted phenols in the aprotic solvent, acetonitrile (186). These workers found that, with the exception of the ortho substituted phenols, the stability of the $RHCl^-$ complex increases with the acid strength of the phenol in acetonitrile. Comparison of their data with the gas phase acidities of McMahon *et al*

(174) shows that the hydrogen-bond strength in acetonitrile follows the gas phase acidity.

Unfortunately, Kolthoff and Chantooni did not use the same set of substituted phenols as in this work and so no direct quantitative comparison between hydrogen-bonding in an aprotic solvent and the gas phase may be made. Since the chloride affinities of the phenols correlate with their gas phase acidities, which in turn correlate with their chloride affinities in acetonitrile, it may be inferred that the order of chloride affinities of the phenols will be the same in the gas phase as in an aprotic solvent.

Bordwell and coworkers (187) have shown that there is a general correlation between gas phase acidities and acidities in an aprotic solvent, dimethyl sulfoxide, for a series of ketones and nitriles. They suggested that the intrinsic acidity of a molecule in the gas phase is also manifested in its acidity in dimethyl sulfoxide. The results of Kolthoff (186) and Bordwell (187) in solution therefore suggest that the environment around an ion in an aprotic solvent resembles that around an ion in the gas phase.

(c) Chloride Affinities of Ketones

Inspection of the ketones measured (see Table XIV) shows that the order of chloride affinities is CH_3COCH_3 <

$C_6H_5COCH_3 < C_6H_5CH_2COCH_3 < (CH_3CO)_2CH_2$. This order also follows the gas phase acidity order as shown in Figure 5.21. The correlation is good for the first three ketones but acetyl acetone lies some distance from the line.

Pople (188), on the basis of *ab initio* SCF MO theory, has calculated the electron distribution on the separate atoms of acetone and shown that the hydrogens are slightly positively charged in the methyl groups.

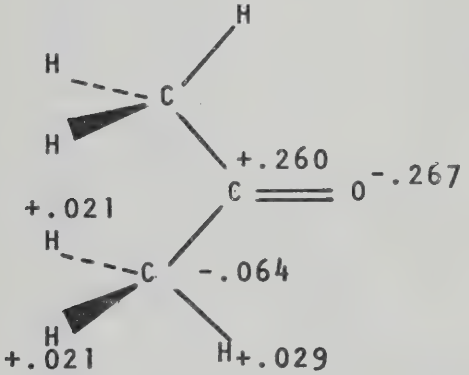

XVII

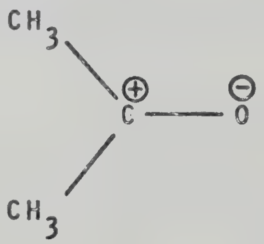

XVIII

There are five possible interactions between Cl^- and acetone. The chloride ion could interact in a formal hydrogen bond with one of the hydrogens. If the chloride ion interacts with more than one hydrogen, it could interact symmetrically with the three hydrogens of a methyl group or symmetrically with four hydrogen atoms (two from each methyl group), since they are close enough for this to occur. A fourth possibility is that the chloride ion may attack the central carbon since this is the most positively charged atom in the isolated molecule according to Pople's calculations. However, as

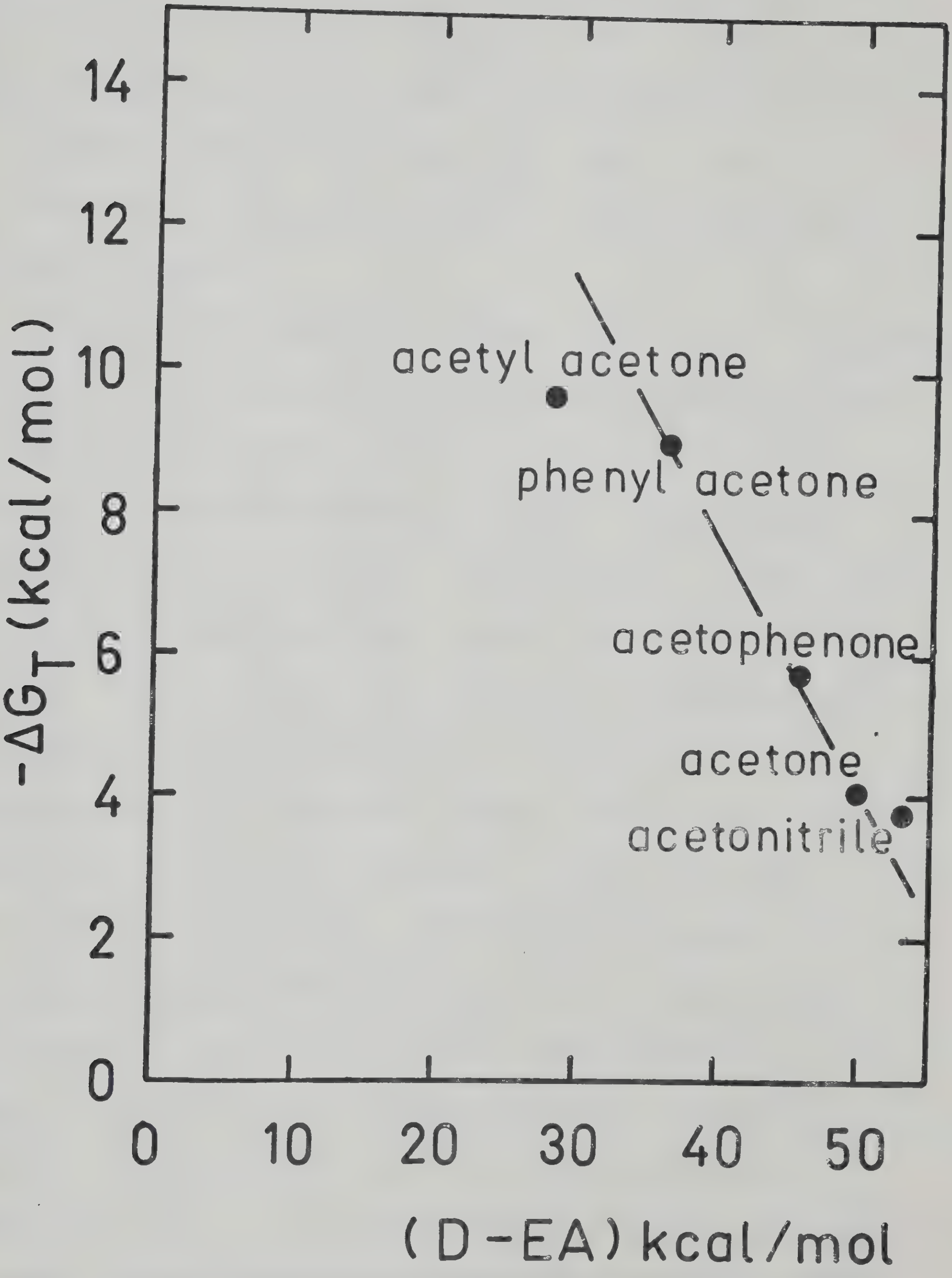

FIGURE 5.21. Correlation of Gas Phase Acidities *versus* Chloride Affinities Relative to 1,4-pentadiene for a Series of Ketones and Acetonitrile.

the chloride ion approaches the molecule the electron distribution will change. Therefore the calculated electron populations serve only to indicate where the possible positions of attachment may be. Finally the fact that acetone can also exist in the enol form must also be considered.

Three of the possible structures of the $Cl^-.CH_3COCH_3$ complex may be discounted. Electrostatic calculations (183) on the $Cl^-.CH_3CN$ system have shown that closer agreement with experimentally measured $\Delta H^o_{0,1}$ values is obtained when the chloride ion interacts symmetrically with all three hydrogen atoms rather than with a single hydrogen. Therefore the occurrence of a hydrogen bond to Cl^- is unlikely with acetone. If the chloride ion interacted with four hydrogen atoms from the two methyl groups, the rotation of the methyl groups about the C-C bonds would be restricted. The hindered movement of the methyl groups would imply a large value of $\Delta S^o_{0,1}$ for this compound. However, Table XII shows that $\Delta S^o_{0,1}$ for acetone is significantly lower than other compounds measured. Interactions with four hydrogen atoms is therefore unlikely. If acetone existed in the enol form in the gas phase, the chloride ion would most probably attach to the hydroxyl hydrogen. However, the enol form is thought to be unimportant in the gas phase (173) and thus a complex of this type will probably not occur.

Therefore the structure of the $Cl^{-}.CH_3COCH_3$ complex will either take the form of a symmetrical interaction with the methyl hydrogens or attachment to the central carbon.

The electron distribution in XVII shows that the contribution of resonance structure XVIII is quite important and that a small amount .007 of an electronic charge is donated from the methyl group to the central carbon. When one of the methyl groups is replaced by a phenyl ring the π electrons on the ring donate .028 electrons to the central carbon (189) leaving the ring slightly positive. The chloride ion may attach to acetophenone in three ways: via the methyl group, to a ring hydrogen or interact with the π electrons by "sitting" on the ring. The deficiency of π electrons in the phenyl ring may indicate that the chloride ion will interact with these electrons.

In the case of phenyl acetone the chloride may attack the methylene hydrogens or the methyl hydrogens since they are both adjacent to a carbon which has a positive charge in the resonance form XIX. However,

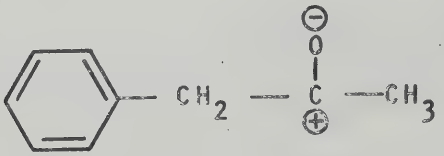

XIX

steric effects may restrict the approach of Cl^{-} to the

methyl hydrogens.

Figure 5.21 shows that the chloride affinity of acetyl acetone is greater than that of acetone. This may be explained by the fact that the central methylene group in acetyl acetone is influenced by two adjacent carbonyl groups. The chloride ion probably attaches to the two hydrogen atoms on the central carbon atom.

Acetonitrile, from previous measurements in this laboratory (72), is also included in Figure 5.21 in order to compare the ketones with another unsaturated functional group. Acetonitrile and acetone are very similar in chloride affinity and gas phase acidity and are in the same order (see Chapter 6).

The electrostatic calculations performed by Davidson (183) found that 95% of the total stabilization energy E_t of an ion cluster was due to the ion-dipole interaction i.e. $E_t \approx E_{dip}$. He found E_{dip} for the $Cl^-.CH_3CN$ complex was 14.51 kcal/mol. Assuming a simple relationship between E_{dip} and the dipole moment an approximation of E_{dip} for $Cl.CH_3COCH_3$ may be made. The dipole moment of acetonitrile is 3.97D and that of acetone is 2.88D (190). Therefore

$$E_{dip} \simeq - \frac{14.51 \times 2.88}{3.97}$$

$$E_{dip} \approx E_t \simeq -10.5 \text{ kcal/mol} \qquad (5.29)$$

Corrections for the zero point energies of the three new

vibrations in the ion-molecule complex are about -2 kcal/mol (155) such that $E_t + 2 \simeq \Delta H^o_{0,1}$. In this case $E_t + 2 =$ -12.5 kcal/mol and the measured $\Delta H^o_{0,1}$ for acetone was -13.7 kcal/mol. Therefore from this rough calculation the ion-dipole energy gives a good estimate of $\Delta H^o_{0,1}$, the difference in the two values was probably due to the polarizability term. More rigorous calculations are necessary to obtain more accurate results but the electrostatic model gives a good indication of the magnitude of the chloride affinity.

(d) Chloride Affinities of Carbon Acids

The gas phase acidities have been measured for only a few carbon acids. Figure 5.22 shows that there is no consistent correlation between the gas phase acidites and chloride affinities of several carbon acids.

In the case of the alkyl benzenes, the chloride ion may attach to the alkyl group or the ring. The electron populations, calculated by Pople (189), are shown for benzene (XX), toluene (XXI) and for the distribution of the π electrons in toluene. The electron population of toluene indicates that the chloride ion may interact with the ring hydrogens or interact symmetrically with the hydrogen atoms of the methyl group.

The chloride affinity of toluene is greater than that of benzene. Further enlargement of the alkyl group

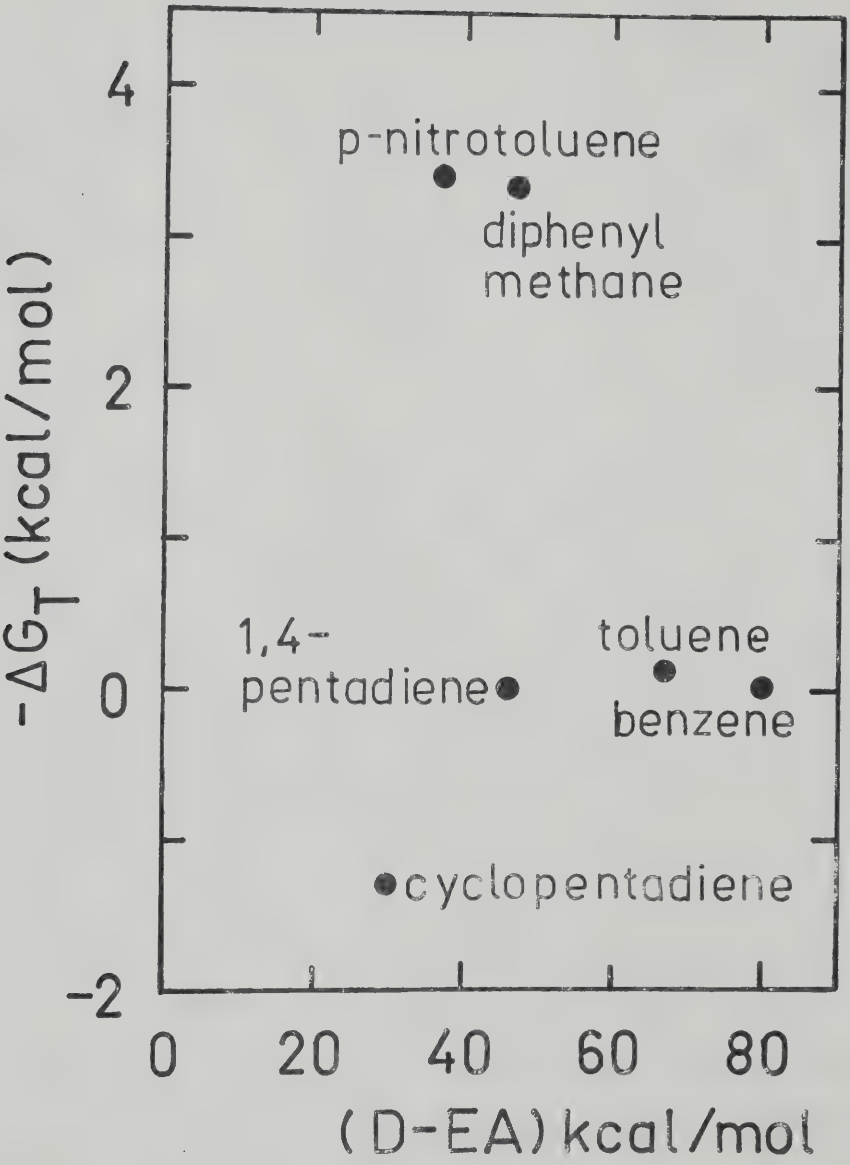

FIGURE 5.22. Correlation of Gas Phase Acidities *versus* Chloride Affinities Relative to 1,4-pentadiene for Various Carbon Acids.

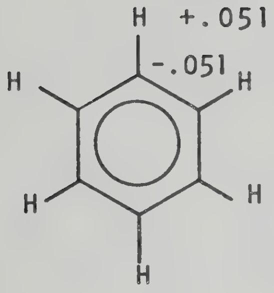

XXI

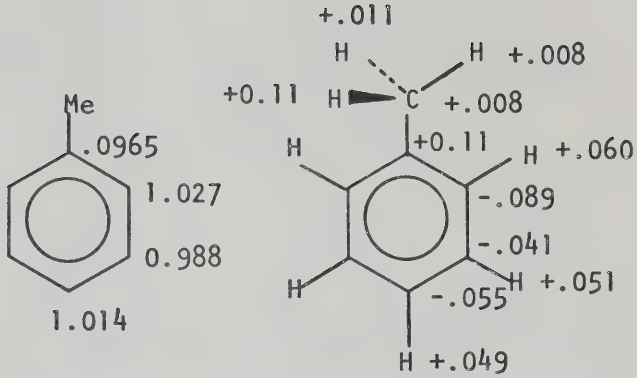

XXI

establishes the order of chloride affinities as H < Me < Et < n-Pr < i-Pr. Since this is the order of increasing electron donation to the ring, the chloride ion is probabily not interacting with the ring hydrogens as increasing substitution would destabilize the cluster. This indicates that the chloride ion probably attaches to the alkyl groups, since the "acidity" of the hydrogens on these groups increases with increasing alkyl substitution. The above order may also be explained in terms of the polarizabilities of the alkyl groups, which was first proposed by Brauman to explain the acidities of aliphatic alcohols (31,161). In the series of alkyl benzenes the chloride ion probably interacts with the diffuse positive end of the dipole, which is spread over an alkyl group. The polarizability of the alkyl group enhances the charge separation with the molecule which is necessary to form a stable cluster with Cl^-. Since the polarizability of the alkyl group increases with size,

the chloride affinity also increases in this order.

The chloride affinities of some methyl substituted benzenes are in the following order (Table XIV):

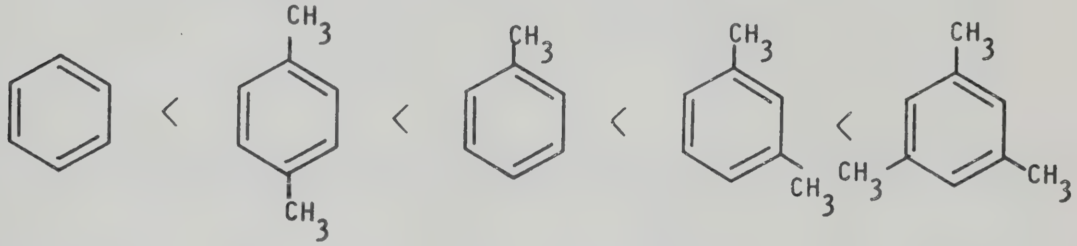

Para-xylene appears to be out of order. Since the $G^{o}_{0,1}$ values of toluene and p-xylene were found to be quite similar, experiments were conducted to check that this was not an experimental error. A mixture containing equal partial pressures of toluene and p-xylene was made and the intensities of Cl^- and the two cluster ions were monitored. The cluster of toluene with Cl^- was found to be slightly more intense than that with p-xylene, confirming that the chloride affinity of toluene is greater. The position of p-xylene in the above order is therefore correct. Tha anomalous behaviour of p-xylene cannot be explained by the inductive effect, since p- and m- xylene would have similar chloride affinities. Hyperconjugation may be invoked to explain the behaviour of p-xylene. When hyperconjugation occurs in m-xylene, the negative charge is in a β position to an alkyl group and the separation of the proton from the alkyl group assists in the interaction with an approaching chloride ion.

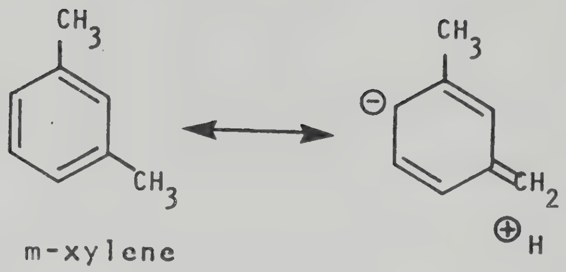

In the hyperconjugated structure of p-xylene a negative

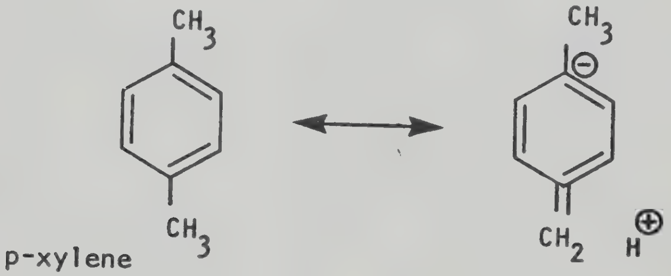

charge is situated at a carbon adjacent to an alkyl group, which is also donating electrons to the ring. This hyperconjugated form is therefore unfavourable and does not contribute to the structure of p-xylene. Although hyperconjugated structures of neutral molecules are probably not important in the gas phase, the approach of a chloride ion to m- or p-xylene will promote charge separation within the molecule and the structures may contribute to the stability of the cluster. Since the hyperconjugated structures for m-xylene are more stable than those for p-xylene, the interaction between Cl^- and m-xylene will be greater, which is the order observed experimentally. This explanation indicates that the chloride ion probably interacts with the

methyl group since the same argument would not hold if the chloride ion attached to the ring.

Brauman and Blair's investigations of unsaturated systems (164) showed that the gas phase acidity of toluene was greater than that of p-xylene. This is the same order as their chloride affinities. The agreement between the gas phase acidity and chloride affinity orders constitutes evidence that the attachment of the chloride ion occurs to the methyl hydrogens since otherwise this correlation would be difficult to explain.

The gas phase acidity of cyclopentadiene is quite large for a carbon acid. This is explained by the fact that cyclopentadiene obtains aromatic character when it loses a porton. The fact that cyclopentadiene is not observed to cluster with Cl^- may be construed as evidence that Cl^- attaches to the ring in the alkyl benzenes. However, a cluster of Cl^- with 1,4 pentadiene is observed. Since 1,4 pentadiene is the open chain analog of cyclopentadiene, with the same number of π electrons, the above argument seems unlikely.

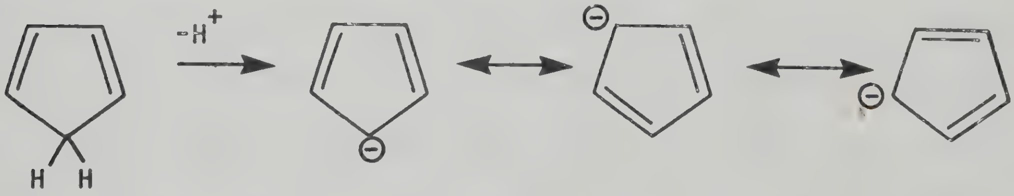

The gas phase acidity order for the phenylmethanes is expected to be $C_6H_5CH_3 < (C_6H_5)_2CH_2 < (C_6H_5)_3CH$. Experiment has verified the relative order of acidities of toluene and diphenyl methane (72) but the formation of the triphenylmethyl anion is expected to be favoured because the negative charge can be delocalized over three phenyl rings. The chloride affinities for these compounds are in the order: toluene < triphenyl methane < diphenyl methane. The interaction of Cl^- with triphenylmethane must be restricted due to steric hindrance of the three phenyl groups. If it is assumed that the chloride ion interacts with the lone hydrogen then it is possible that the chloride ion cannot approach closely enough to form a hydrogen bond. The order of chloride affinity does not follow the expected gas phase acidity for these compounds. This situation is somewhat analogous to the gas phase Brönsted and Lewis basicity orders of the methyl substituted amines. The Brönsted basicities increase regularly from NH_3 to $(CH_3)_3N$ (162). The measurement of the Lewis basicities towards the much bulkier Lewis acid, K^+ shows that the basicities increase from NH_3 to $(CH_3)_2NH$ and then decrease for $(CH_3)_3N$ (191). This effect may also be attributed to steric hindrance by the bulky substituent groups.

In general, the chloride affinities of the carbon acids do not follow the gas phase acidities, whereas

the substituted phenols correlate very well, as discussed in section (b). The correlation was attributed to the phenol being able to stabilize both the anion and charge separated structures by resonance. The phenol is able to form stable resonance structures because the oxygen possesses lone pairs which are mobile and can move around the ring without breaking the O-H bond. In the carbon acids the equivalent structures can only be achieved by hyperconjugation i.e. a carbon-hydrogen bond has to be broken. These structures are therefore not very important in the gas phase and the inability to stabilize these charge separated structures means that the clusters with Cl^- are very weak and do not follow the gas phase acidities.

(e) Chloride Affinities of Benzenes with Hetero Atom Containing Substituents

Examination of Table XIV shows that the chloride affinities of the benzenes containing hetero atom substituents are slightly greater than the alkyl substituted benzenes. No gas phase acidities of the hetero atom compounds are available for comparison with their chloride affinities.

McMahon and Kebarle have shown that the gas phase acidities of the substituted benzoic acids (71) and substituted phenols (174) correlate very well with the

σ^o values of Taft (170). It is possible that the same factors which determine the chloride affinities in the substituted phenols may also affect the substituted benzenes. The σ^o values are a measure of the electron-attracting or electron-donating power of a substituent by resonance or induction. The more electron-attracting a substituent is, the more positive the σ^o for the para position.

Lau and Kebarle (73) have measured the proton affinities of various substituted benzenes. They showed that there was good correlation between the proton affinity and the σ^o value of the substituent. They proposed that if the proton affinity correlated well with the σ^o value, then the proton was attaching to the ring to give a σ complex. The results shown in Figure 5.23 may also be interpreted in a similar manner. It has already been demonstrated that the chloride ion interacts with the phenolic hydrogen of phenol (section (b)). The -OH substituent also lies some distance from the lines of the σ^o plot. This is therefore consistent with the assumption that Cl^- interacts with the ring of compounds that fit the σ^o plot. The nitro group also does not fit the σ^o plot. The resonance structures of nitrobenzene may be represented by:

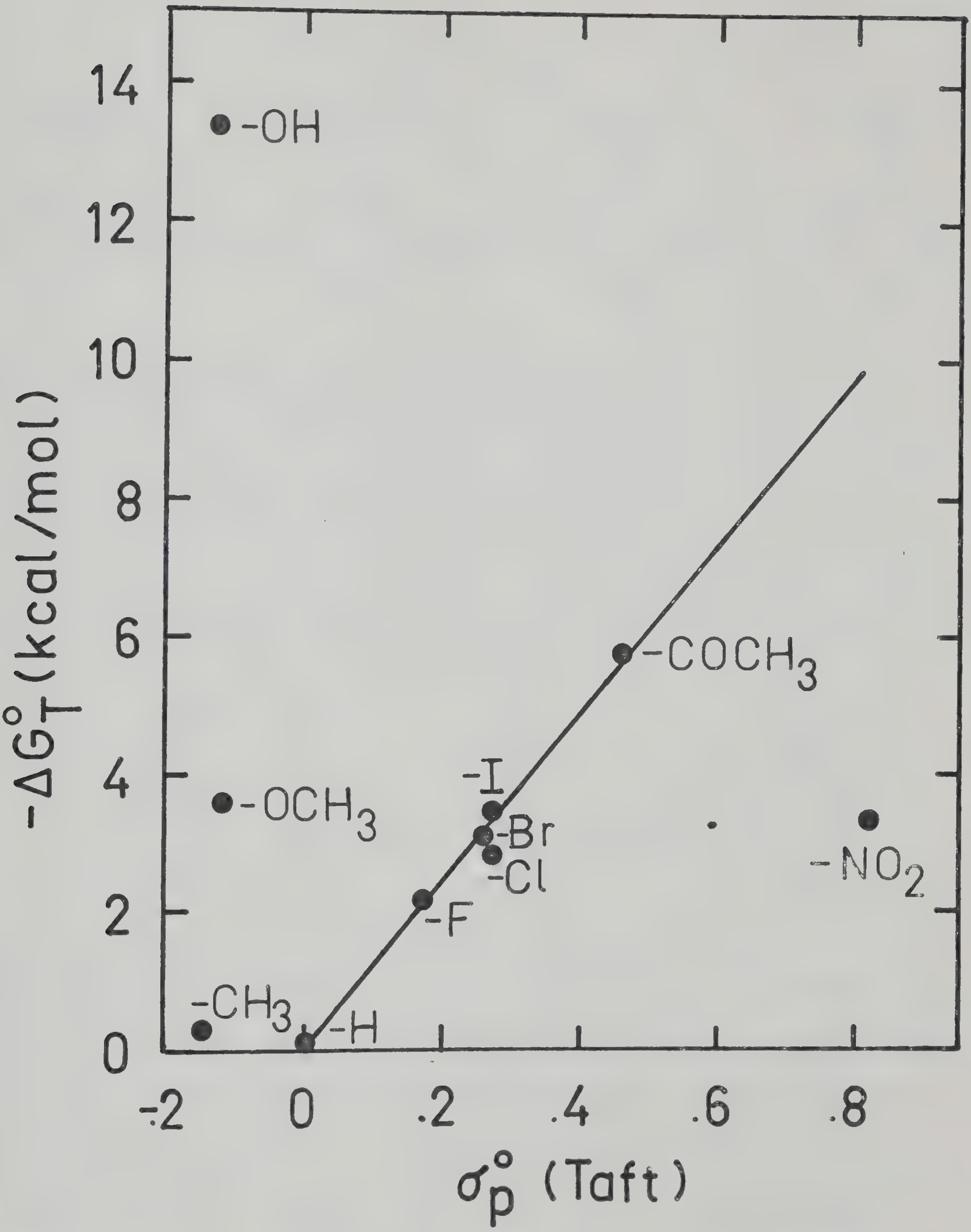

FIGURE 5.23. Plot of ΔG°_T for the Substituted Benzenes *versus* the σ° Values of Taft.

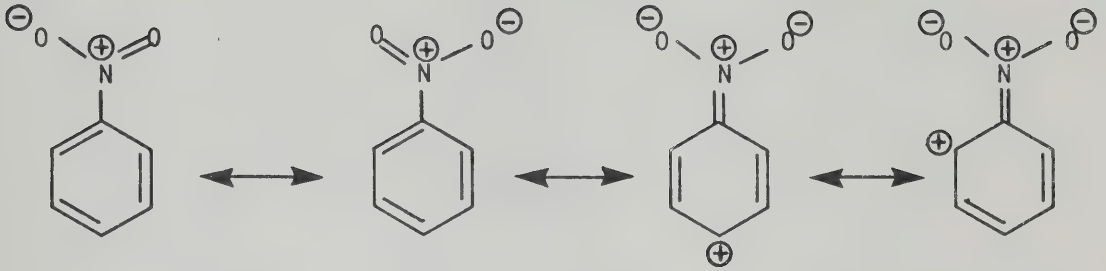

The nitrogen possesses a postive charge in each structure. It is therefore possible that the chloride ion interacts with the nitrogen atom instead of the ring and as a result does not fit the σ^{o} plot. The methoxy substituent donates electrons to the ring by structures such as:

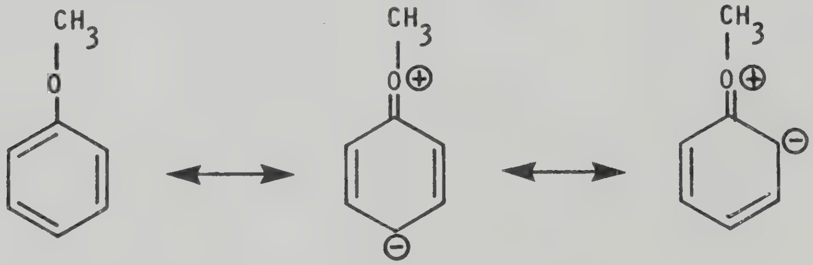

The chloride ion may attach to anisole via the methyl hydrogens since they are in a region of excess positive charge. The possibility of the chloride ion attaching to the methyl group in toluene was discussed in the previous section. Toluene also lies some distance from the line.

The structure of the cluster, where the chloride ion interacts with the ring, may be envisaged as:

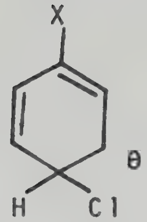

Similar structures may be drawn for the case where the chloride ion attaches to the meta position.

The order of $-\Delta G^o_T$ for the halobenzenes is benzene < fluorobenzene < chlorobenzene < bromobenzene < iodobenzene. Therefore the order of the stabilizing effect of the halogens substituents is F < Cl < Br < I. This is the same order as the gas phase acidities of the halosubstituted acetic acids studied by Kebarle _et_ _al_ (168). Other measurements of the gas phase acidities of compounds containing halogens have also indicated the same order (174, 175). The evidence from these observations therefore suggests that the inductive order in the gas phase is opposite to that in solution. The reversal is probably due to the higher polarizability of the larger halo substituents similar to the polarizability effect of the alkyl groups suggested by Brauman (161). Therefore clusters of halobenzenes with a chloride ion are more favourable with the larger halogen substituents because the resultant negative charge of the clusters can be dispersed over a large volume.

An analogous example is the formation of the halide ions X_3^- in aqueous solution. I_3^- is very stable in

aqueous solution whereas the smaller equivalent ions are rarely observed (192). Therefore I_3^- is probably stable because the excess negative charge may be dispersed over the three large, polarizable iodine atoms.

(f) Correlation of Chloride Affinities with Dipole Moment

Since electrostatic calculations have shown that ion-dipole interaction contributes nearly all of the stabilization energy to a cluster (183), the chloride affinity may be expected to depend on the dipole moment of the molecule. Figure 5.24 shows a plot of $-\Delta G^o_T$ plotted versus the dipole moment of RH. When all of the points are considered a rough correlation exists. When a group of similar compounds (i.e. phenols) are considered, it is found that the dipole moments are approximately constant within the group. However the chloride affinities differ within the group. Thus it may be expected that the chloride affinities will not correlate very well with the dipole moments because they do not take into account the distance between the chloride ion and the molecule. As discussed earlier (183) good agreement with experiment is observed in electrostatic calculations only if the charge distribution of the dipole is taken into account.

FIGURE 5.24 Plot of $-\Delta G_T^o$ for all the Compounds Studied *versus* Their Dipole Moment. Oxygen Acids (●), Pyrrole (○), Ketones (△), Acetonitrile (▲), Chloroform (▼), Halobenzenes (□), Substituted Benzenes (◇), Carbon Acids (■).

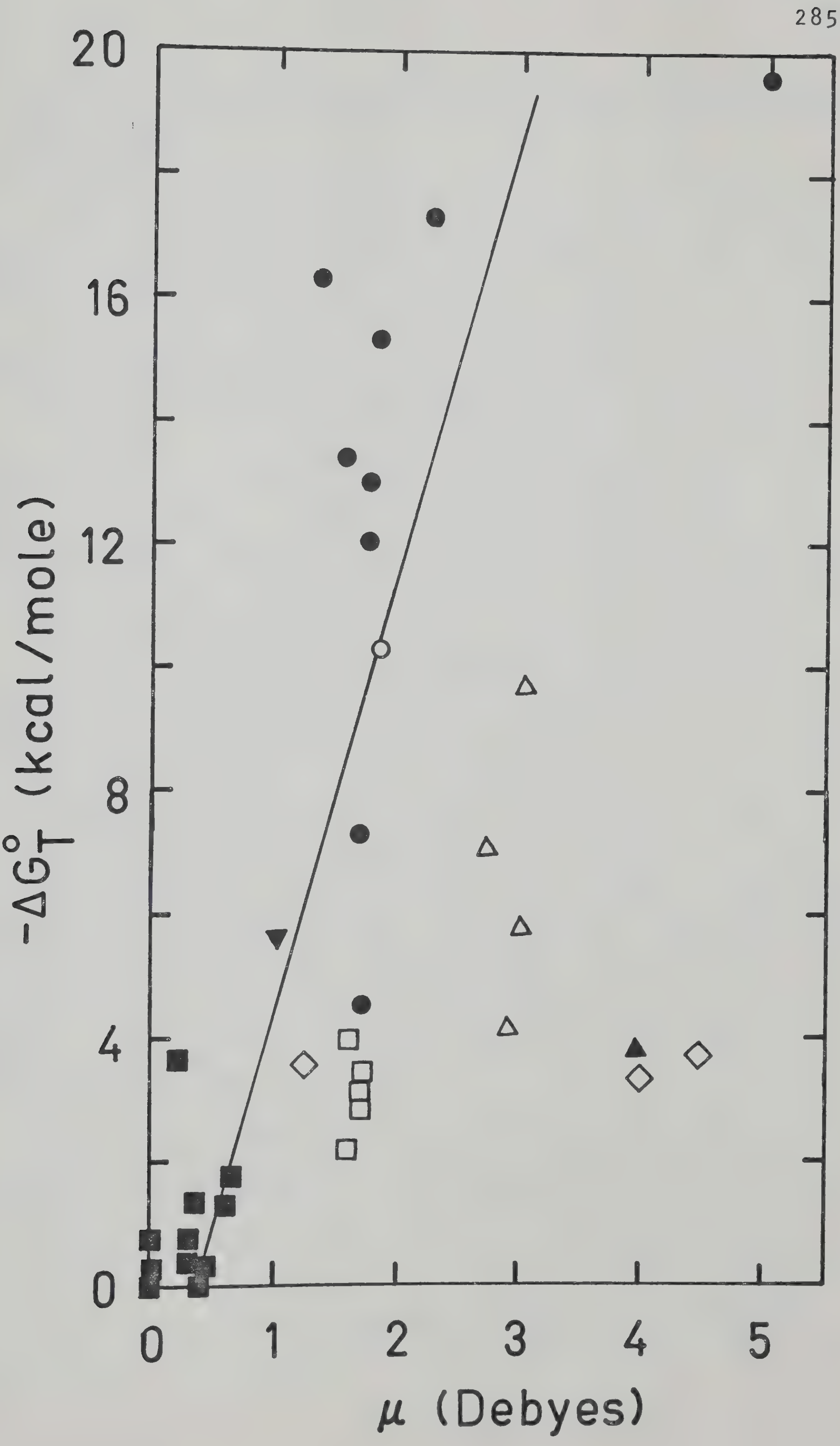
20
16
12
8
4
0
$-\Delta G^\circ_T$ (kcal/mole)
0
1
2
3
4
5
μ (Debyes)

(g) Comparison with Recent Studies of $RHCl^-$ Complexes in Solution.

Recently the attachment of chloride ions to weak acids has been studied in different solvents by Benoit et al (193). They investigated the chloride affinity in sulfolane and acetonitrile for the same series of compounds that Yamdagni and Kebarle (156) had studied in the gas phase. The order of the enthalpies in sulfolane was: $Cl_3CH < HOH < CH_3OH \sim CH_3COOH < C_6H_5OH < HCOOH < HCl$ whereas the order of the equivalent gas phase measurements of $\Delta H^o_{0,1}$, was: $HOH < CH_3OH < Cl_3CH < C_6H_5OH < CH_3COOH < HCl << HCOOH$. The two scales disagree on the position of chloroform. Also the positions of acetic acid and phenol are interchanged as the formic and hydrochloric acids. However if the $\Delta H^o_{0,1}$ values remeasured in this work are included the order becomes: $HOH < CH_3OH < Cl_3CH < CH_3COOH < HCl \sim C_6H_5OH < HCOOH$. The order of acetic acid and phenol now agrees with that of Benoit, the only disagreement is the position of Cl_3CH and HCl which were not measured in this work.

Benoit found that the calculated enthalpy change for reaction (5.30) does not vary greatly with the solvents studied indicating that the interaction with Cl^-

$$Cl^-(\ell) + RH(g) \longrightarrow RHCl^-(\ell) \qquad (5.30)$$

does not change with solvent. This result may have been expected for aprotic solvents such as acetonitrile and DMSO because they resemble the gas phase in many respects.

5.8 Conclusions

In the study of gas phase acidities the fundamental aspect that governs the acidity of a compound is its ability to form a stable anion. Factors which contribute to the stability of the ion are inductive and resonance effects. When clusters of a compound RH, with Cl^- are studied, an "acidic" hydrogen has to be present to promote the formation of the cluster. Since RH is neutral, the important principle in the formation of clusters with Cl^- depends on the ability of RH to support charge separation within the molecule itself. Therefore it is not certain that hydrogen bond energy can be equated with gas phase acidity since the former is determined by the ability of RH to stabilize charge separation whereas the latter depends on the ability of R^- to support a negative charge. In the case of the substituted phenols the oxygen possesses lone pairs which have the ability to shift around the ring facilitating both stabilization of the negative charge in the anion and of charge separation in the neutral compound. Carbon acids do not possess a lone pair which can aid charge separation without breaking a C-H bond and the correlation with acidity is not very good.

The possible geometries of the chloride ion clusters were examined for the different types of compounds. It was found that the chloride ion does not interact with all of the compounds in the same manner. In the case of the substituted phenols, the chloride ion attaches to the phenolic hydrogen rather than the ring hydrogens. Examination of a group of ketones shows that symmetric interaction with the alkyl hydrogens or attack on the carbonyl carbon is possible. In the case of the alkyl benzenes the evidence points to interaction with the alkyl groups whereas interaction with the ring is more likely for several hetero atom substituents. Therefore, considering the different types of interactions, it is not surprising that there is no correlation between the chloride affinities and the gas phase acidities. Rigorous electrostatic calculations would distinguish between the different possible structures of the clusters.

CHAPTER 6

REMEASUREMENT OF THE RELATIVE GAS PHASE ACIDITES OF ACETONE AND ACETONITRILE

6.1 Introduction

The relative acidities of acetone and acetonitrile have been measured previously in this laboratory by McMahon and Kebarle (72). They measured the ΔG for the equilibrium (6.1) which is equal to the gas phase acidity difference between the two compounds. They found that acetonitrile was more acidic than acetone by 2.5 kcal/mol.

$$CH_3COCH_3 + CH_2CN^- \rightleftharpoons CH_3COCH_2^- + CH_3CN \quad (6.1)$$

Bohme *et al* (166) have also investigated reaction (6.1), using the flowing afterglow technique to measure the forward and reverse rate constants. These workers found that acetone was a stronger gas phase acid than acetonitrile which is opposite to McMahon's relative order.

A recent measurement by Bordwell *et al* (187) reported a good correlation between gas phase acidities and acidities in the aprotic solvent dimethyl sulfoxide. They also found that acetone was a stronger acid in DMSO than acetonitrile. Therefore if Bordwell's correlation holds, acetone should be the stronger acid in the gas phase.

In view of the evidence that the relative acidity order of the two compounds measured in this laboratory may be wrong, it was decided to repeat the measurement. The need for such a remeasurement was also indicated by the following aspects of McMahon's results: the anion intensities observed for equilibrium (6.1) were unusually low and he had set a large error limit for this result. Furthermore a competitive reaction the nucleophilic substitution (6.2), had been suggested by McMahon which depletes the

$$CH_2CN^- + CH_3CN \longrightarrow CH_3CH_2CN + CN^- \qquad (6.2)$$

ion concentration of CH_2CN^-. McMahon attempted to eliminate the occurrence of reaction (6.2) by making the partial pressure of acetonitrile equal to a tenth of that of acetone.

6.2 Experimental

McMahon generated the negative ions in reaction (6.1) with sulphuryl fluoride. Electron bombardment of SO_2F_2 was assumed to produce F^- ions. HF is a very weak acid and thus acetonitrile and acetone proton transfer to F^- by reactions (6.3) and (6.4) producing the deprotonated anions.

$$F^- + CH_3CN \longrightarrow HF + CH_2CN^- \qquad (6.3)$$

$$F^- + CH_3COCH_3 \longrightarrow HF + CH_3COCH_2^- \qquad (6.4)$$

As mentioned before, the ion signals in McMahon's measurement were extremely weak. The measurement was initially repeated using McMahon's conditions: 700 torr CH_4, 10 torr SO_2F_2 and 10 torr each of acetone and acetonitrile in the bulb. The anion signal under these conditions was barely detectable even under constant irradiation of the electron beam. McMahon had used SO_2F_2 for the generation of F^- since the NF_3 which had been used earlier in this lab to produce F^- ions had all been consumed. An examination of the ions obtained with SO_2F_2 in the absence of any other acids showed that little F^- is produced by this compound. Therefore in the present experiments NF_3 was used again instead of SO_2F_2 and the anion signal was much stronger.

Different mixtures of acetone and acetonitrile were used to test if reaction (6.2) could be eliminated.

6.3 Results and Discussion

Figures 6.1 and 6.2 show two examples of the experiment performed under different conditions. Figure 6.1 shows the ion decay curves obtained when the partial pressures of acetone and acetonitrile are equal. It can be seen that the intensity of $CH_3COCH_2^-$ is five times greater than the sum of CN^- and CH_2CN^-. Therefore there is no possibility of acetonitrile being the stronger

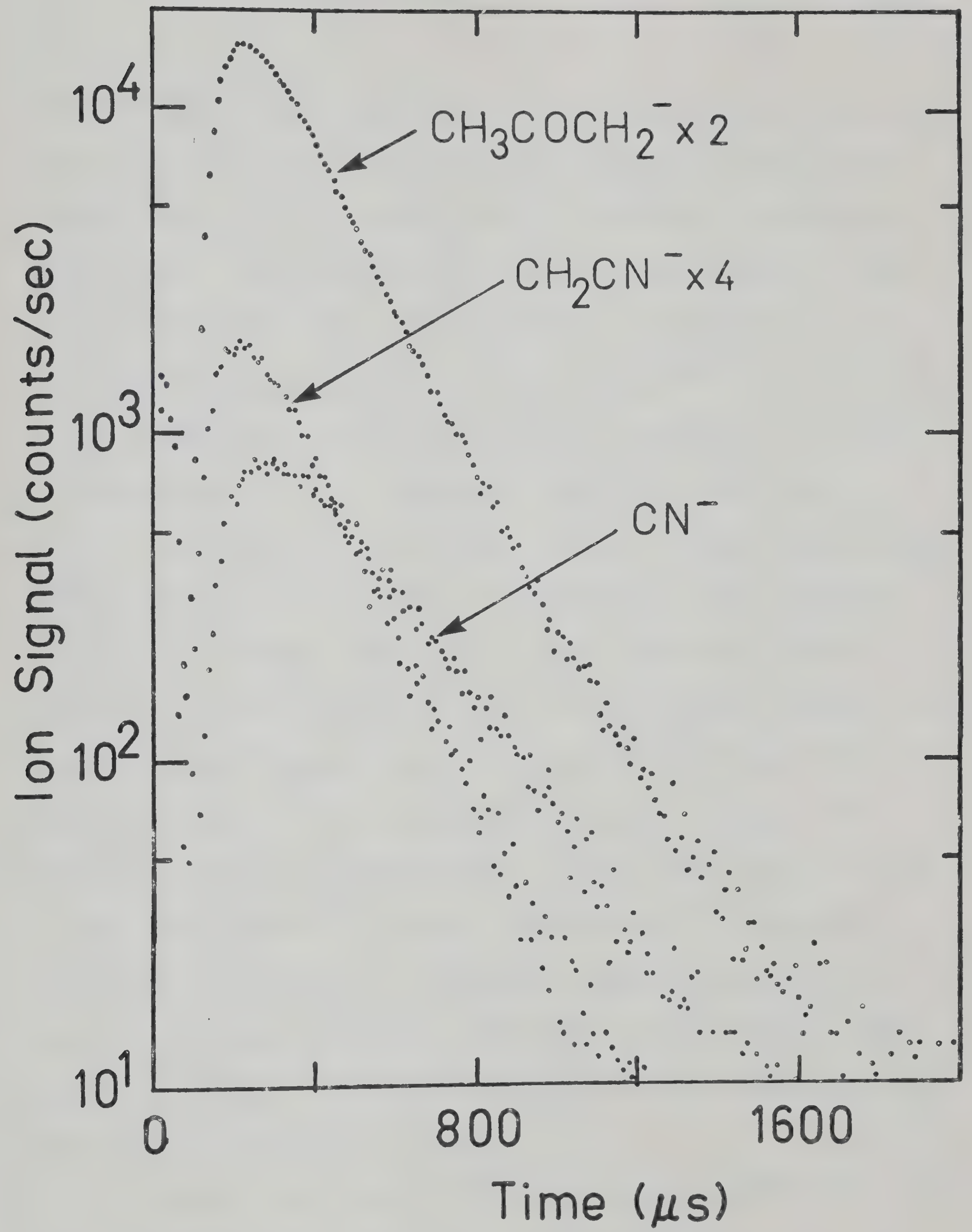

FIGURE 6.1. Observed Ion Signal in 2.8 torr CH_4 Containing a 1:1 Ratio of Acetone to Acetonitrile at 256°C

acid. Figure 6.2 shows the ion decay curves for the same ions when the partial pressure of acetone is ten times greater than that of acetonitrile, similar to McMahon's conditions. The intensity of CN^- is approximately the same as in Figure 6.1, the intensity of CH_2CN^- is about ten times smaller. Therefore the intensity of CN^- appears to be independent of the pressure of acetonitrile which is unexpected if CN^- originates from reaction (6.2).

The results are shown in Table XV and the average ΔG^o was -2.8 ± 0.2 kcal/mol. Acetone had been measured with several other compounds in previous measurements (173) so its D-EA value was well established. Acetonitrile had only been measured against acetone therefore it was the D-EA value of this compound that was wrong. The new D-EA value of acetonitrile is therefore 52.9 instead of the 47.6 kcal/mol obtained previously. A possible reason for the error in McMahon's measurement may be a reaction between $CH_3COCH_2^-$ and SO_2F_2 which reduces the intensity of the ion and gives an erroneous equilibrium constant for reaction (6.1).

Recent results in this laboratory (194) have shown that the large CN^- intensity observed is due to an impurity of HCN in the nitrogen trifluoride. By purifying the gas it was demonstrated that reaction (6.2) is negligible and the CN^- observed is due to the proton transfer reaction (6.5). The D-EA value for HCN is approximately

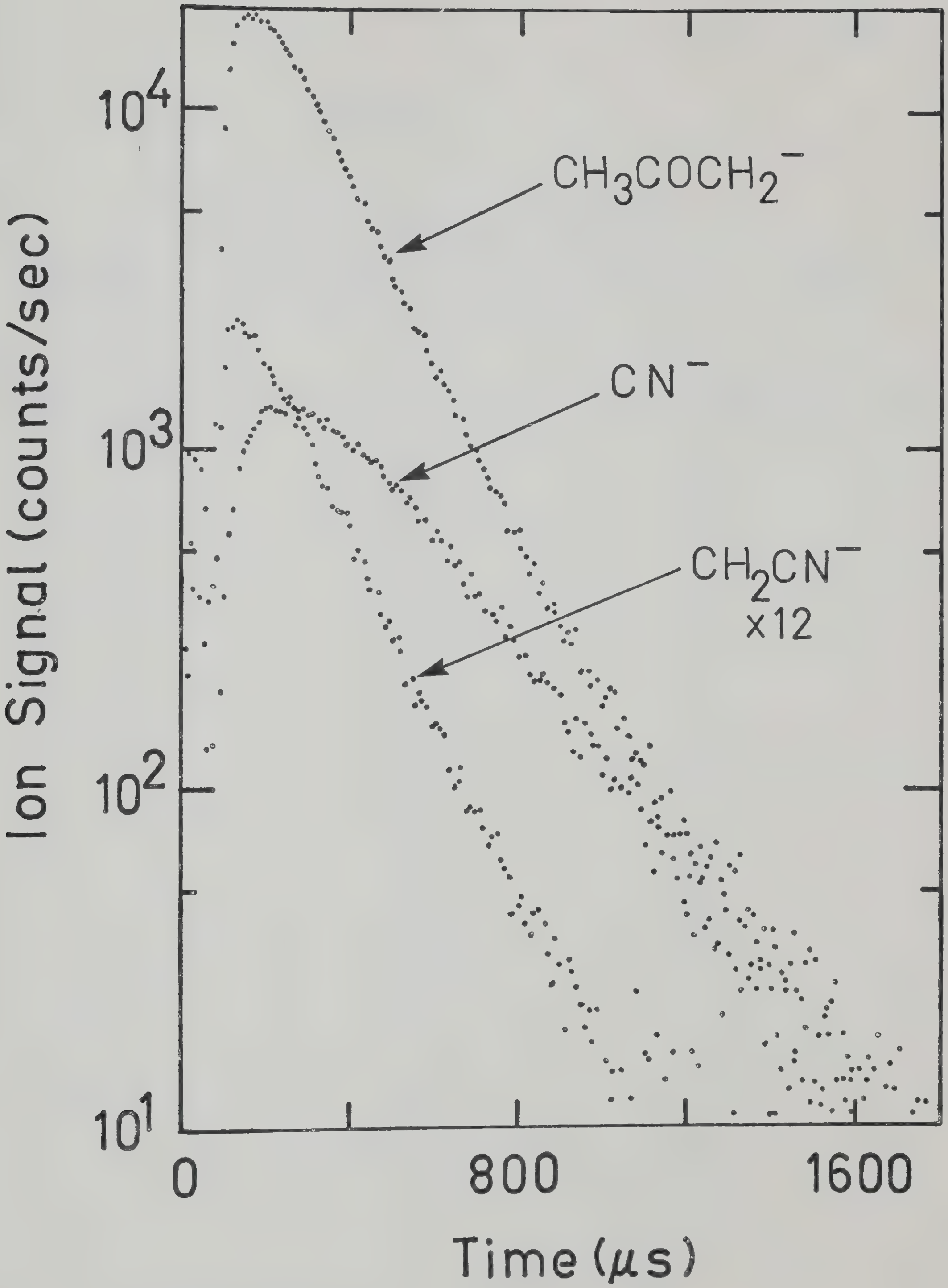

FIGURE 6.2. Observed Ion Signal in 3.2 torr CH_4 Containing a 10:1 Ratio of Acetone to Acetonitrile at 257°C.

TABLE XV

ΔG^o Values for the Equilibrium

$$CH_3COCH_3 + CH_2CN^- \rightleftharpoons CH_3CN + CH_3COCH_2^- \text{ at } 257°C$$

$P_{CH_3CN}/P_{CH_3COCH_3}$	$-\Delta G^o$	Ion Source Pressure (torr)
1:10.2	2.58	1.1
"	3.09	2.1
"	2.60	3.2
"	2.52	4.1
1:5.1	2.92	1.4
"	2.81	2.6
"	3.03	2.7
"	2.73	3.6
"	2.65	3.8
"	2.62	4.4
1:1	3.10	1.7
"	3.10	2.8
"	3.18	3.5

Average $\Delta G^o = -2.8 \pm 0.2$ kcal/mol

$$CH_3COCH_2^- + HCN \rightleftharpoons CH_3COCH_3 + CN^- \qquad (6.5)$$

35 kcal/mol (195) and it is therefore a stronger acid than both acetone and acetonitrile. Remeasurement of the ΔG for reaction (6.1) using purified NF_3 yielded $\Delta G^o = -3.0$ kcal/mol which agrees with the data presented in Table XV.

These results will not be discussed further since they were only carried out to check the previous results of McMahon and Kebarle which are discussed fully by them (173).

CHAPTER 7

SUGGESTIONS FOR FURTHER WORK

An ion source has now been built that will enable ion-molecule reactions at below-room temperatures to be studied. This type of ion source can go down to temperatures of -180°C (143). This will allow measurement of the temperature dependence of $K_{0,1}$ in order to give the chloride affinities for compounds such as benzene, toluene and other weak carbon acids. At lower temperatures it may be possible to observe a cluster of Cl^- with cyclopentadiene.

The study of reactions of the type (7.1) enables

$$R^- + H_2O \overset{K_{0,1}}{\rightleftharpoons} R^-.H_2O \qquad (7.1)$$

a similar correlation to be drawn to that investigated in Chapter 5. The measured $\Delta H^o_{0,1}$ of reaction (7.1) will be the hydrogen bonding energy to R^- and may therefore be correlated with the gas phase basicity of R^-.

Some initial experiments were conducted on this system where RH was malonitrile and acetylacetone. Experimentally it was difficult to obtain a clean source of the R^- ions. Previous experiments had shown that R^- could be generated from sulphuryl fluoride (173). F^- is produced by dissociative electron attachment of electrons to SO_2F_2. Since HF is a very weak acid, F^-

rapidly produces R^- by proton transfer:

$$F^- + RH \longrightarrow HF + R^- \qquad (7.2)$$

Unfortunately SO_2F_2 and SO_2F^- are also produced and the choice of malonitrile meant that the hydrated ion $CH^-(CN)_2.H_2O$ occurred at the same mass as SO_2F^-. This problem was overcome by substituting D_2O for water and the hydrated peak moved from 83 to 86, the shift in 3 mass units being caused by complete deuteration of the remaining hydrogen in $CH^-(CN)_2$ to give $CD^-(CN)_2.D_2O$. The deuterate could only be observed when a trace (~1 mtorr) of malonitrile was present in an atmosphere of D_2O in the bulb, otherwise there was a tendency for the dimer $CH_2(CN)_2.CH^-(CN)_2$ to dominate the spectrum.

NF_3 may also be used to produce F^- (167) but is very difficult to obtain from commercial sources. The F^- is produced by near thermal secondary electrons with NF_3 undergoing dissociative electron capture as in reaction (7.3). The generation of F^- by NF_3 is therefore

$$e + NF_3 \longrightarrow NF_2 + F^- \qquad (7.3)$$

very specific compared to SO_2F_2.

The study of the hydration of anions could also be rewarding in explaining some differences between aqueous and gas phase acidities. For example malonitrile is stronger than monochloroacetic acid in the gas phase

by 1.8 kcal/mol. However in aqueous solution chloroacetic acid is 8 pK_a units stronger than malonitrile (72). By studying the system

$$R^-(H_2O)_{n-1} + H_2O \rightleftharpoons R^-(H_2O)_n \qquad (7.4)$$

for both compounds and choosing conditions such that n could be graudally increased from zero, the cross-over point may be observed and the reversal of aqueous and gaseous behaviour may be explained.

In the experiments described in Chapter 5, a neutral acid molecule interacted with a negative ion. Since the chloride ion can be thought of as a sphere of uniform negative charge and more than one RH solvent molecule may be added to the cluster until the inner solvent shell is full. When the negative ion is a molecule with a dipole, the electronic charge is distributed unevenly over the molecule. When the solvent is water only certain orientations of the molecule are possible. By choosing R^- such that it contains several possible bonding sites, the number of water molecules which will attach to R^- gives information on the type of interaction. For example, if R^- is the cyclopentadienyl anion, the ion is stabilized by resonance.

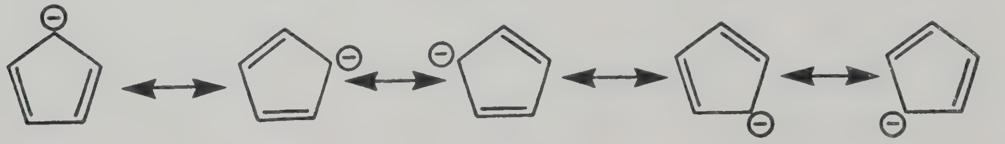

If five water molecules are observed to cluster with cyclopentadiene, the water molecules must be interacting with the five ring hydrogens. Alternatively, if only one or two molecules cluster with the cyclopentadienyl ion, then the water molecules must be laying parallel to the ring with the hydrogens nearest to the ring and interacting with the π electrons. Measurement of $\Delta H^{o}_{n-1,n}$ by reaction (7.4) will reflect which of the two types of interaction is occurring.

REFERENCES

1. J. J. Thomson, Phil. Mag. 24, 241 (1912).
2. A. J. Dempster, Phil. Mag. 31, 438 (1916).
3. H. D. Smyth, Phys. Rev. 25, 452 (1925).
4. T. P. Hogness and E. G. Lunn, Phys. Rev. 26, 44 (1925).
5. V. L. Tal'rose and A. K. Lyubimova, Doklady Akad. Nauk. SSSR 86, 909 (1952) per Chem. Abstracts 47, 2590 (1953).
6. D. P. Stevenson and D. O. Schissler, J. Chem. Phys. 23, 1353 (1955).
7. D. O. Schissler and D. P. Stevenson, J. Chem. Phys. 24, 926 (1956).
8. von H. Gutbier, Z. Naturforsch., A12, 499 (1957).
9. E. W. McDaniel, V. Cermak, A. Dalgarno, E. E. Ferguson, and L. Friedman, "Ion Molecule Reactions" John Wiley and Sons, New York (1970).
10. D. P. Stevenson, D. O. Schissler, J. Chem. Phys. 29, 282 (1958).
11. R. P. Pottie, R. Barker and W. H. Hamill, Rad. Res. 10, 664 (1959).
12. F. H. Field, J. L. Franklin and F. W. Lampe, J. Amer. Chem. Soc. 78, 5697 (1956).
13. F. H. Field, J. L. Franklin and F. W. Lampe, J. Amer. Chem. Soc. 78, 2419 (1956).
14. F. H. Field, J. L. Franklin and F. W. Lampe, J. Amer. Chem. Soc. 79, 2665 (1957).

15. P. Langevin, Annales de Chimie et de Physique, Series 8, 5, 245 (1905).

16. G. Gioumousis and D. P. Stevenson, J. Chem. Phys. 29, 294 (1958).

17. E. E. Ferguson, D. K. Bohme, F. C. Fehsenfeld and D. B. Dunkin, J. Chem. Phys. 50, 5039 (1969).

18. V. L. Tal'rose and E. L. Frankevich, Russian J. Phys. Chem. 34, 1275 (1960).

19. V. L. Tal'rose, Pure Appl. Chem. 5, 455 (1962).

20. T. W. Shannon, F. Meyer and A. G. Harrison, Can. J. Chem. 43, 159 (1965).

21. K. R. Ryan and J. H. Futrell, J. Chem. Phys. 42, 824 (1965).

22. K. R. Ryan and J. H. Futrell, J. Chem. Phys. 43, 3009 (1965).

23. V. L. Tal'rose and G. V. Karachevtsev, "Ion-Molecule Reactions" in "Advances in Mass Spectrometry". Editor W. L. Mead. Vol. 3. Institute of Petroleum. London (1966).

24. A. A. Herod and A. G. Harrison, Int. J. Mass Spectrom. and Ion Phys. 4, 415 (1970).

25. N. A. McAskill and A. G. Harrison, Int. J. Mass Spectrom. and Ion Phys. 5, 193 (1970).

26. A. G. Harrison, Int. J. Mass Spectrom. and Ion Phys. 6, 297 (1971).

27. L. Anders, J. Beauchamp, R. Dunbar and J. Baldeschwieler, J. Chem. Phys. 45, 1062 (1966).

28. J. L. Beauchamp, J. Chem. Phys. 46, 1231 (1967).

29. J. L. Beauchamp and J. T. Armstrong, Rev. Sci. Instr. 40, 123 (1969).

30. J. I. Brauman and L. K. Blair, J. Amer. Chem. Soc. 90, 5636 (1968).

31. J. I. Brauman and L. K. Blair, J. Amer. Chem. Soc. 90, 6561 (1968).

32. J. I. Brauman and L. K. Blair, J. Amer. Chem. Soc. 91, 2126 (1969).

33. J. M. S. Henis, J. Amer. Chem. Soc. 90, 844 (1968).

34. J. M. S. Henis, J. Chem. Phys. 52, 282 (1970).

35. F. H. Field, J. L. Franklin and M. S. B. Munson, J. Amer. Chem. Soc. 85, 3575 (1963).

36. F. H. Field, J. Amer. Chem. Soc. 83, 1523 (1961).

37. F. H. Field and M. S. B. Munson, J. Amer. Chem. Soc. 87, 3289 (1965).

38. F. H. Field and M. S. B. Munson, J. Amer. Chem. Soc. 87, 3294 (1965).

39. M. S. B. Munson and F. H. Field, J. Amer. Chem. Soc. 87, 4242 (1965).

40. M. S. B. Munson and F. H. Field, J. Amer. Chem. Soc. 88, 2621 (1966).

41. F. H. Field, Accounts Chem. Res. 1, 42 (1968).

42. F. H. Field, J. Amer. Chem. Soc. 91, 2827 (1969).

43. F. H. Field, P. Hamlet and W. F. Libby, J. Amer. Chem. Soc. 91, 2839 (1969).

44. F. H. Field, J. Amer. Chem. Soc. 91, 6334 (1969).

45. D. P. Beggs and F. H. Field, J. Amer. Chem. Soc. 93, 1567 (1971).

46. D.P. Beggs and F. H. Field, J. Amer. Chem. Soc. 93, 1576 (1971).

47. F. H. Field and D. P. Beggs, J. Amer. Chem. Soc. 93 1585 (1971).

48. S. L. Bennett and F. H. Field, J. Amer. Chem. Soc. 94, 5186 (1972).

49. S. L. Bennett and F. H. Field, J. Amer. Chem. Soc. 94, 6305 (1972).

50. E. E. Ferguson, F. C. Fehsenfeld and A. L. Schmeltekopf, Adv. Atomic and Mol. Phys. 5, 1 (1919).

51. E. E. Ferguson, Accounts Chem. Res. 3, 402 (1970).

52. E. E. Ferguson, D. B. Dunkin and F. C. Fehsenfeld, J. Chem. Phys. 57, 1459 (1972).

53. H. I. Schiff and D. K. Bohme, Int. J. of Mass Spectrom. and Ion Phys. 16, 167 (1975).

54. D. K. Bohme "Interactions between Ions and Molecules" Editor P. Ausloos, Plenum Press Corporation (1975) p.489.

55. W. L. Fite, J. A. Rutherford, W. R. Snow and V. A. J. van Lint, Disc. Faraday Soc. 33, 264 (1962).

56. J. Sayers and D. Smith, Disc. Faraday Soc. 37, 167 (1964).

57. L. J. Puckett and W. C. Lineberger, Phys. Rev. A, 1, 1635 (1970).

58. E. W. McDaniel "Drift Tube Studies of the Transport Properties and Reactions of Slow Ions in Gases" from "Case Studies in Atomic Collision Physics I". Edited by E. W. McDaniel and M. R. C. McDowell.

59. R. M. Snuggs, D. J. Volz, I. R. Gatland, J. H. Schummers, D. W. Martin and E. W. McDaniel, Phys. Rev. A, 3, 487 (1971).

60. D. A. Durden, P. Kebarle and A. Good, J. Chem. Phys. 50, 805 (1969).

61. A. Good, D. A. Durden and P. Kebarle, J. Chem. Phys. 52, 212 (1970).

62. A. J. Cunningham, J. D. Payzant and P. Kebarle, J. Amer. Chem. Soc. 94, 7627 (1972).

63. A. Good, D. A. Durden and P. Kebarle, J. Chem. Phys. 52, 222 (1970).

64. I. Dzidic and P. Kebarle, J. Phys. Chem. 74, 1466 (1970).

65. J. D. Payzant, R. Yamdagni and P. Kebarle, Can. J. Chem. 49, 3308 (1971).

66. J. D. Payzant and P. Kebarle, J. Chem. Phys. 56, 3482 (1972).

67. M. A. French, L. P. Hills and P. Kebarle, Can. J. Chem. 51, 456 (1973).

68. R. Yamdagni, J. D. Payzant and P. Kebarle, Can. J. Chem. 51, 2507 (1973).

69. J. D. Payzant, A. J. Cunningham and P. Kebarle, Can. J. Chem. 51, 3242 (1973).

70. R. Yamdagni and P. Kebarle, Can. J. Chem. 52, 861 (1974).

71. R. Yamdagni, T. B. McMahon and P. Kebarle, J. Amer. Chem. Soc. 96, 4035 (1974).

72. T. B. McMahon and P. Kebarle, J. Amer. Chem. Soc. 96, 5940 (1974).

73. Y. Lau and P. Kebarle, 24th Annual Conference on Mass Spectrometry, San Diego, (1976).

74. K. HIraoka and P. Kebarle, J. Amer. Chem. Soc. 97, 4179 (1975).

75. K. Hiraoka and P. Kebarle, Can. J. Chem. 53, 970 (1975).

76. E. Lindholm, I. Szabo and P. Wilmenius, Arkiv. Fysik, 25, 417 (1963).

77. H. von Koch, Arkiv Fysik, 28, 529 (1965).

78. P. Kebarle, R. Yamdagni K. Hiraoka and T. B. McMahon, Int. J. Mass Spectrom. and Ion Phys. 19, 71 (1976).

79. G. R. Freeman, "Radiation Chemistry", University of Alberta, Edmonton (1966).

80. F. H. Field and F. W. Lampe, J. Amer. Chem. Soc. 80, 5583 (1958).

81. F. H. Field and F. W. Lampe, J. Amer. Chem. Soc. 81, 3238 (1959).

82. A. Galli, A. Giardini-Guidoni and G. G. Volpi, J. Chem. Phys. 39, 518 (1963).

83. A. M. Hogg and P. Kebarle, J. Chem. Phys. 43, 449 (1965).

84. R. F. Porter "Interactions between Ions and Molecules". Editor P. Ausloos. Plenum Publishing Corporation. New York (1975).

85. K. Hiraoka, E. G. Grimsrud and P. Kebarle, J. Amer. Chem. Soc. 96, 3359 (1974).

86. T. F. Moran and W. H. Hamill, J. Chem. Phys. 39, 1413 (1963).

87. S. K. Gupta, E. G. Jones, A. G. Harrison and J. J. Myher, Can. J. Chem. 45, 3107 (1967).

88. M. T. Bowers and J. B. Laudenslager, J. Chem. Phys. 56, 4711 (1972).

89. T. Su and M. T. Bowers, J. Chem. Phys. 58, 3027 (1973).

90. T. Su and M. T. Bowers, Int. J. Mass Spectrom. and Ion Phys. 12, 347 (1973).

91. T. Su and M. T. Bowers, J. Amer. Chem. Soc. 95, 7609 (1973).

92. H. S. W. Massey, "Negative Ions". Second Edition, Cambridge University Press (1950).

93. D. A. Durden, Ph.D. Thesis, University of Alberta (1968).

94. J. D. Payzant, Ph. D. Thesis, University of Alberta, (1973).

95. O. P. Strausz, S. C. Barton, W. K. Duholke, H. E. Gunning and P. Kebarle, Can. J. Chem. 49, 2048 (1971).

96. S. Dushman, "Scientific Foundation of Vacuum Technique". John Wiley and Sons, New York (1949) p.84.

97. Handbook of Chemistry and Physics. 54th Edition. Chemical Rubber Company Press (1973).

98. M. R. Arshadi, Ph.D. Thesis, University of Alberta, (1969).

99. W. G. Wolber, B. D. Klettke, and P. W. Graves, Rev. Sci. Instr. 41, 724 (1970).

100. J. M. Goodings, J. M. Jones and D. A. Parker, Int. J. Mass Spectrom. and Ion Phys. 9, 417 (1972).

101. W. E. Potter and K. Mauersberger, Rev. Sci. Instr. 43, 1327 (1972).

102. E. W. McDaniel, "Collision Phenomena in Ionized Gases". John Wiley and Sons. New York (1964).

103. S. K. Searles and P. Kebarle, J. Phys. Chem. 72, 742 (1968).

104. A. M. Hogg, R. M. Haynes and P. Kebarle, J. Amer. Chem. Soc. 88, 28 (1966).

105. J. G. Collins, Ph.D. Thesis, University of Alberta (1966).

106. L. J. Kieffer, Atomic Data. Vol. 1. Part 1. (1969). p.19.

107. S. C. Lind, "Radiation Chemistry of Gases". Reinhold. New York (1961) p.25.

108. E. W. McDaniel "The Mobility and Diffusion of Ions in Gases". John Wiley and Sons. New York (1973).

109. W. Schottky, Phys. Z. 25, 635 (1924).

110. "Index of Mass Spectral Data" American Society for Testing and Materials Committee E-14 on Mass Spectrometry (1963).

111. P. Ausloos and S. G. Lias, J. Chem. Phys. 38, 2207 (1963).

112. R. Fuchs, Z. Naturforsch 16a, 1026 (1961).

113. S. Wexler and N. Jesse, J. Amer. Chem. Soc. 84, 3425 (1962).

114. G. A. W. Derwish, A. Galli, A. Gardini-Guidoni and G. G. Volpi, J. Chem. Phys. 40, 5 (1964).

115. G. A. Olah "Carbocations and Electrophilic Reactions". Verlag Chemie. John Wiley and Sons. New York, New York (1974).

116. P. D. Bartlett. "Nonclassical Ions. Reprints and Commentary". Benjamin, New York (1965).

117. G. A. Olah and J. Lukas, J. Amer. Chem. Soc. 89, 2227, 4739 (1967).

118. W. A. Lathan, W. J. Hehre and J. A. Pople, Tetrahedron Lett. 31, 2699 (1970).

119. P. C. Hariharan, W. A. Lathan and J. A. Pople, Chem. Phys. Lett. 14, 385 (1972).

120. A. Gamba, G. Morosi and M. Simonetta, Chem. Phys. Lett. 3, 20 (1969).

121. V. Dycymons, V. Staemmer and W. Kutzelnigg, Chem. Phys. Lett. 5, 361 (1970).

122. M. S. B. Munson, J. L. Franklin and F. H. Field, J. Phys. Chem. 68, 3098 (1964).

123. S. L. Chong and J. L. Franklin, J. Amer. Chem. Soc. 94, 6347 (1972).

124. D. K. Bohme, P. Fennelly, R. S. Hemsworth and H. I. Schiff, J. Amer. Chem. Soc. 95, 7512 (1973).

125. D. K. Bohme, R. S. Hemsworth, H. W. Rundle, and H. I. Schiff, J. Chem. Phys. 58, 3504 (1973).

126. R. S. Hemsworth, H. W. Rundle, D. K. Bohme, H. I. Schiff, D. B. Dunkin and F. C. Fehsenfeld, J. Chem. Phys. 59, 61 (1973).

127. J. L. Franklin, G. J.Dillard, H. M. Rosenstock, J. T. Herron, K. Draxl and F. H. Field. "Nat. Stand. Ref. Data Ser., Nat. Bur. Stand. 26 (1969).

128. W. A. Lathan, W. J. Hehre and J. A. Pople, J. Amer. Chem. Soc. 93, 808 (1971).

129. A. S. Blair, E. J. Heslin and A. G. Harrison, J. Amer. Chem. Soc. 94, 2935 (1972).

130. S. K. Searles, L. W. Sieck and P. Ausloos, J. Chem. Phys. 53, 849 (1970).

131. S. L. Bennett, S. G. Lias and F. H. Field, J. Phys. Chem. 76, 3919 (1972).

132. R. M. Haynes and P. Kebarle, J. Chem. Phys. 45, 3899 (1966).

133. R. C. Pierce and R. F. Porter, J. Phys. Chem. 78, 93 (1974).

134. K. Hiraoka and P. Kebarle, J. Chem. Phys. 63, 394 (1975).

135. D. K. Bohme, R. A. Vane, F. C. Fehsenfeld and E. E. Ferguson, Seventeenth Annual Conference on Mass Spectrometry and Allied Topics, Dallas, Texas (1969).

136. A. G. Harrison. Private communication.

137. K. Hiraoka and P. Kebarle, J. Chem. Phys. 63, 746 (1975).

138. G. M. Barrow. "Physical Chemistry" Second Edition. McGraw-Hill Book Company. New York (1966) p.490.

139. P. J. Robinson and K. A. Holbrook. "Unimolecular Reactions". Wiley. New York (1972).

140. W. H. Hehre, R. F. Stewart and J. A. Pople, J. Chem. Phys. 51, 2657 (1969).

141. W. Th. A. M. Van der Lugt and P. Ros. Chem. Phys. Lett. 4, 389 (1969).

142. P. K. Bischof and M.J.S. Dewar, J. Amer. Chem. Soc. 97, 2278 (1975).

143. K. Hiraoka and P. Kebarle. In press.

144. W. A. Chupka and J. Berkowtiz, J. Chem. Phys. 54, 4256 (1971).

145. N. M. Rodiguin and E. N. Rodiguina. "Consecutive Chemical Reactions". D. van Nostrand Company, Inc. Princeton, New Jersey (1964).

146. J. D. Payzant, A. J. Cunningham and P. Kebarle, Can. J. Chem. 50, 2230 (1972).

147. J. A. Pople. Int. J. Mass Spectrom. Ion Phys. 19, 89 (1976).

148. B. Zurawski, R. Ahlrichs and W. Kutzelnigg, Chem. Phys. Lett. 21, 309 (1973).

149. S. Wexler and L. G. Pobo, J. Amer. Chem. Soc. 93, 1327 (1971).

150. J. F. Coetzee and C. D. Ritchie, "Solute-Solvent Interactions". M. Dekker Inc. New York (1969).

151. P. Kebarle "Modern Aspects of Electrochemistry No. 9". Edited by B. E. Conway and J. O'M. Bockris Plenum Press. New York (1973).

152. J. D. Bernal and R. H. Fowler, J. Chem. Phys. 1, 515 (1933).

153. D. D. Eley and M. G. Evans, Trans. Faraday Soc. 34, 1093 (1938).

154. E. Clementi and H. Popkie, J. Chem. Phys. 57, 1077 (1972).

155. E. Clementi and H. Popkie, J. Chem. Phys. 58, 1689 (1972).

156. R. Yamdagni and P. Kebarle, J. Amer. Chem. Soc. 93, 7139 (1971).

157. J. L. Beauchamp, L. R. Anders and J. D. Baldeschwieler, J. Amer. Chem. Soc. 89, 4569 (1967).

158. J. D. Baldeschwieler, Science 159, 263 (1968).

159. R. G. Pearson and R. L. Dillon, J. Amer. Chem. Soc. 75, 2439 (1953).

160. R. M. Izatt, J. J. Christensen, R. T. Pack and R. Bench, Inorg. Chem. 1, 828 (1962).

161. J. I. Brauman and L. K. Blair, J. Amer. Chem. Soc. 92, 5986 (1970).

162. M. S. B. Munson, J. Amer. Chem. Soc. 87, 2332 (1965).

163. J. I. Brauman and L. K. Blair, J. Amer. Chem. Soc. 93, 3911 (1971).

164. J. I. Brauman and L. K. Blair, J. Amer. Chem. Soc. 93, 4315 (1971).

165. D. K. Bohme, E. Lee-Ruff, L. Brewster-Young, J. Amer. Chem. Soc. 93, 4608 (1971).

166. D. K. Bohme, E. Lee-Ruff, L. Brewster-Young, J. Amer. Chem. Soc. 94, 5153 (1972).

167. R. Yamdagni and P. Kebarle, J. Amer. Chem. Soc. 95, 4050 (1973).

168. K. Hiraoka, R. Yamdagni and P. Kebarle, J. Amer. Chem. Soc. 95, 6833 (1973).

169. D. H. McDaniel and H. C. Brown, J. Org. Chem. 23, 420 (1958).

170. R. W. Taft, J. Phys. Chem. 64, 1805 (1960).

171. M. Taagepera, W. G. Henderson, R. T. Brownlee, J. L. Beauchamp, D. Holtz and R. W. Taft, J. Amer. Chem. Soc. 94, 1369 (1972).

172. A. G. Harrison, P. Kebarle and F. P. Lossing, J. Amer. Chem. Soc. 83, 777 (1961).

173. T.B. McMahon and P. Kebarle, J. Amer. Chem. Soc. 98, 3399 (1976).

174. T. B. McMahon and P. Kebarle, to be published.

175. R. T. McIver and J. H. Silvers, J. Amer. Chem. Soc. 95, 8462 (1973).

176. L. Radom, J. Chem. Soc. Chem. Comm. 403 (1974).

177. G. H. F. Diercksen and W. P. Kraemer, Chem. Phys. Lett. 5, 570 (1970).

178. H. Kistenmacher, H. Popkie and E. Clementi, J. Chem. Phys. 58, 5627 (1973).

179. H. Lishka, T. Plesser and P. Schuster, Chem. Phys. Lett. 6, 263 (1970).

180. M. Arshadi, R. Yamdagni and P. Kebarle, J. Phys. Chem. 74, 1475 (1970).

181. I. Eliezer and P. Krindel, J. Chem. Phys. 57, 1884 (1972).

182. K. Spears, J. Chem. Phys. 57, 1850 (1972).

183. W. R. Davidson and P. Kebarle, J. Amer. Chem. Soc. Submitted for publication.

184. J. H. Beynon "Mass Spectrometry and Its Application to Organic Chemistry" Elsevier Publishing Co.

Amsterdam (1960).

185. R. T. McIver and J. Scott Miller, J. Amer. Chem. Soc. 96, 4323 (1974).

186. I. M. Kolthoff and M. K. Chantooni, J. Amer. Chem. Soc. 91, 4621 (1969).

187. E. G. Bordwell, J. E. Bartmess, G. E. Drucker, Z. Margolin, W. S. Matthews, J. Amer. Chem. Soc. 97, 3226 (1975).

188. W. J. Hehre and J. A. Pople, J. Amer. Chem. Soc. 92, 2191 (1970).

189. W. J. Hehre, L. Radom and J. A. Pople, J. Amer. Chem. Soc. 94, 1496 (1972).

190. A.L. McLellan, "Tables of Experimental Dipole Moments". W. H. Freeman and Co. San Francisco (1963).

191. W. R. Davidson, Ph.D. Thesis, University of Alberta (1975).

192. F. A. Cotton and G. Wilkinson "Advanced Inorganic Chemistry". John Wiley and Sons Inc. (1972).

193. S. Y. Lam and R. L. Benoit, J. Amer. Chem. Soc. 98, 1156 (1976).

194. J. B. Cumming and T. Magnera. Private communication.

195. S. A. Sullivan and J. L. Beauchamp, J. Amer. Chem. Soc. 98, 1160 (1976).

B30175